DELIVERABLE D2.3

REPORT ON ADVANCED COMPONENT TECHNIQUES FOR DVB-NGH

28TH NOVEMBER 2012

Editor: Tero Jokela

University of Turku, Finland

EXECUTIVE SUMMARY

In ENGINES work package two (WP2), individual system architecture components were studied, and the results from these studies have been forwarded to standardization work (DVB-T2 Lite, DVB-NGH). The outcome of WP2 work is collected in five deliverables. Deliverable 2.1 focuses on system architectural work performed by ENGINES partners. Deliverable 2.2 deals with DVB-NGH receiver implementation related issues. Devised advanced component techniques for DVB-NGH are presented in deliverable 2.3. Additionally there is work on overall architectures, including issues not covered by direct standardization that are novel access technologies (deliverable 2.4) and end-to-end system integration (deliverable 2.5).

The advanced component techniques that have been devised or refined in order to solve fundamental issues for reaching required capacity and performance for DVB-NGH are presented in this deliverable. The work on advanced component techniques performed by ENGINES partners for the DVB-NGH is collected here. The topics considered are:

- Forward Error Correction (FEC) coding techniques and constellations for NGH

  Studies on Forward Error Correction (FEC) coding techniques and constellations for data and signalling are presented. Both LDPC and turbo codes are investigated together with Base Band interframe FEC (BB-iFEC) mechanism. Regarding modulation constellations, the application of rotated constellations is studied.

- Time interleaving

  The contributions of the project on optimisation of channel interleaving are presented. Both interleaving mechanism and scheduling are considered.

- Advanced modulation techniques for NGH

  OFDM-OQAM modulation that is particularly efficient against frequency distortions such as Doppler Effect is studied. In OFDM-OQAM no cyclic prefix is inserted between the symbols but a specific pulse-shaping (prototype function) is introduced.

- Interference mitigation and PAPR reduction techniques

  Two contributions related to PAPR reduction techniques are presented. Comparison between several Peak to Average Ratio (PAPR) reduction techniques for DVB-NGH, especially Tone Reservation and Active Constellation Extension is reported. Further, a study on the optimization of the phase and amplitude of the channel estimation pilots, used jointly for PAPR reduction process is performed.

- Time Frequency Slicing (TFS)

  Analysis of Time-Frequency Slicing (TFS) adopted for DVB-NGH is presented. TFS mechanism is depicted and its feasibility and requirements are considered.

- MIMO Techniques

  The outcomes of the multiple antenna technique studies performed within the project are presented. Space Time (Frequency) codes presented for the DVB-NGH are presented together with performance studies. Further, distributed MIMO schemes are considered.

- Relaying for broadcast networks

  A study on relaying on broadcasting networks is presented. Cooperative communications in wireless networks have recently been introduced as a new method to increase the throughput, the reliability and the robustness of wireless systems.

The advanced techniques related to hybrid networks and cognitive radio are presented in Deliverable 2.4.

TABLE OF CONTENTS

1 Introduction 6
2 Forward Error Correction (FEC) coding techniques and constellations for NGH 6
2.1 The Bit Interleaved Coded Modulation Module for DVB-NGH: enhanced features for mobile reception 7
2.2 A double-binary 16-state turbo code for NGH 17
2.3 L1 signalling robustness improvement techniques 25
2.4 BaseBand inter Frame FEC (BB-iFEC) 36
2.5 Rotated PSK and APSK for the satellite component of NGH 46
3 Time interleaving 50
3.1 Time interleaving proposal for NGH 50
3.2 Performance analysis of time interleavers in Land Mobile Satellite conditions 58
4 Study of advanced modulation techniques for NGH 58
4.1 Terrestrial link: OFDM-OQAM modulation 58
4.2 Satellite link: SC-OFDM modulation 85
5 Study of interference mitigation and PAPR reduction techniques 86
5.1 System considerations 86
5.2 Joint PAPR and channel estimation 88
6 Time Frequency Slicing (TFS) 107
6.1 Introduction 107
6.2 TFS Concept 114
7 MIMO Techniques 121
7.1 Candidates of Space-Time (ST) Codes for DVB-NGH 122
7.2 Performance Comparisons among the Candidates 137
7.3 Advanced Modulation and MIMO Schemes 147
7.4 High Diversity Multi-Block Space-Time Code 153
7.5 Distributed MIMO techniques for the future broadcasting systems 162
8 Relaying studies for broadcast networks 172
8.1 Coverage Extension through Cooperative Relaying 172
8.2 Distributed Coding for OFDM-Based Transmission in Cooperative Broadcast Networks 176
8.3 A New Decode-Rotate-and-Forward Strategy for Cooperative Relay Networks 179
8.4 Conclusions 182
9 Summary 183
10 References 183

LIST OF CONTRIBUTORS

- **BBC**
- **CNES**
- **DiBcom**
- **Hispasat**
- **INSA-IETR**
- **MERCE**
- **Nokia**
- **Orange Labs/France Telecom**
- **Teamcast**
- **Telecom Bretagne**
  Catherine Douillard and Charbel Abdel Nour
- **Teracom**
- **Thomson Broadcast**
- **Universidad Politécnica de Valencia/ iTEAM**
- **University of Turku**
  Tero Jokela

1 INTRODUCTION

This deliverable aims at presenting the studies related to advanced component techniques that have been devised or refined in order to solve fundamental issues for reaching required capacity and performance for DVB-NGH.

First, in chapter 2, studies on Forward Error Correction (FEC) coding techniques and constellations for data and signalling are presented. Both LDPC and turbo codes are investigated together with Base Band interframe FEC (BB-iFEC) mechanism. Regarding modulation constellations, the application of rotated constellations is studied.

Chapter 3 presents the contributions of the project on optimisation of channel interleaving. The interleaving mechanism and scheduling are considered.

So-called OFDM-OQAM modulation that is particularly efficient against frequency distortions such as Doppler Effect is studied in chapter 4. In OFDM/OQAM no cyclic prefix is inserted between the symbols but a specific pulse-shaping (prototype function) is introduced.

Chapter 5 presents two contributions related to PAPR reduction techniques. Comparison between several Peak to Average Ratio (PAPR) reduction techniques for DVB-NGH, especially Tone Reservation and Active Constellation Extension is reported. Further, a study on the optimization of the phase and amplitude of the channel estimation pilots, used jointly for PAPR reduction process is performed.

Analysis of Time-Frequency Slicing (TFS) adopted for DVB-NGH is presented in chapter 6. TFS mechanism is presented and its feasibility and requirements are considered.

Chapter 7 presents the outcomes of the multiple antenna technique studies performed within the project. Space Time (Frequency) codes presented for the DVB-NGH are presented together with performance studies. Further, distributed MIMO schemes are considered.

In chapter 8 a study on relaying on broadcasting networks is presented. Cooperative communications in wireless networks have recently been introduced as a new method to increase the throughput, the reliability and the robustness of wireless systems.

2 FORWARD ERROR CORRECTION (FEC) CODING TECHNIQUES AND CONSTELLATIONS FOR NGH

This chapter covers the studies related to error correction coding and constellations that have been performed in the framework of ENGINES in order to increase the robustness of the transmission of data and signalling in the DVB-NGH context.

Section 2.1 presents the enhanced features of DVB-NGH bit interleaved coded modulation (BICM) module. Its elementary components are FEC code, bit interleaver, bit-to-cell demultiplexer, constellations and time interleaver. The section mainly focuses on the new features and performance of NGH compared to T2. Performance results for the DVB-NGH BICM module are shown.

Section 2.2 investigates a double-binary turbo code, similar to the code recently adopted in DVB-RCS2, in order to challenge the DVB-T2 LDPC+BCH code. This FEC code offers high flexibility with respect to block size and coding rate. Therefore, it suits various conditions and environments and delivers better performance than the DVB LDPC codes at low error rates.

Section 2.3 studies the different techniques proposed for the robustness improvement of Layer 1 (L1)

signalling in DVB-NGH. The goal is to investigate the feasibility of three new techniques for L1 signalling robustness and to study which configurations provide the best performance depending on the channel characteristics and operator's requirements.

In Section 2.4, a novel FEC and Time Interleaving scheme is proposed, known as BB-iFEC (Base Band - inter-burst FEC), which aims at providing long time interleaving with fast zapping support. It calls for a split FEC technique, particularly well-suited for satellite transmissions but also proposed for the sheer terrestrial link in DVB-NGH.

Finally, Section 2.5 extends the principle of the rotated constellation technique, adopted in DVB-T2, to PSK and APSK constellations, widely used for satellite transmissions.

2.1 The Bit Interleaved Coded Modulation Module for DVB-NGH: enhanced features for mobile reception

2.1.1 Introduction

In 2009, when the DVB-NGH Call for Technologies [1] was issued, two technical state-of-the-art DVB standards could be used as a starting point for DVB-NGH: DVB-SH [2] and DVB-T2 [3]. Both standards include state-of-the-art Bit-Interleaved Coded Modulation (BICM) modules. In particular, they both use a capacity approaching coding scheme: a turbo coding scheme is used in DVB-SH and a DVB-S2-like LDPC code was adopted in DVB-T2. Moreover, the DVB-NGH Commercial Requirements [4] mention the possibility to combine DVB-NGH and DVB-T2 signals in one Radio Frequency (RF) channel. The natural way for this combination calls for the use of the so-called Future Extension Frames (FEF) of DVB-T2. Although a DVB-T2 FEF can contain BICM components totally different from the DVB-T2 BICM module, the existence of combined DVB-T2/NGH receivers finally pushed the elaboration of a DVB-NGH physical layer strongly inspired by DVB-T2.

According to the above-mentioned considerations, DVB-NGH was designed to provide an extension of the DVB-T2 system capabilities, to ease the introduction of TV services to mobile terminals within an existing terrestrial digital TV network. In particular, keeping reasonable receiver complexity and power consumption and increasing robustness of mobile reception have guided the choice for the BICM components. Therefore, the BICM module in the DVB-NGH standard is mainly derived from a sub-set of DVB-T2 BICM components, with a set of additional features allowing for higher robustness and coverage.

Sub-section 2.1.2 describes the overall structure of the BICM module in DVB-NGH. Sub-sections 2.1.3 to 2.1.6 provide details for its elementary components: FEC code, bit interleaver, bit-to-cell demultiplexer, constellations and time interleaver. The description mainly focuses on the new features and performance of NGH compared to T2. Sub-section 2.1.7 presents some performance results and sub-section 2.1.8 concludes this section.

2.1.2 Overall view of the DVB-NGH BICM module

In the communication theory literature, BICM is the state-of-the-art pragmatic approach for combining channel coding with digital modulations in fading transmission channels [5]. The modulation constellation can thus be chosen independently of the coding rate. The DVB-NGH BICM encoder consists essentially of:

- a forward-error correcting (FEC) code allowing transmission errors to be corrected at the receiver side,

- a bit interleaver whose function is to spread the coded bits within a FEC block in order to avoid undesirable interactions between the bits to be mapped to the same modulation constellation point,
- a bit-to-cell mapper, mapping groups of coded bits to modulation constellation points,
- a set of interleavers intended to fight against channel impairments, e.g. caused by impulsive noise or time-varying channels, by spreading cell error bursts over several FEC blocks.

In DVB-NGH, as in DVB-T2, the input to the BICM module consists of one or more logical data streams. Each logical data stream is carried by one Physical Layer Pipe (PLP) and is associated with a given modulation constellation, a given FEC mode and a given time interleaving depth. The DVB-NGH BICM module structure for data PLPs is described in Figure 1.

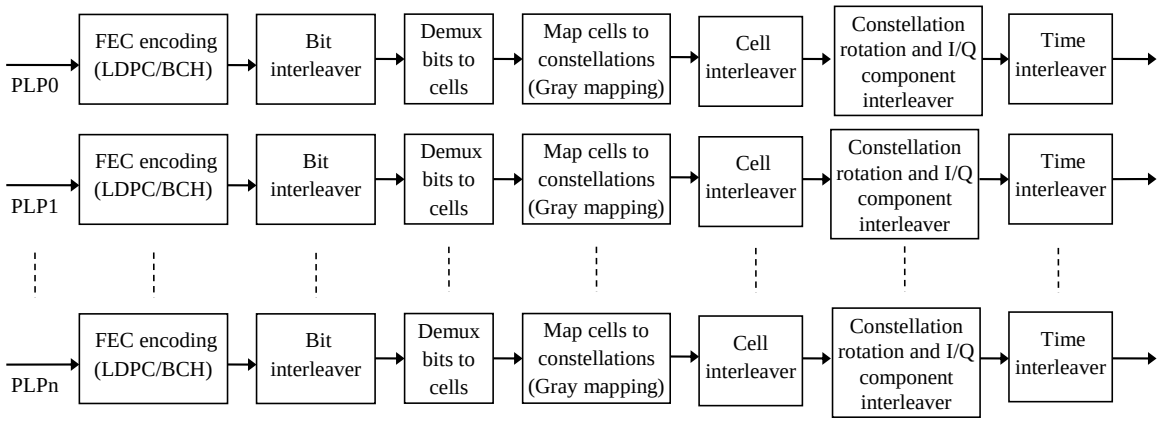

Figure 1: DVB-NGH BICM module structure.

2.1.3 Forward error correction

FEC coding in the first generation of DVB standards was based on convolutional and Reed-Solomon codes. In the second generation, more powerful codes are used, calling for the serial concatenation of a Bose-Chaudhuri-Hocquenghem (BCH) code and Low Density Parity Check (LDPC) code. These codes were designed to provide a *quasi-error free* quality target, defined as "less than one uncorrected error event per transmission hour at the throughput of a 5 Mbit/s single TV service decoder" and approximately corresponding to a transport stream Frame Error Ratio FER < 10^{-7}.

LDPC codes are capacity-approaching codes calling for iterative decoding techniques. The DVB-x2 LDPC codes [6] ensure low-complexity encoding due to their Irregular-Repeat Accumulate (IRA) structure [7]. Moreover, an efficient structure of the parity-check matrix allows for a high level of intrinsic parallelism in the decoding process. In order to reach the quasi error free target without any change in the slope of the error rate curves, an outer *t*-error-correcting BCH code with $t = 10$ or 12 has been added to remove residual errors.

In the main DVB-x2 standards, two FEC block lengths have been defined, Nldpc = 64,800 and Nldpc = 16,200 bits. In DVB-NGH, only the short 16,200-bit LDPC codes have been implemented in order to reduce receiver complexity. Furthermore, the code rate values were chosen to uniformly cover the range 5/15 (1/3) to 11/15, thus providing equidistant performance curves with respect to signal-to-noise ratio. The set of coding rates and blocks sizes are summarized in Table 1.

Table 1: Data coding parameters for DVB-NGH.

LDPC code rate	BCH uncoded block size K_{bch}	LDPC uncoded block size K_{ldpc}	BCH t-error correction
5/15 (1/3)	5 232	5 400	12
6/15 (2/5)	6 312	6 480	12
7/15	7 392	7 560	12
8/15	8 472	8 640	12
9/15 (3/5)	9 552	9 720	12
10/15 (2/3)	10 632	10 800	12
11/15	11 712	11 880	12

The low and high coding rates, 1/3, 2/5, 3/5, 2/3 and 11/15 are directly taken from DVB-S2. On the contrary, rates 7/15 and 8/15 call for new codes specific to DVB-NGH. The BCH code is identical to the one used in DVB-T2 for the short block size.

2.1.4 Bit interleaver and bit-to-cell demultiplexer

DVB-NGH inherited the bit interleaver structure from DVB-T2. It is a block interleaver applied at the LDPC codeword level, consisting of parity interleaving followed by column-twist interleaving. If basic block interleaving – column-wise writing and row-wise reading – were applied directly to the LDPC codewords, many constellation symbols would contain multiple coded bits participating to the same LDPC parity equations, entailing a performance loss in channels with deep fading. To avoid this degradation, the parity interleaver permutes parity bits in such a way that the redundancy part of the parity-check matrix has the same structure as the information part. Then, the information bits and the parity interleaved bits are column wise serially written into the column twist interleaver, and read out serially row wise. The write start position of each column is twisted by an integer value t_c, depending on the code size, the constellation and the column number. In DVB-NGH, parity interleaving is applied to all constellations and for all coding rates, as it was shown to improve low error rate performance in fading channels. Column-twist interleaving is used for all constellations but QPSK.

As in DVB-T2, an additional bit-to-cell de-multiplexer is inserted between the bit interleaver and the constellation mapper. It divides the bit stream at the output of the bit interleaver into a number of sub-streams which is a multiple of the number of bits per constellation cell. In DVB-NGH, the bit-to-cell de-multiplexing parameters have been specifically tuned in order to allow a finer optimization for each constellation size and code rate.

2.1.5 Modulation constellations

DVB-NGH has inherited the four constellations of DVB-T2: QPSK, 16-QAM, 64-QAM and 256-QAM. Except for the 256-QAM, they can be implemented according to two different modes: conventional non-rotated or rotated constellations. Moreover, two new features have been added to the existing scheme: the adoption of non-uniform 64- and 256-QAM and the extension of the rotated constellation principle to four dimensions for QPSK and high coding rates.

2.1.5.1 Non-uniform QAM constellations

Non-uniform constellations are introduced to bridge the observed gap between capacity curves of uniform constellations and the Shannon limit. In fact, when the received signal is perturbed by Gaussian-distributed noise, the mutual information expression is maximised for a Gaussian distribution of the transmitted signal. Applying this assumption leads to the famous Shannon capacity formula. However, the distribution of conventional QAM constellations is far from Gaussian: it is both discrete, as only a limited number of signal values are transmitted, and uniform, since the constellation points are regularly spaced and transmitted with equal probabilities.

Non-uniform constellations try to make the transmitted constellation distribution appear "more" Gaussian. Called shaping gain, the corresponding improvement adds up to the coding gain of coded modulation schemes. It has been shown that the shaping gain of discrete constellations in AWGN channel cannot exceed $10 \log(\pi e/6) \approx 1.53$ dB [8]. Two main shaping techniques have been investigated so far: using a classical constellation with a regular distribution of the signal points and transmitting the signal points with different probabilities or using a constellation whose signal points are non-uniformly spaced and transmitting all the signal points with the same probability. The non-uniform constellations proposed in DVB-NGH belong to the second category.

Constellation point coordinates are chosen to maximise the BICM capacity of the underlying QAM. Let's detail the approach in the simple example of 16-QAM. Non-uniform 16 QAM has not been adopted in DVB-NGH, but the optimisation principle is simpler to explain in this case. If we consider that uniform 16-QAM uses positions $\{-3,-1,+1,+3\}$ on each axis, then we can make a non-uniform version having positions $\{-\gamma,-1,+1,+\gamma\}$, using only one parameter γ. For any particular signal-to-noise ratio (SNR), we can plot the BICM capacity as a function of γ. For example, Figure 2 shows the BICM capacity of the non-uniform 16-QAM at a SNR of 10 dB. γ equal to 3 corresponds to the uniform case, while the maximum capacity is obtained for a value of γ between 3.35 and 3.4. Selecting the values of γ yielding the maximum capacity for a large range of SNRs can provide the basis for the construction of an adaptive non-uniform 16-QAM.

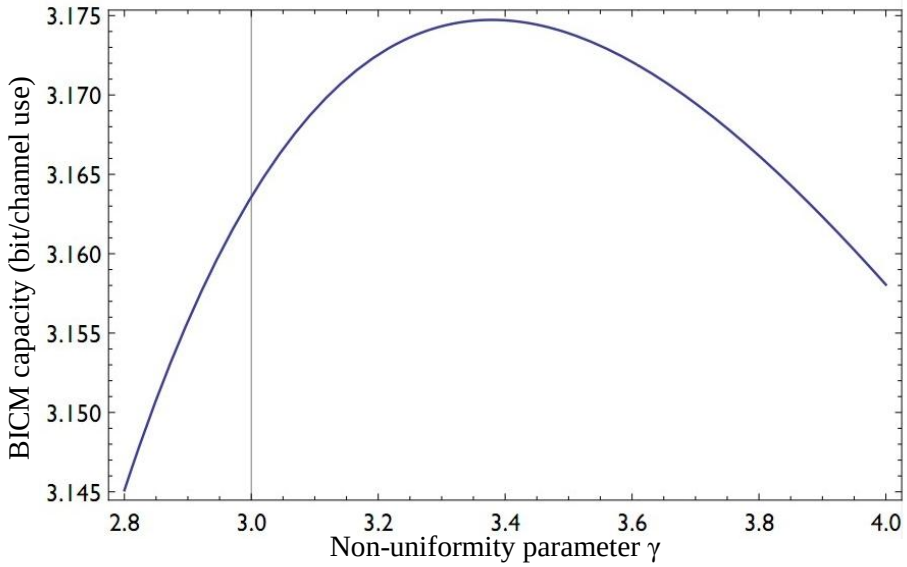

Figure 2: BICM capacity curve as a function of non-uniformity parameter γ for 16-QAM in AWGN at 10 dB SNR (from a report produced by Jonathan Stott Consulting under contract to BBC R&D).

When considering higher order constellations, where larger gains are expected, the capacity maximisation involves more than one non-uniformity parameter: 3 parameters for non-uniform 64-QAM whose

coordinates on I and Q axes are$\{-\gamma,-\beta,-\alpha,-1,+1,+\alpha,+\beta,+\gamma\}$ and 7 parameters for non-uniform 256-QAM whose coordinates on I and Q axes are $\{-\eta,-\zeta,-\varepsilon,-\delta,-\gamma,-\beta,-\alpha,-1,+1,+\alpha,+\beta,+\gamma,+\delta,+\varepsilon,+\zeta,+\eta\}$. A solution to this problem was provided numerically for a large range of SNR. As a consequence of the dependence of the non-uniform constellation points on the SNR, a given non-uniform constellation cannot provide the maximum coding gain for any operation point and accordingly for any code rate. Therefore a specific non-uniform constellation has been defined for each code rate. The corresponding constellation mappings are given in Table 2 and Table 3.

Table 2: Constellation mapping of the I and Q components for the uniform and non-uniform 64-QAM. The I/Q coordinates don't have the form $\{-\gamma,-\beta,-\alpha,-1,+1,+\alpha,+\beta,+\gamma\}$ since a normalization operation was performed in order to keep the same transmit power as for the uniform constellations.

I/Q values		Binary mapping							
		1 0 0	**1 0 1**	**1 1 1**	**1 1 0**	**0 1 0**	**0 1 1**	**0 0 1**	**0 0 0**
Uniform		-7	-5	-3	-1	1	3	5	7
Non-Uniform Coding Rate	***1/3***	-7.2	-5.2	-1.9	-1.4	1.4	1.9	5.2	7.2
	2/5	-7.4	-4.9	-2.0	-1.3	1.3	2.0	4.9	7.4
	7/15	-7.5	-4.6	-2.3	-1.0	1.0	2.3	4.6	7.5
	8/15	-7.5	-4.6	-2.4	-0.9	0.9	2.4	4.6	7.5
	9/15	-7.5	-4.6	-2.5	-0.9	0.9	2.5	4.6	7.5
	2/3	-7.4	-4.7	-2.6	-0.9	0.9	2.6	4.7	7.4
	11/15	-7.3	-4.7	-2.7	-0.9	0.9	2.7	4.7	7.3

Table 3: Constellation mapping of the I and Q components for the uniform and non-uniform 256-QAM.

I/Q values		Binary mapping															
		1 0 0 0	**1 0 0 1**	**1 0 1 1**	**1 0 1 0**	**1 1 1 0**	**1 1 1 1**	**1 1 0 1**	**1 1 0 0**	**0 1 0 0**	**0 1 0 1**	**0 1 1 1**	**0 1 1 0**	**0 0 1 0**	**0 0 1 1**	**0 0 0 1**	**0 0 0 0**
Uniform		-15	-13	-11	-9	-7	-5	-3	-1	1	3	5	7	9	11	13	15
Non-Uniform Coding Rate	***1/3***	-17.2	-12.6	-9.7	-9.3	-3.8	-4.1	-2.5	-2.4	2.4	2.5	4.1	3.8	9.3	9.7	12.6	17.2
	2/5	-17.3	-13.1	-9.4	-8.8	-4.2	-4.3	-2.1	-2.1	2.1	2.1	4.3	4.2	8.8	9.4	13.1	17.3
	7/15	-17.5	-13.1	-9.2	-8.2	-4.7	-4.6	-1.6	-1.7	1.7	1.6	4.6	4.7	8.2	9.2	13.1	17.5
	8/15	-17.5	-13.0	-9.3	-8.1	-5.0	-4.6	-1.6	-1.5	1.5	1.6	4.6	5	8.1	9.3	13	17.5
	9/15	-16.7	-13.1	-10.3	-8.0	-5.9	-4.2	-2.3	-0.9	0.9	2.3	4.2	5.9	8	10.3	13.1	16.7
	2/3	-16.7	-13.1	-10.3	-8.0	-5.9	-4.2	-2.3	-0.9	0.9	2.3	4.2	5.9	8	10.3	13.1	16.7
	11/15	-16.6	-13.1	-10.3	-8.0	-6.0	-4.2	-2.4	-0.9	0.9	2.4	4.2	6	8	10.3	13.1	16.6

Figure 3 shows the performance gain of the non-uniform 256-QAM in the AWGN channel with respect to the classical constellation.

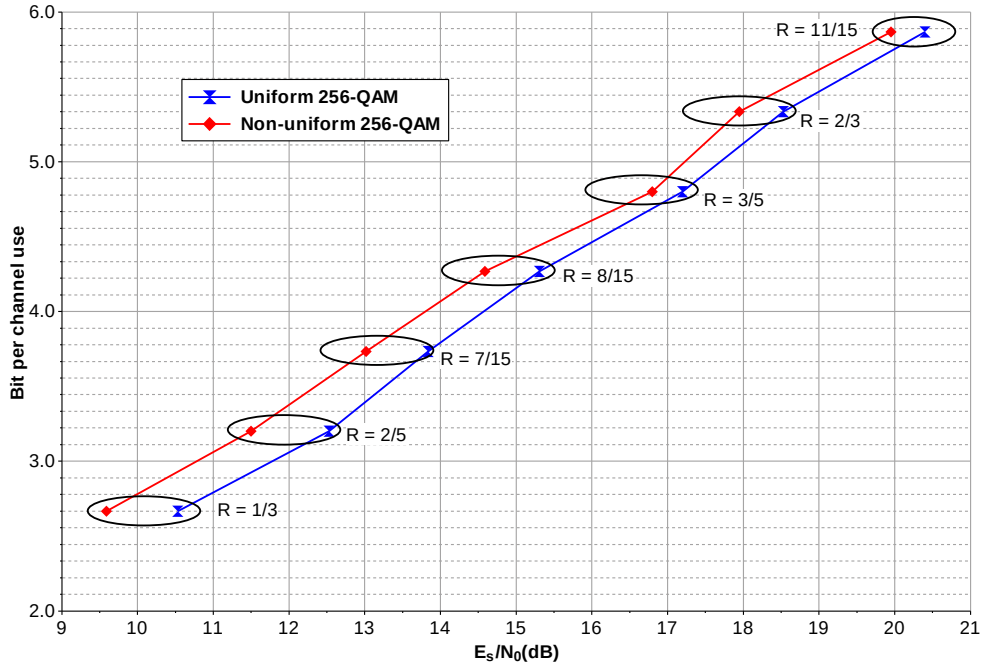

Figure 3: Performance comparison of uniform and non-uniform 256-QAM over AWGN channel. Both curves display the required SNR to achieve a FER=10-4 after LDPC decoding.

2.1.5.2 Rotated Constellations

2.1.5.2.1 A reminder about 2-dimensional rotated constellations

When using conventional QAM constellations, each signal component, in-phase I (real) or quadrature Q (imaginary), carries half of the binary information held in the signal. When a constellation signal is subject to a fading event, I and Q components fade identically. In case of severe fading, the information transmitted on I and Q components suffers an irreversible loss. When a rotation is applied to the constellation, components I and Q both carry the whole binary content of the signal, as every point in the constellation now has its own projections over the I and Q axes. The rotation is performed by multiplying each I/Q component vector by a 2x2 orthogonal matrix:

$$\begin{bmatrix} y_I \\ y_Q \end{bmatrix} = \begin{bmatrix} \cos\Phi & -\sin\Phi \\ \sin\Phi & \cos\Phi \end{bmatrix} \begin{bmatrix} x_I \\ x_Q \end{bmatrix} \qquad (2.1)$$

Next, the Q component of the resulting vector is cyclically delayed by one cell within the FEC block. Consequently, due to the subsequent effect of the cell and time interleavers, the two copies or projections of the signal are sent separately in order to benefit from time or frequency diversity respectively. With this technique, the diversity order of BICM is doubled compared to the case of non-rotated constellation.

2.1.5.2.2 4-dimensional rotated constellations

In DVB-NGH, the constellation diversity has been extended with the adoption of so-called four Dimensional Rotated Constellations (4D-RC). Moreover the cyclic shift delay applied to the quadrature Q component is replaced by a more sophisticated I/Q component interleaver providing a better time separation and channel diversity, when time-frequency slicing (TFS) [9] or multi-frame interleaving is enabled. The 4D rotation is performed by multiplying two vectors consisting of the I/Q components of two adjacent input cells by a 4x4

orthogonal matrix:

$$\begin{bmatrix} y_{0I} \\ y_{0Q} \\ y_{1I} \\ y_{1Q} \end{bmatrix} = \begin{bmatrix} +a & -b & -b & -b \\ +b & +a & -b & +b \\ +b & +b & +a & -b \\ +b & -b & +b & +a \end{bmatrix} \begin{bmatrix} x_{0I} \\ x_{0Q} \\ x_{1I} \\ x_{1Q} \end{bmatrix} \quad (2.2)$$

The four dimensional rotation matrix is characterized by a single parameter r taking values in range [0,1], referred to as the *rotation factor*, which is defined as:

$$r = 3b^2 / a^2 \quad (2.3)$$

Since the rotation matrix is orthogonal, $a^2 + 3b^2 = 1$. Thus, a and b are derived from r as

$$a = \sqrt{\frac{1}{(1+r)}} \quad b = \sqrt{\frac{r}{3(1+r)}} \quad (2.4)$$

The optimal value for r was actually chosen to minimise the bit error rate at the demapper output in Rayleigh fading channels. With 4D-RC, the diversity order of the BICM is quadrupled in comparison with non-rotated constellations. Over fading channels, they only provide gain when used with very low constellation sizes such as QPSK and high code and they show high robustness in case of deep fades or erasures. From a complexity point of view, at the receiver side, M^2 four-dimensional Euclidean distances have to be computed by the demapper for a M-QAM; Finally the use of 4D-RC in DVB-NGH has been restricted to 4D-QPSK for code rates greater than or equal to 8/15. Table 4 summarizes the rotated constellations modes and parameters adopted in the standard.

Table 4: Summary of the rotated constellation modes in DVB-NGH.

Modulation	**Code rate**						
	1/3	***2/5***	***7/15***	***8/15***	***3/5***	***2/3***	***11/15***
QPSK	2D (Φ = 29.0 deg.)			4D (r = 0.4)			
16QAM	2D (Φ = 16.8 deg.)						
64QAM	2D (Φ = 8.6 deg.)						
256QAM	N/A						

Figure 4 shows the performance gain due to the rotated constellations modes of DVB-NGH in a fast fading memoryless Rayleigh channel.

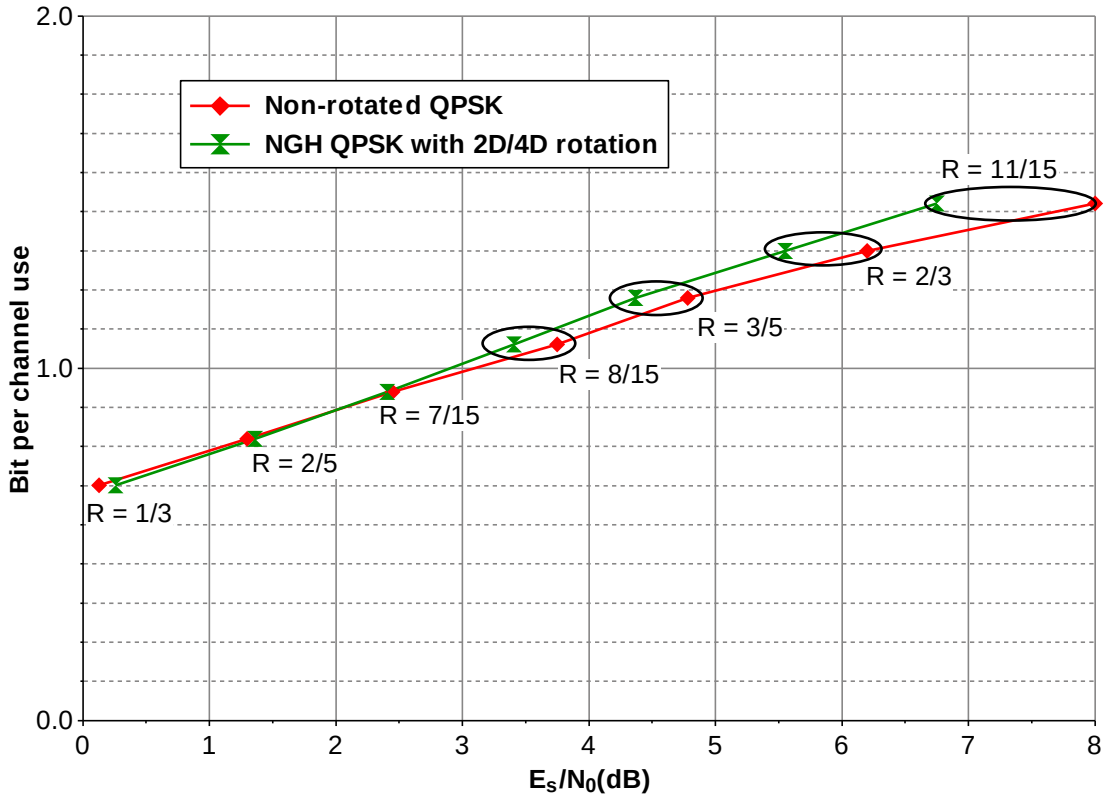

Figure 4: Performance gain due to the constellation rotation modes of DVB-NGH over memoryless Rayleigh channel. Both curves display the required SNR to achieve a FER=10^{-4} after LDPC decoding.

2.1.5.3 Cell Interleaving and I/Q Component Interleaving

1) *Cell Interleaving*: The cell interleaver first applies a pseudo-random permutation in order to uniformly spread the cells in the FEC codeword. It aims at ensuring an uncorrelated distribution of channel distortions and interference along the FEC codewords in the receiver. This pseudo-random permutation varies from one FEC block to the next. In contrast to DVB-T2, it is placed before the I/Q component interleaver.

2) *I/Q Component Interleaving*: It is applied after the 2D or 4D rotation and is performed on each FEC block independently according to the following three steps:

   – The I and Q components of the cells belonging to a FEC block are separately written column-wise into two matrices of the same size;
   – A cyclic shift is applied to each column of the Q-component matrix;
   – The two matrices are read out synchronously row-wise and complex cells are formed by each read pair of a real (I) and an imaginary (Q) component.

The number of rows N_R in the matrices and the values of the cyclic shifts depend on whether TFS is enabled or not. When TFS is off, the component interleaver distributes the $D = 2$ or 4 dimensions of each constellation evenly over the FEC block, the resulting distance between the D components of each constellation signal being $(1/D)^{th}$ of the FEC length. In this case, N_R is equal to D, and the cyclic shifts of all columns are equal to $D/2$. When TFS is on, parameter N_R is a function of the number of RF channels N_{RF} and the cyclic shift can take N_{RF}-1 different values. The values of these parameters are chosen to ensure that the D dimensions of each constellation signal are transmitted over all possible combinations of RF channels.

2.1.6 Time interleaving

The time interleaver (TI) is mainly intended to provide protection against impulsive noise and time-selective fading. It is placed at the output of the I/Q component interleaver or at the output of the cell interleaver, depending on whether rotated constellations are used or not. It operates at PLP level and the TI parameters can vary from a PLP to another.

The total size of the memory for time de-interleaving all PLPs associated with a service cannot exceed 2^{18} memory units for the terrestrial link. A memory unit contains one cell with 64-QAM and 256-QAM modulation. Since QPSK and 16-QAM constellations can afford coarser cell quantization than 64-QAM and 256-QAM, for these low-order constellations a memory unit consists of a pair of two consecutive cells. This case is referred to as *pair-wise interleaving*. It allows higher time diversity for QPSK and 16-QAM constellations, since the TI memory can store up to 2^{19} cells.

The core element is a block row-column interleaver, as in DVB-T2. However, DVB-NGH additionally offers the possibility to combine a convolutional interleaver on top of the core element when interleaving over several NGH frames is enabled. The Interleaving Frame (IF) contains the cells collected for one NGH frame. Since the data rate of each PLP can vary, each IF can contain a variable number of FEC blocks. In the simplest case, the IF is implemented as a single block interleaver. However, this configuration limits the maximum data rate because of the above-mentioned size limitation. To increase the data rate, it is therefore possible to divide the IF into several block interleavers before it is mapped to one NGH-frame. Conversely, for low data rate services, longer time interleaving and hence higher time diversity can be achieved by spreading the IF over several NGH frames. Then, the overall TI is implemented as a combination of a convolutional interleaver with a block interleaver. Figure 5 illustrates this combined structure.

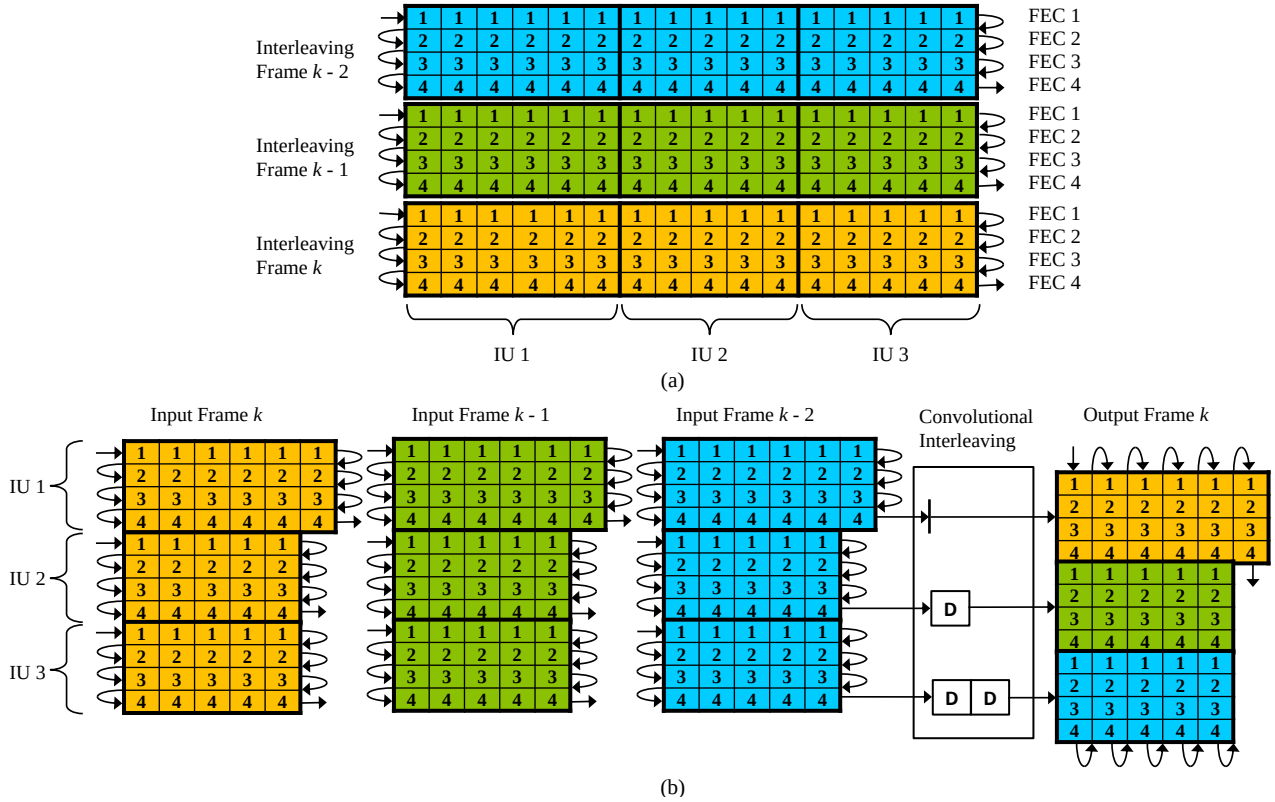

Figure 5: Time interleaving for N_{IU} = 3 in the hypothetical case where each FEC codeword length contains 16 cells and each IF contains 4 FEC blocks.

The cells to be interleaved are written row-wise into the TI memory, FEC block by FEC block (see Figure 5(a)). The IF is then partitioned into N_{IU} Interleaver Units (IU). Each IU is passed in one of the delay lines of

the convolutional interleaver and the cells are afterwards read column-wise, as shown in Figure 5(b). Each input IF is therefore spread over N_{IU} NGH frames. This combined block/convolutional TI structure allows for time interleaving depths greater than 1 sec on the terrestrial segment. The depth can be increased to up to 10 sec for the satellite link, since the TI memory limitation is then 2^{21} memory units.

2.1.7 Performance results

Figure 6 and Figure 7 show simulated performance of the DVB-NGH BICM in AWGN and Rayleigh channels compared to the unconstrained Shannon capacity [10] and DVB-H. The curves display the required SNR to achieve a FER=10^{-4} after LDPC decoding. Over AWGN channel, DVB-NGH outperforms the first generation by around 2.0 to 2.5 dB. Over a Rayleigh fading channel, the gain ranges from 3.0 to 7.0 dB. The gap to Shannon capacity is larger over a Rayleigh fading channel.

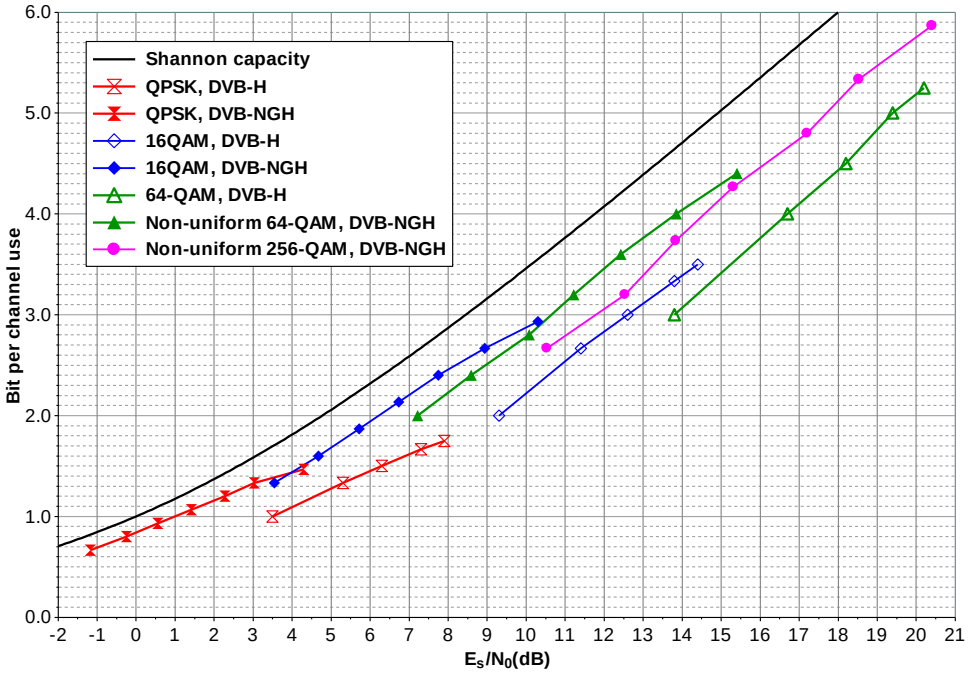

Figure 6: Required SNR to achieve a FER=10^{-4} after LDPC decoding over AWGN channel. Comparison with the Shannon limit and DVB-H.

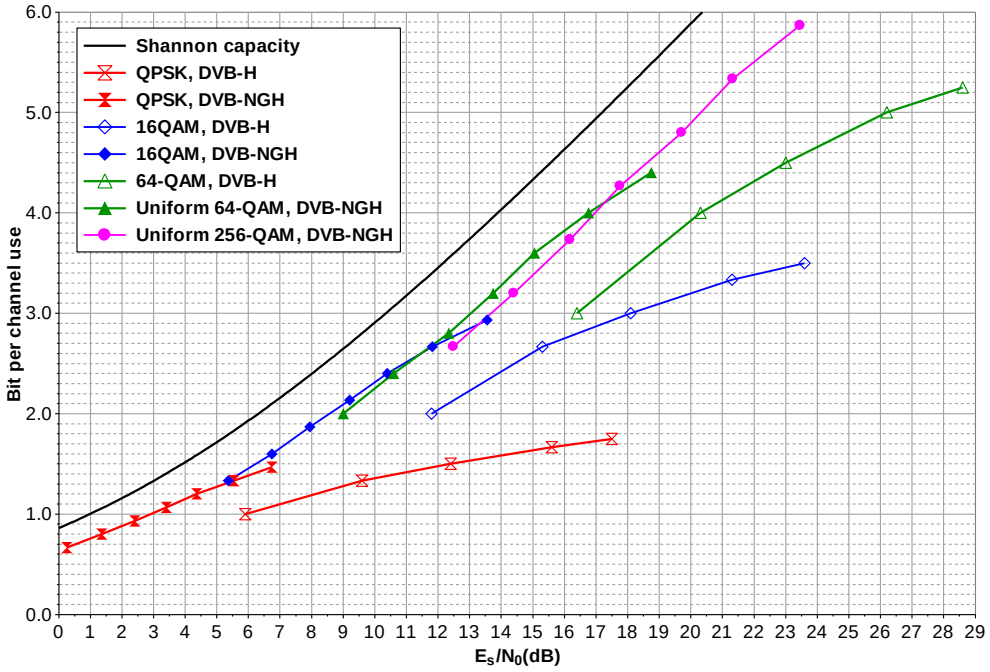

Figure 7: Required SNR to achieve a FER=10^{-4} after LDPC decoding over Rayleigh fading channel. Comparison with the Shannon limit and DVB-H.

2.1.8 Conclusion

The BICM module of DVB-NGH has been devised to extend DVB-T2 operation range to lower SNRs. Moreover, the design of the BICM components has been guided by the need to increase robustness for mobile reception and to keep reasonable receiver complexity and power consumption. The overall performance of the BICM module has only been partially assessed so far. The next step involves the thorough performance evaluation in mobile channels and in quasi-error free conditions.

2.2 A double-binary 16-state turbo code for NGH

This study was carried out by Telecom Bretagne. The outcomes of this work have been presented to the DVB TM-H group, through 10 different contributions.

Due to the "family of standard" approach currently in force in DVB, the main second generation DVB standards (DVB-S2, DVB-T2 and DVB-C2) have adopted the same family of FEC codes, based on the association of a Low Density Parity-Check (LDPC) code with the addition of an outer BCH code, allowing the residual error floor to be lowered.

For DVB-NGH, two previous DVB standards could be taken as starting points: DVB-T2 and DVB-SH (Satellite Handheld). The former resorts to the above-mentioned LDPC+BCH code while the latter calls for a binary turbo code (TC), derived from the 3GPP2 standard. In order to challenge the DVB-T2 LDPC+BCH code, we have proposed a 16-state double-binary turbo code (DB-TC), similar to the code recently adopted in DVB-RCS2. This FEC code offers high flexibility with respect to block size and coding rate. Therefore, it suits various conditions and environments and delivers better performance than 3GPP2 code, especially at low error rates. It can also be associated with a BCH code if required.

Telecom Bretagne carried out an extensive study of the double-binary 16-state TC. It involves the search for code parameters (block sizes, interleaver parameters, puncturing patterns) and the comparison with the DVB-

T2 code in terms of performance, hardware complexity and power consumption.

2.2.1 The turbo encoder structure

The structure of the proposed encoder is depicted in Figure 8. It is based on the parallel concatenation of two 16-state double-binary recursive systematic convolutional (RSC) encoders, fed by blocks of k bits ($N = k / 2$ couples). Internal permutation Π deals with blocks of N double-binary symbols. Both component encoders have identical features:

- 16-state double-binary convolutional code,
- polynomials 23octal (recursivity) and 35octal (redundancy),
- first bit (A) on tap 1, second bit (B) on taps 1, D and D^3,
- circular termination for both component encoders.

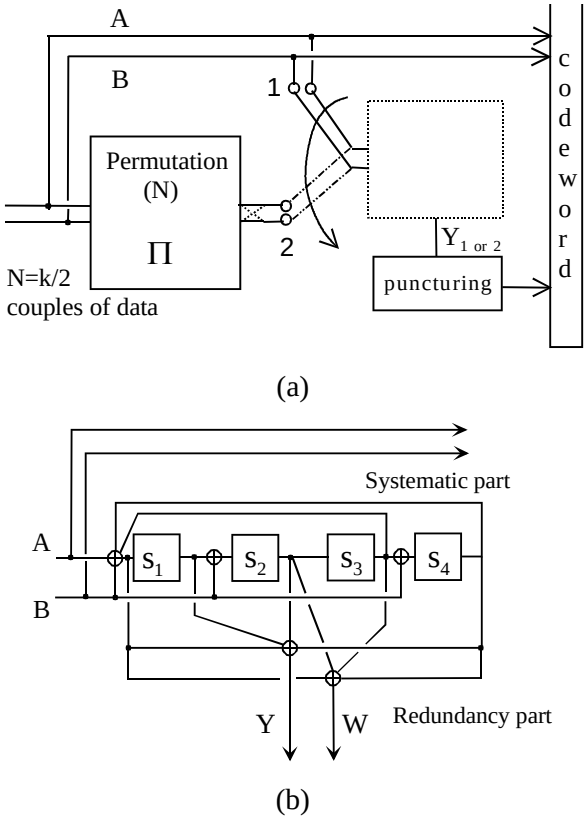

Figure 8: The proposed 16-state DB-TC (a) Global structure. (b) Component encoder: for $R \geq 1/2$, redundancy W is not transmitted; for $R < 1/3$, input B is set to zero and is not transmitted.

The natural coding rate of the TC depicted in Figure 1 is $R = 1/3$. The usual way of increasing the coding rate of a TC consists of puncturing, that is to say not transmitting some redundancy bits. We have adopted the easiest way to perform puncturing through applying periodic puncturing patterns.

The permutation law Π

We proposed a two-layer permutation Π, as already adopted by the DVB-RCS and DVB-RCS2 TCs: the inter-symbol permutation is an Almost Regular Permutation (ARP) as described in [12]. In addition to the main inter-symbol permutation, intra-symbol permutation is also performed to increase the minimum Hamming distance of the code even further. In practice, the bits in the double-binary symbols are permuted once every other time before second encoding, the process beginning with the permutation of the first couple. The selection of the permutation parameters has been performed according to the method described

in [13], which calls for an iterative combinatorial optimization on the correlation graph of the TC. Moreover, we have only kept permutation parameters providing low weight codewords with low input weights, thus making possible the association of the TC with an outer BCH code.

2.2.2 Performance comparison

The proposed double-binary turbo code was compared to the DVB-T2 LDPC for different coding rates and several transmission channels. The comparison was carried out in two steps:

- Comparison over static channels (Gaussian, Rayleigh, Rayleigh with erasures);
- Comparison over mobile channels (TU-6) for different Doppler frequency values f_d.

Both codes were compared for coding rates R=1/5, R=1/3 and R=2/3 and QPSK and 16-QAM constellations. The LDPC code was decoded using 50 iterations of the sum-product algorithm and the TC was decoded using 10 iterations of the BCJR algorithm.

Figure 9, Figure 10 and Figure 11 show some examples of performance comparisons for three different block sizes, coding rates and transmission channels.

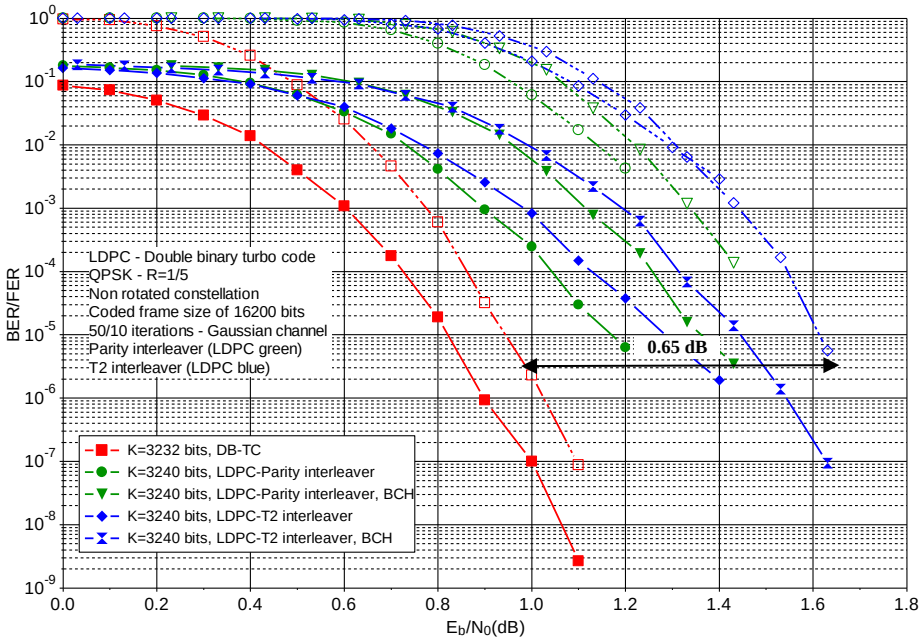

Figure 9: BER and FER comparison of the proposed DB-TC with the DVB-T2 LDPC+BCH. k= 3,232 bits for the DB-TC and k= 3,240 bits for the DVB-T2 code. Coding rate R = 1/5, QPSK constellation, Rayleigh channel.

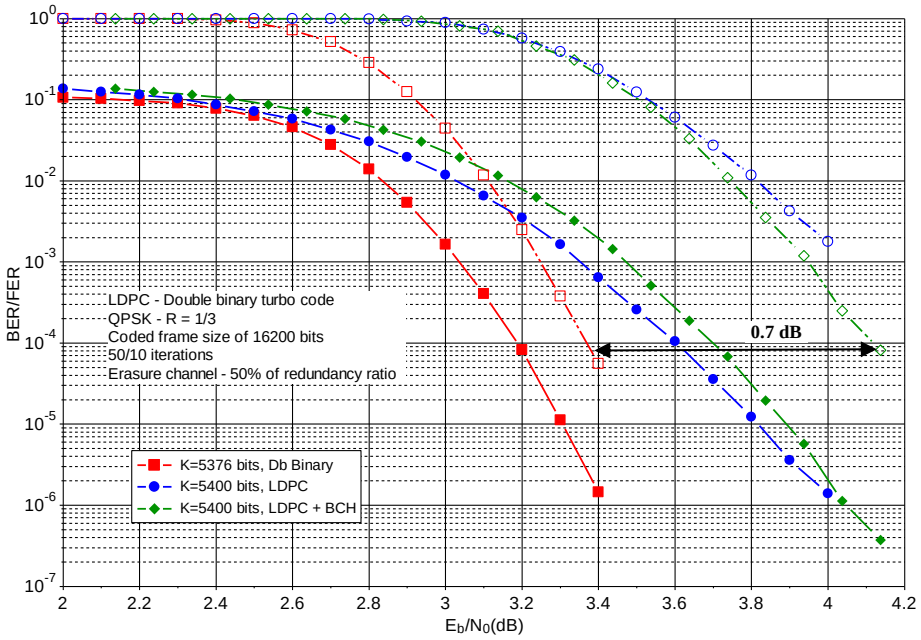

Figure 10: BER and FER comparison of the proposed DB-TC with the DVB-T2 LDPC+BCH. *k*=5,376 bits for the DB-TC and k=5,400 bits for the DVB-T2 code. Coding rate *R* = 1/3, QPSK constellation, Rayleigh channel with erasures.

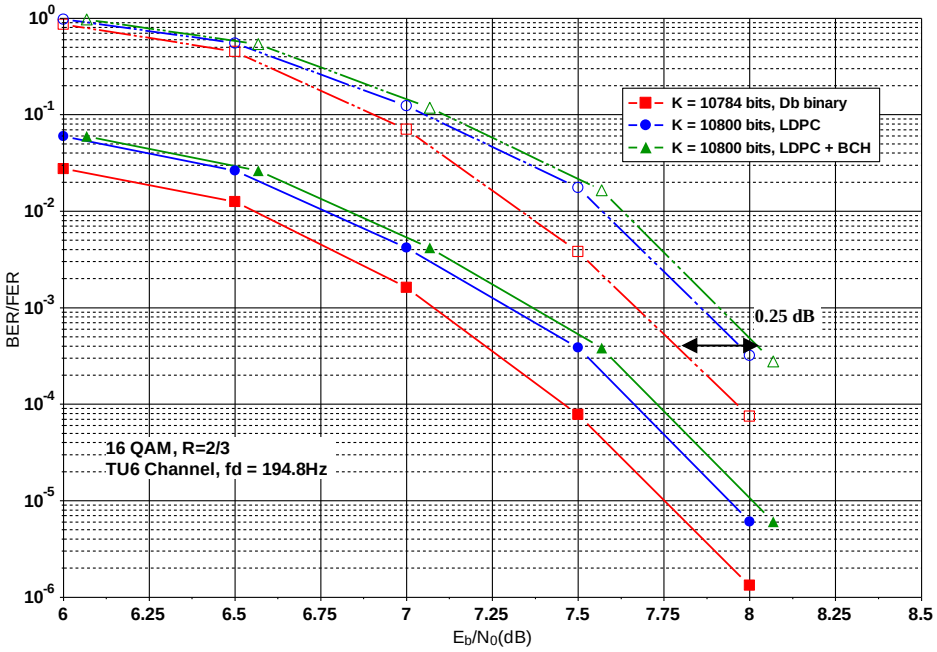

Figure 11: BER and FER comparison of the proposed DB-TC with the DVB-T2 LDPC+BCH. *k*=10,784 bits for the DB-TC and *k*=10,800 bits for the DVB-T2 code. Coding rate *R* = 2/3, 16-QAM constellation, TU-6 channel with Doppler frequency f_d=194.8 Hz.

Table 5 and Table 6 provide an overview of the gain in E_b/N_0 observed between the proposed DB-TC and the DVB-T2 LDPC+BCH code for the different simulated configurations.

Table 5: E_b/N_0 gain in dB observed between the proposed turbo code and the DVB-T2 LDPC+BCH code over static channels at FER = 10^{-5}.

		Coding Rate		
		1/5	1/3	2/3
AWGN	QPSK	0.6	0.3	0.25
	16QAM		0.3	0.35
Rayleigh	QPSK	0.55	0.4	0.3
	16QAM		0.4	0.25
Rayleigh with erasures	QPSK	0.5	0.7	0.2
	16QAM		0.45	0.0

Table 6: E_b/N_0 gain in dB observed between the proposed turbo code and the DVB-T2 LDPC+BCH code over mobile channels at FER = 10^{-4}.

		Coding Rate		
		1/5	1/3	2/3
TU-6 channel f_d=33.3 Hz	QPSK	0.75	0.3	0.25
	16QAM		0.5	0.25
TU-6 channel f_d=194.8 Hz	QPSK	0.7	0.5	0.25
	16QAM		0.4	0.25

2.2.3 Complexity comparison

A three-point complexity comparison of the two families of codes was carried out. The following criteria have been considered:

- Identify the required number of iterative decoder iterations for every family of codes to achieve a target error rate performance given a particular coding rate and constellation size.
- Complexity comparison, in terms of number of logic operations and memory accesses, based on realistic hardware architectures of LDPC and turbo decoders, given the number of identified iterations.
- Area estimate based on partial logic synthesis.

Figure 12 and Figure 13 illustrate some outcomes of the first point of the comparison. For coding rate 1/3 and QPSK constellation, the proposed turbo code, decoded with 5 iterations, outperforms the DVB-T2 decoder using 50 iterations, both over static and mobile channels.

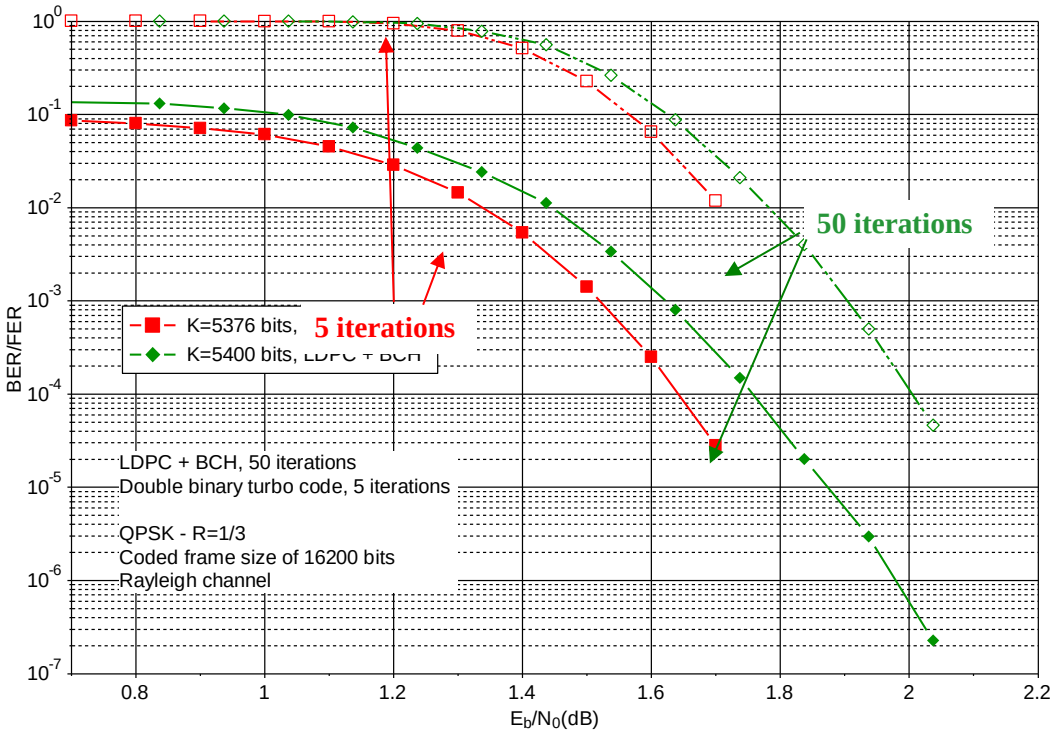

Figure 12: Comparison of the proposed DB-TC – 5 and 10 iterations – with the DVB-T2 LDPC+BCH code – 25 and 50 flooding iterations – over Rayleigh channel. QPSK constellation, coding rate 1/3.

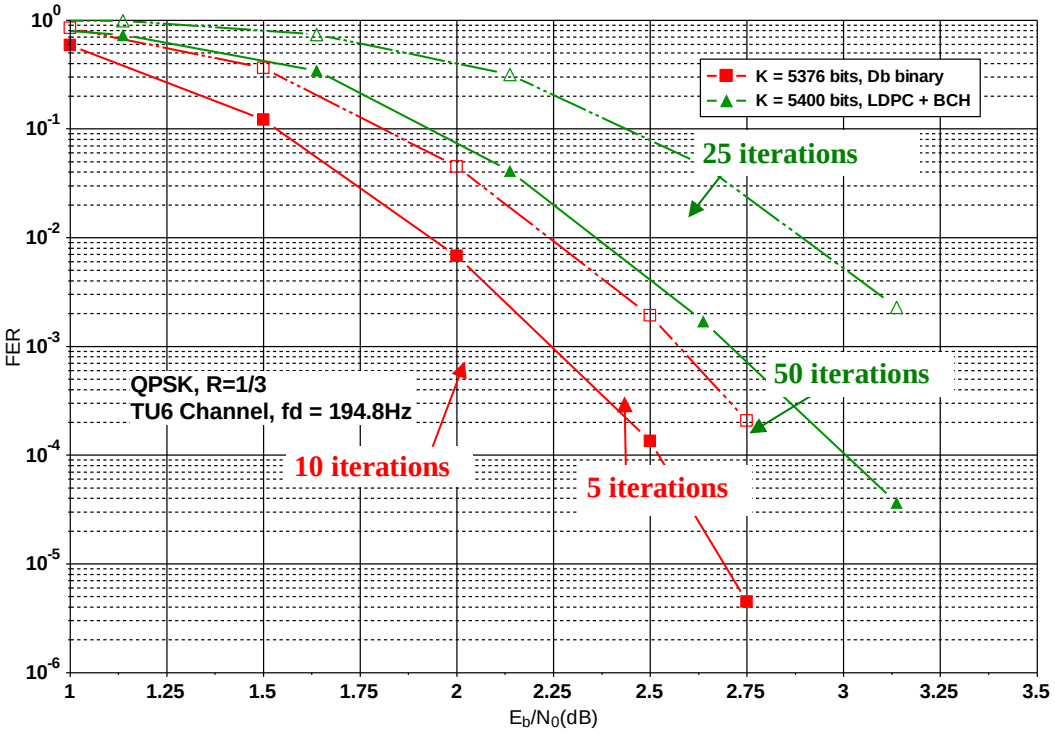

Figure 13: Comparison of the proposed DB-TC – 5 and 10 iterations – with the DVB-T2 LDPC+BCH code – 25 and 50 flooding iterations – over TU-6 channel with f_d = 33.3 Hz. QPSK constellation, coding rate 1/3.

It was finally shown that, for R = 1/5, 4 iterations of DB-TCs show better performance than 50 flooding or 25 layered of the LDPC code over static and mobile channels. For R = 1/3, 5 iterations of DB-TCs show quasi-identical performance to 50 flooding or 25 layered iterations of the T2 LDPC code over Gaussian and

Rayleigh channels. For R = 2/3, 6 iterations of DB-TCs are needed.

A second stage of the comparison is based on a joint work with Panasonic Langen in Germany. Floating-point decoder models of the turbo and the LDPC decoders were elaborated. For the turbo decoder, both the Log-MAP and the Max-Log-MAP decoding algorithms were considered. For the LDPC decoder, the model was based on the sum-product algorithm using the Gallager computation of the hyperbolic tangent function (low-complexity but challenging for a real implementation, due to the detrimental effect of quantization on performance). Based on these models, a Graphical User Interface (GUI) application was developed in Matlab in order to compare both architectures in terms of number of logic operations and memory accesses. Table 7 shows the figures provided by the Matlab GUI for a target data throughput of 4 Mbit/s, as agreed in the DVB-NGH working group.

From these figures, the comparison of the logic requirement for both types of decoders is not straightforward: the number of required additions is higher for the TC decoder than for the LDPC code. However, in the GUI Matlab application, floating-point additions are considered for the LDPC decoder whereas the turbo decoder only needs integer additions. From the memory requirement point of view, for a decoder implementing coding rates from 1/5 to 2/3, the LDPC decoder memory requirement is 217% the TC decoder requirement. Concerning the total number of memory accesses, which is directly related to the decoder power consumption, the LDPC decoder requires from 320% to 570% more memory accesses than the TC decoder, depending on the coding rate. This important difference indicates that the LDPC decoder should logically be less power efficient than the TC decoder. This has an important impact on battery life since a mobile application is targeted.

Table 7: Number of operations and memory accesses required for the implementation of an LDPC and turbo decoder, targeting a information data throughput of 4 Mbit/s. For the turbo decoder, both the Log-MAP (blue figures) and the Max-Log-MAP (red figures) algorithms are taken into account. Figures provided by Panasonic.

	16K LDPC decoder			16K turbo decoder		
	R=1/5	R=1/3 @42Mhz	R=2/3 @48Mhz	R=1/5	R=1/3 @42Mhz	R=2/3 @48Mhz
Input memory size (LLRs)	16,200	16,200	16,200	16,200	16,128	16,176
Extrinsic memory size (LLRs)	48,600	54,000	54,000	3,240	8,064	16,176
Internal memory size	96	120	120	512	512	512
Input memory read	1,215,000	1,350,000	1,350,000	155,520	215,040	323,520
Extrinsic memory read	1,215,000	1,350,000	1,350,000	49,680	145,152	355,872
Extrinsic memory write	1,215,000	1,350,000	1,350,000	24,840	72,576	177,936
Internal memory read	1,215,000	1,350,000	1,350,000	414,720	430,080	1,035,264
Internal memory write	1,215,000	1,350,000	1,350,000	414,720	430,080	1,035,264
Number of additions (floating point additions for LDPC)	4,860,000	5,400,000	5,400,000	6,246,720 4,639,680	14,757,120 10,563,840	34,487,232 24,393,408
Number of LUT accesses	2,430,000	2,700,000	2,700,000	6,246,720 0	7,096,320 0	17,081,856 0
Number of adders	96	96	48	168 / 122	370 / 262	362 / 254
Number of LUTs	48	48	24	242 / 0	252/ 0	252 / 0
Info. throughput [Mb/s]	n/a	4.0	4.6	n/a	4.2	4.0

A third comparison point is based on an actual implementation performed by the technical university of Kaiserslautern, taking into account the target throughput of 4 Mbit/s.

shows the area estimate obtained from the logic synthesis results. It appears that the logic area represents less than one quarter of the overall area and cannot be used alone to compare the complexity of the two decoders. In a DVB-NGH context, the turbo decoder is shown to be 20% less complex than the DVB-T2 LDPC decoder and 30% less complex than the LDPC+BCH decoder while guaranteeing a higher efficiency.

Table 8: Area estimate of a 16-state double binary TC and a LDPC decoder for DVB-NGH block sizes and coding rates, targeting a information data throughput of 4 Mbit/s. Figures provided by the technical university of Kaiserslautern.

	ASIC 65nm@300MHz after synthesis, real memory cuts	
	DB-TC decoder	**LDPC decoder**
Logic	**0.09**	**0.05**
Memories	**0.31**	**0.46**
BCH decoder		**0.08**
Overall area (mm^2)	**0.40**	**0.59**
Decoding algorithm	Max-Log-MAP+ ESF 8 iterations	Lambda 3-Min 40 iterations
Parallelism	1 ACS	8 CNs, serial CN
Payload throughput/iter	17 Mbit/s (R≥1/3) 10 Mbit/s (R<1/3)	15 Mbit/s (R= 3/4) 4 Mbit/s (R=1/5)
Efficiency [14] (**Mbit/s/mm^2**)	42.5 (R≥1/3), 25.0 (R<1/3)	29.4 – 7.8

2.2.4 Conclusion

The 16-state DB-TC proposed for DVB-NGH was compared in terms of performance and decoding complexity with the reference DVB-T2 LDPC+BCH code. This work was carried out in the framework of the Constellation, Coding and Interleaving (CCI) working group in DVB-NGH. The performance and complexity superiority of the 16-state DB-TC was demonstrated and acknowledged by the TM-H group.

Finally a two-fold standardization approach was adopted by the group:

– T2-mobile and NGH-phase 1: following a strong request from broadcasters, a first version of the standard will be closely aligned with DVB-T2. Thus the DVB-T2 LDPC code is kept for this first version.

– NGH-Phase 2: a second version of the standard is under study, which should be more closely aligned with the broadcast mode of the mobile networks (LTE e-MBMS). Then a TC-based FEC solution should be adopted.

2.3 L1 signalling robustness improvement techniques

This section describes a study carried out by Universidad Politécnica de Valencia/ iTEAM Research Institute (UPV-iTEAM) on the different techniques proposed for the robustness improvement of Layer 1 (L1) signalling in DVB-NGH.

2.3.1 Introduction

The sheer terrestrial profile in DVB-NGH has adopted three new mechanisms in order to enhance the robustness of the layer 1 (L1) signalling: 4K LDPC codes (mini-codes), Additional Parity (AP), and Incremental Redundancy (IR). These mechanisms substitute the L1 repetition scheme from DVB-T2, being the use of In Band signalling optional in DVB-NGH.

The headers of Layer 1 have also been optimized (L1-Configurable and L1-Dynamic). New techniques have been adopted to reduce the overhead in the transmission such as the periodic transmission of L1-Pre and L1-Configurable and Self-decodable L1-Configurable.

The goal of this section is to investigate the feasibility of the new techniques for L1 signalling robustness and to study which configurations provide the best performance depending on the channel characteristics and operator's requirements. First, a summary of the L1 Robustness in DVB-T2 issue is given. Then, the abovementioned robustness mechanisms adopted are explained and, finally, the new techniques for reducing and optimising the L1 headers are argued.

2.3.2 Summary L1 Robustness in the Sheer Terrestrial NGH Profile

It is observed that L1 signalling in DVB-T2 does not have enough time diversity, and it is only spread in few OFDM symbols. In contrast, the data path is spread in time and it could be more robust than L1 signalling in mobile channels.

The L1 signalling robustness in DVB-T2 can be increased by transmitting in each frame the signalling related to the current frame and the following frame. This mechanism is known as L1 repetition. L1 repetition implies an increment in the zapping time in case the first frame is received erroneously. In addition, this mechanism increases the signalling information and less data can be signalled. Another technique that enhances the L1 signalling robustness is known as In-Band Signalling and consists of transmitting the signalling information though out the data path. This technique enhances the continual reception and provides the same robustness as data has. However, In-Band signalling introduces some problems in first synchronization and initial zapping. As a consequence, there is a need to improve the signalling robustness and an overhead reduction for mobile environments.

DVB-NGH improves L1 signalling robustness by adopting several mechanisms. These mechanisms are divided in two groups: 1) mechanisms that enhance the L1 signalling robustness by getting more time diversity in the signal and better performance in reception, and 2), those mechanisms which aiming at optimization and overhead reduction.

16K LDPC codes are used in DVB-T2 for L1 signalling with padding and puncturing methods in order to adapt the information to the code word, but robustness is reduced. DVB-NGH 4k codes were introduced to optimize the performance provided by the 16K codes used in DVB-T2, providing several advantages. The abovementioned mechanisms that enhance the time diversity of signalling are Incremental Redundancy (IR) and Additional Parity (AP). In IR 8K LDPC codes are used, the L1 repetition mechanism is replaced and more additional parity bits than 4K LDPC code are provided. AP enhances the robustness by transmitting the

punctured bits and, optionally, adopting the In-Band scheme signalling from DVB-T2.

The signalling structure in DVB-T2 allows each PLP to have completely independent parameters and features. In contrast, in DVB-NGH this is unfeasible since the signalization has been re-structured. The PLPs are associated by configurations with the same features, optimizing the L1 headers. Moreover, in DVB-T2 transmissions, the properties of the channel signalled in L1-Pre and the configuration and features of each PLP signalled in L1-Configurable are transmitted in every T2 frame. The values of these two fields seldom change per super frame and can be considered constants. In DVB-NGH these fields are split in *n* frames, and in every frame a portion will be sent at the same position reducing de L1 overhead.

These new mechanisms and methods adopted are detailed in the following points.

2.3.2.1 4KLDPC Codes

In DVB-T2, the L1 signalling is protected with 16K LDPC with a fixed code rate 1/5 for the L1-pre and a code rate 4/9 for the L1-post. The L1 signalling information of DVB-T2 does not generally fill one 16K LDPC code word. In order to keep the code rate effectiveness, the LDPC code word needs to be shortened and punctured, which degrades the performance. DVB-NGH adopts for L1 signalling new 4K LDPC codes of size 4320 bits.

The shrunk size of 4K LDPC codes is more suitable for signalling, and considerably reduces the amount of shortening and puncturing, see Table 9. The code rates adopted for L1-pre and L1-post in DVB-NGH are 1/5 and 1/2, respectively.

Table 9: 4K Codes vs 16K Codes

LDPC Codes	Code Rate	Information bits	Parity bits	NGH L1 Signalling	Shortening bits	Puncturing bits
4K	1/5	864	3456	640	224	896
4K	1/2	2160	2160	640	1520	1520
16K	4/9	7200	9000	640	6560	8200
16K	1/2	8100	8100	640	7460	7460

16K LDPC codes provide a better performance than 4K LDPC codes without padding and puncturing. However, due to the reduced size of the L1 signalling information, 4K LDPC codes actually outperform in the order of 1-2 dB 16K LDPC codes. The main benefits of 4K codes are fast convergence, lower power consumption and fast detection. 4K codes consume less power thanks to reduced number of padding and puncture bits, so less iteration is needed to obtain the L1 signalling information bits and get better performance in compare with 16K. Reduced number of padding and puncturing methods consume less power and L1 are detected faster (fast convergence).

2.3.2.2 Additional Parity (AP)

The technique of AP replaces the L1-Repetition mechanism in DVB-T2. AP consists of transmitting punctured LDPC parity bits on the previous NGH frame and exploiting the time diversity of the mobile channel, resulting in an increase of the L1 signalling robustness but reducing the effective code rate. This new technique obtains a better performance in comparison with just repeating the information in the frame (L1-repetition).

L1-post signalling is coded by an inner BCH and 4K LDPC outer code. Shortening and puncturing methods allow maintaining the global code rate according to the information length, as shown in Figure 14. The key

issue of AP are the puncturing method and how to use profits of this method.

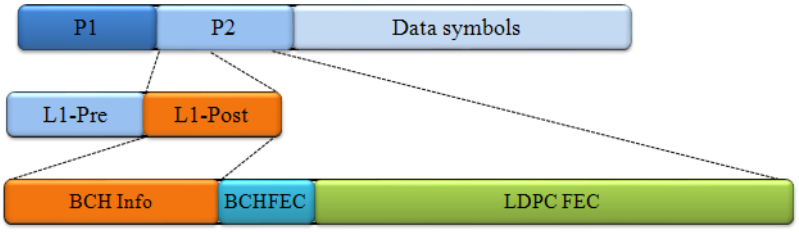

Figure 14: L1-Post encoding.

Puncturing Method

This method is used to maintain the global code rate depending on the amount of signalling information bits. All LDPC parity bits denote by $\{p_0,p_1,\ldots\ldots,p_{Nldpc\text{-}Kldpc}\}$ are divided into Q_{ldpc} parity groups where each parity group is formed from a sub-set of the LDPC parity bits as follows:

$$\boldsymbol{P_j = \{p_k |\, k\ mod q = j, 0 \le k < N_{ldpc} - K_{ldpc}\} \quad for \quad 0 \le j < q}$$

Equation 1: Parity group calculation, where Pj represents the j-th parity group

Each group consists of 360 parity bits and the total number of Q_{ldpc} groups depends on the LDPC parity length. (Q_{ldpc}= LDPC parity length /360), as illustrated in Figure 15.

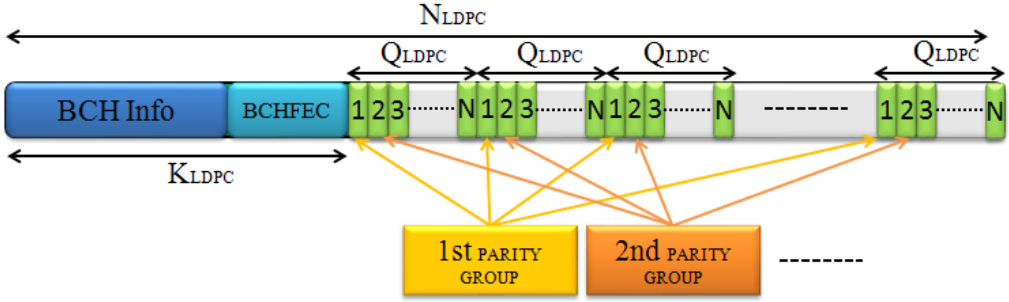

Figure 15: Parity bit groups in an FEC Block

Puncturing of LDPC parity bits is performed on a bit-group basis following the order predetermined by the standard, *i.e.* puncturing pattern. The puncturing pattern depends on the modulation and code rate employed, and shows which Q_{ldpc} groups have to be punctured depending on the signalling information length. As illustrated in Figure 16, specific parity groups have been punctured according to the puncturing pattern.

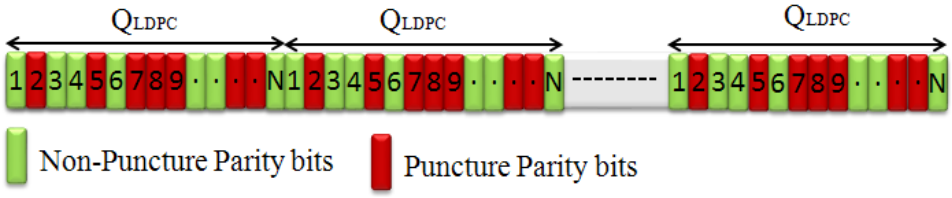

Figure 16: Puncturing of LDPC parity groups

AP Generation rule

AP extends the new 4K LDPC with additional parity bits to provide additional robustness. These additional bits are the punctured bits. When AP is applied, the new configuration of the codeword results as shown in Figure 17.

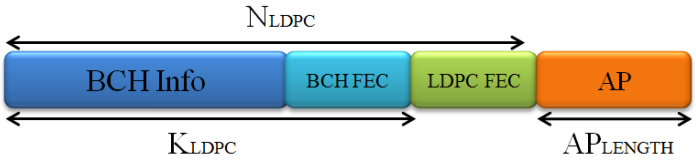

Figure 17: The resulting LDPC code word with Additional Parity bits

The length of this additional part is denoted AP length, and it is obtained from Equation 2, where K is defined as 1/3, *AP_RATIO* {0,1,2,3,..}, and $p(L1_{post})$ gives the number of parity bits corresponding to the *L1_Post_block*.

$$AP_{LENGTH} = K \cdot L1_{APRATIO} \cdot p(L1_{POST})$$

Equation 2 : Additional Parity length calculation

Advantages

The main advantage of using AP is that the effective coding rate for L1 signalling could be reduced without any LDPC matrix. The following table shows the effective code rate achieved for different configurations with parameter K=1/3.

Table 10 : Additional Parity benefits

Num PLP	CR	K_sig	Parity bits	AP bits			Code Rate Achieved		
				AP_Ratio=1	*AP_Ratio*=2	*AP_Ratio*=3	*AP_Ratio*=1	*AP_Ratio*=2	*AP_Ratio*=3
1	1/2	610	610	204	408	612	0.4284	0.3747	0.333
1	1/5	610	1830	610	1220	1830	0.2	0.1667	0.1429

Note that in the AP mechanism, punctured bits are transmitted first. For a given frame, its parity is sent in two consecutives frames. The additional parity is sent in the previous frame as incremental redundancy, and the basic FEC is sent with information at the same time, as depicted in Figure 18, where I, B, P and AP, are the information fields, BCH FEC bits, basic parity bits and additional parity bits, respectively.

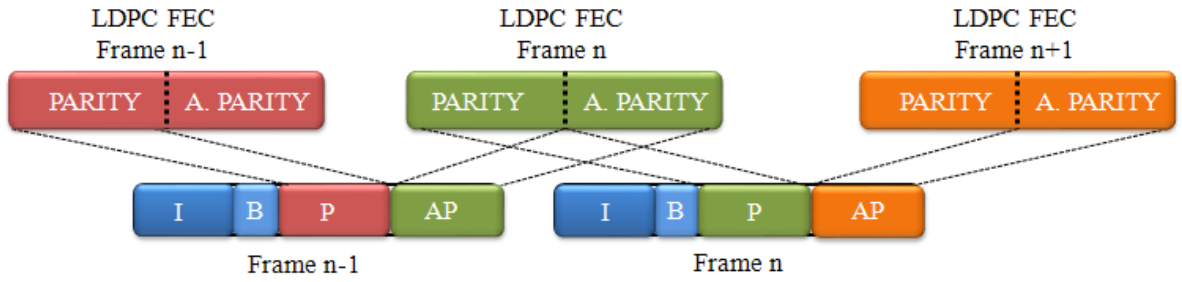

Figure 18: The resulting LDPC code word with Additional Parity bits

2.3.2.2.1 Incremental Redundancy (IR)

IR replaces the L1 repetition mechanism and introduces a new FEC scheme. Initially, IR is thought to get additional bits when are required. As a starting point, IR uses 4K LDPC mini codes in order to reduce latency and decoding complexity at a low code rate. The main idea behind IR is to extend this new 4K LDPC with additional parity bits (another 4K codeword) to provide additional robustness. IR only applies with 1/2 code rate, resulting an extended codeword at 1/4 code rate.

IR Generation rule

The basic FEC 4K is the conventional FEC, where the LDPC encoder code rate input is R_0=1/2, where $R_0 = K_{ldpc}/ N_{ldpc}$. K_{ldpc} are the output bits from the BCH encoder, and that output is a systematic codeword of length N_{ldpc}. The last N_{ldpc} - K_{ldpc} bits of this codeword are the LDPC parity bits, named as LDPC FEC at Figure 19.

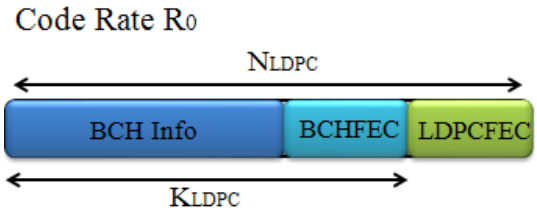

Figure 19 : Basic FEC 4K.

IR uses special 8K LDPC codes (8640 bits) for coding L1 signalling information bits. These codes have been created to obtain the same parity bits as 4K LDPC codes, taken into account the first 4K bits, and they have special properties.

The resulting codeword of applying the IR mechanism can be differentiated in two parts: the first part corresponds to the basic FEC and in the second part the additional parity bits are located. This basic FEC concerns as a 4K LDPC code has been used to code the signalling information bits, and the additional parity bits are going to be used as IR and named M_{IR} in Figure 20.

The codeword length is, thus, 8K bits, and it is composed by $N_{ldpc,1} = N_{ldpc} + M_{IR}$. The LDPC encoding with IR can be considered as one encoder of code rate $R_1 = K_{ldpc}/N_{ldpc,1}$, initially R_1 = 1/4, where the output is split into two 4K codeword, basic FEC and an IR part. The relationship between original codeword and extended codeword can be seen in Figure 21.

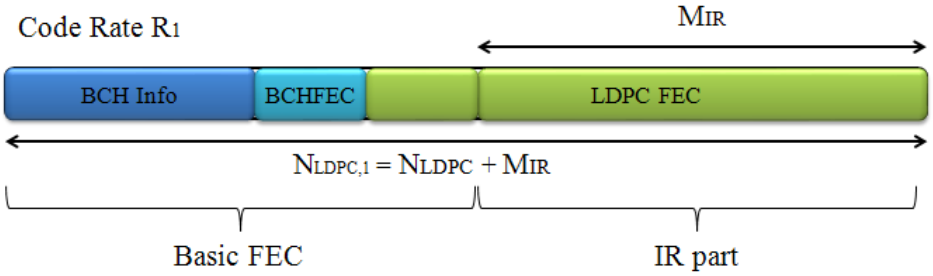

Figure 20 : Extended Codeword. Basic FEC+ IR part (8K codeword)

IR Method

When IR is applied, the amount of LDPC parity bits has increased to N_{ldpc} - K_{ldpc}+ M_{IR}. However, the main property of the 8K LDPC code is that the first $N_{ldpc} - K_{ldpc}$ parity bits are identical to the parity bits of the 4K basic FEC with 1/2 code rate. In addition, the codeword is divided into two parts: the first Nldpc bits are the basic FEC part, while the remaining MIR bits are the IR part to be used as additional parity at the receiver. This IR part (M_{IR} bits) is sent in different transmission times in the following way: first, the basic FEC is sent, and then, the IR part if it is needed. IR replaces L1 Repetition from DVB-T2, avoiding sending the same information in consecutives frames. IR sends a 4K codeword with new parity bits.

Thus, depending on the channel characteristics it is ensured that the decoding of the received codeword is possible in good channel conditions with a R_0–rate decoder, which only takes into account the basic FEC part, while the extended codeword, consisting of both basic FEC and IR part, permits the decoding with a R_1-rate decoder in bad channel conditions.

The main advantage of IR is that the IR part can be ignored by the receiver unless it is needed.

The main objective of this section is to analyze the most effective transmission mode and which receiver parameters are the most suitable. Finally, the operator will decide the use of IR or not depending on the transmission characteristics.

2.3.3 L1 Signalling overhead reduction and optimization

2.3.3.1 L1-Configurable overhead reduction

In DVB-T2 the signalling mechanism allows each PLP to have completely independent parameters in the signalling process. In all realistic situations there will only be a very limited number of PLP configurations used in a given transmission. This means that several PLP will use exactly the same features as MODCOD. For this reason, DVB-NGH suggests a re-structure of the signalling method, associating the PLPs with the same features.

The PLP signalling loop in L1 Configurable from DVB-T2 defines all the features of each PLP. These features are the characteristics of each PLPs, as the name (ID) of each PLP, the modulation and code used, the PLP location inside the NGH frame and its length. These features can be repeated in different PLPs. The properties that are the same are grouped in PLP configurations. With different configurations, each PLP is linked to its associated configuration. As a consequence, each PLP is not more independent form others, reducing the L1 signalling overhead.

For this reason, the signalling loop in L1 Configurable from DVB-NGH is split into two different loops. The first loop defines the different PLP configurations and associating each configuration with a short code (PLPMODE_ID). On the other hand, the second loop is a loop over PLP_IDs that defines the PLPs themselves. This second loop associates each PLP_ID with the code above.

In this way there are only 6 bits per PLP in the PLP loop and only a very limited number of PLP configurations are required inside the PLP configuration loop. This solution allows for a totally general case, with unique configurations for up to 255 PLPs, but in the typical use cases the required amount of L1-Config is radically reduced.

In addition, the L1-Config format from DVB-T2 is very general and supports a lot of features as aux streams, reserved fields, possibility to send a PLP only in certain frames, TFS, more than one PLP group, time interleaving over 255 frames, etc. However, in a particular use case, only a few of these features will be probably used and, hence, the others could be removed or reduced in size. In this case, the introduction of a flag field in the beginning of the L1-config can signal whether the feature is available or not. This flag field

will be one bit per feature. The new L1-Config format is illustrated in Table 11.

The overhead savings for L1-Configurable and L1-Dynamic have been calculated. The study has been done assuming the number of required PLP modes or configurations are 1/4 of the total number of PLPs. The savings using this reduced overhead are ~0.85%, considering quite extreme cases in terms of number of PLPs (the more PLPs, the higher savings). Figure 21 shows the comparative of different overhead structures.

The main advantage of applying this signalling structure is that the zapping time is not affect; it is only about how the signalling structure is defined. [18][19].

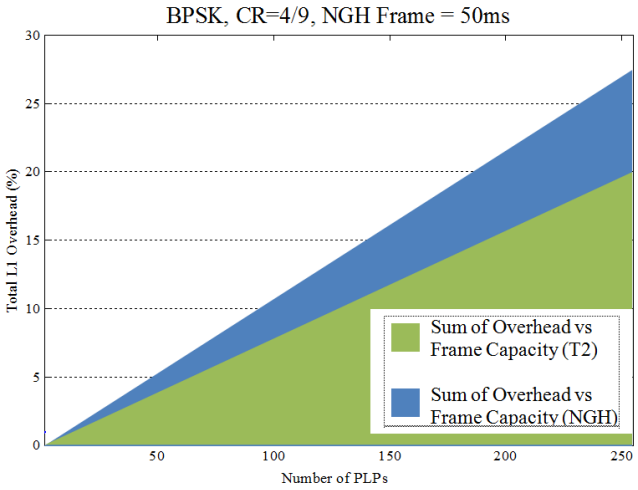

Figure 21 : Comparison between different overheads structures.

Table 11 : The new L1-Config format for DVB-NGH

FIELD	SIZE (Bits)
L1_POST_OPTIONS	18
NUM_PLP	8
NUM_PLP_MODES	6
SUB_SLICES_PER_FRAME	10
NUM_AUX	4
AUX_CONFIG_RFU	8
NUM_NGH_FRAMES	8
NUM_CELLS_NGH_FRAME	22
for i=0:NUM_RF-1{	
L1_RF_FREQUENCY	32
}	
for i=0:NUM_PLP-1{	
PLP_ID	8
PLPMODE_ID	6
PLP_GROUP_ID	8
FIRST_FRAME_IDX	8
PLP_REP_INT	3
RESERVED_1	3
}	
for i=0:NUM_PLP_MODES-1{	
PLP_TYPE	3
PLP_PAYLOAD_TYPE	5
PLP_COD	3
PLP_MOD	3
PLP_ROTATION	1
PLP_FEC_TYPE	2
PLP_NUM_BLOCKS_MAX	10
FRAME_INTERVAL	8
TIME_IL_LENGTH	8
TIME_IL_TYPE	1
IN_BAND_A_FLAG	1
IN_BAND_B_FLAG	1
STATIC_FLAG	1
STATIC_PADDING_FLAG	1
PLP_MODE_REP_INTERVAL	3
RESERVED_2	10
}	
RESERVED_3	32
for i=0:NUM_AUX-1{	
AUX_STREAM_TYPE	4
AUX_PRIVATE_CONf	28
}	

L1_POST_OPTIONS	Bits
TYPE_2	1
AUX	1
L1_CFG_PERIODIC	1
L1_MODE_PERIODIC	1
DETERM_L1_SCHED	1
PLP_GROUPING	1
RSV_FLAG	12

2.3.3.2 N-periodic L1-Pre and L1-Configurable transmission and Self-decodable L1-configurable

In T2 transmissions, L1-Pre and L1-Configurable are transmitted in every T2 frame. L1-Pre signals the properties of the channel (GI, PP, L1 ModCod...), it has a fixed length of 200 bits and it is fixed BPSK-modulated with a 1/4 code rate. L1-Pre is used for accessing L1-Config. On the other hand, L1-Config signals the configuration of the PLPs (ModCod, time, interleaver settings, frequencies..). The values of these two fields may change per superframe, but in practice only change when the multiplex of the RF-channel is reconfigured and this rarely happens.

As these values do not usually change, the transmission of L1-Pre and L1-Configurable can be split in *n* frames. The split part of L1-Pre and L1-Configurable will be at the same position but their length is reduced by a factor of *n*. A portion of these fields of every frame will be sent and the contents of L1-Pre and L1-Configurable will be completed after *n* frames.

The spreading of quasi static signalling contents to several frames, improves the time diversity, and reduces the signalling overhead by a factor *n*.

Figure 22 is meant to clarify the concept of *n*-periodic transmission, and illustrates the case when L1-Pre and L1-Configurable fields are spread by a *n* factor of 4.

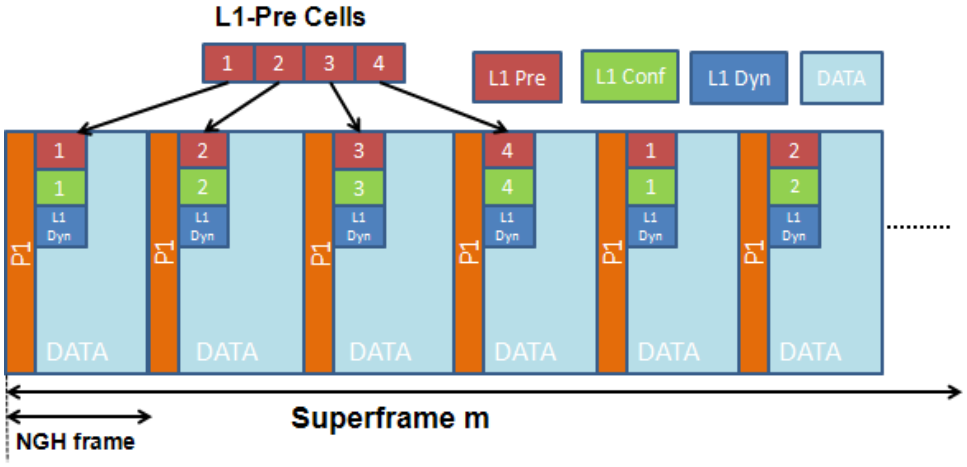

Figure 22 : Comparison between different overheads structures.

The selection of the parameter n is a trade-off between channel scanning time and signalling overhead. Table 12 shows the results of the capacity savings with *n*-periodic signalling.

Table 12 : Parameters for overhead calculation: 8K FFT, GI 1/4, 50ms Frame duration, BPSK, CR 1/3 for L1-Pre and L1-Config [19]

Capacity savings with n-periodic Signaling							
PLPs	**DVB-T2 Capacity**	**N-periodic Signaling**					
		L1-Pre + L1-Config		**L1-Config Only**		**L1-Pre Only**	
		***n* = 4**	***n* = 8**	***n* = 4**	***n* = 8**	***n* = 4**	***n* = 8**
1	1.28%	0.72%	0.8%	0.13%	0.16%	0.59%	0.64%
4	1.62%	0.89%	0.99%	0.30%	0.35%	0.59%	0.64%
8	2.07%	1.11%	1.25%	0.52%	0.61%	0.59%	0.64%
16	2.98%	1.56%	1.77%	0.97%	1.13%	0.59%	0.64%
32	4.78%	2.43%	2.79%	1.84%	2.15%	0.59%	0.64%

However, the channel scanning time increases when the receiver is switched on for the very first time. Joint encoding for L1-Configurable and L1-Dynamic degrades the L1-configurable robustness since a single error makes all L1-Configurable parts useless. N-periodic transmission increases the initial acquisition delay by n factor. This is a major problem in case of TFS since the receiver will not be able to know which the next frequency is.

To mitigate these disadvantages, instead of splitting the L1-Configurable into n blocks based on the basis of guaranteeing the same length of L1-Configurable portions, the L1-Configurable has to be divided into fixed-length portions of self-decodable L1-configurable information.

Applying this fixed length of L1-Configurable new advantages appear. No delay can be obtained for the constant signalling information, which is desirable since signalling information cannot tolerate any delay (TFS info or FEF info). The PLP delays are also controlled: PLPs which cannot tolerate any delay can be sent with zero delay.

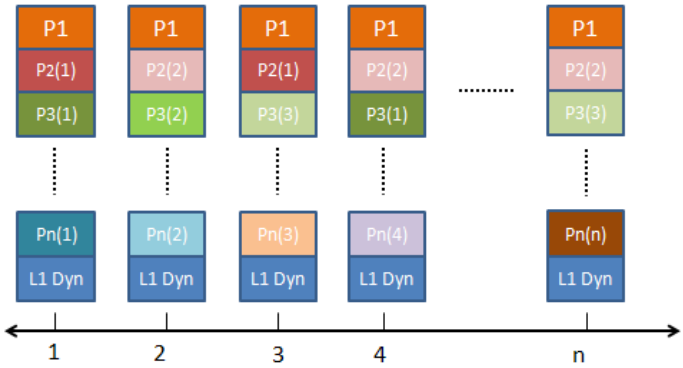

Figure 23 : Transmission mode of PLPs as a function of their repetition interval

The PLPs are sorted as a function of their repetition interval, i.e. PLPs with lower repetition interval are transmitted first. For the PLPs with the same repetition rate the PLP with the lower PLP_id is transmitted first. This sorting allows the receiver to know in advance some PLPs that will be signalled in the following frames.

The receiver starts decoding every portion of L1-Configurable. Figure 24 shows the signalling of the PLPs that are known before decoding.

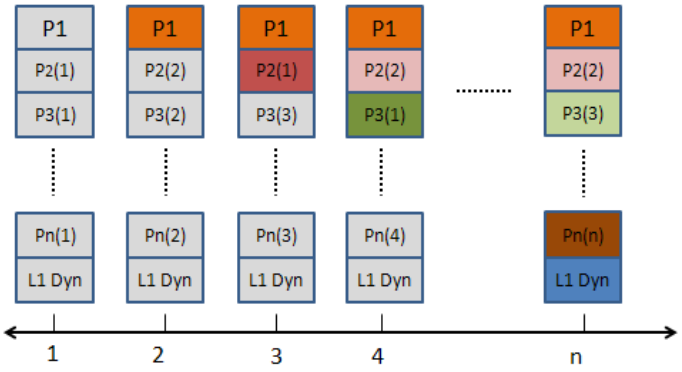

Figure 24 :Reception exemple, assuming L1-Configurable is decoded correctly in every frame

Using fixed portions of L1-Configurable, the probability of correct detection increases every time more information of L1-configurable is available. Zero delay is guaranteed for the constant signalling (e.g. TFS info or FEF info) and it is provided a better trade-off between overhead reduction and zapping delay, controllable on a PLP basis according to the PLP's corresponding service requirement.

In addition, superposed correlation sequence is used to detect the portions and the order of the L1-pre portions. A virtual QPSK with superposed PRBS sequence is used to detect n sequences within a single NGH-frame and estimate the order of the L1-pre portions. As Figure 25 illustrates, both I and Q paths transmit the signalling data. The Q path is cyclically shifted and XOR connected with the PRBS sequence.

The detection can be possible even at negative SNR, and the decoding performance is not degraded compared to usual BPSK due to LLR combining of the I and Q path [15][16].

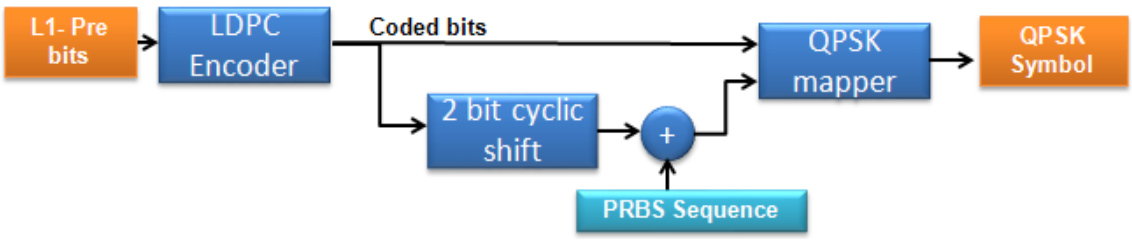

Figure 25 : The Q path is cyclically shifted and XOR connected with the PRBS sequence

2.3.4 Performance of L1 Robustness

The objective of the simulations is to check and validate the solutions adopted mentioned above for different channels. The following tables summarize the simulation conditions used to study the different mechanism adopted.

Table 13 : L1-Post Signalling Fields

L1 Signalling	
Parameter	*Value (bits)*
L1conf_est	142
L1conf_var	34
L1conf_PLPCONF	61
Num_PLPCONFIG	4
L1dyn_est	49
L1dyn_var	8
CRC	16
BCH	100

A) **The signalling fields of Configurable L1-post signalling**

L1 Signalling length equations
L1conf = L1conf_est+Num_PLP*L1conf_var+ L1conf_PLPCONF*Num_PLPCONFIG
L1dyn = L1dyn_est+Num_PLP*L1dyn_var
K_post =L1conf+L1dyn+CRC
K_sig = K_post + BCH

B) **L1-post signalling length calculation as a function of the number of PLPs**

Table 14 : Robustness Mechanism Simulations Framework

Simulation Framework			
	Parameter		Value
L1 Robustness Mechanism	Additional Parity	L1_AP_RATIO	1
		L1_AP_K	1/3
	Incremental Redundancy		8K LDPC CR=1/4

Code Rate 1/2

Additional Parity Mode

Num_PLP	K_post	L1_Conf	L1_Dyn	K_sig	Parity bits	Puncture bits	AP bits	Code Rate Achieved
1	510	420	57	610	610	1550	204	0,4283
4	636	522	81	736	736	1424	246	0,4284
8	804	658	113	904	904	1256	302	0,4284
-	-	-	-	2160	2160	0	0	0,5

Incremental Redundancy Mode

Num_PLP	K_post	L1_Conf	L1_Dyn	K_sig	Parity bits	Puncture bits
1	510	420	57	610	1830	4650
4	636	522	81	736	2208	4272
8	804	658	113	904	2712	3768
-	-	-	-	2160	6480	0

Code Rate 1/5 (1/4)

Additional Parity Mode

Num_PLP	K_post	L1_Conf	L1_Dyn	K_sig	Parity bits	Puncture bits	AP bits	Code Rate Achieved
1	510	420	57	610	1830	1410	610	0,2
4	636	522	81	736	2208	1032	736	0,2

2.3.4.1 AWGN Channel

Table 15 : AWGN channel simulations framework

	Parameter		Value
OFDM	FFT Size		8192 (8K)
	BW		8MHz
	NGH Frame		50ms
Channel	Channel Model		AWGN
L1 Signalling	Number of PLPs		1,4,8
	MODCOD	Constellation	BPSK, CR 1/2 1/5
		Coding	4K LDPC
		Decoding	50 iterations, Fabrice Decoder

2.3.4.2 TU-6 Channel

Table 16 : TU-6 Channel Simulations Framework

	Parameter		Value
OFDM	FFT Size		8192 (8K)
	BW		8MHz
	NGH Frame		50ms
Channel	Channel Model		TU6
	Doppler		10Hz, 33.3Hz, 194.8Hz
L1 Signalling	Number of PLPs		1,4,8
	MODCOD	Constellation	BPSK, CR 1/2 1/5
		Coding	4K LDPC
		Decoding	50 iterations, Fabrice Decoder

2.3.5 Future Work

The next step is to focus on the determination of the optimum parameters according to the use case and the settings of coding-interleaving parameters for data. Moreover, the evaluation of the overhead due to the L1 signalling and determine the use case of additional parity bits and Incremental redundancy mechanism for the different configurations.

2.4 BaseBand inter Frame FEC (BB-iFEC)

This section describes a study carried out by Universidad Politécnica de Valencia/ iTEAM Research Institute (UPV-iTEAM). It presents a novel Forward Error Correction (FEC) and Time Interleaving (TI) scheme, known as BB-iFEC (Base Band - inter-burst FEC) [20], proposed for both satellite and terrestrial profiles of DVB-NGH. BB-iFEC aims at providing long time interleaving with fast zapping support. This feature is key for satellite transmissions, because the Land Mobile Satellite (LMS) channel is characterized by long signal outages (e.g., due to the blockage of the line of sight with the satellite caused by tunnels, buildings, trees, etc.), which can only be compensated with a long time interleaving duration (in the order of 10 s) [21]. But long time interleaving with fast zapping is also of interest for terrestrial transmissions, because it allows exploiting the time diversity of the mobile channel in high-speed reception scenarios (e.g., vehicles, trains).

Although other technical solutions have been proposed in DVB-NGH to increase the diversity of the mobile channel in other dimensions (e.g., in the frequency domain with time-frequency slicing TFS, or in the spatial domain with multiple-input multiple-output MIMO antenna configurations), there is no doubt that in some scenarios and for some applications time diversity can provide very important gains (e.g., vehicles, trains) [22], [23] . One of the features of BB-iFEC is that it is backwards-compatible, in the sense that it allows the coexistence of terminals with and without BB-iFEC. Therefore, it is also proposed as an optional feature for the terrestrial profile of DVB-NGH.

2.4.1 BB-IFEC Overview

BB-iFEC is based on the link layer MPE-iFEC (Multi Protocol Encapsulation inter-burst FEC) scheme of DVB-SH [24]-[27]. The main differences are that it is integrated in the physical layer, that it allows for both soft and hard decoding at the receivers, and that it re-uses the 16K LDPC codes adopted in DVB-NGH instead of using a Reed-Solomon code. The time interleaving is similar to the time interleaving of MPE-iFEC with sliding window Reed-Solomon encoding, although it is not identical.

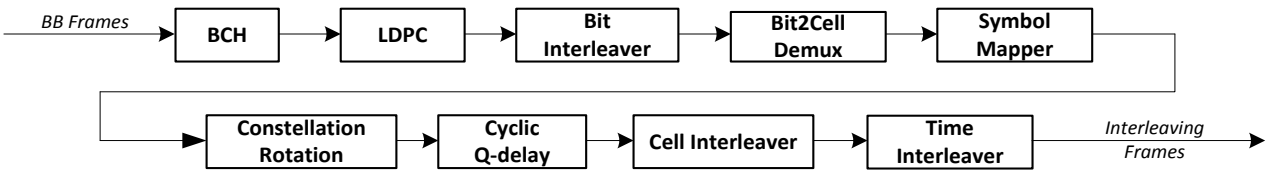

Figure 26: DVB-T2 BICM (Bit Interleaved Coding and Modulation) module at the transmitter.

Figure 26 shows the complete BICM (Bit Interleaved Coding and Modulation) module of DVB-T2. The FEC is based on the concatenation of an LDPC (Low Density Parity Check), which performance approaches within 1 dB the Shannon limit, and a BCH (Bose Chaudhuri Hocquenghem), that removes the error floor of the LDPC. The bit interleaver and the bit2cell demultiplexer compensate the unequal bit protection performed by the LDPC code, assigning the less protected bits to the more robust constellation points. Rotated constellations are used to provide additional robustness to the transmission, by transmitting in different instants (in time and frequency) the I and Q components of each constellation symbol [27]. The time interleaver is a block interleaver that operates with cells (constellation symbols). It allows inter-frame interleaving, but it does not provide fast zapping support [29]. The average zapping time is approximately 1.5 times the time interleaving duration [30].

BB-iFEC introduces an additional FEC and an additional time interleaver (TI). Therefore, there are two FECs and two TIs, denoted as inner and outer, respectively. Fig. 2 shows the modifications to the DVB-T2 BICM module of DVB-T2 at the transmitter to introduce BB-iFEC. Four new blocks are introduced: transmission delay block, data spreading block, outer FEC block, and parity spreading block. The main configuration parameters of each block are:

- Transmission delay block: data delay, *D*.
- Data spreading block: data spreading factor, *B*.
- Outer FEC block: outer FEC code rate, CR_{outer}.
- Parity spreading block: parity spreading factor, *S*.

The outer TI corresponds to the data and parity spreading blocks. It should be pointed out that each TI makes use of a specific time de-interleaver (TDI) memory. Hybrid satellite-terrestrial terminals require an external TDI memory to account for the long TI requirements at the physical layer. With BB-iFEC, the external TDI

memory is managed by the Outer TI, and the on-chip memory is used by the Inner TI. The Outer TI interleaves bits/LLRs instead of cells like the Inner TI.

As shown in Figure 27, BB-iFEC generates an additional PLP, known as iFEC PLP. The proposed scheme is configurable on a PLP basis, and thus it allows different levels of protection (interleaving duration and/or code rate) for different data PLPs. Moreover, it allows co-existence of terminals with and without BB-iFEC.

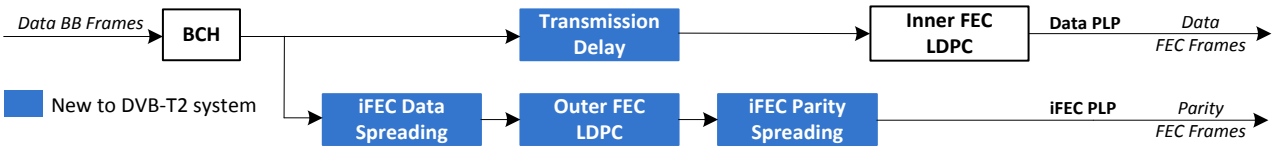

Figure 27: Modifications required at the DVB-T2 BICM module at the transmitter to include BB-iFEC. The iFEC PLP only transmits the parity generated by the Outer FEC. The only modification to the Data PLP is one buffer at the transmitter.

BB-iFEC operates on a burst basis, being possible to recover from completely erroneous bursts (i.e., it provides inter-burst FEC protection). The recommended cycle time is 1 sec, in order to provide fast zapping. The Inner TI can be limited to intra-frame interleaving, but it can also perform inter-frame interleaving within 1 sec (typical trade-off between power saving due to time-slicing versus increased time diversity of continuous transmission). This way, the Outer TI does not interleave BB frames (packet data units of the DVB-T2 physical layer) which are already interleaved by the Inner TI. At the transmitter, after reception of a new data burst, all BB frames are first encoded with the BCH code, and then a parity burst is generated after data spreading, outer FEC, and parity spreading. Simultaneously, the original data burst can be encoded with the Inner FEC and subsequently transmitted.

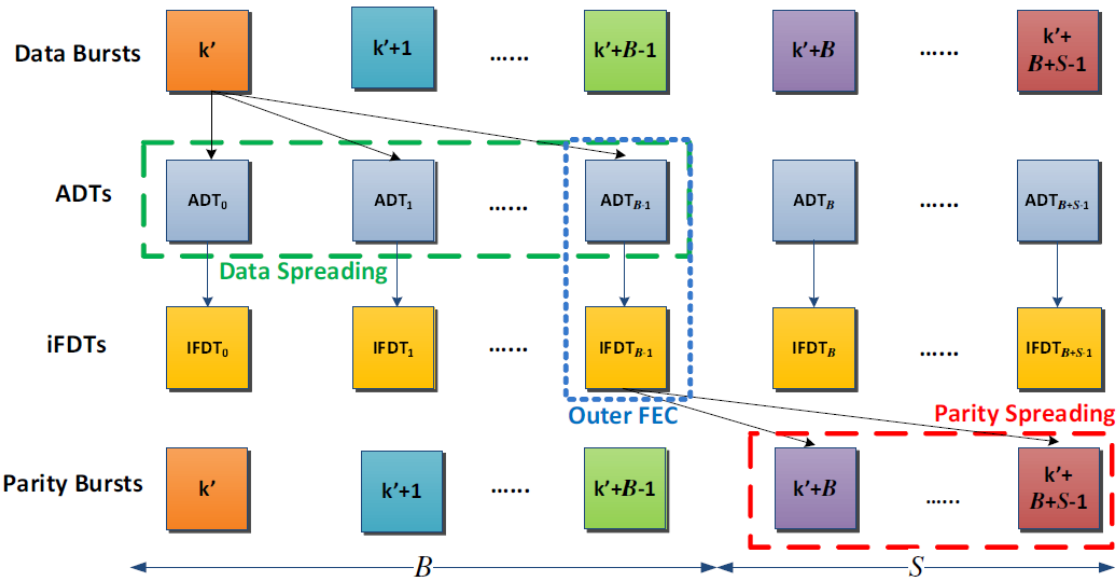

Figure 28: Inter-burst interleaving with BB-iFEC with the parity transmitted after the data (D = 0). The interleaving depth in number of interleaved bursts M, is equal to the data spreading factor, B, plus the parity spreading factor, S.

The interleaving depth in number of interleaved bursts, M, is given by both the data and parity spreading processes ($M = B + S$), with two possible values of D. Either $D = 0$, where the parity bursts are transmitted after the data bursts (see Figure 28), or $D = B + S$, where the parity bursts are transmitted before the data

bursts. The two spreading processes employ a sliding window approach similar to sliding Reed-Solomon encoding in MPE-iFEC in DVB-SH [25]. In the data spreading process, the sliding window encloses *B* Application Data Tables (ADTs) which receive data BB frames from one data burst. At the transmitter, there are M ADTs. After reception of one data burst, one ADT is completely filled, and one iFEC Data Table (iFDT) is generated by the Outer FEC. In the parity spreading process, the sliding window encloses *S* parity bursts which receive BB frames from the generated iFDT. For each data burst, one parity burst is generated. Every burst the data and parity spreading sliding windows are shifted one element.

In Figure 27, it can be seen that with BB-iFEC there are three FEC encoding processes:

- BCH encoding of the data BB frames.
- Inner LDPC encoding of the Data PLP.
- Outer LDPC encoding.

Without considering the overhead introduced by the BCH, the overall code rate can be expressed as follows:

$$CR_{total} = 1/(1/CR_{inner} + 1/CR_{outer} - 1)$$

The code rate distribution for BB-iFEC represents a trade-off between fast zapping performance and overall performance. The protection after zapping is given by the Inner FEC of the Data PLP, whereas the Outer FEC exploits the long time interleaving. In general, it is recommended to put most of the protection in the outer FEC. BB-iFEC is a split FEC scheme, and there is a loss in performance with respect to single FEC encoding in static channels, where the performance is given by the most robust code rate. Table 17 shows typical examples of code rates for BB-iFEC.

Table 17: Examples of code rate distributions for BB-iFEC.

CR_{total}	CR_{inner}	CR_{outer}
1/3	2/3	2/5
1/3	1/2	1/2
1/4	1/2	1/3
1/4	2/5	2/5
1/5	1/2	1/4
1/5	1/3	1/3

For a given outer code rate CRouter and target interleaving depth *M*, the interleaving parameters of BB-iFEC *B*, *S*, and *D* can be derived as follows:

$$B = \lfloor M \times CR_{outer} \rfloor$$
$$S = M - B$$
$$D = B + S$$

where $\lfloor \cdot \rfloor$ denotes the *floor* function. This configuration minimizes the transition time between fast zapping mode and full protection mode, and guarantees a quasi-uniform time interleaving. This is elaborated in detail in the next section.

2.4.2 Main features of BB-IFEC

2.4.2.1 Transparency towards Upper Layers

BB-iFEC is not an upper layer FEC scheme but a physical layer FEC. Therefore, it is *fully transparent to the upper layers*, being compatible with any encapsulation protocol used. This feature is especially relevant in DVB-NGH, because two transmission protocol profiles are supported, in particular MPEG-2 Transport Stream (TS) and IP (Internet Protocol) [31].

2.4.2.2 Backwards-Compatibility

Since BB-iFEC generates an additional PLP, it *allows the co-existence of terminals with and without long time interleaving support without any drawback*. The only modification to the Data PLP is a delay in the transmission by an entire number of bursts. This feature is key in DVB-NGH, because the commercial requirements specify that the optional satellite component should not affect sheer terrestrial terminals [31].

Moreover, it also allows long time interleaving to be introduced as an optional tool in sheer terrestrial networks.

2.4.2.3 Soft and Hard Decoding Support

One of the main differences of BB-iFEC with respect to MPE-iFEC is that it allows to perform soft decoding, re-using the soft output of the Inner LDPC decoder. But BB-iFEC *allows both hard and soft decoding at the receivers*, being thus a scalable solution. There is a trade-off between memory consumption and performance. For hard decoding, two memory bits are required per information bit, since it is needed to denote three possibilities: 0, 1, or erased. For soft decoding, typically only four memory bits per LLR are required for satellite transmissions (e.g., in DVB-SH). Terminals with hard BB-iFEC decoding require thus half of the TDI memory than terminals with soft BB-iFEC decoding. However, in static conditions, the protection is only given by the Inner FEC. The Outer FEC protection is only useful in mobile conditions, and there is also a degradation compared to soft decoding.

2.4.2.4 Reduced Signalling

BB-iFEC *requires very little signalling*. Only 12 bits are required to signal the value of the four BB-iFEC configuration parameters: outer FEC code rate CRouter (3 bits), data and parity spreading factors *B* and *S* (4 bits each), and data delay *D* (1 bit). The rest of the configuration parameters of the iFEC PLP would be the same than the parameters of its associated Data PLP.

2.4.2.5 Reduced VBR Signalling

For Variable Bit Rate (VBR) services, BB-iFEC requires to signal information about previously transmitted bursts to help the receivers to perform the time de-interleaving. The amount of signalling can be significant, especially for continuous transmission, since it is possible to interleave 40-50 frames. This information has to be transmitted in the dynamic field of the L1 (layer 1) signalling, which is very heavily protected for satellite transmissions (the data can be protected with QPSK 1/5). However, BB-iFEC *requires very little VBR signalling*. The reason is that the receivers only need help to perform the inverse of the parity spreading process (this is further elaborated in Section V). Furthermore, the combination of two levels of inter-frame interleaving with the Inner TI and Outer TI for the case of continuous transmission reduces the requirements for VBR signalling quite significantly, to a similar amount than for the case of discontinuous transmission.

2.4.2.6 Reduced BCH and BB Frame Overhead

In DVB-T2, each 16K LDPC BB frame carries 168 bits for BCH and 80 bits for the BB frame header [29]. This overhead is fixed, regardless the code rate, but lower code rates imply higher overheads because more

BB frames are transmitted for the same amount of data. BB-iFEC can achieve very robust code rates with reduced overhead due to BCH and BB frame header. The reason is that the BB frames of the iFEC PLP do not carry BCH nor BB frame headers. The overhead is only due to the Inner FEC of the Data PLP.

2.4.2.7 TDI Memory Requirements

BB-iFEC is a very efficient solution from the TDI memory point of view due to two reasons. First of all, BB-iFEC requires less memory than a sheer block time interleaver like the one adopted in DVB-T2. The memory requirement is similar to a convolutional interleaver with uniform profile, and it is proportional to the factor $(M + 1)/2$ instead of M. Therefore, *the memory saving with respect a block interleaver tends to 50%.*

The second reason is that BB-iFEC *interleaves bits (LLRs) instead of cells (constellation symbols)*, like the DVB-T2 time interleaver. This is more efficient for the low order constellations considered for the DVB-NGH satellite profile (i.e., QPSK and 16-QAM). For cell interleaving, it is needed to store three components for each cell: real part, imaginary part, and channel state information. In DVB-T2, it is recommended to employ 10 memory bits for storing the real and imaginary parts [30]. BB-iFEC requires only 4 memory bits per bit/LLR (for soft decoding).

It should be pointed out that the required TDI memory in DVB-NGH with BB-iFEC is lower than the requirement in DVB-SH [27]. The reason is that BB-iFEC is applied on a PLP basis, not across the whole multiplex like in DVB-SH.

2.4.2.8 External TDI Memory Access

The power consumption when accessing the external TDI memory depends on the size of the Interleaving Units (IUs). The larger the IU size, the lower the power consumption. In DVB-SH, the IU length of the (bit) TI is 126 bits/LLRs [27].

The outer time de-interleaving of BB-iFEC operates with data BB frames after Inner LDPC decoding, which size depends on the code rate of the Inner FEC (e.g., for a code rate 2/3, the IU size is 10800 bits/LLRs [29]), and with parity BB frames of constant size (the IU size in this case is 16200 bits/LLRs). Therefore, BB-iFEC *makes a very efficient access of the external TDI memory*, with IUs significantly larger than in DVB-SH.

2.4.2.9 Fast Zapping Support

The main feature of BB-iFEC is that *it allows fast zapping while providing long inter-frame interleaving* (e.g., 1 sec zapping time, 10 sec time interleaving). BB-iFEC has two operation modes as MPE-iFEC, known as early decoding and late decoding [25]. In early decoding mode, the data is protected only with the Inner FEC of the Data PLP, and the zapping time is given by the Inner TI. In late decoding mode, the protection is given by both Inner FEC and Outer FEC, but it cannot be achieved before receiving B + S bursts.

In a discontinuous transmission (time-slicing), if the Inner TI is configured to perform only intra-frame interleaving, it is possible to display the content after receiving the first burst if the reception conditions are good enough, such that the Inner FEC of the Data PLP correctly decodes the data. Assuming one burst per second, the average zapping time would be around 0.5 s. For continuous transmission, as mentioned before it is recommended to perform inter-frame interleaving with the Inner TI within 1 s, keeping the operation frequency of the Outer FEC and thus a fast zapping time.

Terminals in very good reception conditions would stay always on early decoding, but otherwise at some point terminals need to do a transition from early to late decoding to achieve full protection. The transition time from early decoding to late decoding is $B - 1$ bursts when the parity is transmitted before data (i.e., $D = B + S$), and $B + S - 1$ bursts when the parity is transmitted after the data (i.e., $D = 0$).

The solution adopted to perform this transition for MPE-iFEC in DVB-SH is based slowing down the audio and video display rate, see [32] and [33]. For BB-iFEC, other solutions are currently under investigation,

based on simply buffering and replaying. The key is that the transition time is much lower than in DVB-SH, because with BB-iFEC most of the protection is in the outer FEC. When the parity is transmitted before the data, the lower the code rate, the lower the transition time between early and late decoding. For 10 sec time interleaving, the transition time is only 1 sec for CR_{outer} 1/4, which can be considered to directly provide fast zapping, and 3 sec for CR_{outer} 2/5.

2.4.3 BB-IFEC Transmitter Implementation

2.4.3.1 Data Delay Buffer

The transmission delay block is the only modification to the Data PLP. This block is just a buffer, which delays the transmission of the data bursts an entire number of T2 frames, denoted with the parameter *D*, in analogy to the MPE-iFEC specification in DVB-SH [27]. It should be pointed out that there is no need for a buffer at the receivers.

Two values of *D* are possible. $D = 0$, where the parity data is transmitted after the source data (as shown in Figure 28); and $D = B + S$, where the parity data is transmitted before the source data. The latter configuration increases the end-to-end latency, but reduces the transition time from early decoding mode to the late decoding mode. In particular, for $D = 0$, the transition period is $B + S - 1$ bursts, and for $D = B + S$, the transition period is reduced to $B - 1$ bursts.

2.4.3.2 Data Spreading

The data spreading process is the responsible for assigning the BB frames of each data burst to its corresponding *B* ADTs (Application Data Table) enclosed by the data spreading sliding window, see Figure 29. Data bursts are split into *B* subblocks, in such a way that the maximum difference between one sub-block and the rest is only one BB frame. Each subblock contains an entire number of consecutive BB frames (i.e., BB frames are not split into several ADTs). Each subblock is then assigned to one ADT.

It should be noted that for Constant Bit Rate (CBR) services, the number of data BB frames per burst is constant, and the size of the ADTs is the same than the size of the data bursts.

For Variable Bit Rate (VBR) services, the number of data BB frames per burst changes over time, and thus the size of the ADTs is not constant. The size of each ADT depends on the size of the B bursts that generate the ADT, but always corresponds to an entire number of BB frames.

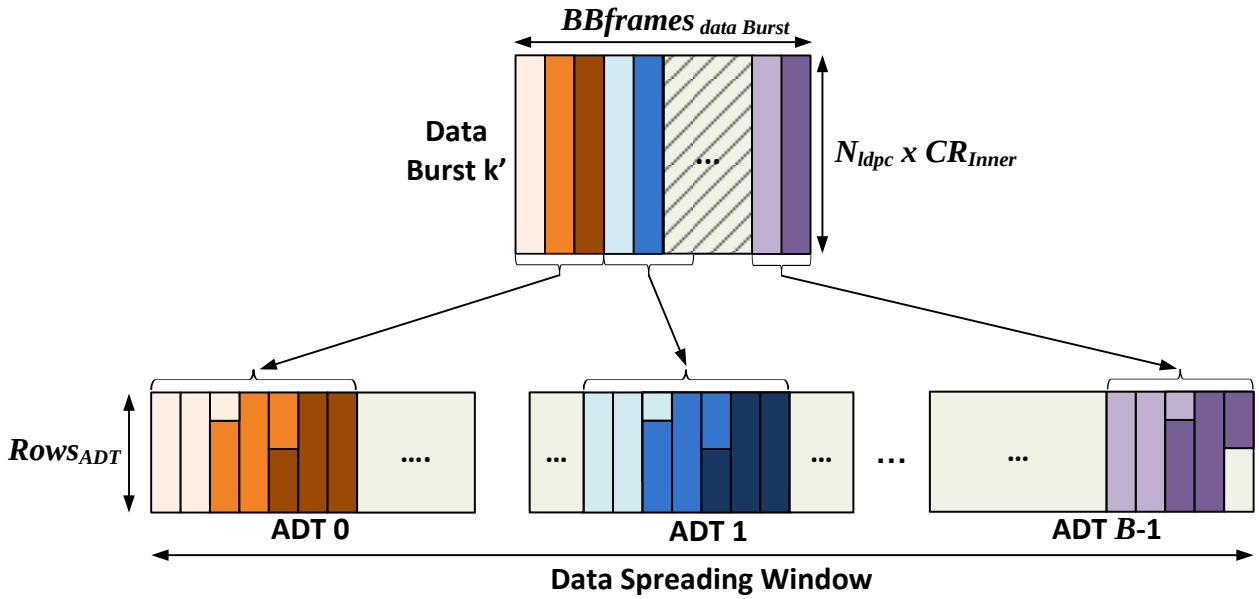

Figure 29: Illustration of the data spreading process. The data spreading process is performed from one data burst to B ADTs (Application Data Tables). The parity spreading process is performed from one iFDT (iFEC Data Table) to S parity bursts. Each ADT/parity burst contains an entire number of consecutive BB frames of the data burst/iFDT. The maximum difference between ADTs/parity bursts is one BB frame.

2.4.3.3 Outer FEC

The Outer FEC process generates the parity data to fill one iFDT (iFEC Data Table) taking as input data one filled ADT. Figure 30 shows the BB-iFEC encoding matrix (ADT + iFDT). The total number of columns is constant, and it is given by the size of the outer LDPC (i.e., N_{ldpc} = 16,200). The number of columns of the ADT, $Columns_{ADT}$, and iFDT, $Columns_{iFDT}$, depend on the code rate of the outer LDPC:

$$Columns_{ADT} = 16{,}200 \times CR_{outer}$$

$$Columns_{iFDT} = 16{,}200 \times (1 - CR_{outer})$$

The number of rows of the ADT and iFDT, $Rows_{ADT,iFDT}$, is adjusted in such a way that the amount of padding in the ADT is minimized. The number of padding bits in the ADT is at most $(16{,}200 \times CR_{inner} - 1)$ bits. That is, it depends on the code rate of the Inner FEC, since it determines the size of the data BB frames. It should be pointed out that the padding bits of the ADT table are not transmitted, and thus they do not reduce the effective capacity. The number of rows is fixed for CBR services and dynamic for VBR services. Once known the number of data BB frames in the ADT, BBframesADT , the number of rows can be computed as:

$$Rows_{ADT,iFDT} = \lceil BBframes_{ADT} \times CR_{inner}/CR_{outer} \rceil$$

where $\lceil \cdot \rceil$, denotes the *ceiling* function.

Once the ADT is filled (including padding), LDPC encoding is performed row by row. Before encoding one row of the ADT, bit interleaving of the data is performed, as depicted in Figure 31. After decoding, the generated parity bits are also interleaved before writing them into one row of the iFDT. The bit interleaving is based on a block interleaver, with the number of columns equal to the data or parity spreading factor (B for data interleaving, and S for parity interleaving). Data is written by columns and read by rows, in a similar

way than the bit interleaver of DVB-T2 [29].

Once the iFDT is written, it may be possible that some padding bits need to be included in the last parity BB frame. These padding bits need to be transmitted in order to avoid puncturing at the receivers. One interesting alternative is to use those bits to transmit in-band signalling, see [29] and [30]. In DVB-T2, there are two types of in-band signalling: type A (with updated L1 and L2 signalling information), and type B (with information related to the input processing of the Data PLP). In DVB-NGH, type A in-band signalling is optional, whereas type B is mandatory.

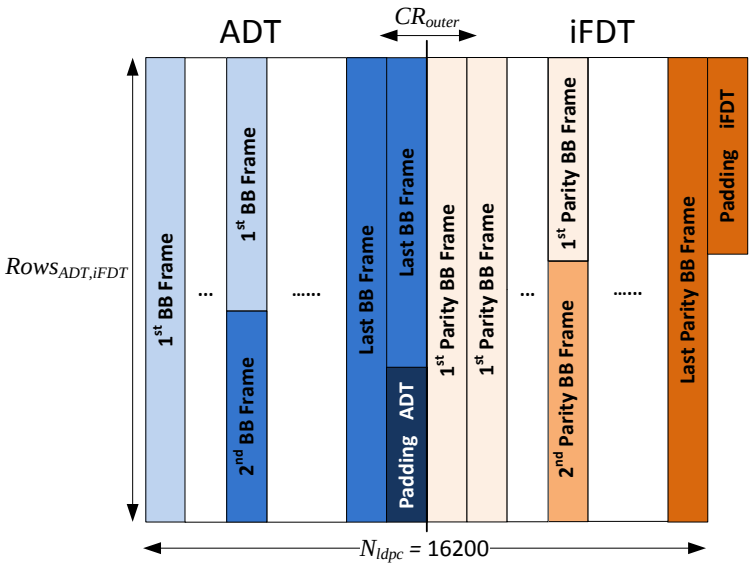

Figure 30: BB-iFEC encoding matrix. ADT (Application Data Table) and iFDT (iFEC Data Table). The padding bits of the ADT are not transmitted. The padding bits of the iFDT can be used to transmit in-band signalling.

Figure 31: Outer FEC process with bit interleaving of the ADT row before LDPC encoding and bit interleaving of the generated parity bits before writing them into one row of the iFDT. The bit interleaver is simply a block interleaver with the number of columns equal to the data spreading factor B and parity spreading factor S, for data and parity interleaving, respectively.

2.4.3.4 Parity Spreading

Once the iFDT is filled, a second spreading process is performed to distribute the parity BB frames to the S parity bursts enclosed by the parity sliding window. The number of parity BB frames in the iFDT can be easily derived from the number of rows of the ADT and iFDT, and the code rate of the Outer FEC:

$$BBframes_{iFDT} = \lceil Rows_{ADT,iFDT} \times (1 - CR_{outer}) \rceil$$

The spreading process from the iFDT to the parity bursts is exactly the same than the spreading process from one data burst to the ADTs, depicted in Figure 29. The only difference is the number of elements enclosed by the sliding window (*B* ADTs in the data spreading process and *S* parity bursts in the parity spreading process). The iFDT is split into *S* sub-blocks. Each sub-block contains an entire number of consecutive parity BB frames. Each sub-block is then assigned to one parity burst.

2.4.4 BB-IFEC Receiver Implementation

2.4.4.1 Decoding Process

Figure 32 shows a block diagram of a BB-iFEC receiver. In early decoding mode, the protection is given only by the Inner FEC of the Data PLP, and therefore the decoding process is the same than in DVB-T2 (inner LDPC first, and then outer BCH). The decoding process in late decoding mode, when the protection is given by both Inner and Outer FEC, is the following (recall that BB-iFEC operates in a burst basis):

1) Perform Inner LDPC decoding to all data BB frames of the burst of the Data PLP.
2) Send the decoded data, either soft or hard LLR values2, to the Data De-Interleaver block, which performs exactly the same spreading process than the Data Spreading block at the transmitter (see Figure 32). In case of soft decoding in the Outer FEC, it is possible to store hard values (i.e., +/- 1 LLRs) when the Inner FEC detects that all parity check nodes are correct. This improves the performance and reduces the number of iterations required by the Outer FEC to converge.
3) Send the LLRs, either soft or hard values, of the parity BB frames of the iFEC PLP to the the Parity De- Interleaver block, which performs the inverse spreading process than the Parity Spreading block at the transmitter (see Figure 32).
4) Perform the Outer FEC process, including bit deinterleaving of the data and parity.
5) Perform BCH decoding to all data BB frames.

From the decoding sequence above, it is clear that the receiver needs help in case of VBR services for doing the inverse of parity spreading process, but not for the data spreading process. For each parity burst, the receiver needs to know the amount of BB frames that correspond to each of the S iFDTs enclosed by the parity sliding window. This information should be transmitted in the dynamic field of the L1 signalling. It should be pointed out that the complete decoding process can be performed sequentially with only one LDPC hardware chain. BB-iFEC increases the number of LDPC decodings per burst with respect to a single FEC scheme. However, assuming 50 LDPC iterations per codeword as reference, the overall number of iterations can be kept without impacting the performance. For example, during early decoding mode, the outer FEC is not performed, and thus the Inner FEC can perform as many iterations as for single FEC. The Outer FEC is also not used in good reception conditions. In late decoding mode, in static conditions the overall performance is given by the FEC with more robust code rate, and thus this FEC should perform more iterations. On the other hand, in mobile conditions, it is possible to benefit when the Inner FEC is correct to speed up the convergence of the Outer FEC.

2.4.4.2 Receiver Implementation with Memory Pointers

One possibility for implementing BB-iFEC at the receivers is to use a double pointer structure, as described in the DVB-SH Implementation Guidelines for VBR memory management with MPE-iFEC [14]. The first pointer level would point to M encoding matrixes, the memory requirements of a sheer block interleaver. The second pointer level would point only to $(M + 1)/2$ encoding matrixes (optimized memory requirements, similar to a convolutional interleaver with a uniform profile). BB-iFEC only needs to manage M pointers per level (B pointers for the data and S pointers for the parity), much less than in MPE-iFEC, which requires M times the total number of columns of the ADT plus iFDT (i.e., 255) [27].

2.4.4.3 Receiver Implementation with Ring Buffers

Because of the regular structure of the BB-iFEC encoding process, the time de-interleaving at the receivers can be also implemented with ring buffers like traditional convolutional interleavers. Two convolutional interleavers are needed for the data and for the parity. The IU size of the convolutional interleaver for the data depends on the code rate of the Inner FEC (i.e., 16,200 × CR_{inner} bits/LLRs), whereas the IU size of the convolutional interleaver for the parity is constant and equal to 16,200 bits/LLRs. The number of delay lines

equals the number of BB frames of the data PLP and the iFEC PLP. The delay values range from 0 to $M-1$, with several lines having the same delay value (there are only M different values). Different interleaving configurations can be seen as different profiles of the convolutional interleaver. For the VBR case, the memory management is similar to one convolutional interleaver with dummy cells.

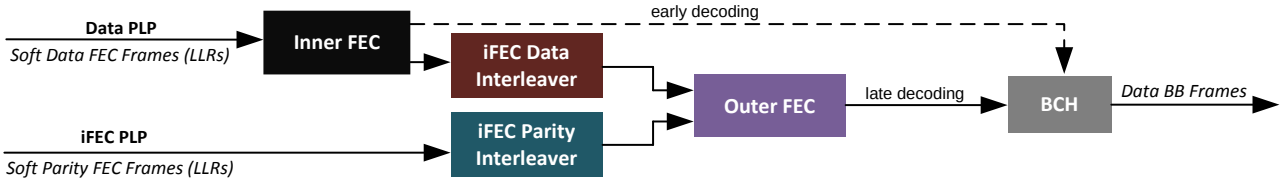

Figure 32: BB-iFEC receiver block diagram. In early decoding mode the protection is given only by the Inner FEC. In late decoding mode the protection is given by both Inner FEC and Outer FEC.

2.5 Rotated PSK and APSK for the satellite component of NGH

In this study, Telecom Bretagne investigated the application of the signal space diversity (SSD) technique called rotated constellation [34] to a constellations such as PSK and APSK, widely used in satellite transmissions. This technique allows the diversity order of the coded modulation in order to improve the transmission robustness over severe channels. It is based on applying a rotation to the constellation and introducing interleaving between the in-phase (I) and quadrature (Q) components of the transmitted signal. This method has been shown to perform well over fading channels with or without erasures [35]. In DVB-T2, Telecom Bretagne's main contribution to this technique was the proposal of new criteria for the rotation angle search. The technique and the rotation angles proposed for 4 to 256 QAM constellations were adopted in the standard. In DVB-NGH, a hybrid terrestrial/satellite coverage is considered. For mobile satellite transmissions, the Land Mobile Satellite (LMS) channel model, calling for a 3-state (line of sight, shadowing, blockage) Markov model, is widely used. The blockage state of the channel infers some erasure events in the transmission. Consequently, the rotated constellation technique is likely to improve significantly the robustness of satellite mobile transmissions. PSK and APSK constellations, widely used for satellite transmissions, have been investigated in this study.

2.5.1 The rotated constellation approach

The transmitter and receiver structure of the proposed SSD scheme is presented in Figure 33.

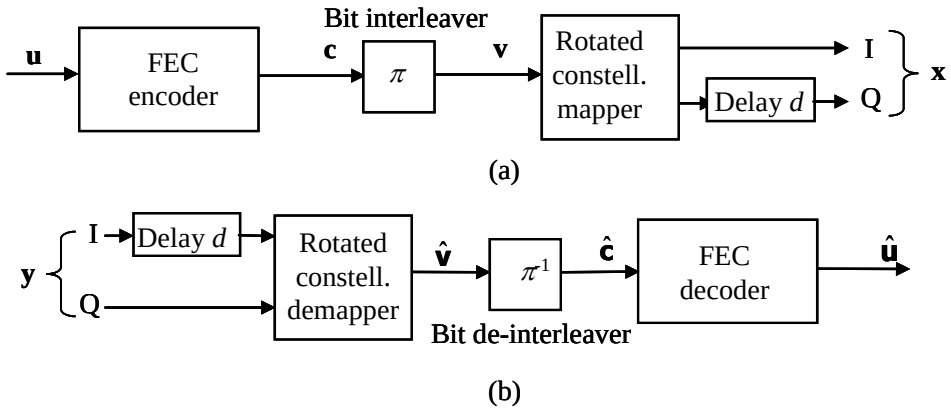

Figure 33: Structure of the proposed coded modulation SSD scheme: (a) transmitter and (b) conventional receiver.

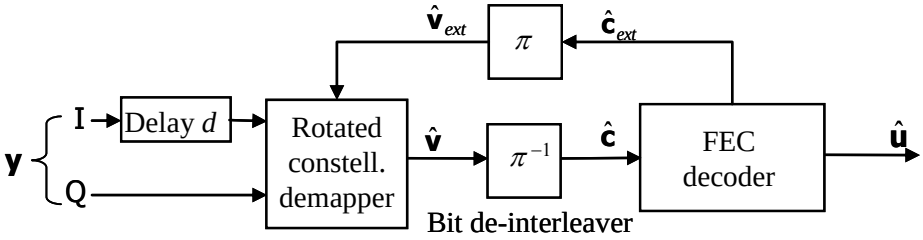

Figure 34: Iterative receiver structure for the proposed scheme.

Due to the constellation rotation and the delay insertion, the binary information contained in each constellation point is transmitted twice over the channel. Consequently, the rotated constellation can be seen in a way as a repetition code proceeding at the constellation symbol level.

From this point of view, the BICM transmitter of Figure 33(a) becomes a serial concatenation of two codes separated by an interleaver. Therefore, at the receiver side, the conventional structure presented in Figure 33 (b) can be beneficially replaced by an iterative structure, as described in Figure 34 in order to get additional gains. Extrinsic information related to every coded bit is then computed by the FEC decoder and fedback at the demapper input as *a priori* information.

The SSD principle had been originally devised for fading channels. However, in the DVB-T2 and DVB-NGH context, some additional erasure events have to be taken into account. Actually, in light of the presence of erasure events, some aspects of the original SSD had to be reconsidered in order to benefit from greater gains. In previous studies, the choice of the rotation angle α was based on maximizing the so-called *product distance* (PD) in order to minimize the pair-wise error probability between two different transmitted sequences. Unfortunately, this criterion is only valid for asymptotical performance, that is for very high values of Signal-to-Noise Ratios (SNR). In practice, actual operating SNRs can be rather low, especially when powerful FEC coding is considered. Consequently, the PD criterion turns out to be suboptimal for the SNR region of interest and the corresponding angles do not lead to the best actual coded performance. Moreover, for erased constellation signals, the distances are measured on the projection of the point on the non-erased axis, I or Q. In this case, a criterion based on a one-dimensional distance had to be introduced.

In order to find rotation angles suited to transmission over fading channels with and without erasure events, the following design criteria were proposed [35]:

- Maximizing the *minimum product distance* (PD), as already mentioned, in order to minimize the asymptotical Bit Error Rate (BER) at the output of the demapper over fading channels without erasures;
- Maximizing *the minimum 1-dimensional distance* ($1D_{min}$) between any two constellation points after their projection onto I or Q, in order to minimize the asymptotical BER at the output of the demapper in the presence of erasures;
- Minimizing the *average Hamming distance* between any two adjacent constellation symbols ($d_{H,avg}$) and the Hamming distance between any two adjacent constellation symbols at distance 1Dmin ($d_{H,1D}$) after their projection onto I or Q: these mapping-related distances play a role in the presence of erasures. In order to minimize the number of bits in error when a wrong constellation symbol is chosen, $d_{H,avg}$ and $d_{H,1D}$ should be kept as low as possible.

Unfortunately, in practice, these criteria are in conflict and their simultaneous application leads to different values of the rotation angle. Thus, a compromise has to be found.

2.5.2 Optimizing the rotation angle for PSK and APSK constellations

In the context of DVB-NGH, these design criteria have been applied to 8-PSK, 16- and 32-APSK. For instance, Figure 35 displays the different distance curves for the 8PSK constellation.

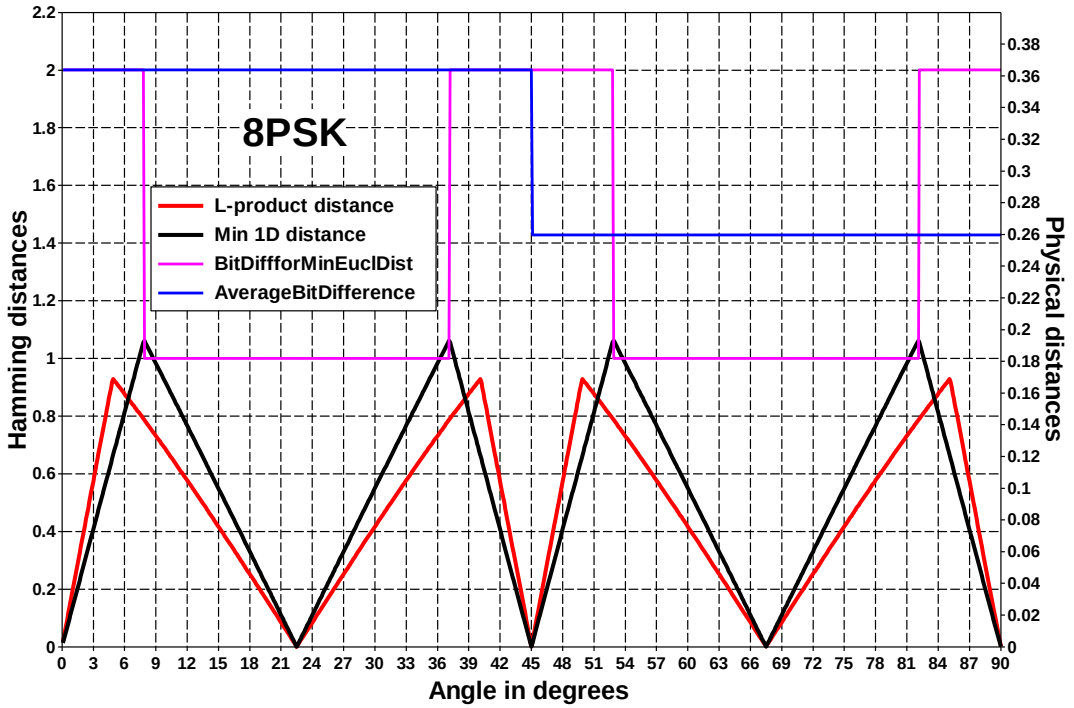

Figure 35: distance values as a function of the rotation angle α for constellation 8-PSK. Red curve: minimum product distance PD. Black curve: minimum 1-dimensional distance $1D_{min}$. Blue curve: average Hamming distance $d_{H,moy}$. Magenta curve: average Hamming distance $d_{H,min}$.

From this figure, we kept the rotation angles α such that $1D_{\min}(\alpha) \geq 1D_{\min}(\alpha_1)$, where α_1 is the angle corresponding to the nearest peak of the product distance: $49.9° \leq \alpha \leq 58.5°$ and $76.5° \leq \alpha \leq 85.1°$.

The same procedure was applied to 16-APSK and 32-APSK constellations.

2.5.3 Simulation results

For each constellation under study, simulations have been carried out over two different channel types: the Rayleigh fading channel and the Rayleigh fading channel with 15% of erasures.

Figure 36 and Figure 37 compare the Bit Error Rate (BER) at the output of the non-rotated and rotated 8-PSK demappers for different acceptable values of angle α. One can observe a performance gain in favour of the rotated 8-PSK constellation for all values of signal to noise ratios (SNR) considered. In the presence of erasures, this gain is greater than 1 dB even for very lows SNRs.

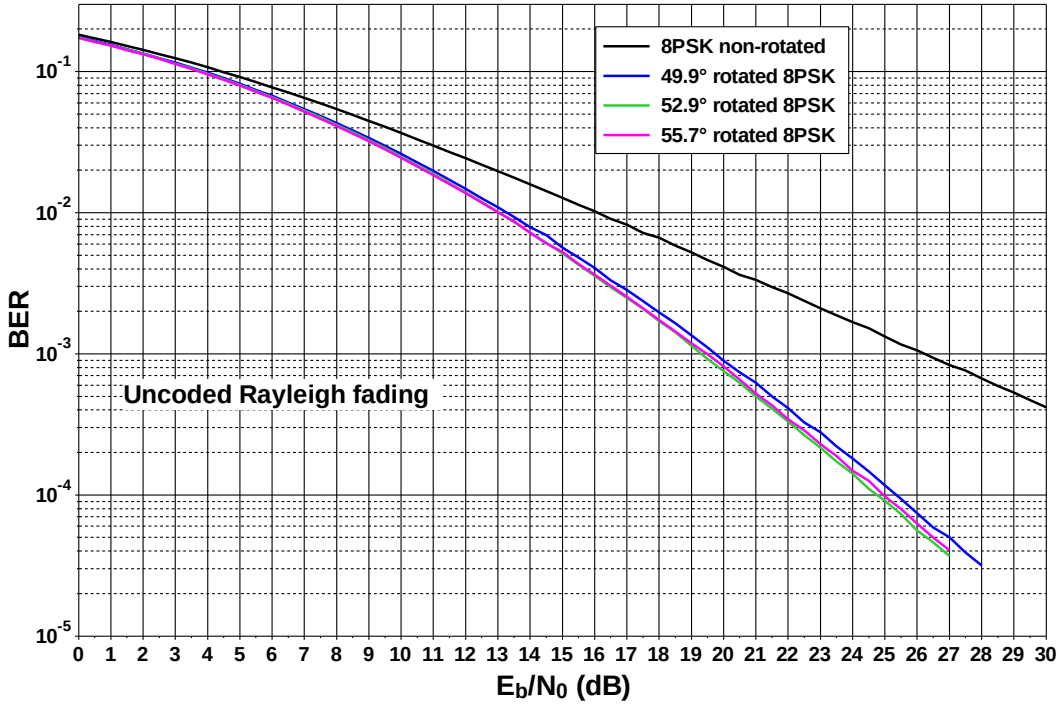

Figure 36: BER comparison at the output of a non-rotated and of a rotated 8-PSK demapper. Uncoded transmission over a flat fading Rayleigh channel.

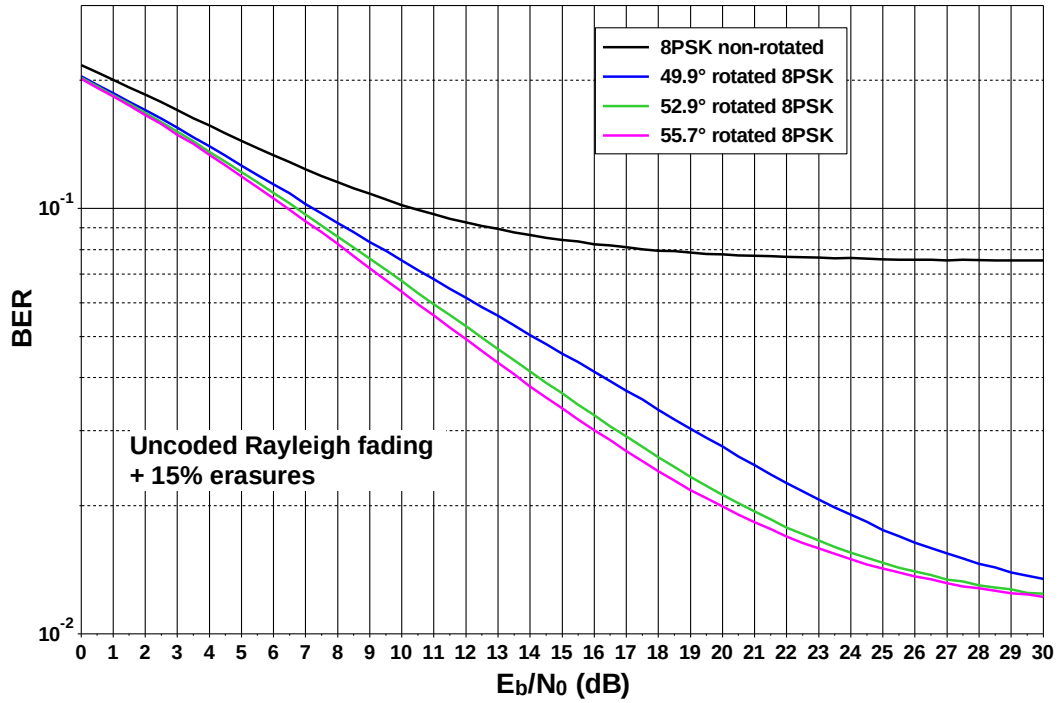

Figure 37: BER comparison at the output of a non-rotated and of a rotated 8-PSK demapper. Uncoded transmission over a flat fading Rayleigh channel with 15% of erasures.

2.5.4 Proposed angle values

The distance curve analysis combined to subsequent simulations led to the proposal for DVB-NGH of the angle values provided by Table 18.

Table 18: Angle recommendations for rotated 8-PSK and APSK constellations in DVB-NGH.

Angle recommendations		
8-PSK	16-APSK	32-APSK
$\alpha = 55.7°$	$9.9° \leq \alpha \leq 10.3°$	$\alpha = 94.4°$

3 TIME INTERLEAVING

DVB-NGH being dedicated to mobile applications, some research has been undertaken to optimize the DVB-T2 channel interleaver in order to reduce the time interleaver memory in the receiver and to take into account the hybrid satellite/terrestrial mode of NGH.

Section 3.1 presents the results of the studies that led to the adoption of a combination of block and convolutional interleaving in the DVN-NGH baseline. Section 3.2 gives the summary of an analysis of time interleavers in Land Mobile Satellite conditions, which is presented in details **ENGINES Deliverable 2.4**.

3.1 Time interleaving proposal for NGH

Teracom was deeply involved in the design of a time interleaver structure appropriate to DVB-NGH. This section presents a synthesis of their work.

3.1.1 Introduction

The time interleaving (TI) proposal for NGH was originally heavily based on the block interleaving (BI) used in the DVB-T2 standard, including the possibility to interleave over several frames. For complexity reasons it was however found desirable to reduce the TI memory by 50%. This would however severely limit the possible time interleaving depth, especially since lower order constellations like QPSK, which are quite likely to be used for NGH, allows a shorter interleaving depth for a given number of cells in the TI memory and for a given PLP bit rate. For these reasons, but also to allow for shorter zapping time (especially in connection with the hybrid satellite/terrestrial mode of NGH) convolutional interleaving (CI) was suggested as an alternative to block interleaving. CI had however already been studied and rejected for DVB-T2, due to certain problems (e.g. TFS and VBR). However, after some analysis a solution was agreed: to combine BI and CI in such a way that BI is done internally in an NGH frame in a similar way as for T2, but the interleaving across NGH frames is done by CI. In this way the previously known problems with CI would vanish but there would still be significant memory gains and gains in zapping time.

3.1.2 I/Q shift for rotated constellations

When rotated constellation is used it is important for the original I and Q components of a cell to be transmitted with large separation in time and frequency, so that e.g. a bad RF channel or a badly received NGH frame (due to fading or interference) will not contain both components. In T2 this was not ensured, but for NGH it has been suggested to use a shift of one Interleaving Unit (IU) for the Q component before cell interleaving. This will ensure that the I and Q are always transmitted in different NGH frames, see Figure 38:

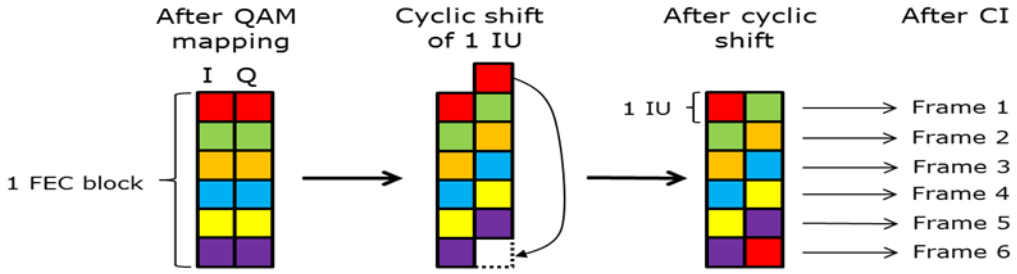

Figure 38: Proposed I/Q shift for DVB-NGH

3.1.3 Hybrid convolutional/ block time interleaver structure

With CI each FEC block needs to be spread over several frames. The way this is achieved is to divide each FEC block into a number of so-called Interleaving Units (IUs), with number of IUs equal to the time interleaving depth expressed in number of NGH frames. In order to minimise power consumption the highest possible IU size should be used.

Figure 39 shows the way the CI works. The upper figure shows the situation before CI and the lower figure after CI. There is one column per NGH frame and four IUs per FEC block. There are two PLPs – one "red PLP" and one "green PLP".

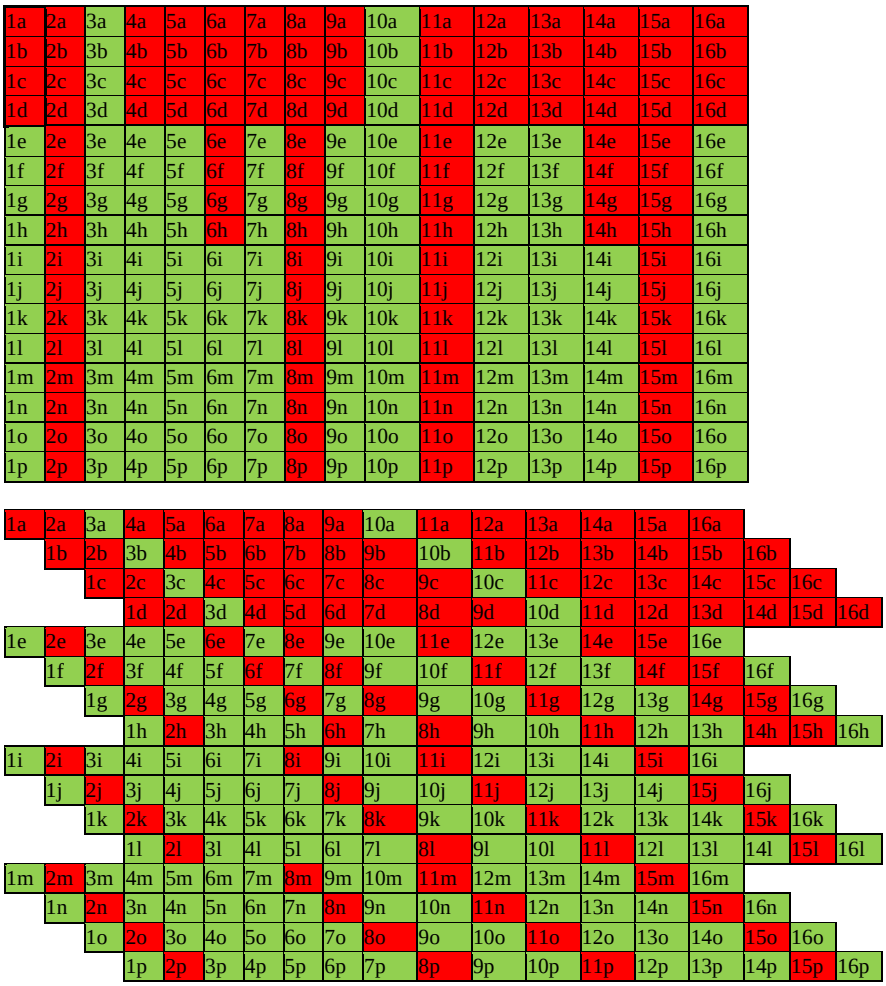

Figure 39: Illustration of the proposed IU-based CI process

The starting point for the interleaving process is that we have an integer number of 16,200 bit FEC blocks per PLP for each NGH frame.

Unfortunately it is not always possible to divide a FEC block into equally large IUs using all the constellations QPSK, 16-QAM, 64-QAM and 256-QAM. In some combinations of constellation and interleaving depth (number of NGH frames N) some IUs get one cell more than the others (these cases are: 16-QAM N=4, 256-QAM, N=2, 4, 6). This does not have any effect on the CI as such, but will affect the number of cells per frame for a given PLP.

In each NGH frame BI is performed for each PLP individually. The BI is shown in

Figure 40.

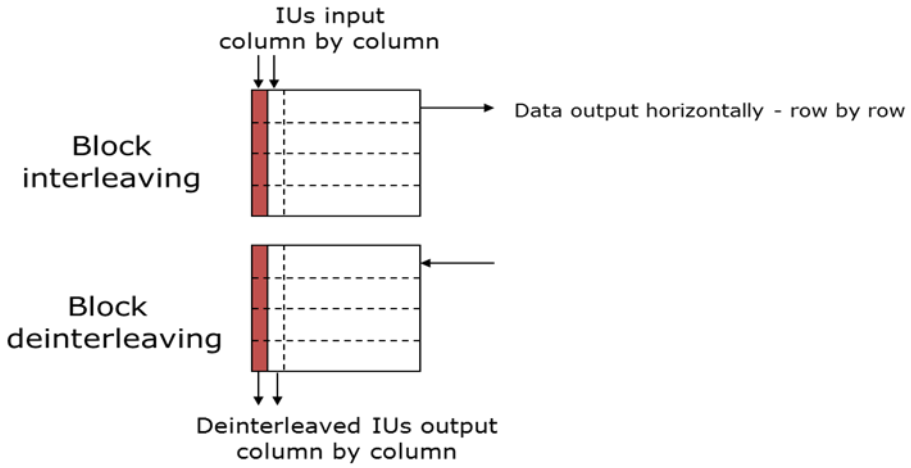

Figure 40: IU-based BI

For a given PLP each IU is inserted vertically in a column. The result is read out horizontally, row-by-row. Due to the slightly different IU lengths (for a given configuration) the IUs will in general not perfectly fit a column – some IUs will, but others will be "one cell short". There will thus be some empty space at the end of the BI. These empty positions are simply discarded when the data is read out, as can be seen from Figure 41.

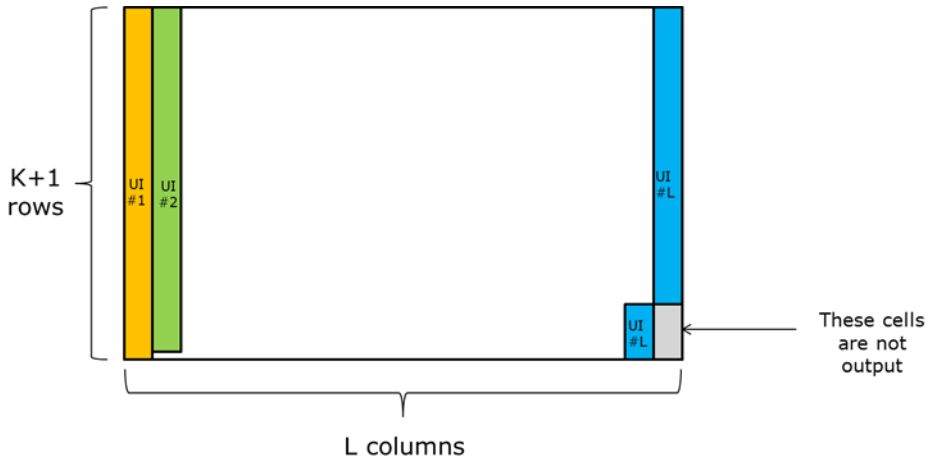

Figure 41: Insertion of IUs into the BI

3.1.4 Scheduling of PLPs

After the BI the PLPs are put on top of each other in a cell-based matrix, according to Figure 42.

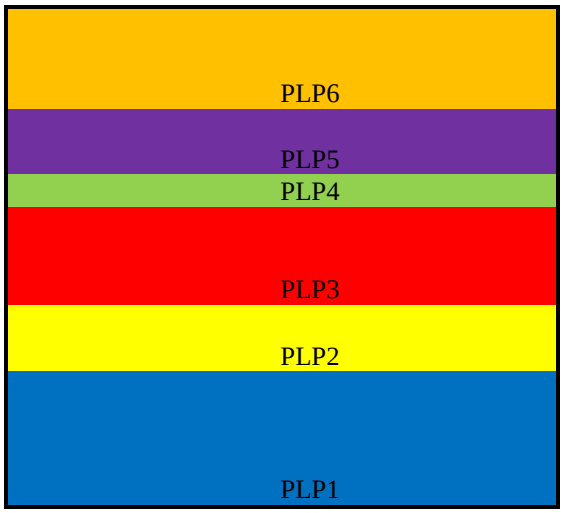

Figure 42: PLP arrangement after the BI

The number of columns in the matrix equals “number of RF channels” multiplied by “number of sub-slices per RF channel”. When this condition is fulfilled (including any necessary padding cells in the top row), a deterministic scheduling of the cells into the NGH frame can be done in the way outlined below.

First step: Divide the matrix into "number of sub-slices per RF channel" (here two) and put one half on top of the other, see Figure 43:

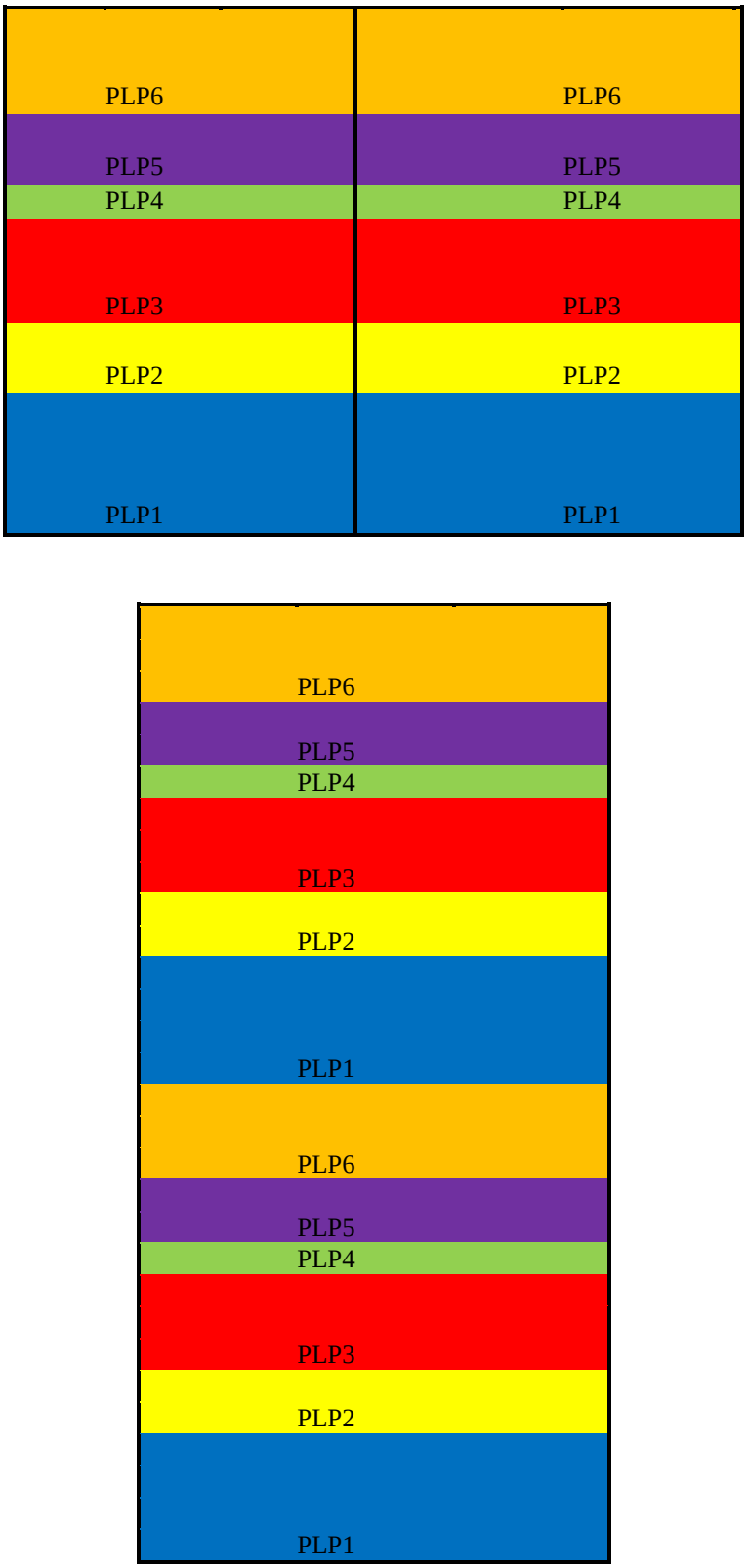

Figure 43: Result of the first scheduling step

Second step: Divide the resulting structure into “number of RF channels” (here three in Figure 44):

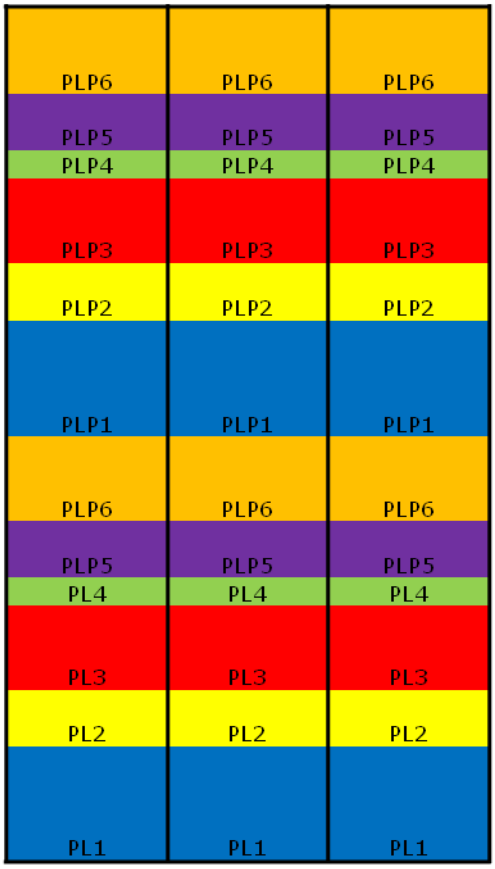

Figure 44: Result of the second scheduling step

Third step: Perform time shifting and folding back, according Figure 45. The time shift makes the PLPs evenly distributed in order to allow for good time diversity and time/frequency hopping.

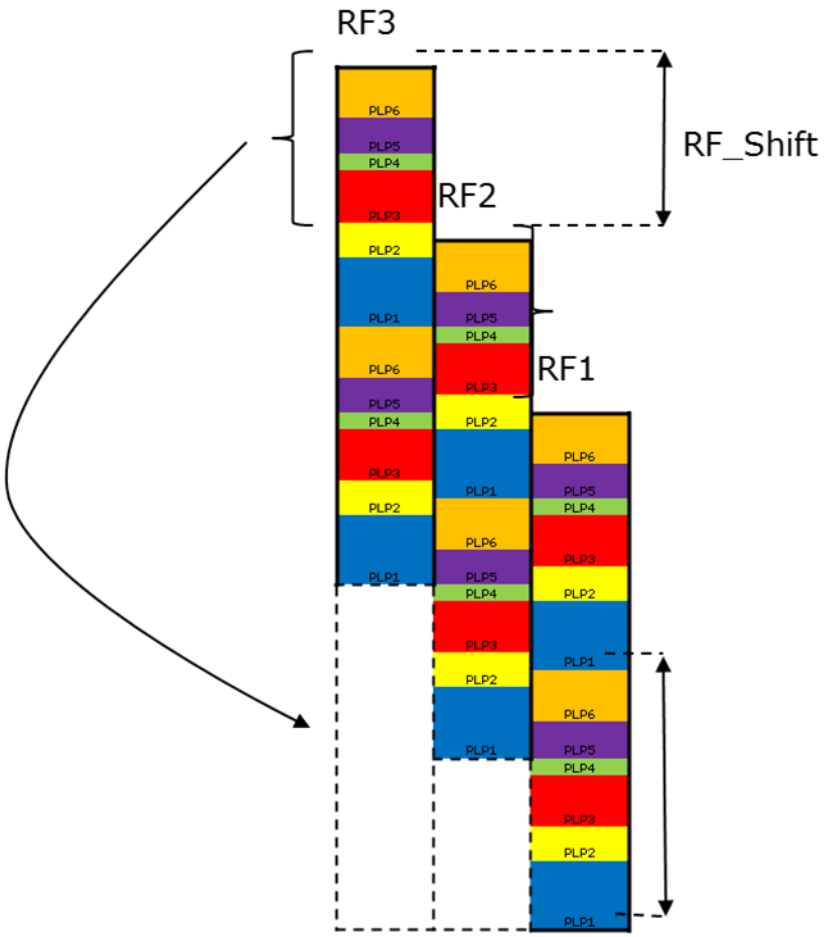

Figure 45: Result of the third scheduling step

End result of scheduling process

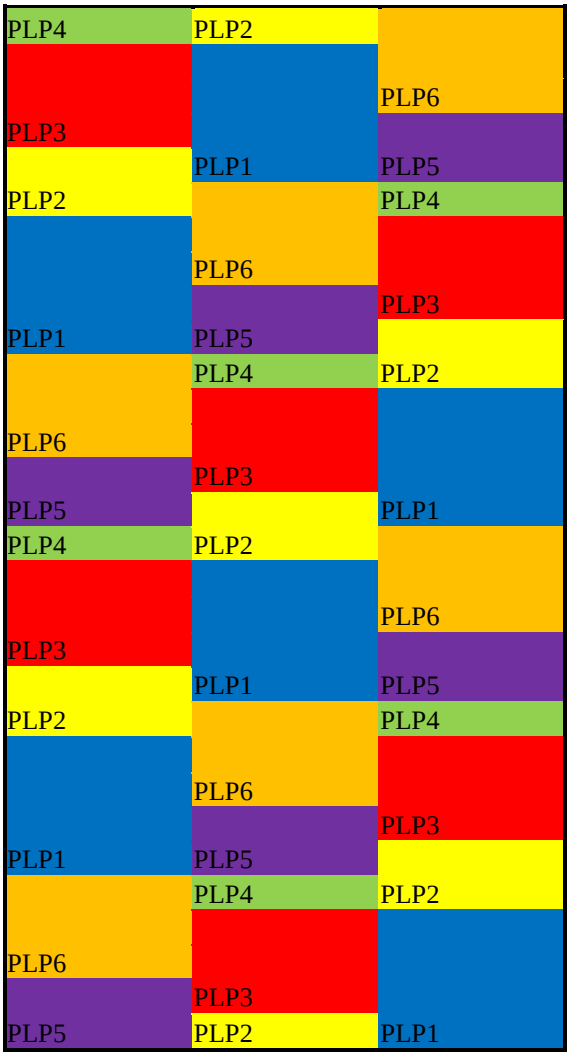

Figure 46: End result of scheduling

It should be noted that the previous process has not yet filled the scheduled cells with data – only allocated the positions in the frame.

Time interleaved PLP cells are introduced into sub-slices in the natural time sequence, independently of RF channel

The first time interleaved cell is therefore introduced in the first cell position of the first sub-slice of the PLP (in whichever RF channel it appears). A receiver performing the frequency hopping will therefore receive the time interleaved cells in the right order.

3.1.5 Frequency Interleaving

Frequency interleaving is performed in each symbol using a time varying frequency interleaver. This allows for each OFDM symbol to be differently frequency interleaved and therefore spreads the IUs to potentially all OFDM carriers in the frame to maximize frequency diversity. This allows also for a simpler BI since there is no need to use the approach adopted for T2 of splitting an input block (a FEC block in T2) into five columns.

3.2 Performance analysis of time interleavers in Land Mobile Satellite conditions

This study was carried out by CNES. It can be viewed as a common task of Task Forces 1 and 4, since TF4 deals with hybrid access technologies. Thus, this report only contains an executive summary of this study. For an extensive description, please refer to **ENGINES Deliverable 2.4**.

For a satellite part, a long interleaver is needed to cope with the fluctuation of the shadowing effect seen by the mobile receivers while the code rate is tightly tuned to the optimisation of the satellite link budget and the compromise with data throughput.

Two solutions have been introduced in DVB-SH: one solely on the physical layer with the class 2 physical time interleaver, and the other one on the link layer with the class 1 physical time interleaver.

The class 2 interleaver must be implemented at the physical layer. This solution leads to the best performance in terms of decoding capability but it has zapping and service access times higher than those expected with NGH standards. The class 2 interleaver is a good compromise between robustness and zapping time.

The interleaver added with MPE-IFEC on top of class 1 physical interleaver is less performing but it allows lower zapping and service access time.

The use of a return channel may improve the performance of this solution as well in a compromise to be done with the additional use of the forward link it will trigger.

4 STUDY OF ADVANCED MODULATION TECHNIQUES FOR NGH

DVB-T2 multi-carrier modulation is based on a classical Cyclic Prefix (CP) Orthogonal Frequency-Division Multiplexing (OFDM). Two ENGINES members, Orange Labs/France Telecom and MERCE studied and proposed two alternative solutions for DVB-NGH. Orange Labs/France telecom investigated the so-called OFDM-OQAM modulation, particularly efficient against frequency distortions such as Doppler Effect. This study is detailed in Section 4.1. Besides, MERCE proposed Single-Carrier (SC)-OFDM modulation for the satellite component of the DVB-NGH system. This contribution is summarized in Section 4.2. For an extensive description, please refer to **ENGINES Deliverable 2.4**.

4.1 Terrestrial link: OFDM-OQAM modulation

The most common OFDM scheme transmits QAM symbols thanks to the use of a basic Inverse Fast Fourier Transform (IFFT) at the transmitter and an FFT at the receiver. Because of the sensitivity of such a scheme to multipath channels, a Cyclic Prefix (CP) is usually inserted at the transmitter side and removed at the receiver side. This procedure can cancel inter-symbol interference (ISI) if the length of the CP is larger than the largest echo of the channel. This scheme referred to as CP-OFDM has the advantage to provide good performance for a reasonable complexity. Nevertheless several issues are pending. The CP does not fight against frequency distortions such as the Doppler Effect; so inter-carrier interference (ICI) remains and the cyclic prefix may be seen as redundancy leading to a spectral efficiency loss. Finally the use of a simple IFFT at the transmitter, *i.e.* modulating the symbols over each sub-carrier by a rectangular function, leads to non-negligible out-of-band radiations. This latter item implies that in practical systems consequent filtering has to be applied to meet spectrum masks requirements. In this document we focus on an OFDM scheme, proposed for DVB-NGH that can solve, partially or completely, the aforementioned issues. In this document, this specific OFDM modulation scheme often referred as OFDM/OQAM is described (where the OQAM

term stands for Offset-QAM).

In OFDM/OQAM no cyclic prefix is inserted between the symbols but a specific pulse-shaping (prototype function) is introduced that in the meantime satisfies some orthogonality constraints. Among the OFDM/OQAM prototype function, we can find the Isotropic Orthogonal Transform Algorithm (IOTA) that has been proposed in 1995 by France Telecom in the case of a transmission over a time-frequency dispersive channel. However, since this date, other prototype functions either optimized in continual-time such as the Extended Gaussian function (EGF), or in discrete-time using the Time-Frequency Localization (TFL)[38] criterion have also been proposed. Some of the basic features of these main functions are presented in this document. In order to illustrate the hardware feasibility of OFDM/OQAM, we also present the France Telecom OFDM/OQAM demonstrator.

4.1.1 Time-frequency representation

Time-frequency representations are particularly appropriate for multi-carrier modulation schemes that can indeed have different features in the time and frequency domains. Figure 47 represents the time-frequency lattice for the OFDM and OFDM/OQAM modulations. In this scheme the lattice density is measured by the inverse of the product of the distance between two elements on the vertical and horizontal axis.

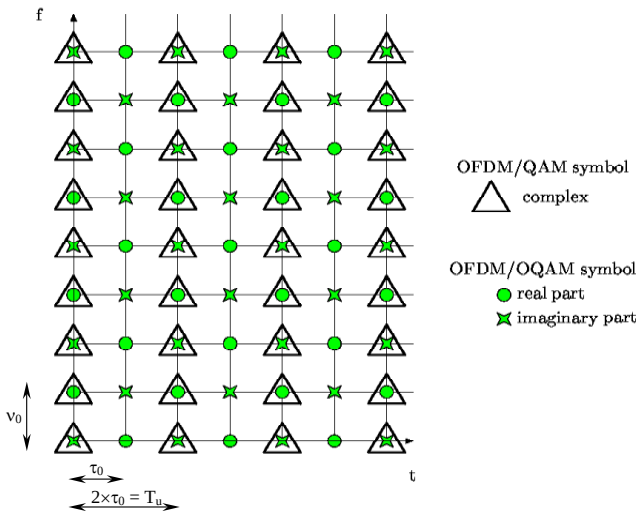

Figure 47: Time-frequency lattice for OFDM and OFDM/OQAM.

It can be seen that, if the frequency spacing, denoted here by $\upsilon_0 (= F_0)$, is identical for both modulation schemes, it is not the case for the time spacing. Indeed, as previously mentioned, the real OFDM/OQAM symbols have a duration τ_0 that is half the one of the useful time duration, denoted here $T_u (= T_0)$, of complex OFDM symbols. So, in theory, both modulation schemes can achieve a similar maximum bit rate. In practice OFDM is always less efficient with a guard time interval (also called cyclic prefix), T_g that introduces a loss of spectral efficiency. Otherwise stated the OFDM/OQAM spectral efficiency is, in theory, $(T_g + 2\tau_0)/2\tau_0$ times higher than the one of OFDM.

4.1.2 Continual time formulation

In the OFDM/OQAM scheme, instead of transmitting a QAM symbol, $s_{m,n} = s_{m,n}^{\mathrm{Re}} + j.s_{m,n}^{\mathrm{Im}}$ at a given rate T_0

on each sub-carrier, the real (Re) and imaginary (Im) are transmitted separately at rate $\tau_0 = T_0/2$, with a time-offset of τ_0 (m: sub-carrier index, n: symbol index). That means either the real or the imaginary part is delayed of one half-symbol duration. The constraint is to keep a phase difference of $\pi/2$ between adjacent symbols in time and frequency. This so-called staggering rule, which is summarized in Table 19 leads to the OQAM transmission scheme. As the sub-carriers have to be grouped by pairs, we naturally have *M* (total number of sub-carriers) even.

Table 19: Coding scheme for OQAM symbols.

	$(2m-1)F_0$	$(2m)F_0$	$(2m+1)F_0$
$nT_0 - T_0/2$	$s^{\mathrm{Re}}_{2m-1,n-1}$	$j.s^{\mathrm{Im}}_{2m,n-1}$	$s^{\mathrm{Re}}_{2m+1,n-1}$
nT_0	$j.s^{\mathrm{Im}}_{2m-1,n}$	$s^{\mathrm{Re}}_{2m,n}$	$j.s^{\mathrm{Im}}_{2m,n}$
$nT_0 + T_0/2$	$s^{\mathrm{Re}}_{2m-1,n}$	$j.s^{\mathrm{Im}}_{2m,n}$	$s^{\mathrm{Re}}_{2m+1,n}$

Based on this coding principle we get the modulator scheme that is depicted in Figure 48.

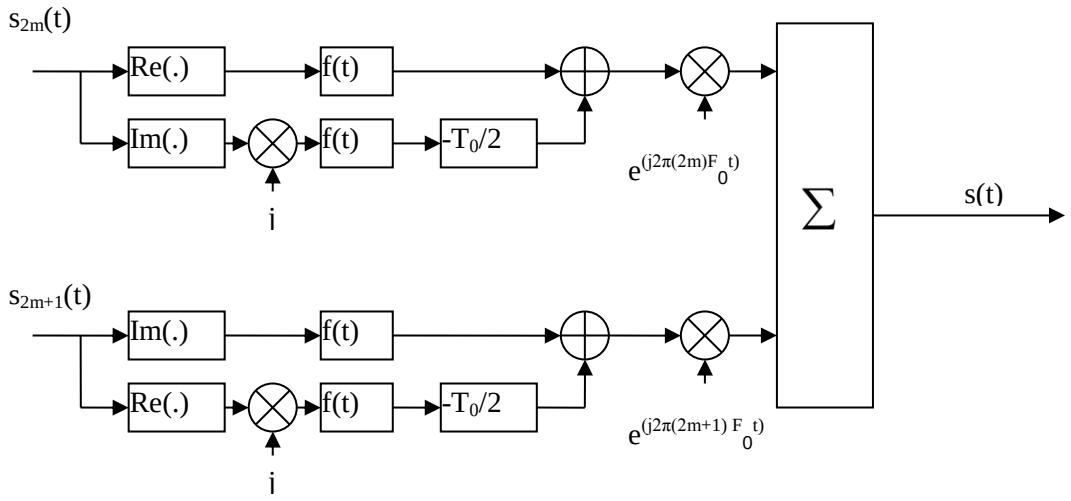

Figure 48: OFDM/OQAM modulator in its analog form (continual-time).

From Figure 48, it can be seen that the baseband OFDM/OQAM signal $s(t)$ is obtained as the combination of 4 signals that are shifted in time by τ_0, the duration of one real symbol, and in frequency by F_0, the spacing between two successive carriers. With a direct formulation it can be seen that $s(t)$ is obtained as a summation in time and frequency of 4 terms. This expression can be simplified in order to get the following unified formulation where the baseband OFDM/OQAM signal is written as follows:

$$s(t) = \sum_{n=-\infty}^{\infty} \sum_{m=0}^{M-1} a_{m,n} f_{m,n}(t)$$

Where the base of modulation can be expressed as a Gabor family:

$$f_{m,n}(t) = f(t - n\tau_0) e^{j2\pi m F_0 t} e^{j\varphi_{m,n}} \qquad (1)$$

The phase term $\varphi_{m,n}$ is directly related to the OQAM staggering rule so it has to be such that:

$$\varphi_{m,n} = \begin{cases} 0 & \text{if } m \text{ and } n \text{ have the same parity} \\ \frac{\pi}{2} & \text{if } m \text{ and } n \text{ have a different parity} \end{cases} \quad (2)$$

It is important to note that the family of functions in (1) does not form an orthonormal basis for a lattice with $F_0 T_0 = 1$. Therefore the Balian theorem which states that is not possible to get an orthonormal basis for $L^2(R)$ for a Gabor system with $F_0 T_0 = 1$ and a bounded time-frequency localization product does not hold for OFDM/OQAM. So if for OFDM it is not possible to get a prototype function being well-localized in time and frequency the situation is different for OFDM/OQAM.

But, in this latter case, the demodulation basis, the same as the modulation one, has to be based on the **real** scalar product of $L^2(R)$. Then at the receiver side the real symbols are recovered by:

$$\hat{a}_{m,n} = \left\langle f_{m,n} \middle| s \right\rangle_R = \mathrm{Re}\left\{ \int_{-\infty}^{+\infty} f_{m,n}^*(t) s(t) dt \right\}$$

Then the orthogonality condition can be checked with the following relation:

$$\mathrm{Re}\left\{ \int_{-\infty}^{+\infty} f_{m,n}^*(t) f_{m',n'}(t) dt \right\} = \delta_{m,m'} \delta_{n,n'}$$

With this expression it can be checked that a phase rotation has a direct impact on this orthogonality condition which means that indeed the phase term cannot be arbitrarily chosen. In the case of continual-time OFDM/OQAM, the definition used by Hirosaki was the one given in (2). As $\varphi_{m,n}$ may be defined modulo π, in fact we need $\varphi_{m,n} = \varphi_0 + \frac{\pi}{2}(m+n)$. To simplify we can only choose $\varphi_{m,n} = \frac{\pi}{2}(m+n)$.

4.1.3 Discrete time formulation

Sampling the continual-time signal at the Nyquist rate T_0/M, we get the discrete-time version of OFDM/OQAM:

$$s[k] = \sum_{n \in Z} \sum_{m=0}^{M-1} a_{m,n} \underbrace{f[k - n\frac{M}{2}] e^{j\frac{2\pi}{M}(k-L-1)} e^{j\varphi_{m,n}}}_{f_{m,n}[k]}$$

Where L is the length of the so-called prototype filter f [k].

Then the orthogonality of the family of discrete-time functions $f_{m,n}[k]$ can be checked using again the real scalar product for this discrete-time function, i.e.:

$$\mathrm{Re}\left\{ \sum_{k \in Z} f_{m,n}^*[k] f_{m',n'}[k] \right\} = \delta_{m,m'} \delta_{n,n'}$$

This discrete-time formulation naturally leads to filter-bank-based realization schemes.

4.1.4 OFDM/OQAM prototype functions

Among the main prototype functions that could have been candidates in DVB-NGH standard, we can list:

- The IOTA function that constitutes a remarkable case of OFDM/OQAM modulation by many specific aspects. Probably the most surprising is the double orthogonalization procedure which, to the best of our knowledge, was never used before. However, the IOTA prototype function is time-continual and defined in an infinite interval that is not very convenient for burst transmission.
- The EGF prototype function that is a variant of the IOTA one. The EGF is given by a closed-form expression and it keeps the parameter, i.e. it is possible to favour with value, the time or the frequency dimension.
- The TFL prototype function that results from an optimization of the waveform carried out directly in discrete-time. Its main advantage is the possibility to get short prototypes, with duration (T_0) less than for CP-OFDM, that are well suited for transmission over time and frequency dispersive channels.
- The Frequency Selective (FS) prototype is also designed directly in discrete-time and is particularly appropriate for channels that are only selective in frequency.

Note also that some other prototype filters are available from the state-of-the-art on OFDM/OQAM [39] or on filter banks [40].

4.1.5 PAPR

It has been shown in [41] that OFDM/OQAM has a similar Complementary Cumulative Density Function (CCDF) as OFDM, as long as its prototype is orthogonal (TFL, FS) or nearly orthogonal (IOTA, EGF). Otherwise stated, the PAPR values and impact are identical with an OFDM or an OFDM/OQAM modulation scheme.

4.1.6 Main key points of CP-OFDM and OFDM/OQAM modulations

Table 20 gives a general idea of the main difference between CP-OFDM and OFDM/OQAM modulations.

Table 20: List of the main key points of OFDM and OFDM/OQAM modulations

Parameters	CP-OFDM	OFDM/OQAM
Symbols	Complex (QAM)	Real (PAM)
CP	Yes	No
Symbol rate	T0+CP	T0/2
Prototype function	Rectangular	IOTA, EGF, TFL …
Equalization	One tap	One tap
Implementation	FFT (T0)	FFT (T0/2) + polyphase filter
Orthogonality	Complex	Real
PAPR	0	0
Robustness to Doppler	+	++
Robustness to band limited interferers	+	++
Robustness to SFN	++	-

4.1.7 Hardware implementation

Figure 49 shows the hardware implementation block diagram that reflects what has already been prototyped by France Telecom; this hardware implementation has allowed the comparison of the main differences between CP-OFDM and OFDM/OQAM modulation in terms of complexity.

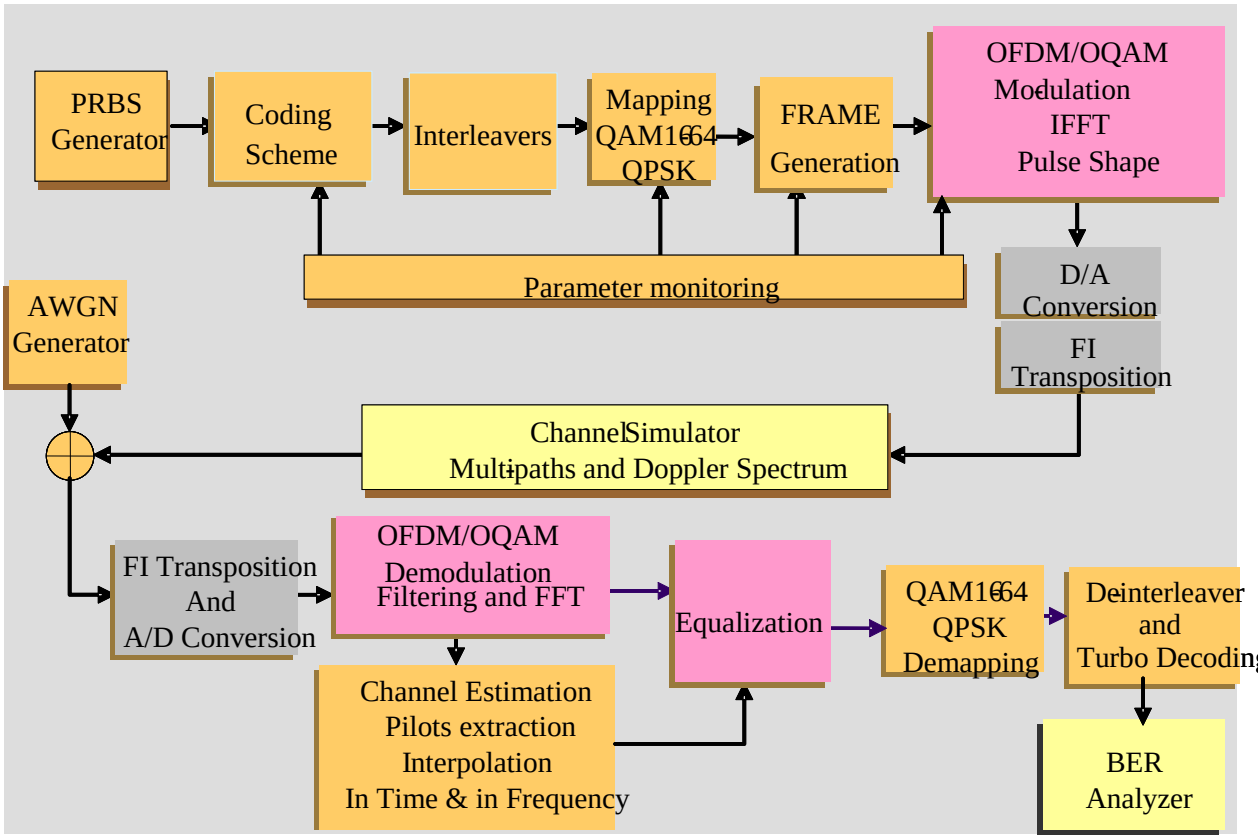

Figure 49: Example of hardware implementation block diagram

4.1.8 Implementation considerations

This section aims at introducing main differences between CP-OFDM and OFDM/OQAM at the hardware level.

Except the synchronization techniques using CP for correlation process, all the other synchronisation methods, which don't use the cyclic prefix, i.e. based on pilot sequence correlation known by the receiver, can still be used.

The hardware implementation impact, with regard to conventional OFDM, is mainly due to the prototype function pulse shaping. The complexity of this process greatly depends on the type of the chosen prototype function (e.g. IOTA, EGF and TFL).

The modulation requires some additional processing:

- OFDM/OQAM pulse shaping requires a set of $2L$ real multipliers (where L is the length of the truncated prototype function, e.g. L = 1,2 or 4) and $2L$ FIFO symbol memories.
- Inverse FFT requires doubling the process speed but still remains equivalent to OFDM IFFT because data are real.

The choice of the OFDM/OQAM prototype function can be carried out in relation with the propagation channel characteristics. This flexibility can be considered in hardware implementation by changing the waveform according to the scenario (fixed / portable / mobile).

4.1.9 OFDM/OQAM modulator

This section gives the implementation guidelines of an OFDM/OQAM modulator.

In a first step a complex symbol is split in real and imaginary parts; the $\pi/2$ rotation is added on each cell $a_{m,n}$ by (i^{m+n}) ("m" for frequency index). This modulation is performed in the real domain.

The modulator uses the inverse fast Fourier transform, which is similar to OFDM. The prototype filter is applied, in time domain, to the symbol; then after the τ_0 offset applied on the imaginary part, both parts are added at the end of the process.

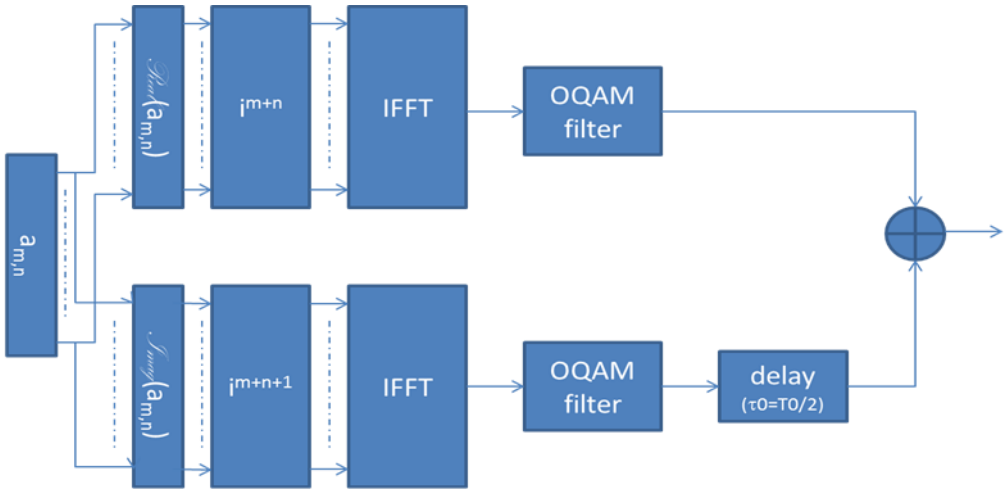

Figure 50: OFDM/OQAM Modulator

4.1.10 OFDM/OQAM demodulator

In this section, OFDM/OQAM demodulator is described. The blocks are the dual functions of those included in the modulator. The algorithm of "OQAM filtering" is equivalent to a windowing function of FFT (Fast Fourier Transform).

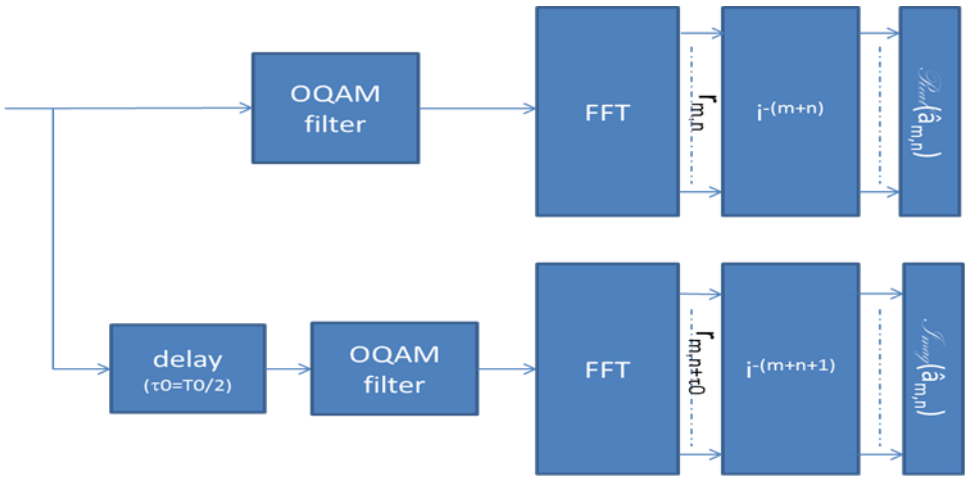

Figure 51: OFDM/OQAM demodulator

4.1.11 Complexity issue

A compared analysis of the hardware complexity of the CP-OFDM and OFDM/OQAM modulators and demodulators led to the results shown in Table 21 and Table 22.

Table 21: Result of the complexity analysis of the CP-OFDM and OFDM/OQAM modulators

CP-OFDM Mod (clk/2)	Logic cells		LC registers		Memory	
	Nb	%	Nb	%	Nb bits	%
CP insertion	204	1.90	69	0.84	262144	39.71
Time interleaver	1522	14.19	685	8.48	65536	9.93
IFFT (mode burst buffered)	7500	69.93	6518	80.67	262144	39.71
Framing	182	1.70	96	1.19	0	0.00
Mapping	447	4.17	188	2.33	0	0.00
Turbo encoder	870	8.11	524	6.49	70304	10.65
total	10725	100	8080	100	660128	100
	Logic cells		LC registers		Memory	
OFDM/OQAM Mod	Nb	%	Nb	%	Nb bits	%
TFL1 Filtering	223	1.52	175	1.59	106496	10.38
IFFT (streaming)	7238	49.38	6208	55.91	327680	31.98
Framing	405	2.76	257	2.31	0	0
Interference Matrix	3768	25.71	2916	26.26	393216	38.38
Rephase	212	1.45	112	1.01	0	0
Time interleaver	1549	10.57	712	6.41	65536	6.4
Mapping	386	2.63	197	1.77	61440	6
Turbo encoder	876	5.98	526	4.74	70240	6.86
total	14657	100	11103	100	1024608	100
Increase (%)	36.66		37.41		55.21	

Table 22: Result of the complexity analysis of the CP-OFDM and OFDM/OQAM demodulators

CP-OFDM Demod	Logic cells		LC registers		Memory	
	Nb	%	Nb	%	Nb bits	%
CP Cancellation	295	0.70	133	0.48	155648	8.08
IFFT	7453	17.70	6301	22.58	327680	17.02
Equalization	7336	17.42	3712	13.30	1024	0.05
Time Interpolation	667	1.58	479	1.72	360496	18.72
Freq. Interpolation	1970	4.68	1344	4.82	375792	19.51
Time de-interleaver	1204	2.86	768	2.75	262144	13.61
DeMapping	108	0.26	85	0.30	0	0.00
Turbodecoder	23076	54.80	15087	54.06	442880	23.00
total	42109	100	27909	100	1925664	100
	Logic cells		LC registers		Memory	
OFDM/OQAM Demod	Nb	%	Nb	%	Nb bits	%
TFL1 Filtering	334	0,83	202	0,75	245776	9,68
FFT	7209	17,93	6201	22,90	327680	12,90
Rephase	257	0,64	132	0,49	0	0,00
Equalization	4563	11,35	2636	9,74	1024	0,04
Time Interpolation	1688	4,20	735	2,71	942080	37,10
Freq. Interpolation	2108	5,24	1343	4,96	375792	14,80
Time de-interleaver	1204	3,00	768	2,84	262144	10,32
DeMapping	231	0,57	139	0,51	0	0,00
Turbodecoder	22604	56,23	14919	55,10	384708	15,15
total	40198	100,00	27075	100,00	2539204	100
Increase (%)	-4.54		-2.99		31.86	

According to the reported comparison tables we find that the OFDM/OQAM receiver needs 31.86% extra memory compared with CP-OFDM system but less logical cells and registers. It is worth mentioning that the reported values are obtained from the basic implementation VHDL without any sophisticated design from the efficiency point of view by the experts.

4.1.12 Performance description

4.1.12.1 Presentation of TFL1 OQAM filter, proposed for DVB-NGH

For DVB-NGH, France Telecom proposed the so-called **TFL1 filter**, among the large family of OFDM/OQAM filters. This filter exhibits better performances against Doppler effect and its length is equal to the FFT length; the complexity is proportional to the length of the filter (L=1). The coefficients of this filter, in 2K FFT mode, are represented in Figure 52.

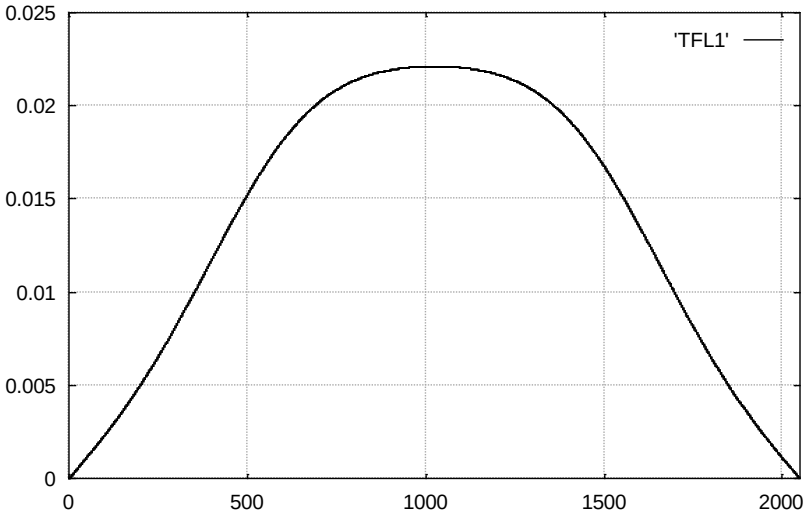

Figure 52: Coefficients of TFL1 OQAM filter for 2K FFT case

4.1.12.2 Performance of OFDM/OAQM against SFN and Doppler

Performance of OFDM/OQAM modulation in an SFN scenario and its robustness to Doppler effect induced by speed of the receiver (mobile scenario) has been obtained in France Telecom simulation chain with the following components:

- A random data generator;
- A double- binary turbo encoder of 1504 info size bits (mother code rate 1/2);
- A bit interleaver of the same size for both systematic and redundancy parts;
- A puncturing component in order to achieve the 1/2, 7/12, 2/3, 3/4, 5/6 and 11/12 coding rates;
- A pre-mapping block that optimizes the results for low SNR values (LSB and MSB bit partitioning);
- A mapping component allowing QPSK, 16QAM, 64QAM and 256QAM mappings to be generated;
- DVB-T framing in 2K mode;
- A framing module that inserts the scattered pilots (and that will allow to process the intrinsic interference produced on the pilot by the neighbouring data);
- A phase component that corresponds to the ambiguity function of the OFDM/OQAM filters;
- A 2K FFT modulation;
- The OFDM/OQAM prototype filter: TFL1.

Figure 53 and Figure 54 present the performance results of OFDM/OQAM-TFL1 filter and CP-OFDM for a target BER=10^{-4}, the first figure corresponding to the resistance to a Doppler shift and the second figure corresponding to the performance in an SFN channel (two paths with 0dB).

The parameters of the simulation chain are: 64QAM, coding rate 1/2, no time interleaver, 2K FFT mode.

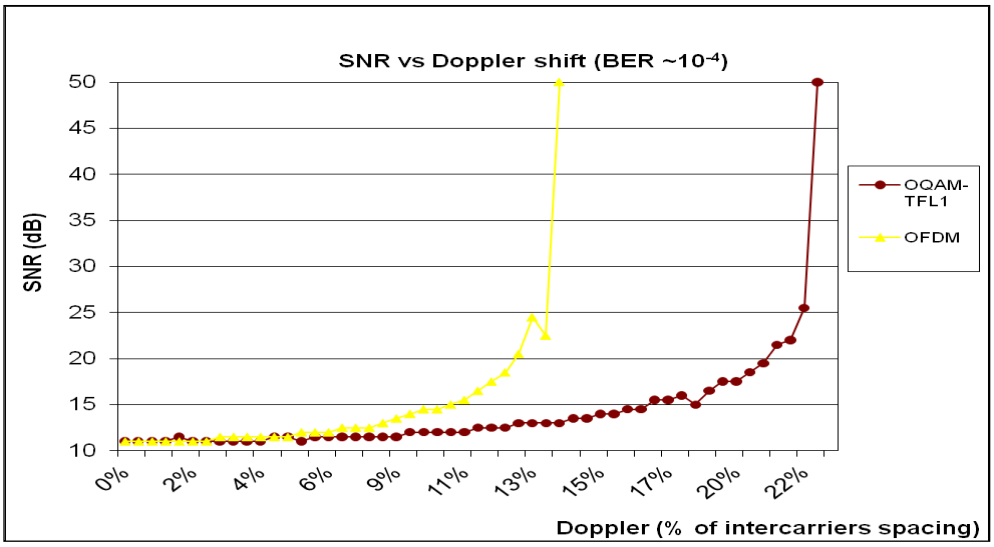

Figure 53: Performance of OFDM and OFDM/OQAM-TFL1 against Doppler shift.

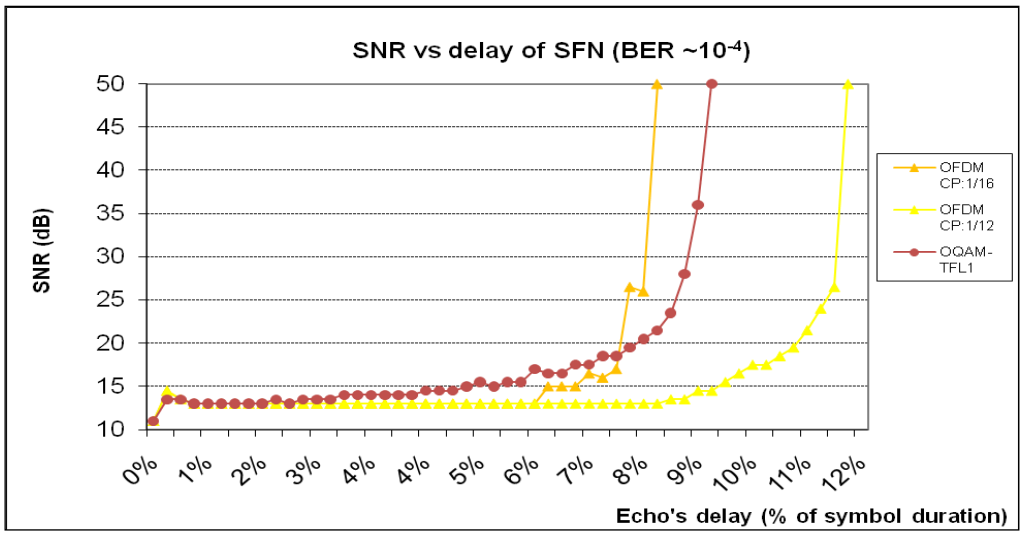

Figure 54: Performance of OFDM and OFDM/OQAM-TFL1 against SFN channel

It is possible to improve the performance of the OFDM/OQAM chain in an SFN channel with a shift of the window on receiver side, searching for a synchronisation around the barycentre of the channel impulse response. Figure 55 shows the performance improvement for this chain as a function of the window shift, keeping a target BER=10^{-4}. Figure 56 shows the effect of the delay value on Doppler performance (single path, no SFN).

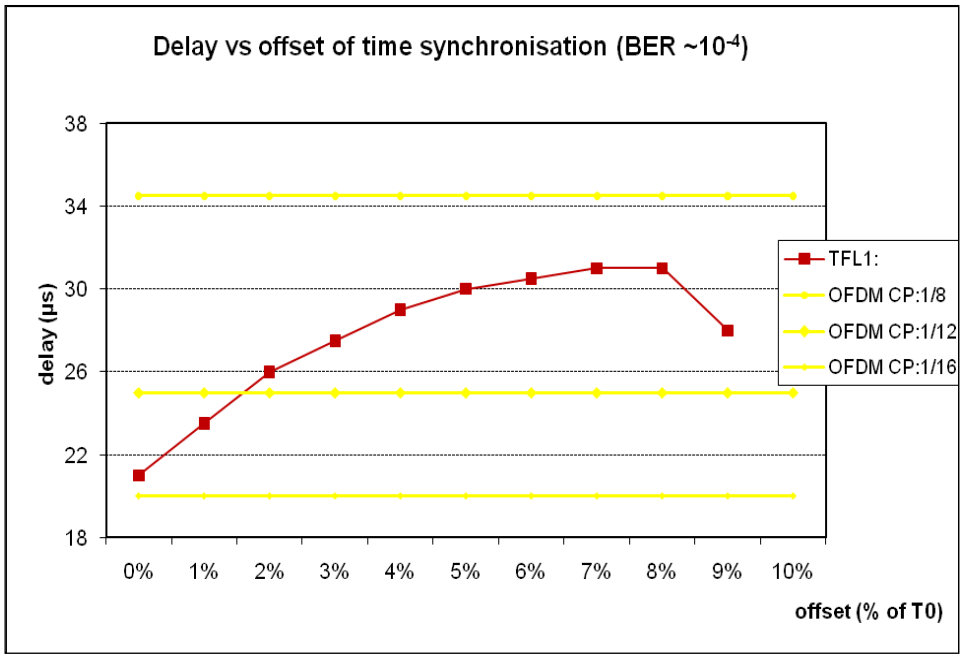

Figure 55: Performance of OFDM and OFDM/OQAM-TFL1 against SFN channel with window offset.
Comment: the maximum robustness of the OFDM/OQAM receiver, with this window offset, is close to the OFDM case with a cyclic prefix equal to 1/8.

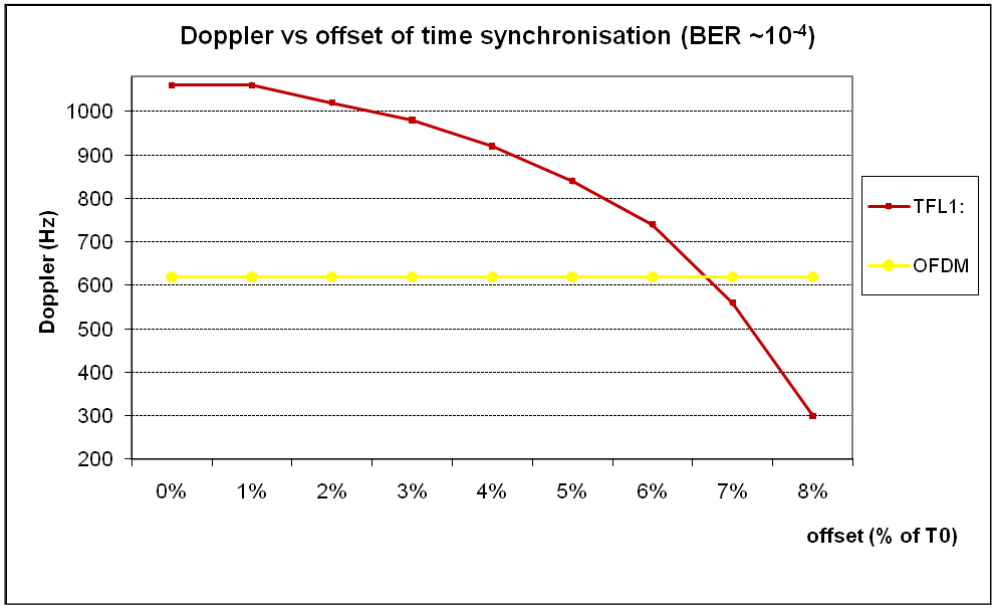

Figure 56: Performance of OFDM and OFDM/OQAM-TFL1 against Doppler with window offset

With a window shift less than 7% of T0 (symbol duration), OFDM/OQAM modulation still outperforms classical CP-OFDM modulation.

4.1.12.3 Extension of these results for different FFT sizes

The performance for "OFDM-OQAM-barycentre" corresponds to a shift of the windows filter, in this case the shift is equal to 5% of symbol duration. The results displayed in Figure 57 arise from the interpolation of the performance of FFT-2k.

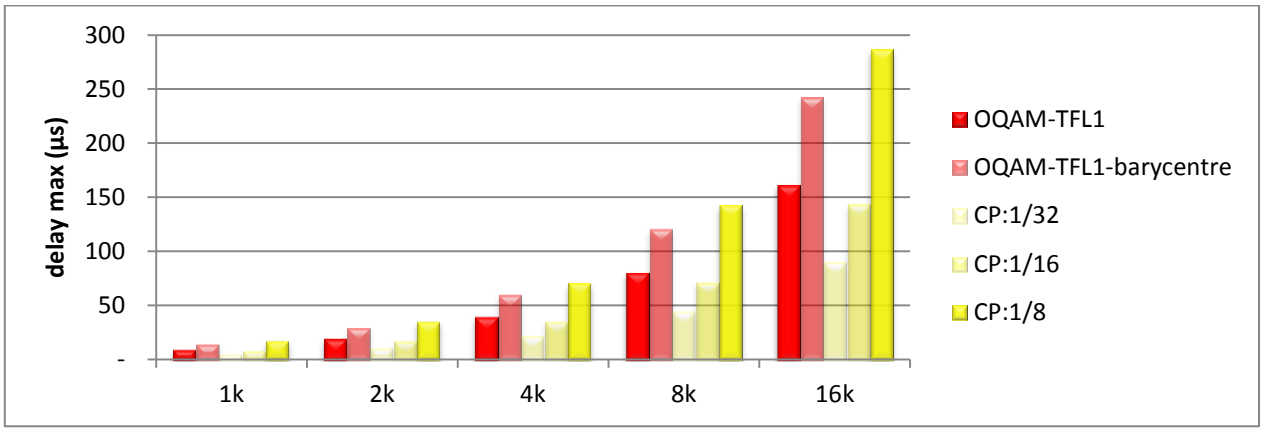

Figure 57: Performance comparison of CP-OFDM and OFDM/OQAM-TFL1 for different FFT sizes (window shift = 5% T0)

4.1.13 Specific framing for DVB-NGH with OFDM/OQAM

In this section we describe some specific adaptations in terms of framing through some cases:

- Association between OFDM and OFDM/OQAM.
- Cancellation of intrinsic interferences for scattered pilots and continual pilots.
- Scattered pilot patterns as a function of the performance of OFDM/OQAM-TFL1 and as a function of channel estimation.

4.1.13.1 Cancellation of intrinsic interferences

OFDM/OQAM modulation is orthogonal only in the real domain; but the propagation channel is complex and for this reason it is necessary to cancel the intrinsic interference of the scattered pilots "P". This operation is possible directly on modulator side. To do so, it is necessary to compute the intrinsic interference coming from TFL1 filter.

For example if "P" is the position of the scattered pilot, the intrinsic interference noted "I" is dependent of the value of the data near the pilot tone on one side and of the coefficients "$Ci_{m,n}$" on the other side, coefficients described in the table below:

Table 23: Coefficients of the intrinsic interference of the OFDM/OQAM-TFL1 filter

m

0,007	0	-0,007
-0,022	0,040	-0,022
-0,112	0	0,112
-0,228	0,538	-0,228
-0,281	P	0,281
-0,228	-0,538	-0,228
-0,112	0	0,112
-0,022	-0,040	-0,022
0,007	0	-0,007

n

For example, considering the scattered pilot $P_{m,n}$, the position of the specific element "I" used to cancel interference on "P" will be in coordinates (m+1,n) and the value of this element will be :

$$I_{m+1,n} = -\frac{1}{Ci_{m+1,n}} \sum_{n-1}^{n+1} \sum_{m-4}^{m+4} Ci_{m,n} \cdot d_{m,n} \quad \text{with} \quad Ci_{0,0} = 0$$

The performances of intrinsic interference cancellation scheme on imaginary part of scattered pilot depends on the number of the coefficients (described in Table 23) used.

The couple of pilots scattered "P" and interference cancellation "I" is equivalent to a complex scattered pilot in OFDM system.

4.1.13.2 Insertion of pseudo continual pilots

In broadcasting system it is necessary to evaluate the common phase error (CPE) between two successive symbols. This evaluation will be carried out by continual pilots in OFDM system.

For OFDM/OQAM system we use "pseudo" continual pilots to achieve this function, because intrinsic interferences cannot be easily cancelled with continual pilots (similar to conventional OFDM). However if the framing provides a couple of pilots, it is possible to evaluate the CPE between this pilots. The typical related framing will be presented below.

With "d" for data, "C" for pseudo continual pilot and "Ic" pilot for cancellation of intrinsic interferences on imaginary part of pilot "C".

This framing allows the estimation of the common phase error (CPE) every OFDM/OQAM symbol under τ_0 (T_0/2) sampling.

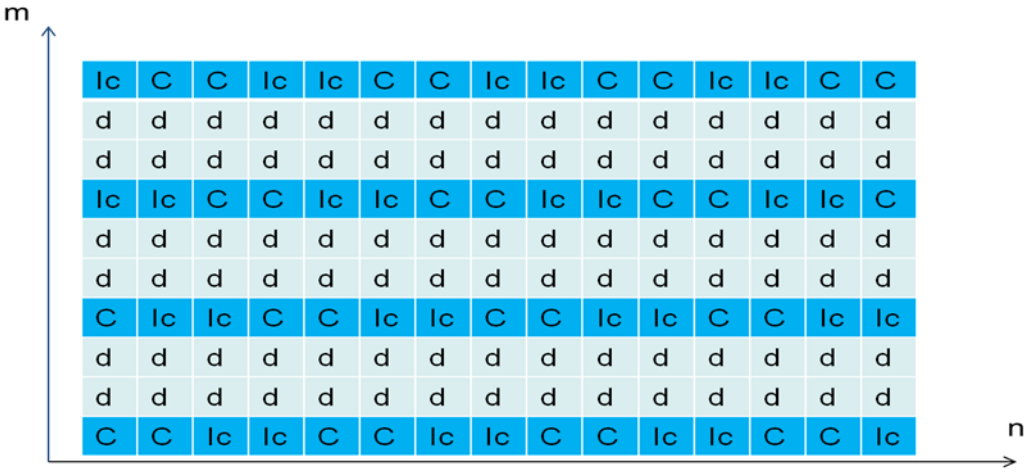

Figure 58: Framing for pseudo continual pilots

4.1.13.3 Association between OFDM and OFDM/OQAM symbols

DVB-NGH system could be transmitted in DVB-T2 Future Extension Frame. One constraint already exists at the beginning of this FEF: a P1 symbol will be the first symbol of the frame. This symbol is an OFDM modulated symbol.

Nevertheless it is possible to associate OFDM symbols with OFDM/OQAM symbols. One possible

configuration is presented in Figure 59.

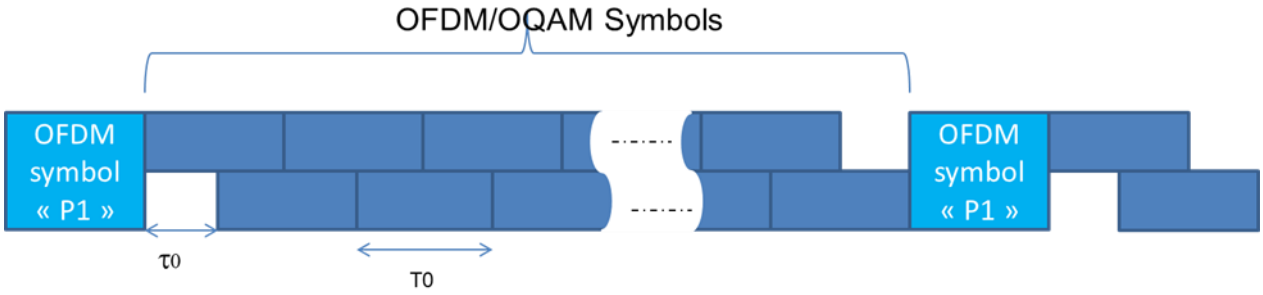

Figure 59: Framing for OFDM and ODFM/OQAM symbols

Only half a symbol is wasted at the end of the frame because an overlap-add operation is done between real and imaginary parts of a symbol, so the loss in spectral efficiency is really not significant considering realistic frame lengths. It is possible to define a synchronization symbol looking like P1 but using ODFM/OQAM modulation.

4.1.14 Scattered pilot insertion

The scattered pilot patterns must be adapted to the performances of OFDM/OQAM-TFL1 filter in regards to the channel variations in time and frequency domains.

The scattered pilots are used to estimate the propagation channel. The periodicity in time allows following the Doppler effect and the periodicity of scattered pilots in frequency domain allows to estimate the variation due to the multiple echoes.

The periodicity in time is D_y=4, where "D_y" corresponds to the OFDM/OQAM sampling D_y=4*τ_0.

The periodicity in frequency domain is equal to X=12*f_0 with f_0=1/T_0.

This means that after time interpolation there is one pilot each "D_x=6" sub-carrier in frequency domain. Figure 60 gives this repartition of scattered pilots optimized for OFDM/OQAM/TFL1 filter.

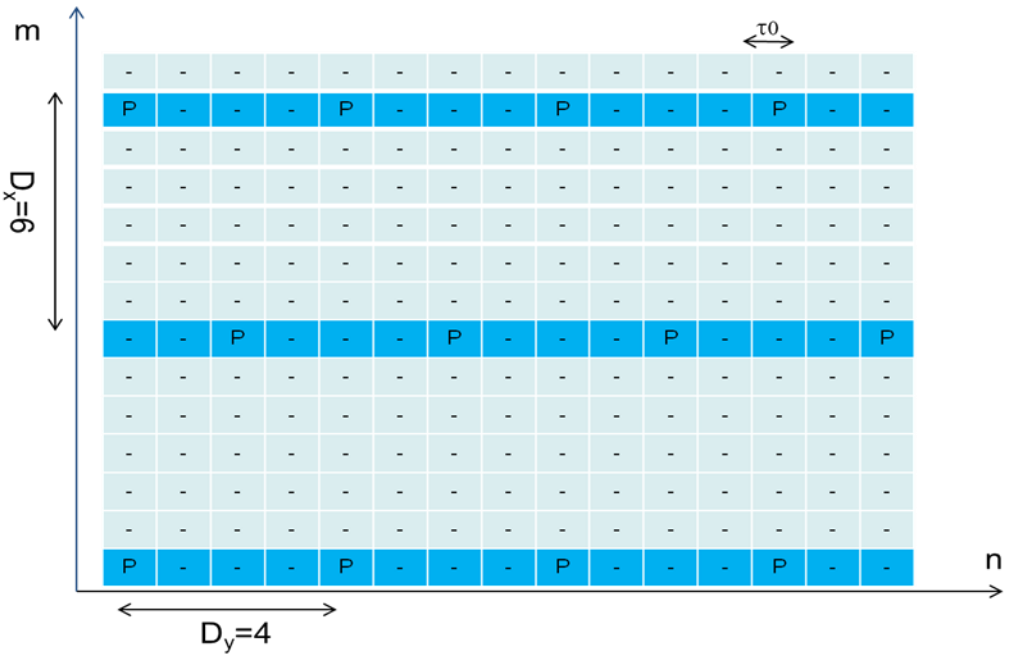

Figure 60: Scattering pilots for ODFM/OQAM framing

4.1.15 Alamouti coded OFDM/OQAM

One of the major problems for the OFDM/OQAM system is its intrinsic interference, which causes a difficulty in operating Alamouti encoding. The conventional Alamouti coding scheme cannot work properly with OFDM/OQAM. The most recently published research, i.e. [41], gives a possibility for OFDM/OQAM using Alamouti block encoding at the cost of memory increase on the receiver side or spectral efficiency lost by zero padding.

4.1.16 Complexity reduction of the FBMC/OQAM transmitter

In a previous section, we have proposed an alternative to the well-known OFDM modulation which undoubtedly remains the flagship of all multicarrier modulation schemes because of its simple principle and ease of realization. Indeed, its principle which is to split a broadband signal into a set of narrowband signals makes it robust for transmission over multipath channels. Furthermore, its implementation can take advantage of Fast Fourier Transform (FFT) algorithms. However, OFDM requires the addition of a Cyclic Prefix (CP) which reduces its useful data rate and, moreover, its rectangular shape leads to a poor frequency behaviour. On another hand, there is a Filter Bank MultiCarrier (FBMC) scheme that can get rid of these two drawbacks while keeping most of the simplicity and efficiency features of OFDM. Its basic idea, introduced a long time ago [42] is to cleverly split the complex QAM symbols that have to be transmitted into their real and imaginary parts leading to the OFDM with Offset QAM (OQAM) mapping. With this principle, orthogonality only needs to be satisfied in the real field, thus leaving room to the introduction of pulse shapes being well localized in time and frequency and, therefore, for which no CP is required. Therefore in previous sections we have proposed this filter bank-based scheme known as FMBC/OQAM or OFDM/OQAM. Though the corresponding proposal has not been retained for the DVB-NGH standard, it is still supported in other types of applications, e.g. in cognitive radio [43], [44], and is constantly being improved by various researchers from academy and industry. Here we want to highlight significant improvements of the FMBC/OQAM systems that could be of interest for future terrestrial broadcast systems. A first one described here is a proposal for a fast implementation of the FBMC/OQAM modulator while in Section 4.1.17 we introduce a new equalization scheme that takes advantage of the generally discarded imaginary component which is present in the OFDM/OQAM receiver.

4.1.16.1 Introduction

The double advantage provided by OFDM/OQAM, no CP and good time-frequency localization, has nevertheless a price. Indeed, due to the OQAM time offset which corresponds to half a QAM symbol duration, for FBMC/OQAM, as explained in previous sections, the Inverse FFT (IFFT) has to operate at a double rate compared to the one used for OFDM in similar bit rate conditions. Furthermore, though the OQAM symbols are real-valued, there are no obvious simplifications for the IFFT algorithm. Indeed, a pre-processing stage is required to implement the OQAM staggering rule and to insure the overall system to be causal, so that the IFFT inputs are no longer real-valued [45]. Consequently, the IFFT computational complexity of FBMC/OQAM is twice compared to the one of the conventional OFDM. Moreover, since the FBMC/OQAM prototype filter is no longer rectangular, the filtering stage adds an additional computational complexity to FBMC/OQAM system, compared to OFDM one. However, in practical setup, this extra complexity is less than the one added by the IFFT as, for a given prototype filter length, it decreases when the number of sub-carriers increases (see Table 24 and comparison of IFFT and filter complexities). The previous attempts [46][47][48] to reduce the OFDM/OQAM modulator complexity did not take into account the system causality, i.e., the reconstruction delay. Thus, they cannot be directly applied in practice.

In this deliverable, we consider the causal FBMC/OQAM systems that are described in [45]. The key idea we propose to exploit, in order to reduce the computational complexity, takes advantage of a conjugate-symmetry relation between the outputs of the IFFT stage. Then, an appropriate selection over the IFFT output indices opens the possibility to use a pruned IFFT algorithm. So that compared to a standard inverse Fourier transform the computational cost can be reduced by more than one half.

Our presentation is organized as follows. Section 4.1.16.2 shortly describes the FBMC/OQAM system model. In Section 4.1.16.3 we derive the conjugate symmetry relations and show how these relations can be used afterwards to reduce the IFFT complexity by the means of a pruned IFFT algorithm. In Section 4.1.16.3.3, a complexity comparison is carried out between OFDM and FBMC/OQAM.

4.1.16.2 FBMC/OQAM System model

The discrete time FBMC/OQAM baseband signal can be written as follows [45]:

$$s[k] = \sum_{n=-\infty}^{+\infty} \sum_{m=0}^{2N-1} a_{m,n}\, \psi_{m,n}[k] = \sum_{n=-\infty}^{+\infty} \sum_{m=0}^{2N-1} a_{m,n} g[k-nN] e^{j\frac{2\pi}{2N}m(k-D/2)} e^{j\phi_{m,n}} \qquad (1)$$

where M=2N is the is the number of sub-carriers and the $a_{m,n}$'s are real data obtained from the real and imaginary parts of a QAM constellation. g(n) is a prototype filter of length L and a delay factor D with the relation L=D+1. For the OFDM/OQAM system, $\psi_{m,n}$ forms an orthogonal basis and the same prototype filter g(n) is used at the receiver (RX) side. The term $e^{j\phi_{m,n}}$ ensures a $\pi/2$ phase difference in time and frequency between the real data $a_{m,n}$. In general, it is chosen such that

$$\emptyset_{m,n} = \frac{\pi}{2}(m+n) \pm \rho\pi nm$$

where $\rho \in \{0,1\}$. Without loss of generality, here we take ρ=0. The FBMC/OQAM modulator is depicted in Figure 61. In this scheme, the polyphase components $G_k(z)$ of the prototype filter h(n) are defined for $0 \leq k \leq M$-1 by

$$G_k(z) = \sum_n h[k+nM] z^{-n}$$

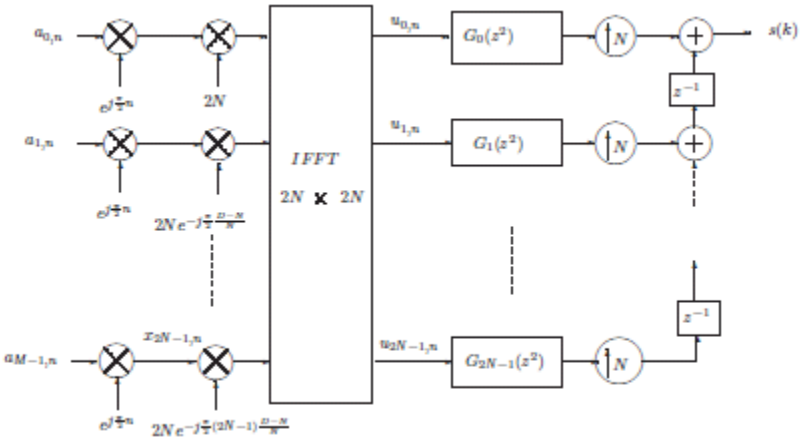

Figure 61: FBMC/OQAM modulator.

4.1.16.3 Complexity reduction method

4.1.16.3.1 Relations between the IFFT outputs

For the causal OFDM/OQAM system, the prototype filter length L has a direct impact on the IFFT outputs because of the last column of multiplications involving $D=L$-1 at the IFFT inputs. For a prototype filter of arbitrary length we can write $L=qM+q_1$, where q and q_1 are integers such that $q\geq 1$ and $0 \leq q_1 \leq M$-1 [49].

Depending on the parity of q_1, we can distinguish the following cases.

Case 1: q_1 is even

In this case, the length of the prototype filter can be written as $L=qM+2p$, where $0 < 2p \leq M$-1. Then, with the restriction that M has to be divisible by 4, depending on the value of $2p$, we have the following relations at the IFFT output.

If $0 \leq 2p \leq M/2$-1: then the expression of the IFFT output at index k is given for $0 \leq k \leq M/4+p$-1, by,

$$u_{k,n} = e^{j\frac{\pi n}{2}} \sum_{m=0}^{M-1} a_{m,n}\, e^{-jm\frac{\pi D-N}{2\ N}} e^{-j2\pi\frac{mk}{M}} = e^{j\frac{\pi n}{2}} \sum_{m=0}^{M-1} a_{m,n}\, (-1)^{mq}\, e^{j\frac{\pi m}{2}} e^{j\frac{\pi m}{2N}} e^{j2\pi\frac{m(k-p)}{M}} \qquad (2)$$

and, as shown in [50],

$$u_{\frac{M}{2}+2p-k-1,n} = (-1)^n u^*_{k,n} \qquad (3)$$

where (.)* denotes complex conjugation.

Furthermore, for $0 \leq k \leq M/4-p$-1, we have:

$$u_{\frac{M}{2}+2p+k,n} = e^{j\frac{\pi n}{2}} \sum_{m=0}^{M-1} a_{m,n}\, (-1)^{mq}\, e^{j\frac{3\pi m}{2}} e^{j\frac{\pi m}{2N}} e^{j2\pi\frac{m(k+p)}{M}}$$

and

$$u_{M-1-k,n} = (-1)^n\, u^*_{\frac{M}{2}+2p+k,n} \qquad (4)$$

If $M/2 \leq 2p \leq M$-1 then $2p$ can be written as $2p=M/2+2p'$ where $0 \leq 2p' \leq M/2$-1, then, for $0 \leq k \leq p'$-1, we have:

$$u_{k,n} = e^{j\frac{\pi n}{2}} \sum_{m=0}^{M-1} a_{m,n}\, (-1)^{mq}\, e^{j\frac{\pi m}{2N}} e^{j2\pi\frac{m(k-p\prime)}{M}}$$

and

$$u_{2p\prime-1-k,n} = (-1)^n\, u^*_{k,n} \qquad (5)$$

Furthermore, for $0 \leq k \leq M/2-p'$-1, we have:

$$u_{k+2p',n} = e^{j\frac{\pi n}{2}} \sum_{m=0}^{M-1} a_{m,n}\,(-1)^{mq}\, e^{j\frac{\pi m}{2N}} e^{j2\pi\frac{m(k+p')}{M}}$$

and

$$u_{M-1-k,n} = (-1)^n\, u^*_{k+2p',n} \qquad (6)$$

In Figure 62 we provide an illustration of the complex-conjugate (CC) relationships (6) at the IFFT ouput in the case of a prototype filter of length $L=qM$.

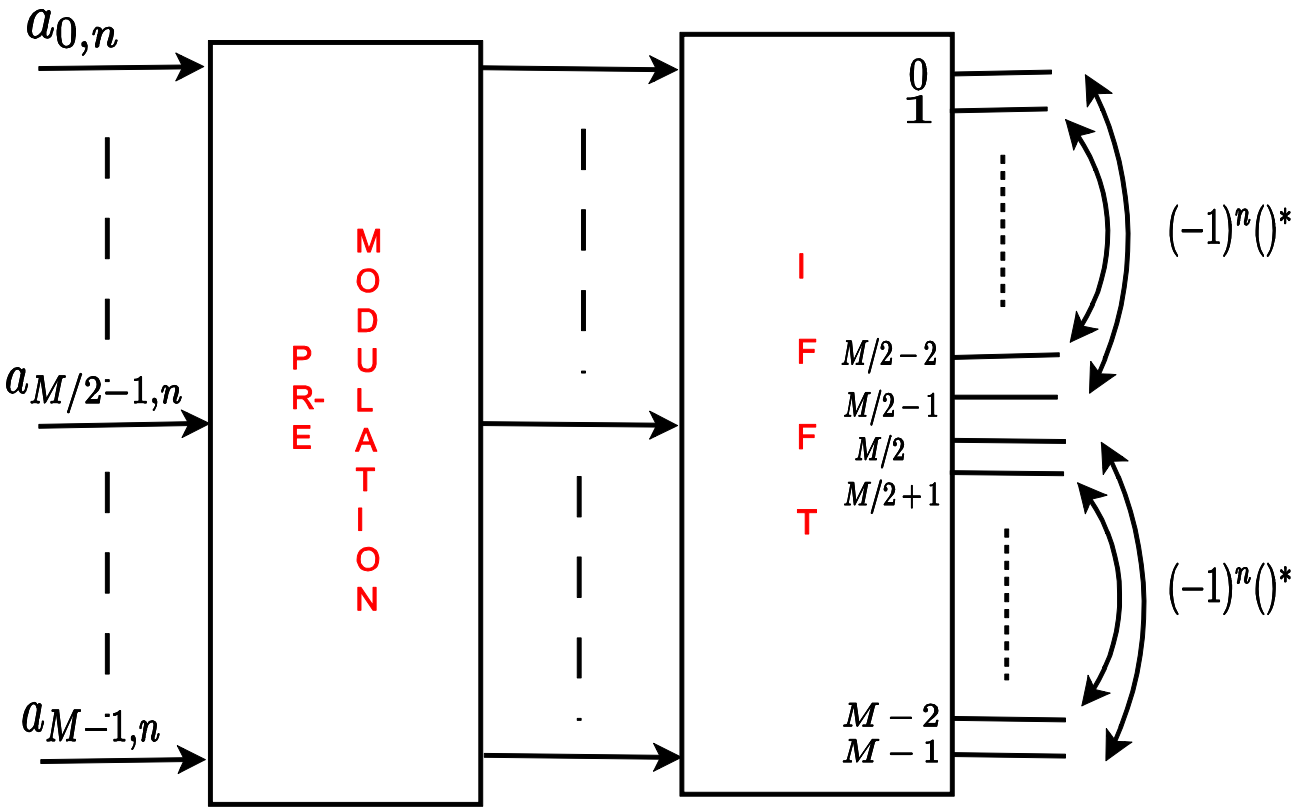

Figure 62: Illustration of the IFFT output relations for a prototype filter of length *L=qM*.

Case 2: q_1 is odd

The length of the prototype filter can be written as $L=qM+2p+1$. In this case, for $0 \le k \le M-1$, the IFFT outputs are given by

$$u_{k,n} = e^{j\frac{\pi n}{2}} \sum_{m=0}^{M-1} a_{m,n}\,(-1)^{mq}\, e^{j\frac{\pi m}{2}} e^{j2\pi\frac{m(k-p)}{M}} \qquad (7)$$

Similarly to [47], the outputs expression (7) is equivalent to the one obtained by an IFFT with real inputs $(a_{m,n}(-1)^{mq})$ for which a circular shift to the left by $M/4$-p is carried out at the output. In Figure 63 we illustrate the case of a real-valued IFFT input together with a circular shift at the output in the case where the prototype filter length is given by $L=qM+2p+1$.

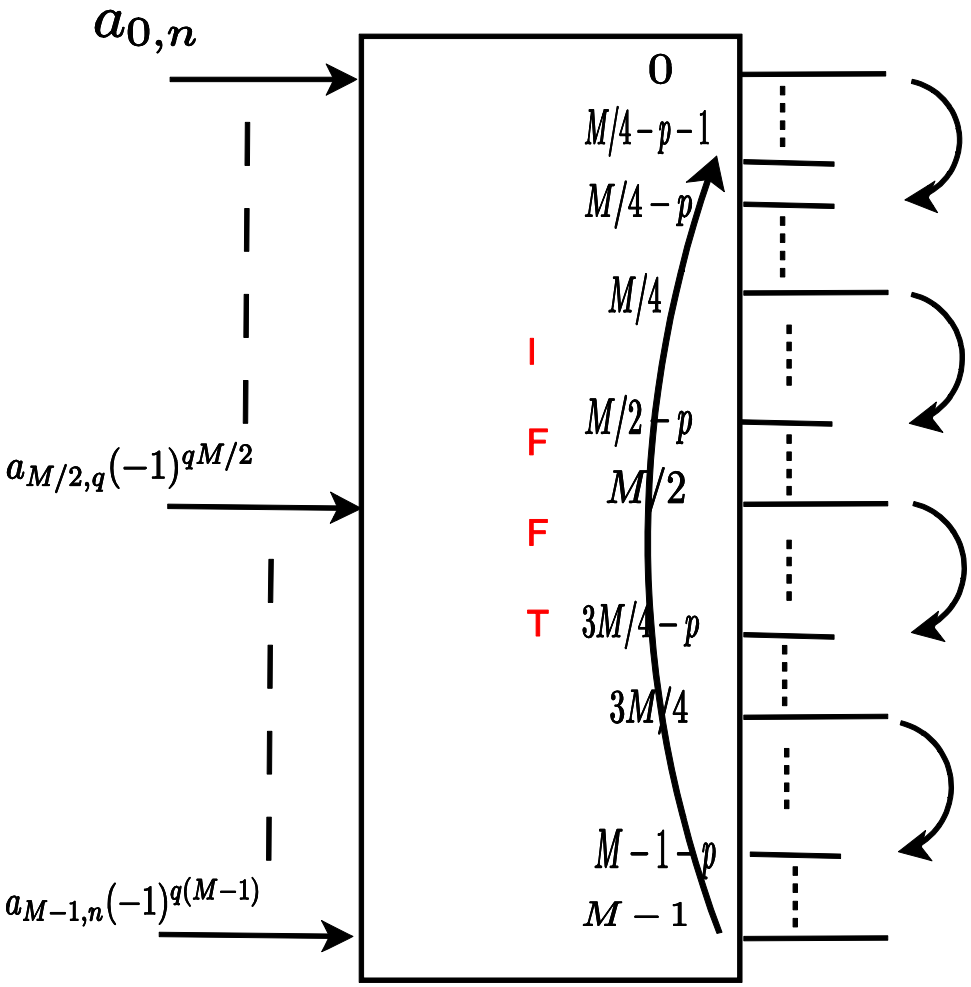

Figure 63: Efficient IFFT implementation in the case of a prototype filter of length $L=qM+2p+1$.

4.1.16.3.2 Pruned IFFT algorithm

Firstly, we consider the case where the prototype filter has an even length, i.e. q_1 is even. In this case, we can see from relations (3) and (4) or (5) and (6) that only half of IFFT outputs are needed to reconstruct the total set of outputs. There are several possibilities to choose the indices for this half IFFT outputs which will participate in the pruned IFFT algorithm.

As it is well known, most of the (I)FFT algorithms, e.g. the "radix-2" [51] or the "split radix" (SR) [52], based on "radix-2" and "radix-4", use elementary "butterfly" structures. To reduce at most the computational complexity, we must select the output indices that will involve a computation with the smallest number of butterflies. If we choose indices implying computation with distant butterflies in the flow chart, we can reach this goal.

According to (3) and (4) or (5) and (6) one can note that these complex conjugate (CC) relationships are between odd indices and even ones. In order to reduce at most the computational complexity, we choose the output indices of the pruned IFFT having the same parity together with a decimation-in-frequency (DIF) algorithm [53]. It is worth noting that the notion of DIF is generally used for FFT algorithms. Here, the DIF algorithm used to compute the IFFT is identical to the one used to compute an FFT, i.e. for decimation of the output indices, we just have to change the sign of the power of the complex exponential in the butterflies.

As an example, let us take the SR algorithm [52] which requires a reduced number of real multiplications and additions compared to other algorithms. For a frequency complex sequence X(m) with m=0,…, M-1and $M=2^r$, the DIF IFFT algorithm considers r stages of decomposition to calculate

$$x[k] = \sum_{m=0}^{M-1} X[m]\, W_M^{mk} \quad with\, W = e^{j\frac{2\pi}{M}}$$

At each stage we have the following decomposition

$$\begin{cases} x[2k] = \sum_{m=0}^{M/2-1} [X[m] + X\left[m + \frac{M}{2}\right]]\, W_{M/2}^{mk} \\ x[4k+1] = \sum_{m=0}^{M/4-1} [X_R[m] + jX_I[m]]\, W_M^m W_{M/4}^{mk} \\ x[4k+3] = \sum_{m=0}^{M/4-1} [X_R[m] - jX_I[m]]\, W_M^{3m} W_{M/4}^{mk} \end{cases} \quad (8)$$

with $X_R[m]=X[m]-X[m+M/2]$ and $X_I[m]=X[m+M/4]-X[m+3M/4]$. This decomposition consists in the computation of the even indices using an IFFT of size $M/2$ and of the odd indices using two IFFTs of size $M/4$ but at the cost of $M/2$-4 non trivial complex multiplications (μ_c), i.e. the multiplications by W_M^m and W_M^{3m} for $m \neq \{0, M/8\}$ and 2 multiplications by the eighth root of unity. Thus, for the pruned IFFT algorithm, it is more advantageous in terms of complexity to calculate the even indices only. According to (8), the computational complexity to calculate the even indices of an IFFT of size M is equivalent to calculate an IFFT of size $M/2$ plus $M/2$ complex additions (to calculate the sum of $X[m]+X[m+M/2]$ for $m=0, .., M/2-1$). As we know, the arithmetic complexity of the SR algorithm [52] is equivalent to $M\log_2 M-3M+4$ real multiplications (μ_R), and $3M\log_2 M-3M+4$ real additions (α_R), using the fact that one μ_c can be implemented with $3\mu_R$ and $3\alpha_R$ [54]. Applying our pruned IFFT algorithm, we reduce the arithmetic complexity of the FBMC/OQAM IFFT stage to $(M/2)\log_2 M-2M+4$ instead of $M\log_2 M-3M+4$ (α_R) and to $(3M/2)\log_2 M-2M+4$ instead of $3M\log_2 M-3M+4$ (α_R), i.e. in both cases, multiplication and addition, the gain is greater than 50%.
Figure 61 shows an example of the SR flow graph to compute a 32-point IFFT. We can see that the arithmetic complexity to calculate the even indices (the upper half) is equivalent to calculate a 16-point IFFT plus 16 complex additions.

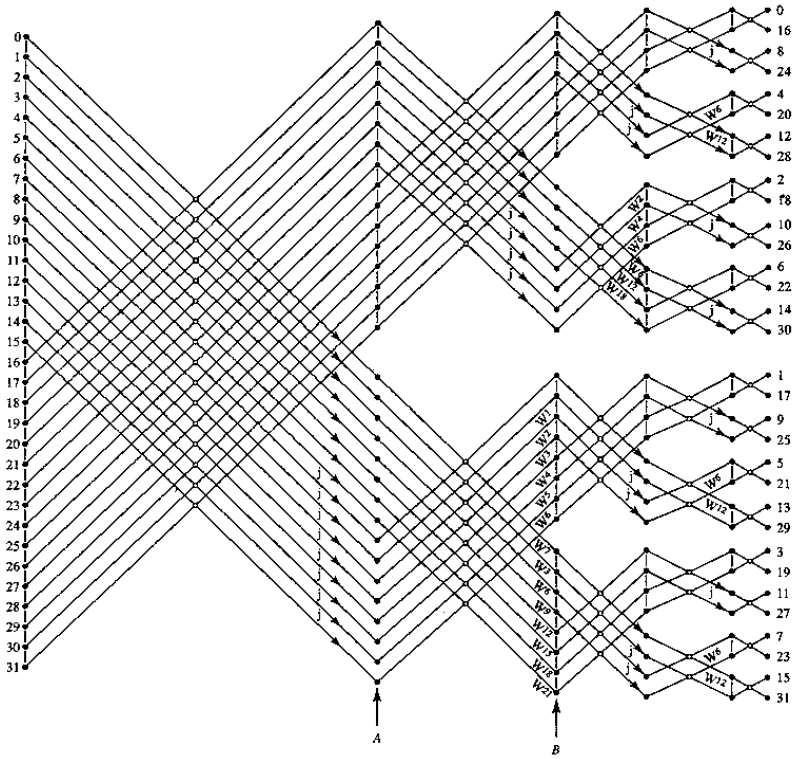

Figure 64: Flow graph for DIF SR algorithm for M=25, W=exp(j2π/32)(resp. exp-j2π/32) for the IFFT (resp. FFT): Source [52].

Similarly, using the radix-2 DIF algorithm, we can easily show that the cost to calculate the even indices of an IFFT of size M is equivalent to calculate an IFFT of size $M/2$ plus $M/2$ complex additions. We have always a gain greater than 50% with respect to μ_R and α_R.
If the prototype filter has an odd length, according to (7), the IFFT has real-valued inputs. Then, using the SR algorithm [55] the arithmetic complexity in this case is equivalent to $(M/2)\log_2 M-(3/2)M+2$ μ_R (gain equal to 50%) and $(3/2)M\log_2 M-(5/2)M+4$ α_R (gain greater than 50%).

4.1.16.3.3 Complexity comparison

To give a more precise view of the gain that can be expected on the overall FBMC/OQAM system by a pruned IFFT implementation for given M and L values, one can report to Table 24. Also in order to get a fair comparison with the OFDM systems, the computational cost takes into account one complex symbol for OFDM and two real data symbols for FBMC/OQAM. Thus, the number of IFFTs is one for OFDM and two for FBMC/OQAM.

Table 24: Complexity comparison between OFDM (for one complex symbol) and FBMC/OQAM systems (for two real symbols) for a prototype filter of length $L=qM$.

	Operation	Pre-modulation	IFFT(SR)	Filtering	Post-polyphase
OFDM	+	0	$3M\log_2 M - 3M + 4$	0	0
	×		$M\log_2 M - 3M + 4$	0	0
FBMC/OQAM before reduction	+	0	$2(3M\log_2 M - 3M + 4)$	0	$(2q-1)M$
	×	$4M$	$2(M\log_2 M - 3M + 4)$	$4qM$	0
FBMC/OQAM after reduction	+	0	$2((3M/2)\log_2 M - 2M + 4)$	0	$(2q-1)M$
	×	$4M$	$2((M/2)\log_2 M - 2M + 4)$	$4qM$	0

For the FBCM/OQAM system, we also have a pre-processing stage which is, arithmetically, equivalent to M (real by complex) multiplications. Table 24 shows the comparison, in terms of real arithmetic operations, between OFDM and FBMC/OQAM, applying or not the complexity reduction for the FBMC/OQAM system. The comparison is carried out for a prototype filter of length $L=qM$. The polyphase filtering stage for FBMC/OQAM system amounts to add the shifted outputs after each polyphase filtering (see Figure 61). In practice, the number of subcarriers may be very large, e.g. up to M=32,768 for the DVB-T2 system, while for FBMC/OQAM the prototype filter length is often limited to $4M$. Thus, the IFFT complexity is the predominant parameter and, if very short prototype filters are used e.g. $L=M$ as in our proposal presented in previous sections, then the difference with OFDM in terms of complexity becomes very small.

4.1.17 FBMC/OQAM equalization using the imaginary interference

4.1.17.1 Introduction

The previous section has highlighted the fact that using a complex conjugation property at the IFFT output could be exploited by an IFFT pruned algorithm to reduce the OFDM/OQAM modulator complexity. However, this technique cannot be applied at the receiver side and then a rough evaluation of the computational complexity tells us that the one of an OFDM/OQAM demodulator may be approximately twice the one of an OFDM one, due again to the FFT which has to be run twice faster. This also supposes that both systems use an equalizer of identical complexity. The common assumption for OFDM is that the equalizer is a one-tap zero forcing (ZF). It is why previously the comparison between both systems is carried out for a 1-tap ZF. If this simple equalizer may be sufficient to provide better results with OFDM/OQAM than with CP-OFDM for high mobility scenarios, it may be insufficient if the signal has to cope with an SFN channel with large delays for which it is required to operate at large signal to noise ratio (SNR), which may be also the case for smaller delays but using high order constellations. In these types of configuration, in spite of the extra complexity (which has also to be evaluated taking into account the overall transmission system, thus relatively reducing the extra complexity due to the modulation/demodulation operations), equalizers being more complex than the simple 1-tap ZF have to be considered. As a recent example we can for instance mention [56]. A common feature of all known OFDM/OQAM equalizers, including the ones in [56] is to process equalization in the complex field related to the frequency domain before extracting the real-valued information and discarding the imaginary component. This way to proceed is totally justified by the fact that, as recalled in Section 4.1.17.2, the OFDM/OQAM modulation only has the real orthogonality property. Nevertheless, we have recently discovered that this imaginary interference could be very helpful for equalization [57]. Indeed, there exists a correlation between the real and imaginary interference components such that the equalization could be able to explore this property. Such equalization is therefore named Equalization with Real Interference Prediction (ERIP) [57]. In this report, we present a general concept of the ERIP and its performance analysis. The interest for this imaginary component is highlighted in Section 4.1.17.3. Then, in Section 4.1.17.4 we derive our proposed ERIP equalization).
In Section 4.1.17.5 we analyze its theoretical behaviour in a multipath channel and provide some insights concerning its computational complexity. Finally in Section 4.1.17.5 we present simulation results.

4.1.17.2 OFDM/OQAM and real orthogonality

Let us recall that the OFDM/OQAM signal is a complex-valued signal defined by equation (1) in section 4.1.16.2. However, one can consider that it transmits real-valued symbols and the way to recover these symbols is based on the real orthogonality. This could be expressed mathematically as following. For any OFDM/OQAM modulated signal $s[k]$, written as, $s[k] = \sum_{n=-\infty}^{+\infty} \sum_{m=0}^{2N-1} a_{m,n}\, \psi_{m,n}[k]$, the orthogonality yields in real-field only, i.e.,

$$\hat{a}_{m,n} = \Re\{< s[k], \psi\hat{} *_{m,n}[k] >\},$$

where <,> is scalar product. On receiver side, this also indicates that only real part components of the equalized signal are retained. Since it is widely agreed (or considered) that the imaginary part components do not contain any useful infomation, they are simply removed after equalization. However, until recently [57], we discovered that the imaginary part components carry some useful information that we can take advantage of for improving the equalization performance and this discovery is original to the best of our knowledge. In the following sections, we share the principle idea and the results of our discovery.

4.1.17.3 Interference correlation analysis: a simple case

The usefulness of the imaginary part components is better understood through a simple case. We start by a time asynchronization, i.e., the equivalent Channel Impulse Response (CIR) yields $h[k] = \delta(k - l_d)$ with l_d the delay in samples. This model will be referred to as the simple delay channel. Based on the OQAM demodulation model [58] the demodulated OQAM signal at the phase-position (m_0, n_0) is written as

$$y_{m_0,n_0} = A_g[-l_d, 0]a_{m_0 n_0} e^{-j2\pi m_0 n_0 l_d/M} + I_{m_0,n_0}$$

With

$$I_{m_0,n_0} = \sum_{p^0,q^0} a_{m_0+p,n_0+q} e^{\frac{j\pi(p+q+pq)}{2}} (-1)^{pn_0} A_g[-qN - l_d, p] e^{-\frac{j\pi(2m_0+p)l_d}{M}}$$

Since the prototype filter is real-valued and symmetrical, $A_g[l, k]$ is real-valued and symmetrical as well. The complex-valued term, $I_{m_0 n_0}$, stands for the interference where $\sum_{p^0,q^0}(.)$ means the summation of all the possible integer pairs (p, q) excluding $(p, q) = (0,0)$.

Let us assume a simple one-tap Zero-Forcing (ZF) equalizer with coefficient $e^{-j2\pi m_0 l_d/M}$ which corresponds to the $m_0{}^{\text{th}}$ output of the M-point discrete Fourier transform of the CIR. Then, the equalized interference, at position (m_0, n_0), yields $J_{m_0,n_0} = ZF[I_{m_0,n_0}]$, i.e.,

$$J_{m_0,n_0} = \sum_{p^0,q^0} a_{m_0+p,n_0+q} e^{\frac{j\pi(p+q+pq)}{2}} (-1)^{pn_0} A_g[-qN - l_d, p] e^{-\frac{j\pi p l_d}{M}}$$

Thus, obviously, its real part is given by

$$J^{\Re}_{m_0,n_0} = \sum_{p^0,q^0} a_{m_0+p,n_0+q} (-1)^{pn_0} A_g[-qN - l_d, p] \cos\left(\frac{\pi(p+q+pq)}{2} - \frac{\pi p l_d}{M}\right) \quad (9)$$

while its imaginary part is written as

$$J^{\Im}_{m_0,n_0} = \sum_{p^0,q^0} a_{m_0+p,n_0+q} (-1)^{pn_0} A_g[-qN - l_d, p] \sin\left(\frac{\pi(p+q+pq)}{2} - \frac{\pi p l_d}{M}\right) \quad (10)$$

It can be easily seen that when $l_d = 0$ the real part (9) is null while the imaginary interference term (cf.(10)) is removed after real part extraction, which is the usual way to proceed. When l_d is nonzero, we propose to use this imaginary term to estimate the nonzero real one.

Indeed, in what follows, we unveil the fact that there exists a correlation between the Real and Imaginary Parts of the Interference, concisely written as RPI and IPI, when one is shifted in time w.r.t. the other. To

derive this correlation, we introduce a time shift factor t,($t \in \boldsymbol{Z}$), to the imaginary component and the covariance between them yields

$$Cov\left[J^{\Re}_{m_0,n_0}, J^{\Im}_{m_0,n_0+t}\right] = E[J^{\Re}_{m_0,n_0}, J^{\Im}_{m_0,n_0+t}]$$

An analytical expression is given in [57] and it turns out that the correlation does exist at certain time shift factor positions.

4.1.17.4 Proposed equalization solution: ERIP

Inspirited by the above-mentioned fact, the ERIP method is proposed to take advantage of the time-shifted imaginary-part interference (i.e., IPI) components so as to predict the real-part interference (i.e., RPI) components. The basic process is explained as following. The correlation between RPI and IPI has been proved to depend only upon the channel coefficients [57]. Thus, as long as the channel state information (CSI) is available, this correlation can be calculated analytically. Furthermore, in [57], we find out that the correlation lies on an approximately linear form, which is to say that the RPI can be predicted by a simple linear regression projection w.r.t. the IPI. The slope of the linear regression is highly related to the correlation calculated. The diagram of the ERIP method is depicted in figure below. For further details of the functionality of the linear regression as well as the slope calculation, please refer to [57].

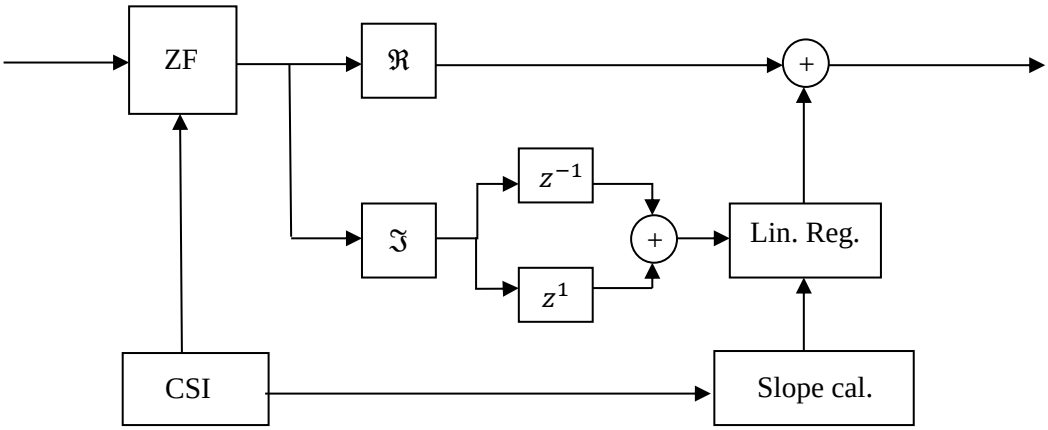

Figure 65: ERIP diagram

The complexity of the ERIP method can be separated into on-line computation and periodic computation. The former indicates the computation that is processed at the transmission symbol rate; while the latter stands for the computation that is required once when the channel state information is updated. Therefore, it is natural that in the case of a moderate mobility channel, the equalization complexity depends more on the on-line computation. In [57], we analyze these two computations, and we conclude that the on-line computation yields only 1 extra real multiplication per modulated subcarrier compared with the conventional ZF equalization.

4.1.17.5 Simulation results

This section presents the simulated results obtained under the following configuration setting. We evaluate the ERIP efficiency comparing it with the conventional ZF equalizer. The main parameters of the transmission system are:

- Sampling frequency: 10MHz;
- Constellation: 64-QAM;
- FFT size: 128;

- Perfect CSI and synchronization;
- No channel coding is applied in our simulation.

The channel model, in our simulations, is a simple two-path Rayleigh channel with Line-of-Sight (LOS) propagation. The complex coefficients of the two paths, named h_1 and h_2, are independently generated and with power profiles (in dB): [0 -4], i.e., $E[|h_1|^2] = 1$ and $E[|h_2|^2] = 0.1995$. Moreover, in order to guarantee the LOS propagation, we set the amplitude of h_1 be at least 4 dB stronger than that of h_2 in each channel realization. Furthermore, the delay profile of this model is set to around 10% of FFT interval ($\approx 1.2\ \mu s$). Note that, the channel coefficients are normalized before being applied to simulations. We assume that the channel remains non-variant during 30 symbols duration ($0.192\ \mu s$). Our BER for each SNR point is averaged over more than 10^4 channel realizations in order to reach an accuracy of 95%.

The simulation results, in BER versus SNR, are depicted in Figure 66. For the conventional ZF equalizer case, it clearly shows a performance error floor before the BER at 10^{-3}, but, with the help of our proposed equalizer, this floor has been effectively lowered. Regarding the latency and complexity issue, ERIP only introduces a latency of one OQAM symbol duration at the beginning of the frame and it leads to a reasonable complexity increase, e.g. at each subcarrier, in this simulation setting, the major periodic complexity yields around 139 real multiplications and the extra online complexity yields 1 real multiplication.

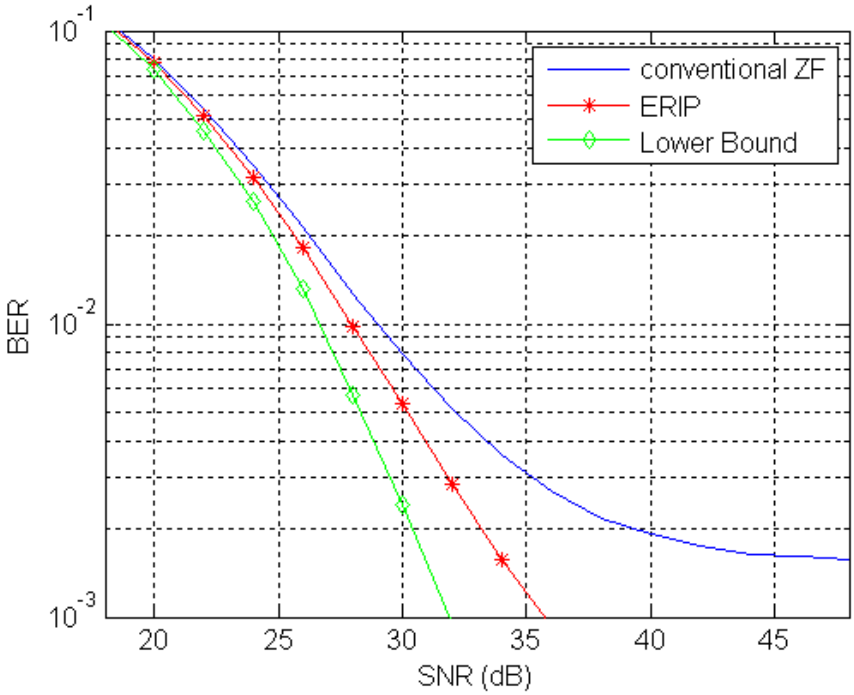

Figure 66: Performance Evaluation

4.1.17.6 Conclusion

The recent outcome on the investigation of the correlation between IPI and RPI at the output of the OFDM/OQAM system has been presented in this section. The fact that the IPI could be effectively taken advantage of to improve the robustness of the conventional one-tap ZF equalizer has been pointed out, which leads to a more robust equalizer, named ERIP. We can conclude two main merits of ERIP equalization: firstly, it can effectively lower the error floor that usually appears in the conventional ZF case; secondly: it has very low extra complexity which remains the advantage of using frequency-domain equalization.

4.1.18 Conclusion

In this section, we have described the multicarrier OFDM/OQAM modulation and the way we have adapted it for DVB-NGH. We have listed the main difference of this modulation compared to conventional CP-OFDM modulation. The main advantage of using OFDM/OQAM modulation is the no cyclic prefix insertion leading to significant gain in terms of spectral efficiency. The performance results have shown that the OFDM/OQAM modulation exhibits better robustness against Doppler than CP-OFDM modulation. In terms of delay spread, TFL1 is better than OFDM with CP equal to 1/12 and with an offset in receiver, it is possible to be close to the performance of OFDM with CP equal to 1/8. In addition we have proposed a framing including scattered pilots, pseudo continual pilots and the association between OFDM and OFDM/OQAM symbols. Further, a proposal for a fast implementation of the FBMC/OQAM modulator and a new equalization scheme that takes advantage of the generally discarded imaginary component which are were presented.

4.2 Satellite link: SC-OFDM modulation

MERCE proposed a modulation scheme, called Single Carrier-Orthogonal Frequency Division Multiplexing (SC-OFDM) modulation, suitable for the satellite component of the DVB-NGH system.

One of the key components in a satellite is the power amplifier (PA) that is due to bring the incoming signal at a level compatible with the receivers sensibility over large areas. In order to guarantee the durability of the satellite, it is critical to keep low the power consumption of the system and thus to optimize the amplifier power efficiency, i.e. to drive the amplifier with small input back-offs. Single Carrier modulations have long been the reference scheme for satellite transmissions for their suitability to achieve low power fluctuations compatible with small input back-offs. However, OFDM modulation is taking over SC schemes thanks to a better flexibility and a comparatively lower complexity when it comes to compensate for high channel degradations. However, the more sub-carriers are added together the more the signal behaves like a Gaussian noise with large power fluctuations. This means either the use of costly power amplifiers with a large linear region at the expense of a poor power efficiency or significant performance degradations due to the saturation of the peaks in the signal when driving the PA with a small input back-off. As its name stands for, the Single Carrier-Orthogonal Frequency Division Multiplexing (SC-OFDM) modulation was derived to combine the best of the two underlying waveforms and more precisely to preserve a lot of commonalities with pure OFDM while significantly reducing power fluctuations. As shown in [36] that depicts the relationships between the OFDM, SC-FDE and SC-OFDM schemes, this is achieved by applying a Discrete Fourier Transform (DFT) on the symbols to be transmitted prior the actual OFDM modulation. A comprehensive description of the SC-OFDM modulation illustrated in Figure 67 is given in the **ENGINES Deliverable 2.4** that specifically addresses the topics related to satellite transmission. It is shown that the SC-OFDM appears as a sensible solution when it comes to transmit over power amplifier with very small input back-offs.

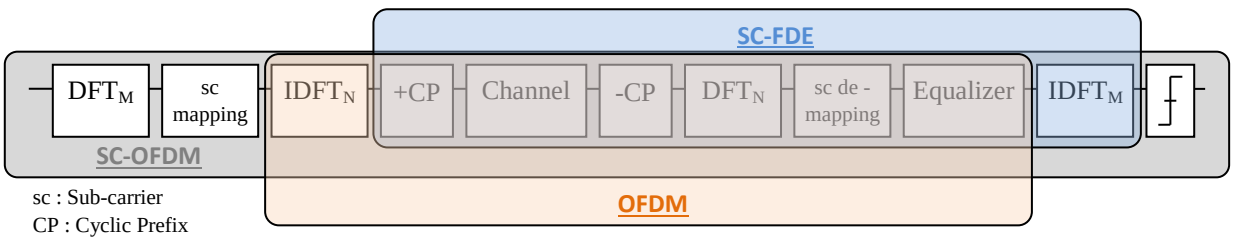

Figure 67: General architecture of an SC-OFDM system.

5 STUDY OF INTERFERENCE MITIGATION AND PAPR REDUCTION TECHNIQUES

Multi carrier communications play a key role in digital communications industry but they suffer from a serious drawback from their high Peak to Average Ratio (PAPR) because it reduces the efficiency of the power amplifier.
Two contributions related to PAPR reduction techniques are reported in this document. In Section 5.1, Thomson Broadcast investigates the comparison between several Peak to Average Ratio (PAPR reduction techniques for DVB-NGH, especially Tone Reservation and Active Constellation Extension. Section 5.2 presents the results of a study carried out by INSA-IETR on the optimization of the phase and amplitude of the channel estimation pilots, used jointly for PAPR reduction process.

5.1 System considerations

Multi carrier communication is playing a key role in digital communications industry but they are suffering of a serious drawback from their high PAPR. It is impacting the design to cost of transmitters and the power efficiency of the High Power amplifier on the transmitter site. Indeed, in one hand, network operators are requiring higher Modulation Error Ratio of the signal being transmitted to the end user and in the other hand they need better power efficiency of their systems to improve the operating expenditure of the entire network. In the past years, it is commonly accepted that the output of transmitter used in the broadcast UHF bandwidth exceeds 35dB but these requirements are clearly made against the efficiency of the transmission system. However, techniques enabling to reduce the PAPR are helping to maintain good performances while improving the efficiency of the transmitter. Moreover, like standard clipping techniques, PAPR techniques help to protect the HPA against overdriving the amplifier.

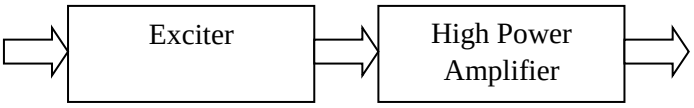

Figure 68 : System under consideration

Choosing a technique is not an easy task and a figure of merit of the techniques has been put in place in order to estimate the gain for the system. Techniques are being also checked for their impact on the receiver design trying to put the complexity of the signal processing into the transmission system and not on the receiver chipset.

Measurements made on Tone Reservation techniques applied to fixed transmission have shown that:

- Power may be increase up to 10% or 0.4dB as well as power effciciency
- MER is increased by 2dB for operating the transmitter at operational transmission

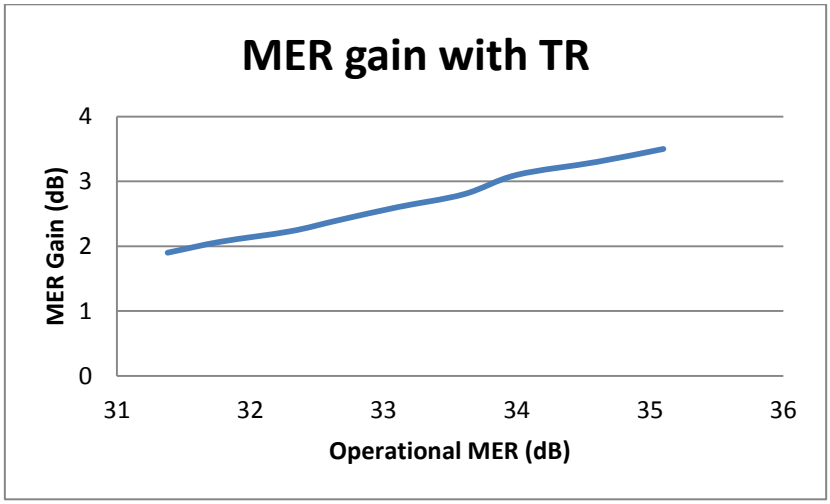

Figure 69: MER gain(dB) versus operational MER(dB) for TR implementation

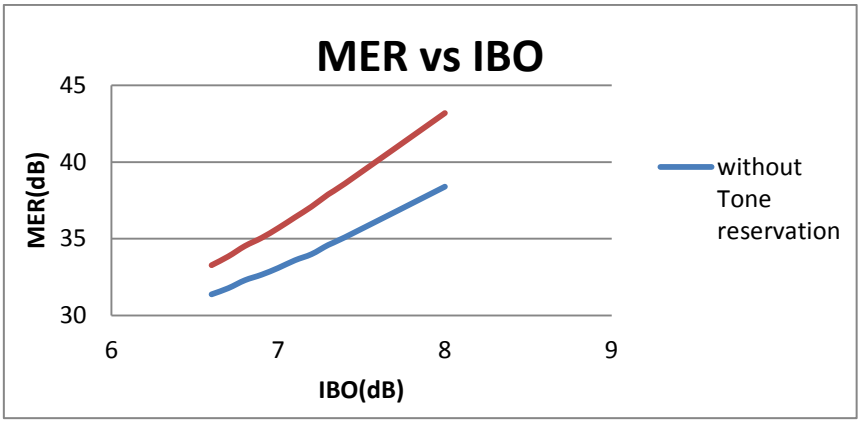

Figure 70 : MER verus HPA IBO

From the chart above, we observe that the gain in MER of tone reservation technique is linearly increasing with the the input back off of the transmitter HPA resulting with higher MER performance for higher MER operatioanl requirements. For instance, in a system requiring a MER of 35dB , an HPA with a back off inferior to 0.4dB can be used improving system efficieny by 10%.

Tone reservation technique is matching the needs for fixed transmission but better gain can be achieved where lower constellations order are available. Better results for mobile transmission with Active Constellation Extension are achieved in QPSK mode (1.5dB power gain has been achieved in previous B21C project). Other techniques (SC-OFDM or Joint PAPR) are being investigated in the project may potentially show superior efficiency for a mobile system.

Input Back Off IBO dB	MER operation dB	MER gain dB	MER with PAPR dB	Out Of Band products (oob) dB	Figure Of Merit Fom
6.6	31.38	1.9	33.28	1.87	0.156875
6.7	31.78	2.07	33.85	2	0.2164375
6.8	32.3	2.23	34.53	2.1	0.2254375
6.9	32.66	2.4	35.06	2.2	0.235
7	33.1	2.6	35.7	2.3	0.24625
7.1	33.6	2.8	36.4	2.4	0.2575
7.2	34	3.1	37.1	2.48	0.274375
7.3	34.6	3.3	37.9	2.5	0.285625
7.4	35.1	3.5	38.6	2.7	0.296875
8	38.4	4.8	43.2	2.9	0.37

Figure 71: Performance table for Tone Reservation

Input Back Off IBO dB	MER operation dB	MER gain dB	MER PAPR dB	Oob dB	Fom
6.7 (QPSK)	33.1	15	48.1	2.3	1.54375
6.7 (16QAM)	33.1	5	38.1	3.3	0.68125

Figure 72: Performance table for Active Constellation Extension on QPSK – 16 QAM

5.2 Joint PAPR and channel estimation

Various approaches have been proposed as summarized in [61][62] to mitigate the PAPR of an OFDM signal. Among them, clipping and filtering technique is easy to implement. However, these schemes yield a broken system performance since clipping is a nonlinear process [63] leading to a signal distortion. An alternative method based on coding was proposed in [63], in which a data sequence is embedded in a longer sequence and only a subset of all these possible sequences is used to exclude patterns generating high PAPR. Moreover, other methods such as partial transmit sequence [64], selected mapping [65] and interleaving [65] are also proposed. The main drawback of these methods is the necessity to transmit side information (SI) to the receiver, resulting in some loss of throughput efficiency.

Some methods recently proposed do not need this SI transmission [66][67]. Indeed, the active constellation extension (ACE) method proposed in [67] reduces the PAPR by changing the constellation of the signal without modifying the minimum distance. However, this technique has some gain limits when the constellation size of the signal increases. Moreover, this technique is not suited for rotated constellation schemes, which have been selected for the second generation digital terrestrial television broadcasting system (DVB-T2). The Tone Reservation (TR) method, proposed by Tellado [67] and adopted in DVB-T2 also, uses allocated subcarriers to generate additional signal that minimizes the PAPR value. However, TR technique reduces the spectrum efficiency since it requires some dedicated pilots for PAPR reduction issues. In DVB-T2, 1% of the subcarriers are dedicated for PAPR. Moreover, an iterative process should be implemented at the transmitter with a special need for a smooth control of the transmitted power on the dedicated subcarriers in order to respect the DVB-T2 spectrum mask requirements (the dedicated pilots should be at a power level less than 10 dB with respect to the data subcarriers power).

With the limitations of ACE technique for rotated constellation schemes and those of TR by spectral

efficiency loss, an innovative technique which could be implemented for rotated constellation and without efficiency loss is clearly needed. In this work, we adopt, as in [61], the TR technique by using the pilots of channel estimation for both PAPR reduction and channel estimation issues. The novelty of our proposition is based on the optimization of the phase and amplitude of the channel estimation pilots, used jointly for PAPR reduction process. Indeed, instead of using orthogonal pilots sequences (OPS), we optimize the transmitted sequence for PAPR issue in terms of phase and amplitude. Using a predefined law between different sequences, the receiver could easily utilize a blind detection of the transmitted sequences.

The proposition of this work is multifold. First, instead of using dedicated pilots for PAPR reduction, we expend the idea of [61] which consists in utilizing existing pilots dedicated for channel estimation for both channel estimation and PAPR reduction issues. In this way, we avoid the use of reserved pilots as proposed in DVB-T2 standard improving thus the spectral efficiency of the system. Second, in order to allow their recovery serving for channel estimation process at the receiver, these pilots have to follow particular laws. Multiplicative law in frequency domain is then proposed and investigated in this work. At the receiver, this law is applied to detect and estimate transmitted pilots in frequency domain. As the detection and estimation of multiplicative law's parameters in continuous frequency domain, i.e., in real space, cause degradations, we propose to operate this law in the discrete frequency domain, i.e., in a predefined discrete set. Third, we show by simulations the validity of our technique using DVB-T2 [1] parameters. Its performance is compared to the DVB-T2 PAPR Gradient algorithm and to the second order cone programming (SOCP) technique proposed in [67][68][70].

5.2.1 OFDM signal and PAPR value

Let $\mathbf{X} = [X_0, \dots, X_{N-1}]$ be a sequence of complex symbols and $\mathbf{x} = [x_0, \dots, x_{N-1}]$ be its discrete inverse Fourier transform. The OFDM baseband signal; in continuous time domain, is expressed as:

$$x(t) = \frac{1}{\sqrt{N}} \sum_{k=0}^{N-1} X_k e^{\frac{j2\pi kt}{TN}} \qquad 0 \le t < NT \tag{1}$$

where $j = \sqrt{-1}$, N denotes the number of subcarriers and T is the original complex signal duration. In practice, only NL equidistant samples of $x(t)$ are considered, where L represents the over-sampling factor [67] used to make the signal as close as possible to the continuous signal. The over-sampled signal is then given by:

$$x_{[n/L]} = \frac{1}{\sqrt{N}} \sum_{k=0}^{N-1} X_k e^{\frac{j2\pi kn}{LN}} \qquad \forall n \in [0\ NL-1] \tag{2}$$

When the over-sampling factor L is large enough, the PAPR value of the OFDM signal is defined as the ratio of its maximum power divided by its average power. It is expressed as [71]:

$$PAPR\{x(t)\} \approx PAPR(\mathbf{x}_L) = \frac{\max_n \left|x_{n/L}\right|^2}{E\left\{\left|x_{n/L}\right|^2\right\}} \tag{3}$$

where $\mathbf{x}_L = \mathbf{Q}_L \mathbf{X}_L$, $\mathbf{X}_L$ is the zero-padded over-sampled vector of $\mathbf{X}$, $E\{\}$ denotes expectation operation and $\mathbf{Q}_L$ is the inverse discrete Fourier transform matrix of size NL. $\mathbf{Q}_L$ is given by:

$$\mathbf{Q} = \frac{1}{\sqrt{\mathrm{N}}}\begin{bmatrix} 1 & 1 & \cdots & 1 \\ 1 & e^{\frac{j2\pi}{NL}1.1} & & e^{\frac{j2\pi}{NL}1.(NL-1)} \\ & \vdots & \ddots & \vdots \\ 1 & e^{\frac{j2\pi}{NL}(NL-1).1} & \cdots & e^{\frac{j2\pi}{NL}(NL-1).(NL-1)} \end{bmatrix} \quad (4)$$

In this study, the PAPR performance is evaluated using the complementary cumulative distribution function (CCDF). It is defined by the probability that the PAPR value exceeds a given threshold γ. For L=1, it can be expressed as [72]:

$$CCDF_{PAPR} = Pr[PAPR(\mathbf{x}_L) > \gamma, L = 1] \approx 11(11e^{-\gamma})^N \quad (5)$$

It is also demonstrated in [72] that the real PAPR value can be approximated independently of L when $L \geq 4$ by:

$$CCDF_{PAPR\{x(t)\}} = Pr[PAPR(\boldsymbol{x}_L) > \gamma, L \geq 4] \approx 1 - (1 - e^{-\gamma})^{2.8\,N} \quad (6)$$

In this work, we consider L=4 and use this expression as a theoretical PAPR reference value of the original OFDM signal.

5.2.2 Existing TR-PAPR reduction methods

5.2.2.1 General principle

In an OFDM based system (like DVB standards), the main idea of the TR technique is to use reserved pilots in order to reduce the PAPR value at the input of the power amplifier of the time domain transmitted signal.

Let us consider M as the number of channel estimation pilots used for PAPR reduction issue and $\mathbf{P} = [P_0, \ldots, P_{M-1}]$ as the M pilot positions dedicated for PAPR reduction, and $\mathbf{C} = [C_0, \ldots, C_{M-1}]$ be the set of M pilots transmitted on these positions, as shown in Figure 73. Then, the N modulated symbols $\{X_k\}_{k=0\ldots N-1}$ of the OFDM symbol in frequency domain are expressed as:

$$X_k = \begin{cases} C_k & if\ k \in \boldsymbol{P} \\ S_k & if\ not \end{cases} \quad (7)$$

where S_k is the data symbol transmitted on subcarrier k and C_k is a pilot symbol used for PAPR reduction.

The OFDM baseband signal in time domain, after pilot insertion, becomes:

$$\mathbf{x}_L = \mathbf{Q}_L\mathbf{X}_L = \mathbf{Q}_L(\mathbf{C} + \mathbf{S}_L) = \mathbf{Z}_L\mathbf{C} + \mathbf{s}_L \quad (8)$$

Where $\mathbf{S}_L$ is the data vector represented in frequency domain of size N (where the values at the pilots positions are set to 0) and $\mathbf{s}_L$ is its time domain representation. $\mathbf{Z}_L$ is given by:

$$\mathbf{Z}_L = \frac{1}{\sqrt{\mathrm{N}}}\begin{bmatrix} 1 & 1 & \cdots & 1 \\ e^{\frac{j2\pi}{NL}1.p_1} & e^{\frac{j2\pi}{NL}1.p_2} & & e^{\frac{j2\pi}{NL}1.p_M} \\ \vdots & & \ddots & \vdots \\ e^{\frac{j2\pi}{NL}(NL-1).p_1} & e^{\frac{j2\pi}{NL}(NL-1).p_2} & \cdots & e^{\frac{j2\pi}{NL}(NL-1).p_M} \end{bmatrix} \quad (9)$$

and L holds for oversampling factor.

The added signal $\mathbf{c}_L = \mathbf{Z}_L\mathbf{C}$ has to cope with PAPR values. In literature, different techniques have been proposed to optimize this signal. Among them, the SOCP and the Gradient solutions are two of the most promising keys which have been extensively studied for optimization purposes. In the next section, we will give a general overview about these techniques. Performance of these techniques will be used as reference in comparison with our proposed technique.

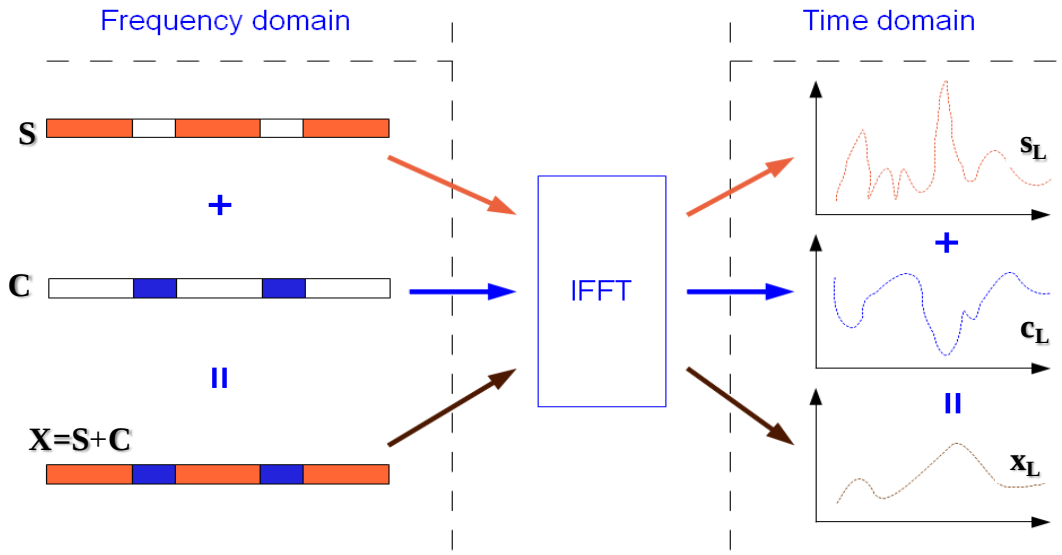

Figure 73: Pilots insertion scheme.

5.2.2.2 SOCP solution

The PAPR reduction problem can be formulated as follows: reducing PAPR value leads to the minimization of the maximum peak value of the combined signal ($\mathbf{s}_L + \mathbf{Z}_L\mathbf{C}$) while keeping the average power constant [12]. Mathematically speaking, this problem can be written as:

$$\min_{\mathbf{C}} \max_{n} \left|\mathbf{s}_L + \mathbf{Z}_{n,L}\mathbf{C}\right| \tag{10}$$

where $\mathbf{Z}_{n,L}^{row}$ denotes the n^{th} row of $\mathbf{Z}_L$.

Equation (10) can be also rewritten as:

$$\min_{\mathbf{C}} \left\|\mathbf{s}_L + \mathbf{Z}_{n,L}\mathbf{C}\right\|_{\infty} \tag{11}$$

where $\|.\|$ denotes the standard uniform norm.

Since the set $\mathbf{C}$ of pilots is used for PAPR reduction, the problem turns out now to find $\mathbf{C}$ which minimizes the PAPR of the current transmitted OFDM symbol. In the continuous domain, i.e. for $\mathbf{C} \subset \mathbb{C}^M$, this search is formulated as a convex optimization problem and solved using SOCP problem [67][68][70]. The optimization process can take the form of:

$$\begin{cases} \text{Minimize} & \beta \\ \text{subject to} & \left\|\mathbf{s}_L + \mathbf{Z}_{n,L}^{row}\mathbf{C}\right\| \leq \beta \\ & \forall\, 0 \leq n \leq NL-1 \end{cases} \tag{12}$$

It has been shown that this technique provides the optimized value in terms of PAPR reduction but it presents a high calculation complexity [67][68][70]. In our study, we will use this technique as a comparison term with other techniques mainly with the proposed joint PAPR reduction and channel estimation scheme.

5.2.2.3 Gradient iterative based method

This method, adopted in DVB-T2 standard, is a suboptimal solution of the SOCP method. It is based on the gradient iterative method using the clipping process. In order to apply this technique, the technical specifications of DVB-T2 allowed 1% of active sub-carriers for PAPR reduction issues. The pilots signal used for PAPR, defined as a reference kernel signal, is given by:

$$p = \frac{N}{N_{TR}} \mathbf{Q}_L[1_{TR}] \qquad (13)$$

where N_{TR} denotes the number of reserved subcarriers, $[1_{TR}]$ denotes the $(N,1)$ vector having N_{TR} elements of ones at the positions corresponding to the reserved carriers and $(N\text{-}N_{TR})$ elements of zeros at the others. This reference signal presents a peak at the position 0.

For each iteration, the peak position k of the initial signal is detected. Reference signal is shifted of k positions in order to allow the reduction of peak signal to a predefined clipping value V_{CLIP}. The reduction principle is described in Figure 74.

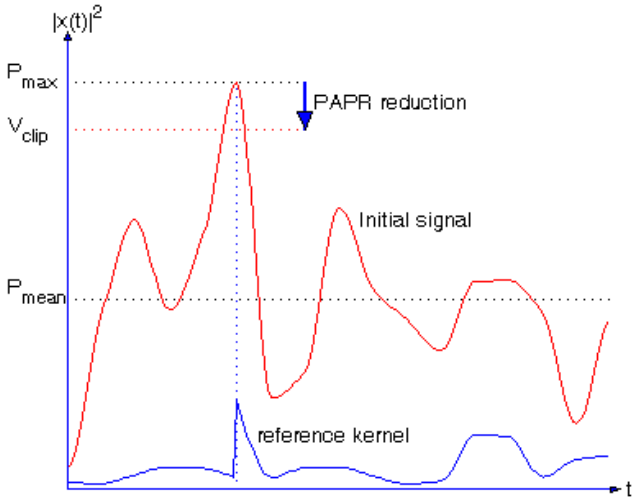

Figure 74: Principle of peak suppression by reference kernel signal.

The procedure of the PAPR reduction algorithm is given as follows:

Initialization:

1. *The initial values for peak reduction signal in time domain are set to zero:*
2. $\mathbf{c}^{(0)}=[0 \ldots 0]^T$ *where* $\mathbf{c}^{(i)}$ *denotes the vector of the peak reduction signal computed at* i^{th} *iteration.*

Iterations:

1. *i starts from 1.*
2. *Find the maximum magnitude of* $(x + \mathbf{c}^{(i-1)})$*, noted* y_i*, and the corresponding sample index* k_i*.*
3. *If* $y_i<V_{CLIP}$ *: go to the step 5.*
4. *If* $y_i > V_{CLIP}$ *: clip the signal peak to this value.*
5. *Update the vector of peak reduction signal* $\mathbf{c}^{(i)}$*.*
6. *If* $i< i_{max}$*, the maximum iteration number, increase* i *by one and return to step 2.*
7. *Terminate the iteration. The transmitted signal is obtained by:* $x'=x+\mathbf{c}^{(i)}$

The overall process of the gradient iterative based method is summarized in Figure 75.

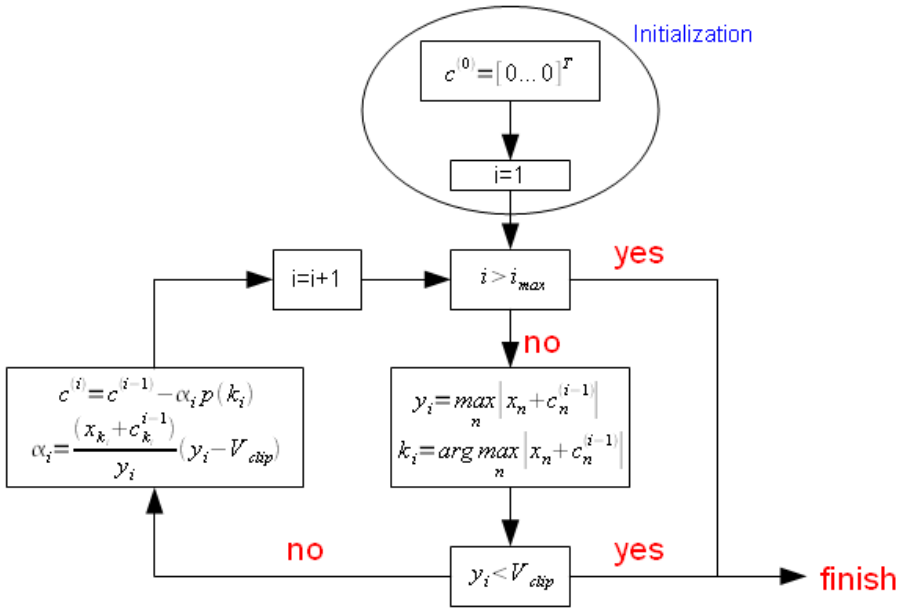

Figure 75: Principle of gradient iterative algorithm proposed in DVB-T2.

5.2.3 Proposed pilot-aided PAPR reduction method

The conventional TR method uses dedicated pilots for PAPR reduction issue leading to a spectral efficiency loss. In this proposition, we use some of the scattered pilots dedicated to channel estimation for both PAPR reduction and channel estimation purposes. The main problem turns out then to find the pilot symbols at the transmitter which minimizes the PAPR value but also to find these pilot symbols at the receiver in order to achieve channel estimation.

That is, in order to achieve both operations, i.e., PAPR reduction and channel estimation, the set $\boldsymbol{C}$ chosen for PAPR reduction has to undergo some particular laws known at the receiver. Figure 76 shows the general principle of the proposed method. In this scheme, the function $f(.)$ reflects the particular law known at both the transmitter and receiver. In our proposition, we consider a simple multiplicative law given by:

$$C_{k+1} = C_k \times \Omega \qquad \forall\, k \in [0, \ldots, M-2] \quad \text{or equivalently} \quad C_k = \Omega^k C_0 \tag{14}$$

where Ω denotes the step between two consecutive pilots and C_0 is the first pilot symbol.

The choice of C_k and Ω could be either in continuous domain, i.e. the pilots could take any continuous value in $\mathbb{C}$, or they could take any discrete value from a discrete predefined set in discrete domain with a discrete value Ω. Since the estimation of the pilots and Ω at the receiver in continuous domain could yield to a residual estimation error, and then to a slight system performance degradation, we propose to perform research in a discrete sub-set of $\mathbb{C}$. Equation (14) becomes:

$$\begin{aligned} C_0 &= \lambda e^{j\phi} \\ \Omega &= e^{j\Delta} \\ C_k &= \lambda e^{j(\phi+k\Delta)} \end{aligned} \tag{15}$$

where λ, ϕ and Δ take values from a predefined set of discrete values. λ is the boost factor applied to the dedicated subcarriers, ϕ is the initial phase value of the first pilot symbol, and Δ is the phase increment. The main reason to select a multiplicative law is due to simplicity issues and boost factor control, i.e. power

control of the transmitted sequences. Indeed, using (15), we can equivalently control the boost factor of all pilots (joint PAPR and channel estimation pilots). Again, we recall that the "discrete domain" means that instead of searching SOCP solution in $\mathbb{C}$, we search it in a predefined discrete set with a different discrete step for ϕ and Δ, called $\mu(\phi)$ and $\mu(\Delta)$ respectively. Figure 77 shows the multiplicative law scheme and the evolution of the pilots from one index to another. λ, ϕ and Δ have to be selected in such a way to optimize the PAPR reduction gain and to limit channel estimation errors. This compromise will be detailed in next sections.

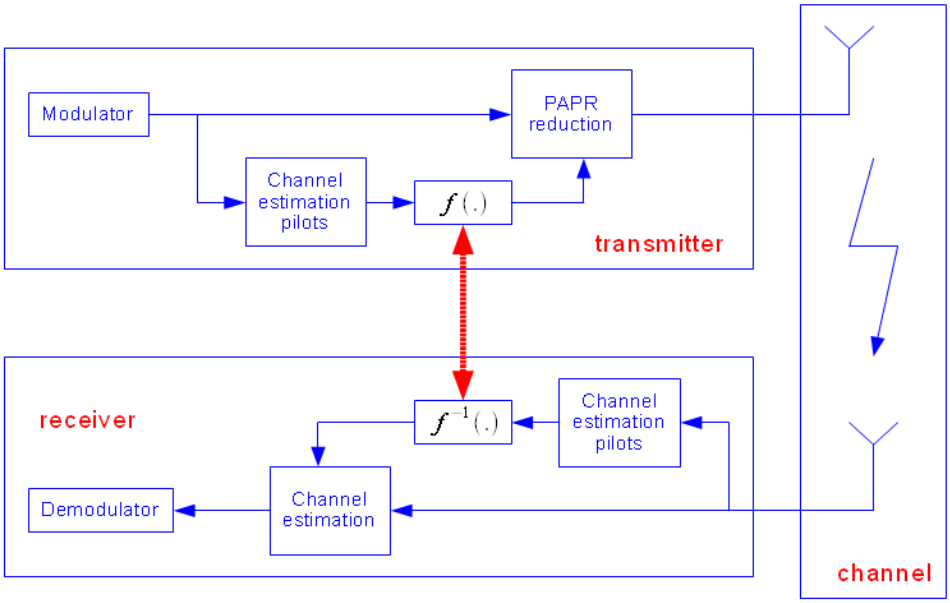

Figure 76: General principle of the proposed method.

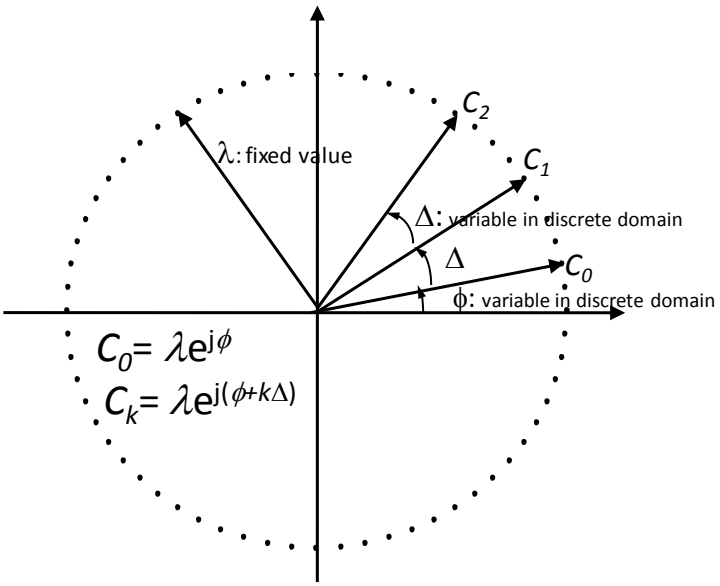

Figure 77: Multiplicative law scheme.

5.2.4 Pilots recovery and channel estimation

In order to describe the channel estimation scheme and pilots recovery, frequency non-selective fading per subcarrier and time invariance during one OFDM symbol are assumed. Furthermore, the absence of Inter-symbol Interference and Inter-carrier Interference is guaranteed by the use of a guard interval longer than the maximum excess delay of the impulse response of the channel. In conventional OFDM schemes and under these assumptions, the received signal at the output of the FFT operation could be written as:

$$\mathbf{R} = \mathbf{HS} + \mathbf{W} \tag{16}$$

where **H** denotes the $N \times N$ matrix which contains the complex channel coefficients and **W** is the additive white Gaussian noise vector.

In conventional OFDM systems, the channel estimation is done by estimating the pilot channel coefficients $\widehat{H}_p$ first and then by filtering the obtained coefficients using some conventional filters (the Wiener filter is widely used). The conventional OFDM channel estimation scheme is represented in Figure 78. Figure 79 shows the proposed channel estimation scheme when some pilots are dedicated for PAPR issues. It is clear that there is a slight difference with the conventional estimation scheme shown in Figure 78. In our scheme, the pilot symbols C_p used for PAPR reduction are not known a priori at the receiver. Therefore, the pilots' recovery and channel estimation procedure is performed in two steps. First, we determine the transmitted sequence $\hat{C}_p$ used for PAPR reduction. In the second step, we determine the actual channel coefficients $\widehat{H_k}$.

In order to accomplish the first step, we assume that the channel is almost constant between two successive OFDM symbols i.e. we assume that $\widehat{\mathbf{H}}^{(l)} \approx \widehat{\mathbf{H}}^{(l-1)}$ where l denotes the OFDM symbol index in time domain. Then, the pilot symbol used for PAPR reduction could be deduced by:

$$\bar{C}_p^l = \frac{R_p}{\widehat{H}_p^{(l-1)}} \quad \forall\, p \in P \tag{17}$$

By considering multiplicative law in discrete domain, received symbols at pilot positions are expressed as:

$$\bar{C}_p^l = \frac{H_p^l C_p^l + W_p^l}{\widehat{H}_k^{(l-1)}} \approx C_p^l + \frac{W_p^l}{H_p^l} \quad \forall\, p \in P \tag{18}$$

By combining (18) with (15), we have:

$$\bar{C}_p^l = \lambda e^{j(\phi + p\Delta)} + \frac{W_p^l}{H_p^l} \quad \forall\, p \in P \tag{19}$$

Since C is in discrete frequency domain, the estimate, $\hat{C}_p^l$, of C_p^l can be obtained from $\bar{C}_p^l$ by a simple quantization operation. As we consider that the boost factor λ is known at the receiver, the set C is characterized by two unknown variables of ϕ and Δ. Considering μ(ϕ) and μ(Δ) the elementary steps of ϕ and Δ in discrete domain, ϕ and Δ can be estimated as follows:

Estimation and decision of Δ:

$$\begin{aligned} \hat{\Delta} &= angle\left[\sum_{p=1}^{M-1} \bar{C}_p^l \left(\bar{C}_{p-1}^l\right)^*\right] \\ \bar{\Delta} &= D\left[\hat{\Delta}\big|_{\mu(\Delta)}\right] \end{aligned} \tag{20}$$

where $D[X|_\alpha]$ denotes decision function of X in discrete domain with a step α.

Estimation and decision of ϕ:

$$\hat{\phi} = angle\left[\sum_{p=0}^{M-1} \bar{C}_p^l e^{-jp\Delta}\right]$$
$$\bar{\phi} = D\left[\hat{\phi}\big|_{\mu(\phi)}\right] \quad (21)$$

In order to evaluate our detection algorithm, we define the error detection probability (EDP) of ϕ and Δ as:

$$\Pr(\Delta) = \Pr\left\{|\bar{\Delta} - \Delta| > \frac{\mu(\Delta)}{2}\right\} \quad (22)$$

$$\Pr(\phi) = \Pr\left\{|\bar{\phi} - \phi| > \frac{\mu(\phi)}{2}\right\} \quad (23)$$

where $\Pr\{|x| > \alpha\}$ denotes the probability that the absolute value of x is greater than α.

In Appendix A, these probabilities are calculated in the case of AWGN channel. We obtain:

$$\Pr(\Delta) = 1 - erf\left(\frac{\mu(\Delta)/2}{\sqrt{2\left(\frac{\sigma^2}{(M-1)^2\lambda^2} + \frac{2(M-1)\sigma^4}{(M-1)^2\lambda^4}\right)}}\right) \quad (24)$$

and

$$\Pr(\phi) = 1 - erf\left(\frac{\mu(\phi)/2}{\sqrt{\frac{\sigma^2}{M\lambda^2}}}\right) \quad (25)$$

The results of this computation are analyzed in next section.

The estimation and detection of ϕ and Δ allow us computing the transmitted pilot sequence. Once the transmitted pilot sequence is obtained, the second step consists of estimating the channel coefficients in the frequency domain. They could be obtained by the simple relationship:

$$\hat{H}_k^l = \frac{R_k}{\hat{C}_k^l} \quad \forall\, k \in P \quad (26)$$

Once the channel coefficients are computed on the pilot positions, the overall frequency channel response can be obtained by a simple Wiener filtering like in conventional channel estimation procedure. Both procedures are shown in Figure 78 and Figure 79 respectively.

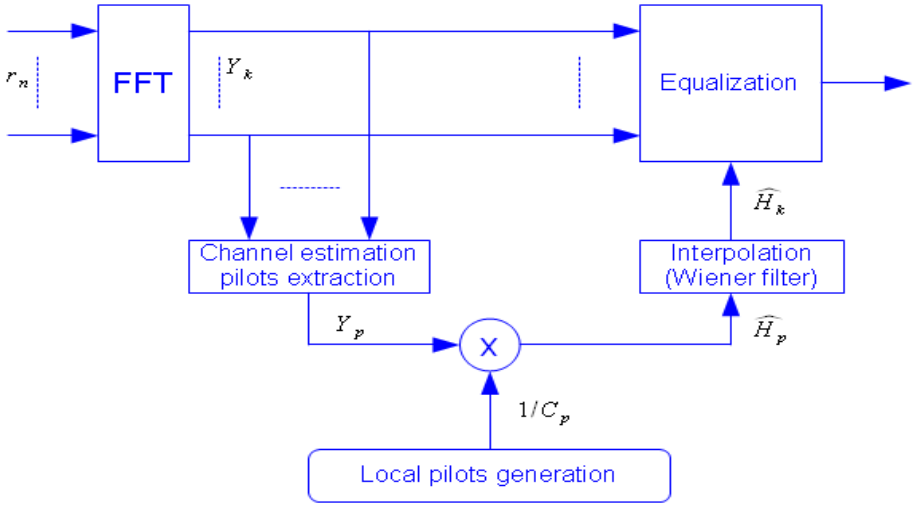

Figure 78: Conventional channel estimation scheme in OFDM systems.

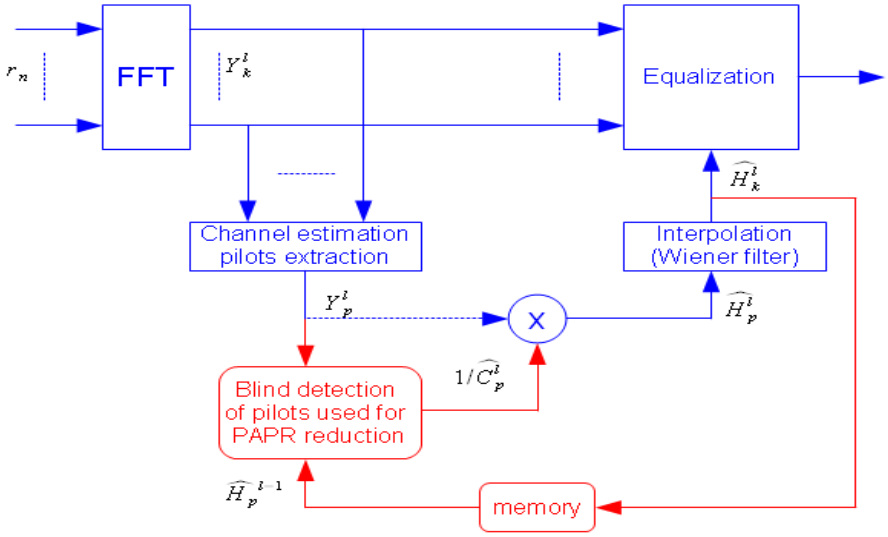

Figure 79: Modified channel estimation scheme.

5.2.5 Simulation results and discussion

Simulation results are performed using DVB-T2 parameters. Some of the main parameters are summarized in Table 25. The PAPR parameters of the proposed method, i.e., λ, Δ and ϕ are variable parameters which allow an optimization of both PAPR reduction and channel estimation processes. They will be specified in each simulation scenario.

Let's consider SOCP solution with a number of pilot tones M equal to 8. In fact, the SOCP solution is not possible using multiplicative law in continuous domain since the problem is not convex. In order to solve the problem, we consider discrete values of ϕ and Δ while maintaining λ in continuous domain. More precisely, we consider λ in continuous domain and we change the values of ϕ from 0 to 2π with a step of $\pi/8$, while Δ varies from 0 to 2π with variable step μ, of $\pi/2$, $\pi/4$, $\pi/8$ and $\pi/16$. The results are presented in Figure 80 in terms of CCDF.

Table 25: Simulation parameters, extracted from DVB-T2 standard.

Mode (OFDM size)	2K
Number of subcarriers	NFFT=2048
Guard Interval length	GI=1/8
Modulation	16-QAM, 64-QAM
Coding rate	R=1/2
Over-sampling factor	L=4
Number of subcarriers used for PAPR reduction	M=8, 16, 32

Figure 80 shows the CCDF of the multiplicative law using SOCP solution with respect to the continuous λ value and different step values μ. The PAPR gain increases when the step value μ decreases since the solution is approaching the continuous domain. Moreover, the solution converges when the step value μ reaches a limit value $\mu_{lim} = \pi/8$. In other words, the PAPR gain increases when the pilots' values are optimized in continuous domain. The results obtained in Figure 80 show first that CCDF simulation results are close to theoretical value given in equation (6). Moreover, this figure shows that with a continuous λ value, a phase discretization using a step $\mu = \pi/8$ is enough to converge to the maximum PAPR reduction gain in the continuous domain.

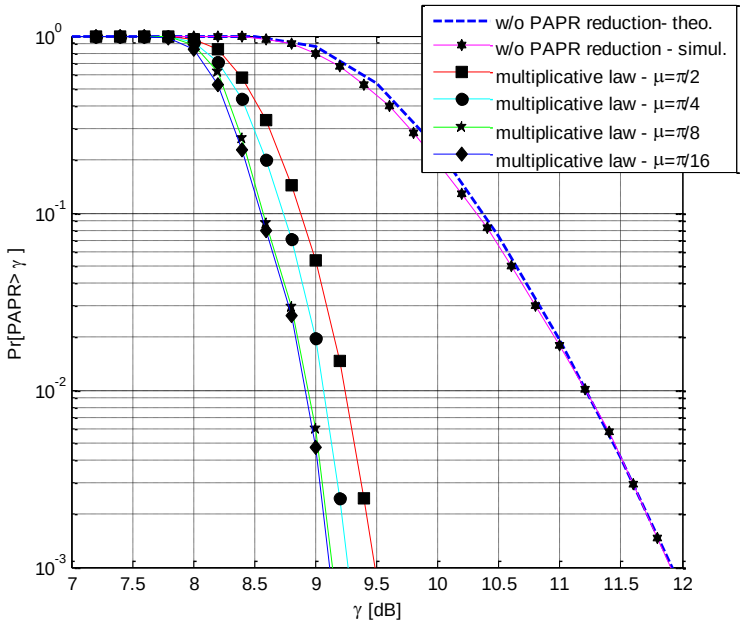

Figure 80: CCDF performance of multiplicative law using SOCP solution, continuous λ, 16-QAM, 2k mode.

5.2.5.1 Multiplicative law performance in discrete domain

We consider now the multiplicative law with ϕ and Δ in the discrete domain while λ takes a value from a predefined set. Firstly, we present CCDF performance for a fixed λ value and for ϕ and Δ varying from 0 to 2π with a step of $\pi/8$. The number of subcarriers used for PAPR reduction is always M=8. In this case, reducing PAPR is not a SOCP problem anymore but becomes a search of the optimum combination minimizing PAPR. At the receiver, pilots are recovered by a detection and estimation algorithm. Figure 81 gives a comparison between different PAPR reduction techniques namely, SOCP solution, Gradient technique and our proposed technique with a predefined power value $\lambda = 20\,dB$. This figure shows that using our solution and this λ value, we obtain slightly better results than in DVB-T2 gradient solution.

However, the Gradient solution requires an iterative complex implementation. Again, we recall that this method avoids the use of dedicated pilots for PAPR reduction issue, improving also spectral efficiency of the system (1% in case of DVB-T2 specification).

In Figure 82, we present the PAPR gain in terms of CCDF, in comparison with the curve obtained without PAPR reduction technique, as a function of λ. We assume that ϕ and Δ change from 0 to 2π with a step of $\pi/8$, $\pi/16$ and $\pi/32$. This gain is evaluated at a CCDF=10-3. It is also compared with the SOCP solution for multiplicative law (λ continuous). Figure 82 shows that the system performance is improved when the step of ϕ and Δ becomes smaller. This is because the number of pilot combinations increases when the step decreases. For each value of this step, there exists one optimum value of λ for which the PAPR gain in terms of CCDF reaches the maximum.

Now, considering a discrete λ value, we compare the performance of the proposed method, for a step of ϕ and Δ of $\pi/8$, when λ=20 dB which is the one maximizing the PAPR gain at CCDF=10-3 and when λ is discrete, varying from 5 dB to 25 dB with a step of 3 dB. The results are presented in Figure 83. For a CCDF=10-3, the performance in terms of PAPR when λ=20 dB is about 0.35 dB worse than the one of SOCP solution. It is about 0.17 dB worse than the case when λ is discrete. In other words, we lose only 0.17 dB when a predefined value of λ is selected instead of using a predefined set of discrete values.

In terms of complexity, the discrete solution is less complex than the SOCP solution (optimal solution). Indeed, our proposed PAPR reduction technique aims at searching the optimal solution in terms of λ, ϕ and Δ in a predefined discrete set of values while SOCP solution applies a search in continuous domain. Moreover, setting a predefined value of λ yields to a reduced complexity implementation in comparison with the discrete λ solution, however, with a 0.17 dB PAPR loss. On the other hand, in terms of channel estimation, setting a predefined value of λ implies an improved performance in comparison with the discrete case since we avoid quantization at the receiver. So, the proposed method with a predefined value of λ presents a good tradeoff between channel estimation performance and PAPR gain.

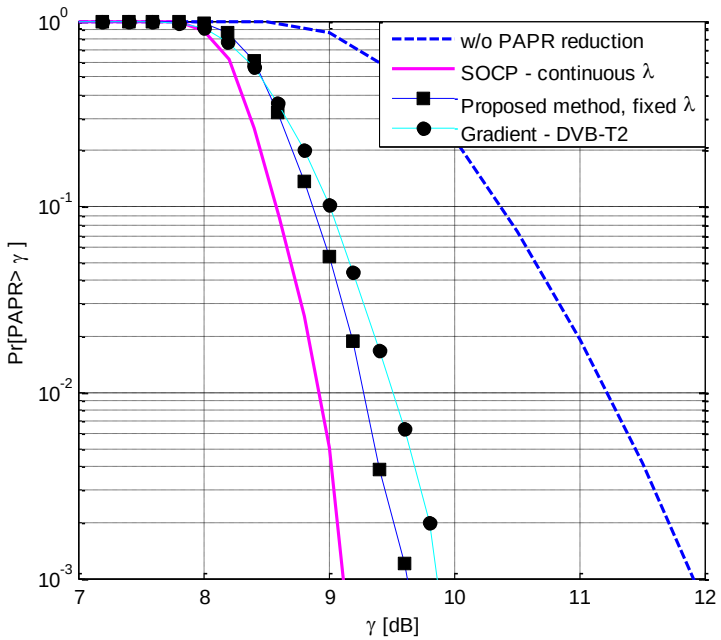

Figure 81: CCDF performance of multiplicative law in discrete domain, 16-QAM, λ = 20 dB

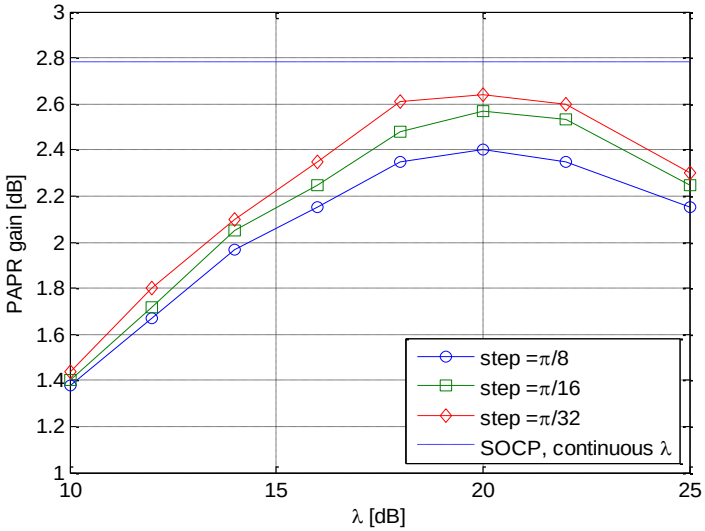

Figure 82: PAPR gain at a CCDF=10^{-3} as a function of λ, M = 8, 16-QAM

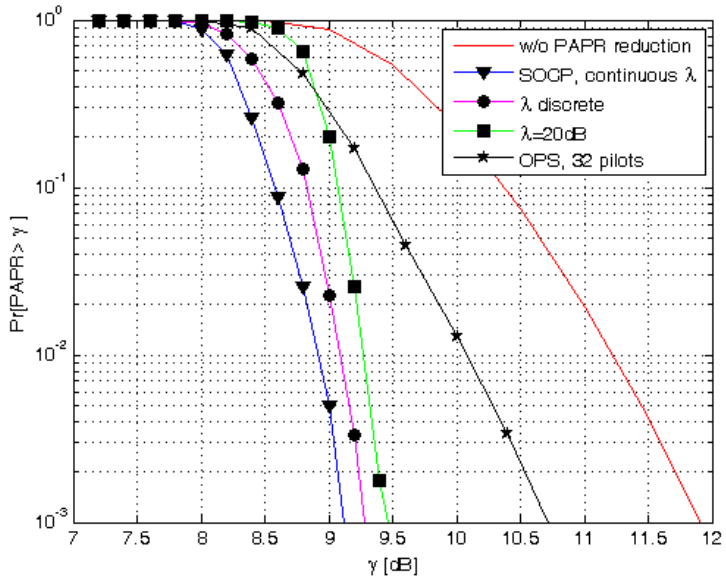

Figure 83: CCDF comparison in two cases: λ = 20 dB and discrete λ, with OPS technique [61], 16-QAM.

In [61], OPS technique using Walsh-Hadamard sequences is chosen in order to make a blind detection of the transmitted sequence at the receiver side. In Figure 83, performance of this technique is given for WH sequences with length Nc= 32 chips. We can easily see that the performance of our proposed method is much better than the one proposed in [61]. A gain from 1.2dB to 1.6dB in terms of PAPR reduction is obtained in this case.

Finally, the performance in terms of PAPR gain is presented in Figure 84 for M=8, 16 and 32 as a function of λ. Figure 84 shows that the PAPR gain performance slightly decreases when M increases, but we note that the optimum value of λ also decreases when M increases. This is important because it means that we can reduce the pilot's power when increasing the number of subcarriers used for PAPR reduction.

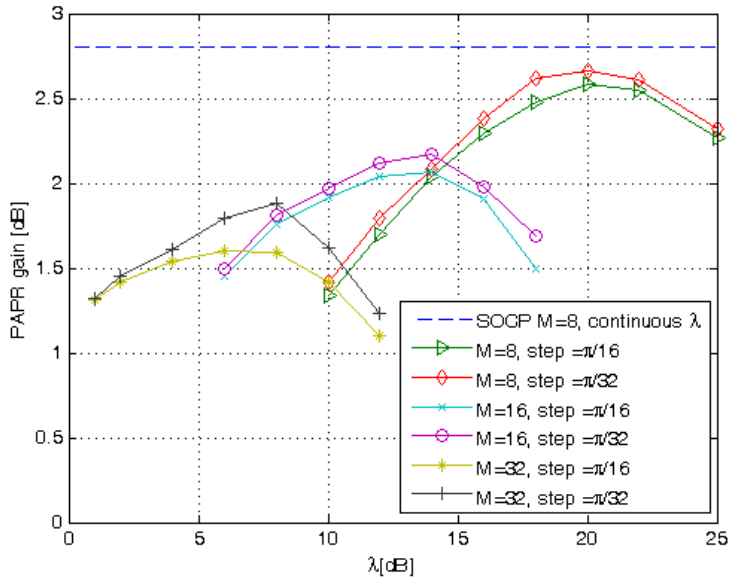

Figure 84: CCDF performance as a function of λ and M, 16-QAM

5.2.5.2 Comparison with DVB-T2 PAPR techniques

First of all, one of the main advantages of this technique is that it could be used with rotated constellation schemes of DVB-T2 standard. This is not the case for ACE technique adopted in DVB-T2 where there is a restriction on rotated constellations. On the other hand, when the pilots are boosted by a factor λ, the transmitted power increases also. So, in order to have a fair comparison, we define the PAPR effective gain as the difference in dB between the PAPR gain ΔG and the power increase ΔE due to the use of boosted pilots (in both techniques), i.e. $PAPR_{eff} = \Delta G - \Delta E$ (Figure 85).

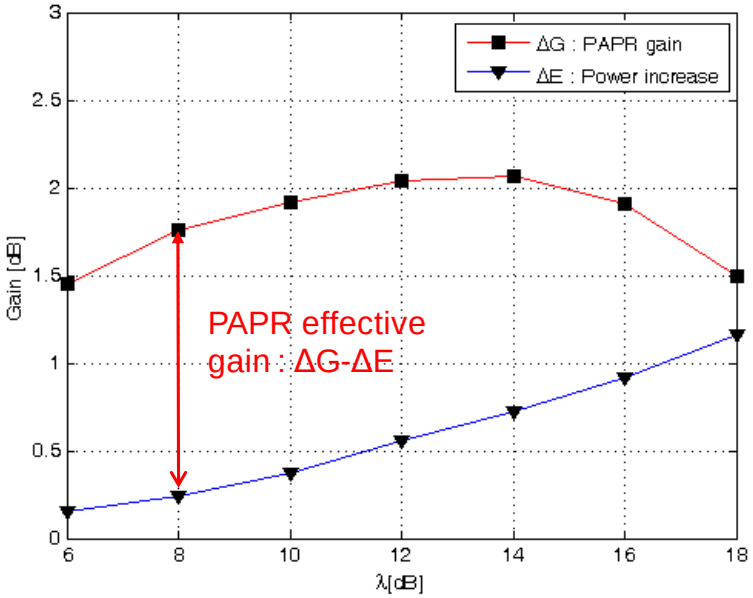

Figure 85: PAPR effective gain

We evaluate in Figure 86 the PAPR effective gain of the proposed method as a function of the pilot power λ, which represents as previously the boost factor of the used pilots for different values of M, and of the elementary step μ. We plot in the same figure the results obtained with the Gradient based method proposed

in DVB-T2. We note that the Gradient solution proposed in DVB-T2 does not specify the boost factor of each dedicated pilot but specifies the maximum permitted power of these pilots. Hence, the boost factor of these pilots in DVB-T2 could change from on symbol to another. In other words, the PAPR gain in Gradient-based solution of DVB-T2 depends on a variable λ value. The obtained results show that the performance of the proposed method is better than the one of the Gradient based method (TR technique) proposed in DVB-T2.

We also note that the optimal boost factor decreases when the number M of channel estimation pilots used for PAPR reduction increase. In DVB-T2 standard, it is specified that the boost factor of the channel estimation pilots could take values between 2 and 7 dB. Then, an optimal tradeoff should be found in terms of number of used pilots for PAPR reduction, PAPR effective gain and channel estimation specifications. The same kind of results and conclusions could be given from Figure 87 for a 64-QAM constellation. In Figure 86 and Figure 87, the performance of the DVB-T2 Gradient algorithm is given as a reference result with a clipping value VCLIP = 5 dB. We note however that the Gradient algorithm needs a smooth control of the transmitted powers of the PAPR pilots. Moreover, using the Gradient algorithm, the allocated powers are varying from one pilot to another.

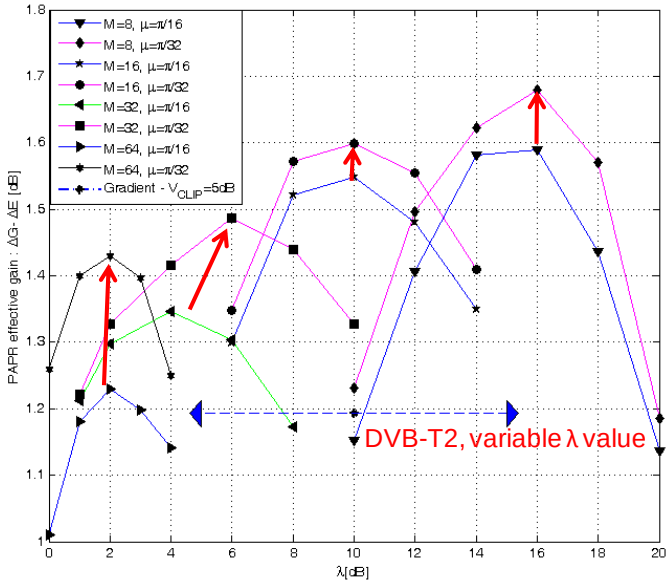

Figure 86: PAPR effective gain: comparison between proposed and DVB-T2 TR techniques, 16-QAM.

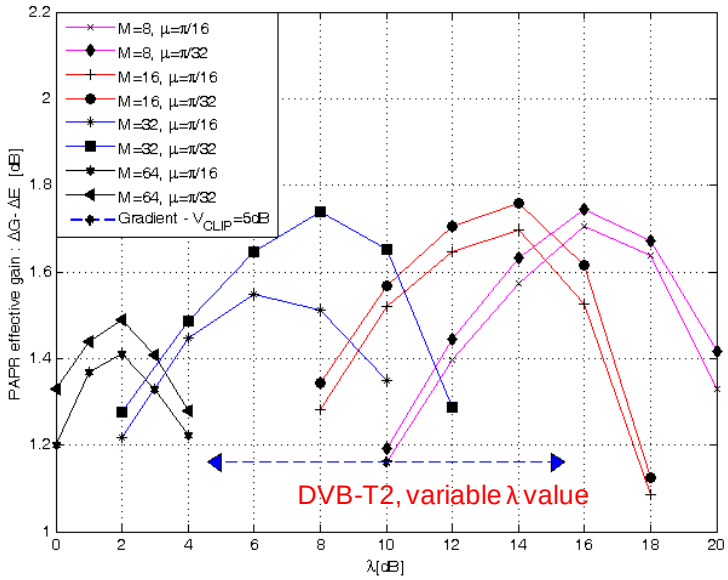

Figure 87: PAPR effective gain: comparison between proposed and DVB-T2 TR techniques, 64-QAM.

5.2.5.3 Channel estimation results

The goal of this section is to show how the system performance is affected by the use of dedicated channel estimation for both PAPR reduction and channel estimation issues.

In order to give more insights about the proposed technique, the error detection probability (EDP) of a sequence used for PAPR and channel estimation is first evaluated. Then, the mean square error (MSE) of channel estimation is performed with respect to the signal to noise ratio (SNR) of the system. The simulation results obtained hereafter are achieved at the output of the Wiener filter. The latter is a 1D filter applied in the frequency domain only. An improvement of the results could be obtained by filtering in 2D, i.e. frequency and time domain.

First, we verify the analytical performance evaluated in expressions (24) and (25). In order to evaluate the EDP values of Δ and ϕ, we consider appropriated elementary step such as for each evaluation, EDP of the other parameter is negligible. For instance, we choose $\mu(\Delta) = \pi/64$ and $\mu(\phi) = \pi/4$ in order to evaluate the EDP of Δ; $\mu(\Delta) = \pi/2$ and $\mu(\phi) = \pi/16$ in order to evaluate the EDP of ϕ. Figure 88 illustrates the comparison between analytical and simulated EDPs for different SNR values. It shows that our theoretical analysis matches perfectly with simulations.

Figure 89 shows the EDP obtained by simulations of the pilot sequence at the receiver as a function of SNR for different values of the elementary steps $\mu(\phi)$ and $\mu(\Delta)$. This figure shows that it is better to quantify the phase difference between two successive pilot symbols with small quantifications steps $\mu(\Delta)$ than quantifying with small steps the possible initial phase value of the first pilot, i.e. $\mu(\phi)$. In other words, it is more efficient to quantify more precisely Δ than the value of ϕ.

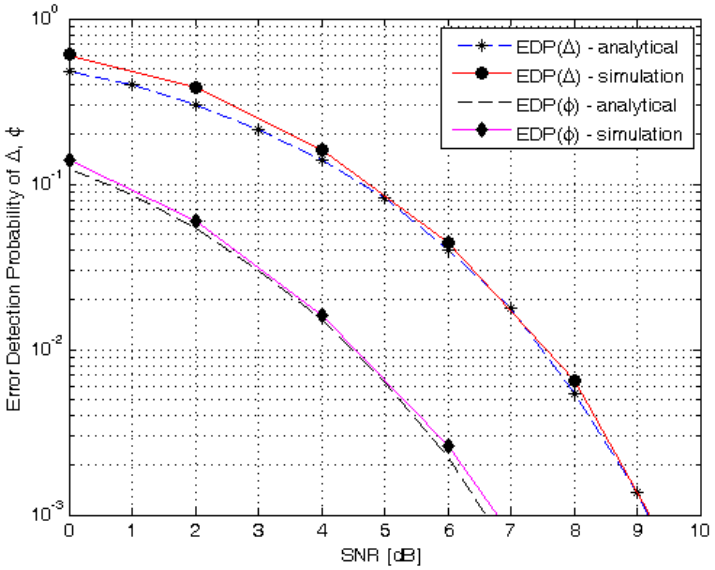

Figure 88: Analytical and simulated Error Detection probability.

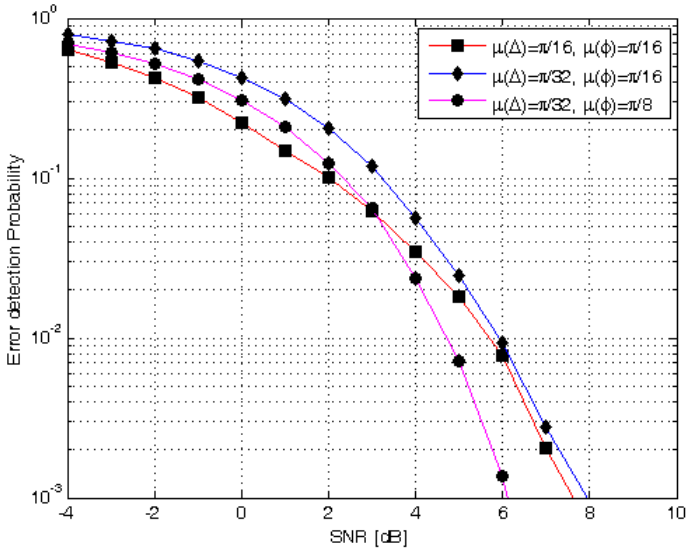

Figure 89: Error detection probability as a function of elementary steps.

Figure 90 presents the MSE of the channel coefficients estimation scheme using a F1 channel proposed in DVB-T2 [1] using the conventional channel estimation scheme presented in DVB-T2 and the proposed channel estimation scheme. The conventional channel estimation relies on a traditional Wiener interpolation based on received channel estimation on pilot positions at the receiver. For the proposed method, as explained in section V, channel response on pilot positions used for PAPR reduction issue is recovered first by using channel response of the previous OFDM symbol. Then channel estimation on all subcarriers is performed using traditional Wiener interpolation. This figure shows that the MSE of the channel coefficients estimated using our method is negligible for a SNR value greater than 6 dB. It is slightly higher than the conventional scheme for smaller SNR values. We recall that, for F1 channel and 16-QAM constellation, the required SNR value to obtain a BER=10^{-7} at the output of the channel decoder is equal to 6.2 dB at a coding rate R=1/2 [1]. The simulation results of this transmission scenario which is the most robust for a 16-QAM constellation are very important. Indeed, since the MSE is independent of the coding rate and, for higher coding rates the DVB-T2 requirements specify higher SNR values to make the system work properly, the

proposed joint channel estimation scheme and PAPR reduction scheme will be always effective for these high SNR values.

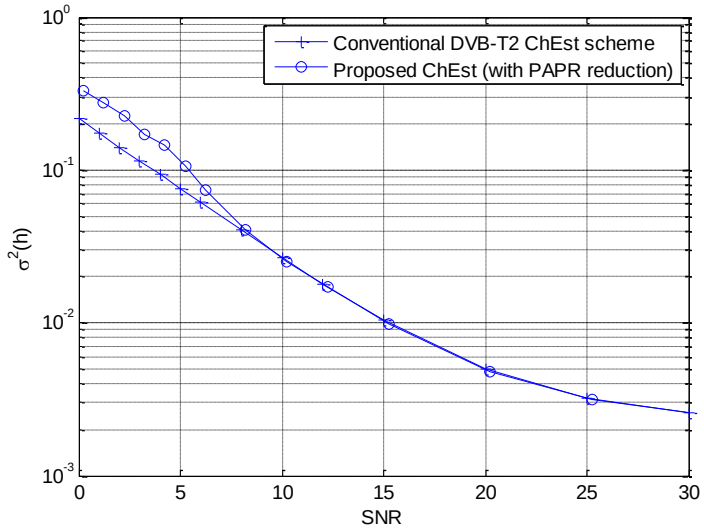

Figure 90: MSE of channel coefficients estimation, 2K mode, 16-QAM modulation, F1 [1].

We also evaluate the Bit Error Rate (BER) of the overall DVB-T2 system. The F1 channel coefficients are estimated through dedicated pilots and then by applying a 2D Wiener filtering. Figure 91 shows the obtained BER performance using the conventional estimation scheme (Figure 78) and the proposed estimation scheme (Figure 79). As expected, the pilot sequence dedicated for channel estimation and used for PAPR reduction is well estimated at the receiver. Hence, the BER performance is not degraded.

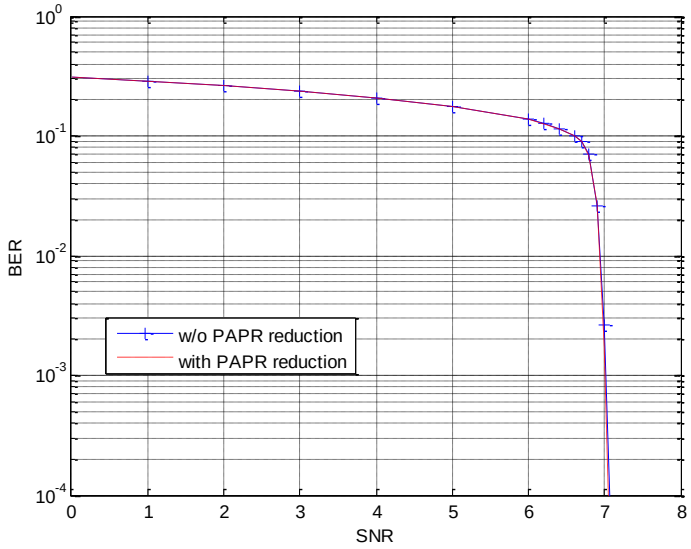

Figure 91: BER performance, 2K mode, 16-QAM modulation, F1 channel.

Now, we consider a time-varying TU6 channel model given in [73]. The Doppler frequency f_d is equal to 33Hz. Figure 92 gives the BER performance for a perfect channel estimation and a Wiener channel estimation without/with proposed PAPR reduction method. The obtained results show that the proposed scheme is efficient with high Doppler frequency scenario. We show in this figure that the overall degradation in comparison with perfect channel estimation is less than 1dB where only 0.1 dB of SNR loss is due to the joint application of PAPR reduction and channel estimation scheme.

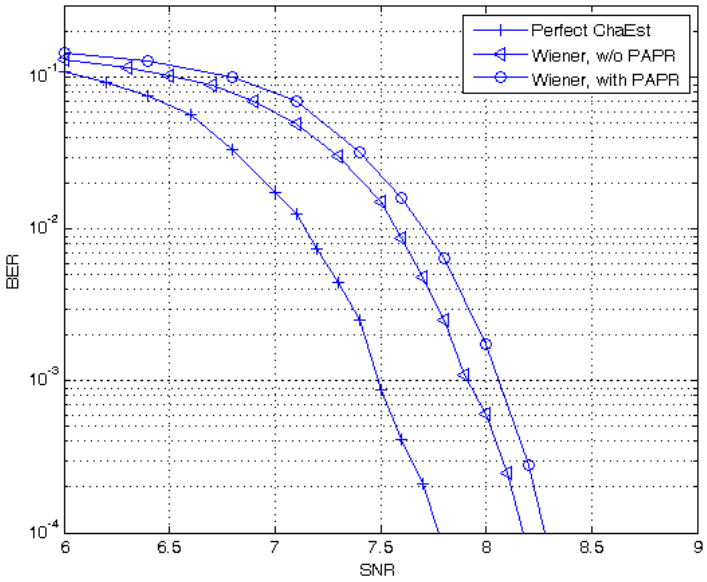

Figure 92: BER performance, 2K mode, 16-QAM modulation, TU6 channel.

5.2.5.4 Results summary

Based on the conclusions given in previous sections, this section summarizes optimal parameters and the corresponding PAPR effective gains using the proposed technique. The different results previously presented have been obtained in the 2k mode. The same analysis has been done in the 8k mode. Table 27 and Table 26 summarize the main parameters chosen as a good tradeoff between PAPR gain, channel estimation performance and optimal transmitted power in the 2k and 8k modes for 16-QAM and 64-QAM modulations. In all cases, the proposed technique presents better PAPR gain than the DVB-T2 TR technique, requires less transmitted power on pilot symbols (the maximum value of the boost factor λ of the PAPR pilots in DVB-T2 is equal to 10 dB) but also a spectral efficiency increase of 1% when it is compared with the actual DVB-T2 standard. It could be also applied using the rotated constellation adopted in DVB-T2. We should note that these parameters, i.e. M, λ, Δ and ϕ are applicable to the context of DVB-T2. However, they should be optimized to other contexts especially when the system parameters like the number of sub-carriers and the constellation size change. Nevertheless, the optimization process remains unchanged.

Table 26- Optimal parameters using the proposed technique, 8K mode.

Modulation	Number of pilots : PP2	M	Elementary steps of ϕ and Δ	λ_{opt}	PAPR effective gain
16-QAM	143	32	μ(Δ)=π/32, μ(ϕ)=π/8	5dB	1.49 dB
	143	DVB-T2 (V_{CLIP}=5dB – 18 pilots)			1.19 dB
64-QAM	143	32	μ(Δ)=π/64, μ(ϕ)=π/16	7dB	1.80 dB
	143	DVB-T2 (V_{CLIP}=5dB – 18 pilots)			1.16 dB

Table 27- Optimal parameters using the proposed technique, 2K mode

Modulation	Number of pilots: PP2	*M*	Elementary steps of ϕ and Δ	λ_{opt}	PAPR effective gain
16-QAM	569	128	$\mu(\Delta)=\pi/64$, $\mu(\phi)=\pi/16$	5dB	1.47 dB
	569	DVB-T2 (V_{CLIP}=5dB – 72 pilots)			1.39 dB
64-QAM	569	128	$\mu(\Delta)=\pi/128$, $\mu(\phi)=\pi/32$	5dB	1.48 dB
	569	DVB-T2 (V_{CLIP}=5dB – 72 pilots)			1.38 dB

5.2.6 Conclusion

A novel PAPR reduction method based on channel estimation pilots is addressed in this work. By using channel estimation pilots to reduce PAPR value, dedicated pilots for PAPR reduction purpose are avoided improving the spectral efficiency of the system. These pilots have to be related by a particular law in order to allow their detection at the receiver side. Multiplicative law in discrete frequency domain is then investigated. Simulations, using the new DVB-T2 standard chain, showed that with appropriate parameters, the proposed method can achieve up to 1.80 dB in terms of PAPR effective gain. In comparison with the Gradient based method initially proposed in DVB-T2, the proposed method presents better performance in terms of PAPR reduction while avoiding the use of dedicated pilots. As a consequence, it allows achieving 1% of spectral efficiency gain. At the receiver side, only a slight modification is required. Simulations have shown that no degradation is caused by this additional function. The obtained results demonstrate the relevance of this method for future broadcasting of OFDM based systems.

6 TIME FREQUENCY SLICING (TFS)

Time-Frequency Slicing (TFS) is a novel transmission technique that consists of transmitting a variable-bit-rate PLP (carrying one or more services) across several Radio Frequency (RF) channels (multiplexes) with frequency hopping and time-slicing (i.e., discontinuous transmission). TFS was originally proposed by Teracom in the standardization process of DVB-T2 (Terrestrial 2nd Generation) [74]. It was initially adopted for the baseline, but finally, it was not specified in the normative part of the T2 specification due to the need of implementing two tuners (front-ends) at the receivers. Instead, the details of TFS were specified in informative annex (Annex E) to the T2 specification [74] to be used for "future implementations". DVB-NGH (Next Generation Handheld) has adopted TFS because it can be operated with a single tuner without adding excessive complexity at the receivers. The reason is the reduced service data rates of mobile TV compared to HDTV DVB-T2 services as well as more realistic use cases for FEF and "guard periods", which makes possible to receive the signal with a single tuner.

This section reports the results of the feasibility analysis of TFS for DVB-NGH performed by **Teracom** and **Universidad Politécnica de Valencia/ iTEAM Research Institute (UPV-iTEAM).**

6.1 Introduction

In a traditional transmission, services are allocated in multiplexes that are distributed over the RF frequency band. The reception of a particular service is performed by tuning the RF channel where the service is transmitted. With TFS, services are allocated over a set of several RF channels, where each such RF channel contains a multiplex in case of non-TFS. Thereby, time slices of one service are transmitted sequentially in a

different RF channel, implementing frequency hopping. This allows services to be potentially spread over the whole RF frequency band. The reception of a particular service is performed by implementing frequency hopping at the receiver side among the RF channels that transmit the time slices of the service. The way TFS works allows services to be spread in the time and frequency domains which supply a large time/frequency diversity that can be exploited in a number of different ways.

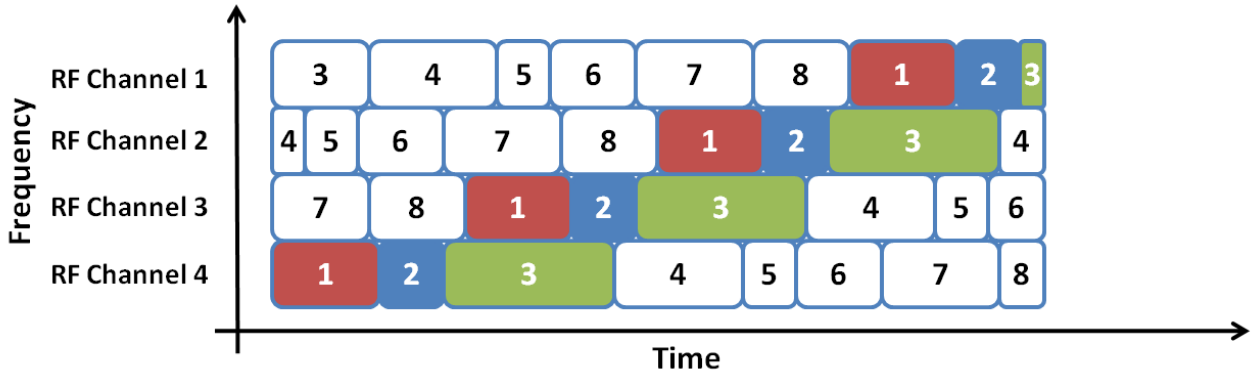

Figure 93: Example of TFS (intra-frame) with 4 RF channels. To receive service 1, receiver must perform frequency hopping between RF channels.

The major advantages of TFS are a gain in capacity and a gain in coverage [75].

The capacity gain of TFS is due to a more efficient Statistical Multiplexing (StatMux) for Variable Bit Rate (VBR) services. StatMux exploits the fact that video codecs generate video streams of a variable bit rate depending on the content encoded. Without StatMux, the capacity of a multiplex should be divided among services considering the maximum (peak) bit rate of each video stream in order to guarantee a correct transmission. This feature implies that, for lower instantaneous bit rates, there would exist an excess of bandwidth that is not being used by any service. Statistical multiplexing takes advantage of the fact that the overall peak bit rate of all video streams together would be significantly lower than the sum of peak bit rates for the individual video streams. This feature makes possible to make a more efficient use of spectrum. Figure 94 shows the bundling of 4 video streams considering the peak bit rate of each service (left) and statistical multiplexing (right). The excess in capacity when using StatMux is defined as the StatMux gain.

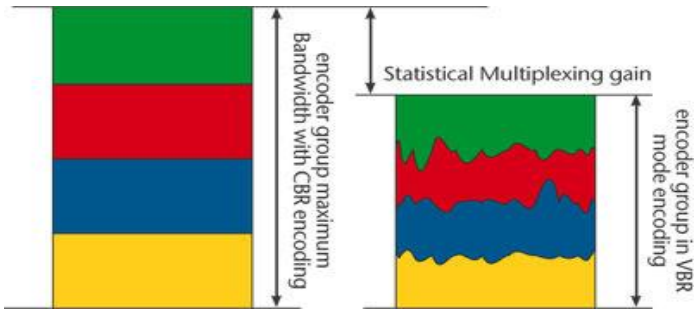

Figure 94: Efficient badwidth use provides StatMux gain when using VBR encoding instead of CBR encoding.

The StatMux gain depends on the number of services jointly multiplexed. Obviously, there is no gain for a single service, but the gain increases as a function of the number of services until saturation.

The coverage gain of TFS is due to increased frequency diversity. The signal of each RF channel is affected by different propagation conditions that not only depend on the characteristics of the scenario but also on the frequency of the RF channel. In a traditional transmission the coverage of a DTT network is determined by

the channel with the worst signal level in each location. With TFS, it is possible to homogenize the coverage of all RF channels in such a way that the service area of the whole set of channels is increased (whereas the area where at least one RF channel is received decreases). Figure 95 shows an example of the coverage of 3 different multiplexes (left) and the effect in the coverage of implementing TFS within the same 3 RF channels.

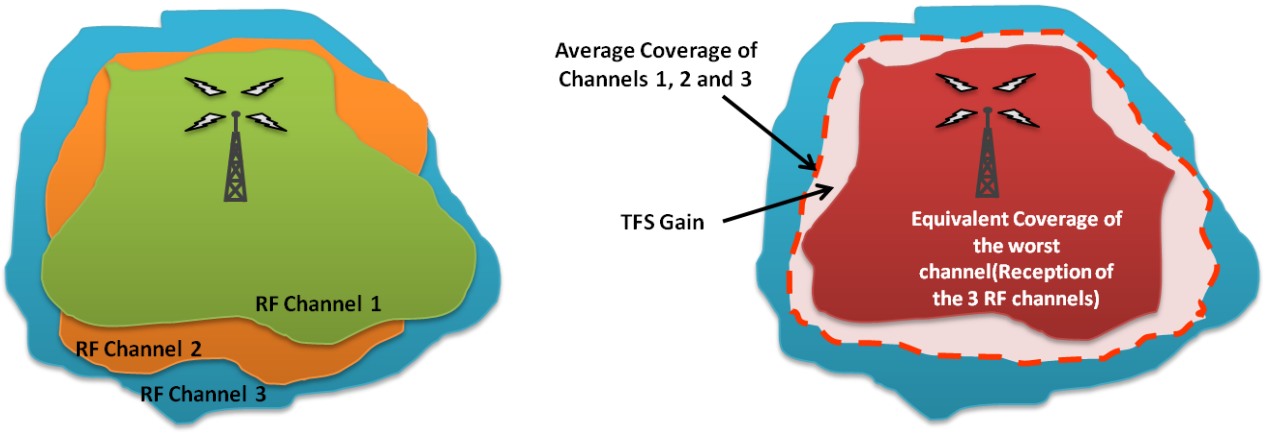

Figure 95. Example of coverage differences between 3 RF channels in a DTT network without TFS (left) and effect of TFS on the coverage of the channels.

The coverage advantage provided by TFS is known as TFS coverage gain and it is closely linked to the number of RF channels involved in transmission and the frequency spacing among them. In general, TFS gain increases with the number of RF channels as this would increase diversity and with frequency spacing as distant channels (in frequency) suffer from different propagation conditions.

6.1.1 TFS in DVB-T2

The main driving force for DVB-T2 was to increase spectral efficiency of the DTT networks for the transmission of high quality services such as HDTV and 3DTV [76]. One of the techniques that could afford this aim is TFS, which was proposed by Teracom, the Swedish DTT operator. However, the inclusion of this technique in the standard was conceived as informative as a result of the necessity of implementing two tuners in the receiver which makes design much more complex and also expensive.

It is a fact that DVB-T2 can provide greater capacity and spectral efficiency than DVB-T; however, the bandwidth requirements of HD services make capacity for this kind of services to be limited within a multiplex. The idea behind TFS was to offer the possibility of combining multiple (up to 6) RF channels to create a high-capacity system that could offer gain in capacity for almost ideal statistical multiplexing across several HD services using VBR encoding. Figure 96 shows an example of the performance of StatMux gain for HDTV services with the number of services.

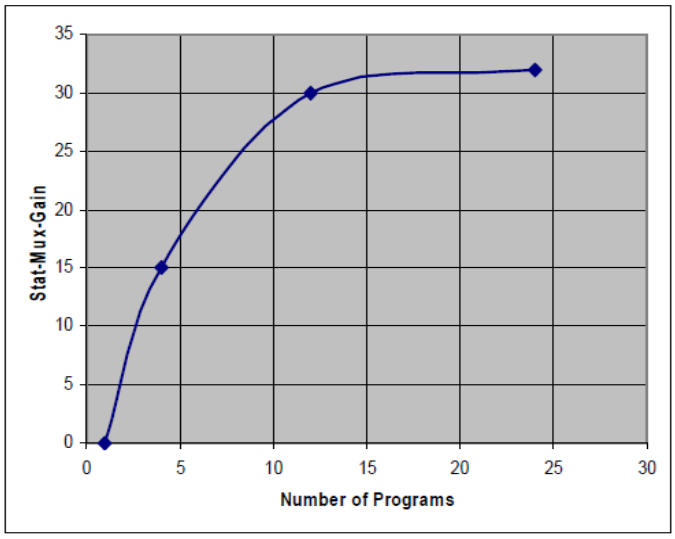

Figure 96: Example of StatMux gain with number of services for MPEG-4 AVC video streams in DVB-T2.

TFS is defined for input mode B, where multiple PLPs are used in transmission. . In this case, P1 symbols, L1 signalling and common PLPs must be repeated simultaneously on each RF channel as these should always be available while receiving any other data. Each type 1 PLP only occurs on one RF channel in one T2-frame but different type 1 data PLPs are transmitted on different RF channels. TFS can operate from frame by frame (inter-frame TFS) for type 1 data PLPs and within the same frame (intra-frame TFS) for type 2 data PLPs. The RF channel for a type 1 PLP may change from frame to frame (inter-frame TFS) or may be the same in every frame (Fixed Frequency) according to the L1 signalling configuration. The sub-slices of type 2 data PLPs are sent over multiple RF frequencies during the T2-frame reaching an interleaving applied both in time and frequency domains.

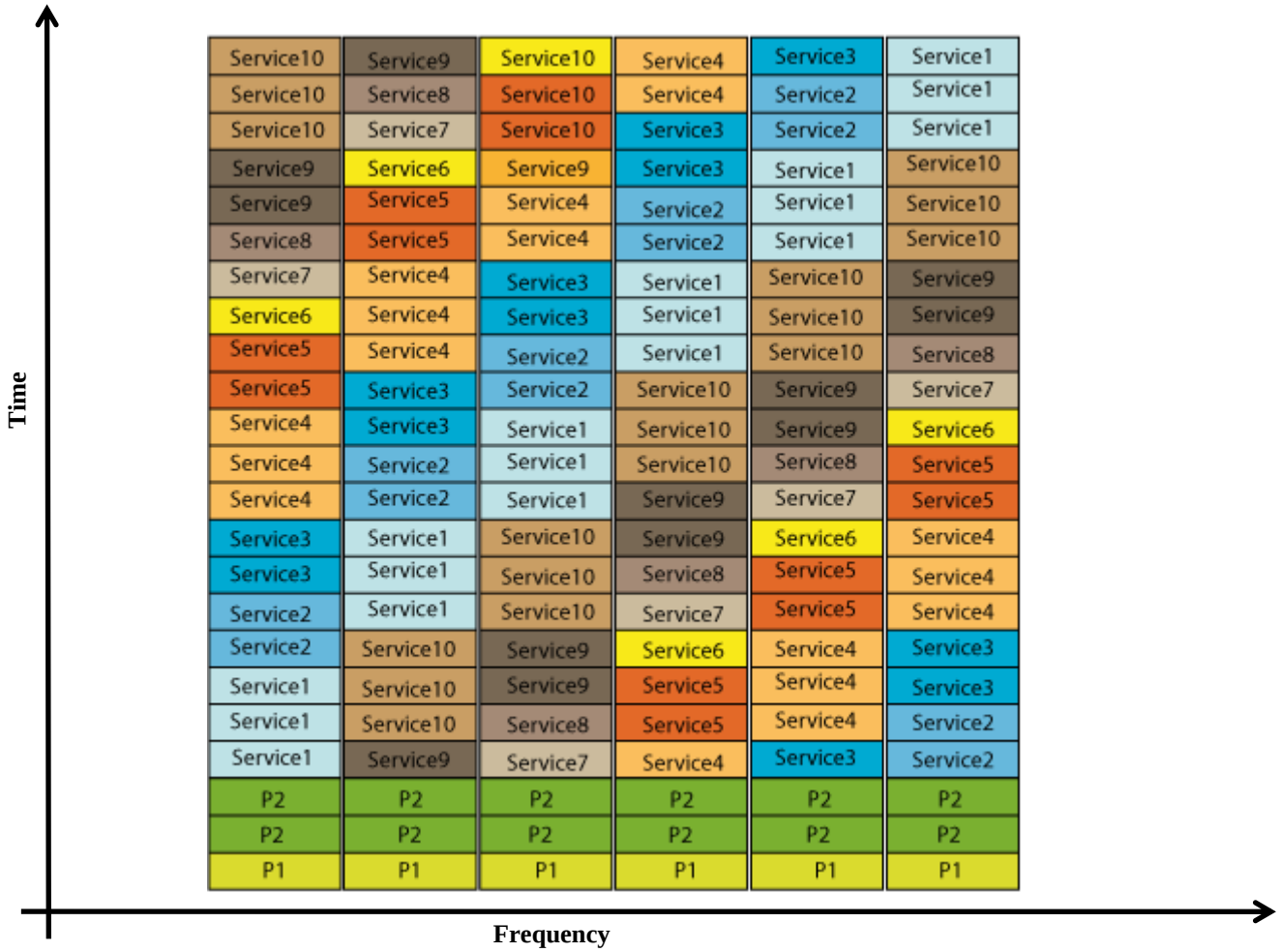

Figure 97: Example of Intra-frame TFS within 6 RF channels.

DVB-T2 Annex E introduces these features, which are not specified for the single profile defined by the standard, but allow future implementation of TFS. The main requirements for TFS implementation in DVB-T2 include both signalling and frame structure. The basic blocks, specified in the DVB-T2 transmission chain, apply when TFS is used; however, frame builder and OFDM generation modules are modified in order to add branches that corresponds to each of the N RF channels.

The major disadvantage that leads to reject implementation of TFS in DVB-T2 is the requirement of providing two tuners at the receiver. It is necessary to guarantee a time interval between slots to perform frequency hopping among RF channels correctly when using a single tuner. Implementation of inter-frame TFS is less strict as there is enough time to perform frequency hopping between slots of the same service; however, implementation of intra-frame TFS requires a complex scheduling in order to assure the necessary time interval. Moreover, it is not always possible to provide a time interval between slots when transmitting high bit rate services. Therefore, the standardization process of DVB-T2 leads to refuse the implementation of intra-frame TFS with a single tuner, which highlighted the need of two front-ends to receive TFS transmissions.

Regarding StatMux gain, previous studies for DVB-T2 have shown that StatMux gain increases with number of VBR statistical multiplexed services in a multiplex. StatMux gain reaches saturation at approximately 9-12 HD programs. High Statmux gain is also obtained for lower number of programs.

Studies are presented as a comparison between a non-TFS case (which almost reaches 15% StatMux gain of

HDTV services) and TFS for 3 and 6 channels which reaches 30% and 32% of StatMux gain assuming HD services of 9.0 Mbps. StatMux gain here referes to the possible bit rate reduction, where (for clarity) a hypothetical 50% reduction would allow a 100% increase in number of services. A 30% bit rate reduction therefore allows about 43% (1/(1-0.30)-1) more services. The increase in capacity is also important as increasing the number of RF channels, capacity is larger. This factor added to additional StatMux gain allows the inclusion of almost 3 HD programs with TFS-6RF and 2 with TFS-3RF. However benefits of StatMux gain appear to be negligible for SD services as large number of programs per RF channel already leads to Statmux gain saturation for a single RF channel. Moreover, there exists a loss in terms of total bit-rate due to the additional overhead of TFS.

Regarding TFS network gain, increased frequency diversity leads to consider two kinds of gain, one related to coverage and the other to interference. A choice of TFS architecture leads to a system where the error correction is applied to each individual service within a TFS multiplex rather than applying the error correction to the TFS multiplex as a whole. Thus, frequency hopping allows for an advantage as a service is affected by disturbance RF channel by RF channel making possible the recovery of each service as good received bursts can compensate bad ones.

Large-scale field measurements show a potential gain of 4-5 dB for TFS-4RF for fixed reception which offer the possibility of increasing the coverage of broadcasted services. These measurements also indicated a similar gain for portable and roof-top reception. This dB gain could also in principle be partly converted to an additional capacity increase, should that be preferred (there is always a trade-off between capacity and coverage/robustness).

Interference gain, although not quantified, was shown to exist in principle in networks based on the frequency allocation plan GE'06. The studies suggest that even higher interference gain could be obtained with changes in the frequency plan.

6.1.2 TFS in DVB-NGH

In a similar way as for DVB-T2, Time-Frequency Slicing could also be very beneficial for NGH, offering a gain in capacity due to efficient StatMux and a gain in coverage due to increased frequency diversity. The point of view from which TFS is addressed in DVB-NGH is slightly different from DVB-T2, as reception conditions and demands from users and operators are not the same in a mobile scenario than for fixed reception. The nature of mobile terminals, in general of reduced dimensions, is not intended to the reception of a service offering of HDTV which can make possible to lower data rates of services. Low data rates in NGH raises the possibility of receiving services with a single tuner that is hopping from RF channel to channel as time constraints turn out to be more relaxed than they were in T2. Moreover, the most important issues that prevail in a mobile communications scenario are related to improvements in coverage and low power consumption at the receiver for longer battery life. Therefore, whereas the main goal of TFS in T2 was increase capacity, NGH would be focused on coverage advantage.

TFS coverage gain in NGH can go beyond the considerations in DVB-T2, where fixed reception was the most important issue. The increased frequency diversity offered by TFS is likely to provide a significant reduction in required C/N. Link budget can be improved for static reception or pedestrian, where time diversity (interleaving) provides little or no gain and space diversity is difficult due to size and cost constraints. Moreover, increased frequency diversity can reduce requirements for time interleaving depth, offering a reduced zapping time for NGH.

From the interference point of view, TFS can also provide additional gains. TFS coverage gain is obtained exploiting the statistical variations of the signal on various frequencies whereas noise remains constant. However, interferences from other transmitters are statistically independent from the signal of the desired

transmitter and will not be the same on all frequencies in the TFS. In general the better C/I performance could be exploited as an improved coverage (the C/I-limited coverage area will increase) and/or a tighter frequency reuse could be used, i.e. more NGH networks could fit within a given spectrum.

The use of TFS over NGH would also offer the potential possibility to find spectrum for NGH services more easily, without causing excessive interference into existing DVB-T/T2 services. The development of TFS technique in NGH is also done taking into account potential interferences caused by the deployment of LTE services in the upper part of the UHF band (channels 61-69) as the result of the digital dividend after DTT transition. There is then the risk that these transmissions will have an adverse effect on broadcast reception on RF channels close to LTE. However, using the TFS principle typically only a small part of the NGH signal (the one close to LTE) would be affected and reception could still be successful thanks to the successful reception of the other parts.

Regarding capacity, TFS capacity gain in DVB-NGH should be analysed in depth as it is not clear to quantify the possible gain when using NGH services allocation in FEFs due to the expected limited capacity of them. Another important issue is that NGH is not intended for the transmission of HDTV services and, SDTV services already achieve very good StatMux gain.

The implementation of TFS in NGH was part of two Call for Technologies responses submitted by Teracom, oriented to a reuse of the T2 specification, and Sony and the Technical University of Braunschweig, oriented to an adaptation of DVB-C2 (2nd generation Cable) specification.

The Sony/TUBS proposal concerning TFS is based on Data Slicing concept (implemented in DVB-C2) that consists of dividing a wide transmission bandwidth of a RF channel (e.g. 8 MHz) in the frequency domain into narrower Data Slices (sub-bands) with a maximum bandwidth of 1.7 MHz. Hence, the receiver only needs to decode a single Data Slice out of the overall transmitted bandwidth which provides the system a very low power consumption on receiver side as segmentation in N bands of the overall channel bandwidth allows the receiver tuner to operate 1/N of the bandwidth and at N times slower rate.

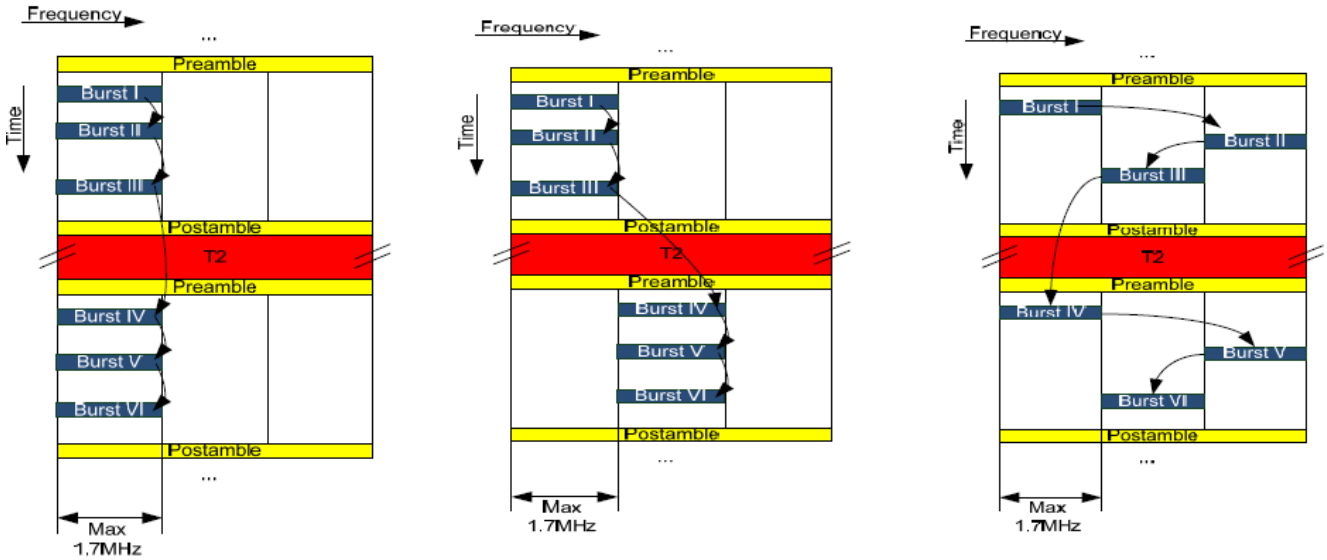

Figure 98: Operation modes of the Sony/TUBS Data-Slicing proposal

Data-Slicing was rejected as a T2-like frame structure achieves better performance in most of the possible NGH scenarios and Data Slice bandwidth (1.7 MHz) is not enough to achieve bit rates higher than 1Mbps at reasonable spectral efficiencies.

Teracom proposal for DVB-NGH consists of an adaptation of TFS mode described in DVB-T2 but with the

requirement of using a single tuner to perform frequency hopping. TFS frequency hopping can be performed by using full bandwidth channels (8 MHz, 7 MHz, 6 MHz, 5 MHz and 1.7 MHz) bundled across RF band (inter-channel TFS) or internally within an RF channel (intra-channel TFS), similarly as Sony/TUBS Data Slicing, which allows almost the same performance as in full bandwidth case but with a notable reduction of power consumption.

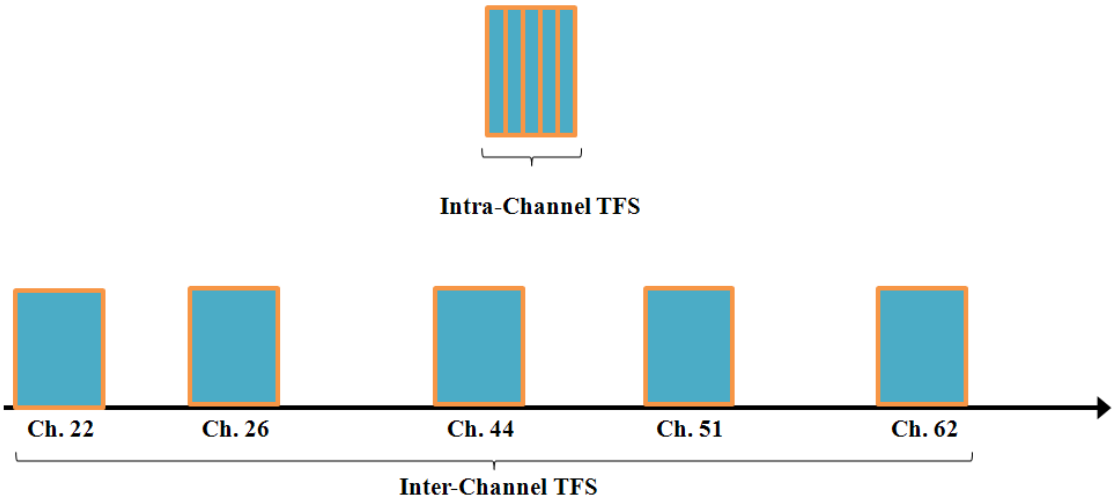

Figure 99: Intra-Channel0 (above) and Inter-Channel (below) modes proposed by Teracom.

TFS can be implemented within the same frame (intra-frame TFS) and frame-by-frame (inter-frame TFS). These two methods are oriented to a particular operation mode for NGH and directly depend on frame size as soon as frames should be large enough to be received with a single tuner.

Intra-frame TFS is thought to be implemented when there exist a whole 250 ms frame entirely dedicated to NGH services. However, NGH is more likely to be implemented in FEFs (Future Extension Frame) of a DVB-T2 frame (in a structure of e.g. 250 ms dedicated to a T2 frame and e.g. 50 ms for a NGH FEF) where inter-frame TFS should be used due to impossibility of using intra-frame due to tuning time constraints with such a reduced frame length.

6.2 TFS Concept

TFS concept is to be developed in two different ways in DVB-NGH. Although NGH services will probably be allocated in the FEFs of DVB-T2 frames, and consequently inter-frame TFS should be the most suitable mode of operation, there exists the possibility of implementing intra-frame TFS within large frames. Nevertheless, both modes of TFS operation should intrinsically involve the use of a single tuner (front-end) in the receiver.

Intra-frame TFS may be implemented as a reuse of the informative T2 Annex E, but assuming a single tuner in the receiver, which is one on the requirements in NGH standardization. The solution for intra-frame TFS works with type 2 PLPs, those which have 2 or more sub-slices in a frame. Time constraints for intra-frame TFS operation with a single tuner implies the necessity of providing enough time for tuning between slots. To achieve this aim frames should be long enough and service data rates lower compared to T2. Using a "guard period" of Type 1 PLPs in each frame, or a FEF between frames, makes it easier to perform the frequency hopping, since hopping at the border between two frames is the most critical case.

When the NGH frame time is short (such as 200 ms T2 frame + a 50 ms NGH in the T2 FEF), there is not enough time to perform frequency hopping inside the frame and it has, instead, to be done between frames.

This case leads to consider implementing frequency hopping between frames (inter-frame TFS) where both type 1 and type 2 PLPs could be used. In this case, when type 2 PLPs are used there is, however, no frequency hopping within each frame only between frames. This use case can be seen as a special case of the FEF bundling, in which an NGH frame is not mapped to a single T2 FEF but could be extended over several FEFs. A T2 FEF could even include the end of one NGH frame and the beginning of the next one.

6.2.1 Intra-Frame TFS

Intra-frame TFS is performed inside the frame. The receiver implements frequency hopping between sub-slices. This mode of operation implies intra-frame time interleaving and it is only possible for type 2 PLPs. In this case, the sub-slices which belong to a service are transmitted in parallel over the set of RF channels. That means sub-slices of all services are spread over the set of RF channels. Critical parameters in intra-frame TFS operation as frame duration, MODCOD and number of subslices should be controlled to guarantee single tuner reception, although, as mentioned above, the use of FEFs and/or guard periods could simplify the frequency hopping.

Scheduling of services for intra-frame TFS shall consider variation in the bit rates of the services that makes sub-slices have a variable length. However it is possible to implement a deterministic scheduling of the amount of services which can lead to a regular distance between sub-slices or an almost constant hopping time between slots. These mechanisms are implemented in the scheduler which is part of the physical layer mechanisms of DVB-NGH.

In general, the service data is written into the frame during the frame duration TF. Each frame consists of different cells which contain data from one service (PLP) and their size depends on the instantaneous bit rate of the services. Moreover, the size of the TFS frame in bits is not constant because of the dynamic size of the subframes and physical channel specific MODCOD parameters. However, the size is constant in OFDM symbols (or useful carriers) per frame.

The starting point for scheduling is a set of PLP cells which are disposed one after the other as a matrix with $N_{subslices} \cdot N_{RF}$ columns.

The size of each cell is determined by the bit rates of the services mapped into the same physical channel. Therefore, cell size may change from frame to frame according to the bit rate variation of the services but the frame size is fixed. In the Figure 100, an example of a matrix with 6 PLPs is shown. In this case, there are 2 sub-slices per RF channel and 3 RF channels (6 columns).

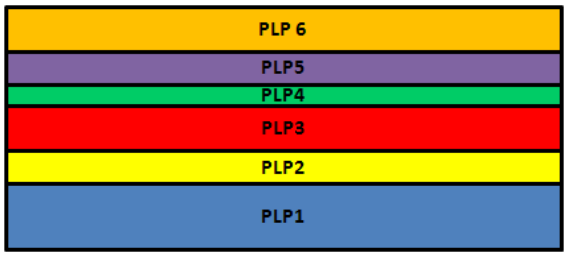

Figure 100: Example of a matrix with 6 PLPs, starting point for the scheduling.

The total number of PLP cells is divided into the number of sub-slices per RF channel ($N_{subslices}$) of equal size. Figure 101 shows the result of this operation.

Figure 101: First step of the scheduling.

All the resultant sub-slices are disposed in column. According to the total number of PLP cells (in this case 6), the parameter sub-slice interval is defined as the distance between two sub-slices of the same PLP cell.

$$Subslice_{Interval} = \frac{Total\ number\ of\ cells}{Total\ number\ of\ subslices}$$

The resultant structure is then divided (by columns) according to the number of RF channels involved in the TFS transmission. For this particular example there exist 3 columns (one for each RF channel) containing slots of the PLP cells.

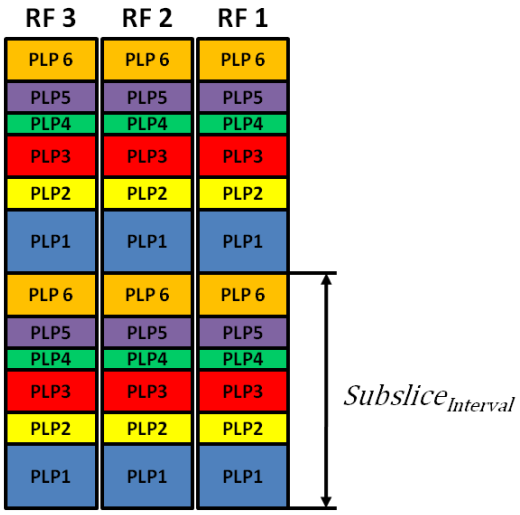

Figure 102: Second step of the scheduling.

Intra-Frame TFS transmission implies that services are transmitter in parallel in each RF channel. However, there should exist some mechanisms that guarantee that a single tuner can perform frequency hopping among channels and receive services regularly and one after the other.

To achieve this feature, a time shift is implemented in the set of slots corresponding to each RF channel.

$$RF_{Shift} = \frac{Subslice_{Interval}}{N_{RF}}$$

Figure 103 shows the effect of time shifting in each RF channel.

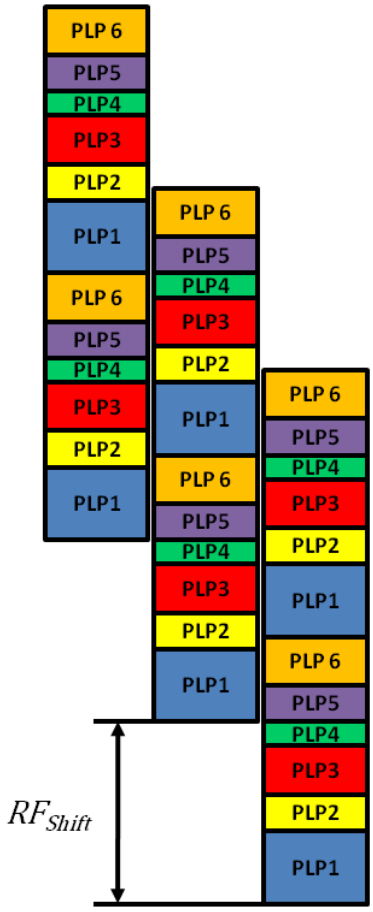

Figure 103: Effect of time shifting in each RF channel.

The slots that exceed the frame length must be folded back. As a result of the time shift and folding the TFS frame is ready to allocate services and to perform frequency hopping.

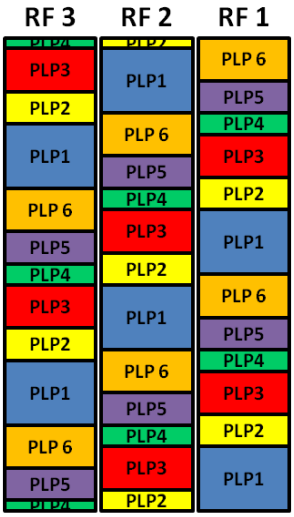

Figure 104: The slots exceeding the frame length are folded back.

It should be noted that the previous process has defined the scheduling for Intra-frame TFS implementation; however, scheduled cells has not yet been filled with data. Only positions in the frame have been defined.

Time interleaved PLP cells are introduced into sub-slices in the natural time sequence, independently of RF channel. The first time interleaved cell is therefore introduced in the first cell position of the first sub-slice of the PLP (independently of the RF channel in which it appears).

6.2.2 Inter-Frame TFS

Another technique to implement TFS for the transmission of NGH services is known as inter-frame TFS. Otherwise than as in intra-frame TFS, frequency hopping is performed between frames and not within the frame. Inter-frame TFS is thought to be implemented when allocating NGH services in the FEFs of DVB-T2 (Figure 105) as frame length makes impossible to implement intra-frame TFS. However, inter-frame TFS can also be used in a dedicated multiplex to NGH services.

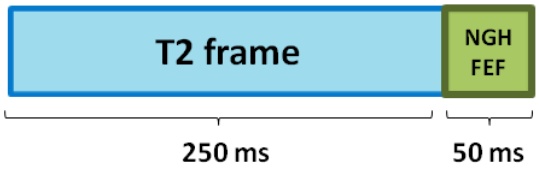

Figure 105: NGH services allocation in FEFs of the T2 frame.

With inter-frame TFS, the slots of the services are not transmitted in parallel over the set of RF channels but are allocated inside FEFs which are distributed in time and frequency along RF channels. Frequency hopping is performed at the receiver side with relaxed time restriction due to the duration of the frames and the large time intervals among them. This makes scheduling of inter-frame TFS transmission to be not as critical as inter-frame TFS.

An example of an inter-frame TFS transmission is shown in Figure 106. As in Figure 105, blue frames correspond to DVB-T2 services whereas green slots correspond to FEFs where NGH services are allocated. Frequency hopping is performed at the receiver within a concrete number of RF channels (in this example, 3 channels).

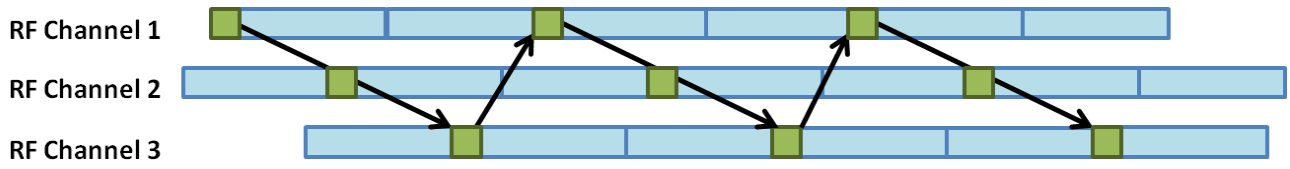

Figure 106: Example of inter-frame TFS transmission.

The main factors involved in this mode of transmission are time interleaving, zapping time and also power saving. The transmission of services among FEFs implies that there must exist some time interleaving among them to guarantee time diversity as the use of only one FEF deals to too little interleaving depth. Power saving control depends on the implementation of Inter-Frame TFS as frequency hopping is one of the most important factors with implication in power consumption. A large spacing in time between FEFs reduces power consumption as frequency hopping is produced less often. However, assuming there exist some time interleaving among FEFs, zapping time is increased with spacing among FEFs. To solve this problem, the

solution proposed is the use of time-shifted superframes as shown in Figure 107 (right).

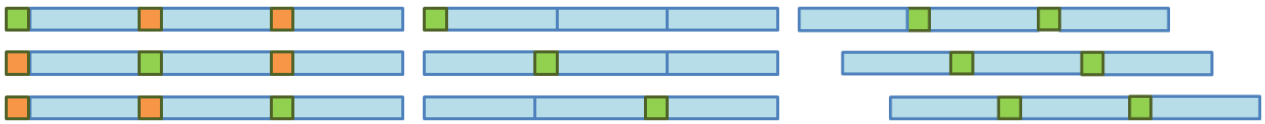

Figure 107: Interleaving over FEFs with frequency hopping between RF channels using co-timedT2 frames (left), time shifted FEFs but co-timed superframes (center), and time-shifted superframes (right).

6.2.3 Time constraints for TFS operation modes

6.2.3.1 Requirements for the tuning time

The transmitter must guarantee that the slots in which services are allocated are separated at least by a certain time interval such that receivers can perform frequency hopping with a single tuner and, therefore, successfully receive TFS transmission. The minimum frequency hopping time period between slots is measured from the end of one slot to the beginning of the next one that belongs to the same service.

Frequency hopping in the receiver implies to perform operations that involve PLL tuning, AGC tuning, fine frequency synchronization and channel estimation. The tuning operations between two slots in the middle of the frame need a time interval for the finalization of channel estimation for the current slot (T_{CHE}), the performance of frequency hopping (T_{tuning}) and finally the reception of the symbols needed for channel estimation and fine synchronization (T_{CHE}). Figure 108 illustrates this timing.

Therefore, the minimum frequency hopping time between data slots is calculated as 2* T_{CHE} + T_{tuning}.

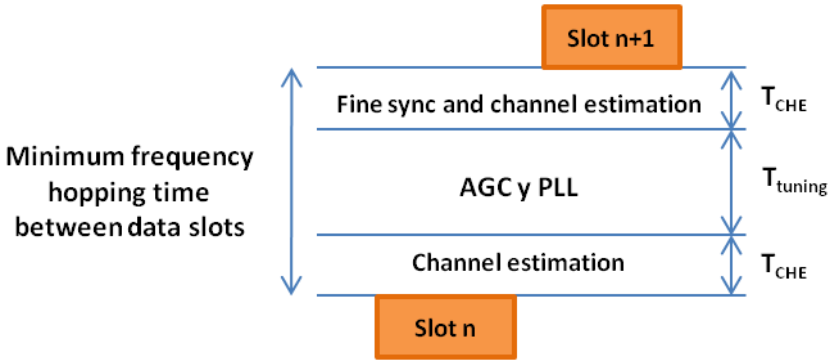

Figure 108: Illustration of the requirements for the tuning time.

It is assumed that the coarse frequency and symbol time synchronizations, which can be estimated from pilot symbols P1 and P2, need to be done before receiving the slot. It is reasonable to assume that PLL and AGC tuning takes about 5 ms. After that at least one OFDM symbol is needed for fine frequency error estimation. In addition to that, some more symbols may be needed in the channel estimation to make the time interpolation.

Table 28 shows the required frequency hopping time between data slots calculated during the T2 standardization process.

Table 28. Values for S_{tuning} (number of symbols needed for tuning, rounded up, for 8 MHz bandwidth), when tuning time = 5 ms for DVB-T2

FFT size	T_U (ms)	Guard Interval						
		1/128	1/32	1/16	19/256	1/8	19/128	1/4
32K	3.584	2	2	2	2	2	2	NA
16K	1.792	3	3	3	3	3	3	3
8K	0.896	6	6	6	6	5	5	5
4K	0.448	NA	11	11	NA	10	NA	9
2K	0.224	NA	22	22	NA	20	NA	18
1K	0.112	NA	NA	10	NA	9	NA	8

Therefore, the frequency hopping time depends on the used mode (FFT size and GI) and the number of symbols assumed to be used in the synchronization/channel estimation. A too tight period of time cannot be assumed, some margin must be left to take into account different implementations and possible effects of the channel.

Related to the minimum tuning time, another important time restriction is the time shift among slots in a frame (the distance in time between the two slots that belong to the same service). This time is required to be larger than the frequency hopping time in order to avoid overlapping and malfunction of the TFS transmission. The minimum shift is calculated as $RF_{shift} \geq Max\_Slot\_Length + 2^{*} T_{CHE} + T_{tuning}$.

Requirements for the guard period between frames

Deterministic scheduling for intra-frame TFS, which has been previously explained, guarantees frequency hopping internally in a frame with a single tuner. However, a guard period is needed at frame boundaries to allow enough tuning time (for e.g PLP 1 in

Figure 109).

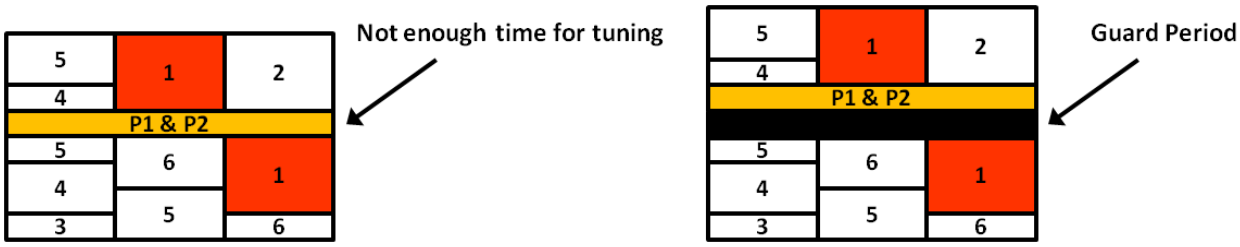

Figure 109: Illustration of the need for a guard period.

Critical jump, produced at the frame boundary between slots carrying the same service when there is not enough time for tuning and receiving preamble, should be avoided during transmission of frames. To enable simple slot allocation algorithms, that avoid complicating the scheduling, it is suggested that an additional time slot of the length of the tuning time is added on every frequency before the signalling symbols P1 and P2 (Figure 109).

The symbols transmitted during the guard period are not redundant, but could be filled with some low bit rate service, like radio or auxiliary (teletext –like) services. Furthermore, it is possible to implement guard periods by means of FEFs between frames or Type 1 PLPs that are located at the beginning of each frame.

Figure 110 shows two methods for implementing the guard period when using large frames entirely dedicated to the broadcasting of NGH services. As said before, to guarantee enough tuning time between

frames, FEF or Type 1 PLP durations could be used as guard intervals.

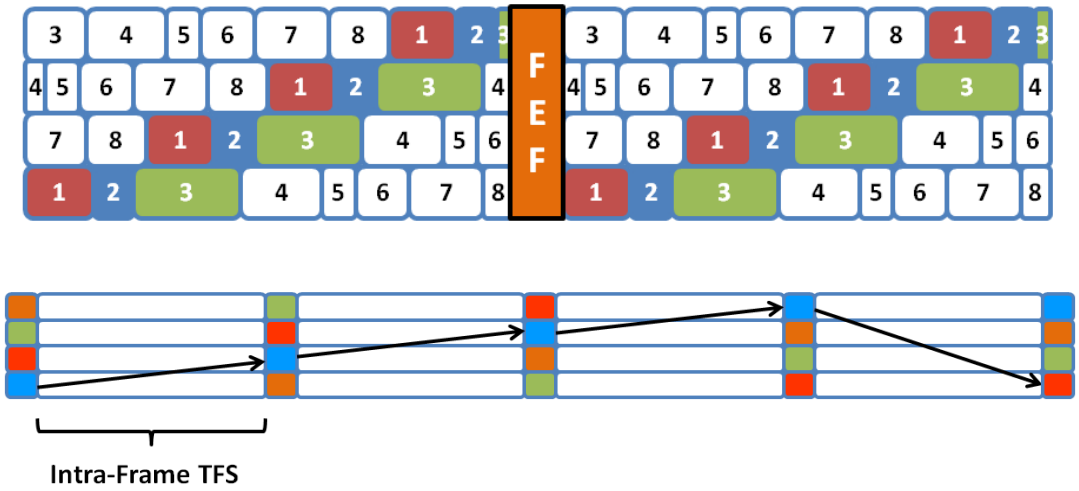

Figure 110: Two possible methods for the guard period implementation.

Inter-frame TFS time constraints are relaxed as there exist the possibility of transmitting more than one frame between two FEFs (slots), increasing the time interval for tuning.

7 MIMO TECHNIQUES

The key issue in the MIMO transmission is to exploit the space dimension offered by the multiple-antenna structure. This is achieved by converting the vector of symbols to be transmitted into multiple coded replicas assigned to each transmit antenna. This leads to a so-called space-time (ST) coding scheme. Similarly to classical channel coding, two different coding approaches are considered in the literature: space-time trellis codes (STTC) and space-time block codes (STBC). This report mainly concerns the latter because it is considered as yielding the best trade-off of performance/complexity when combined with efficient forward error correction (FEC) schemes.

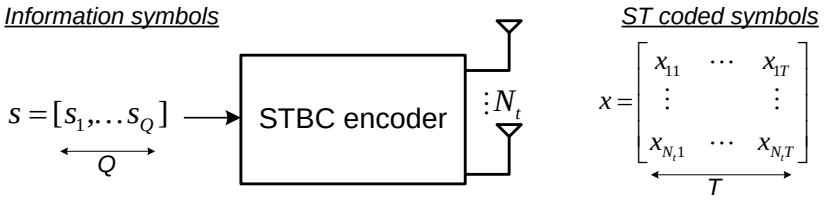

Figure 111: ST encoding.

An STBC scheme employs at the transmitter a STBC encoder which encodes the original information symbols and then assigns each ST-coded symbol to a given antenna for a given time. Figure 111 describes a ST encoder that converts Q symbols, coming for example from a constellation mapper, into T ST-coded symbol vectors spread over N_t transmit antennas. More specifically, the ST encoding is described by matrix **X**:

$$\mathbf{X} = \begin{pmatrix} X_{1,1} & X_{1,2} & \cdots & X_{1,T} \\ X_{2,1} & X_{2,2} & & X_{2,T} \\ \vdots & & \ddots & \\ X_{M_T,1} & X_{M_T,2} & & X_{M_T,T} \end{pmatrix} = f\left\{\begin{pmatrix} S_1 & \cdots & S_Q \end{pmatrix}\right\}$$

where the *i*th row of matrix **X** represents the signal vector that will be transmitted in the *i*th antenna within *T* successive time slots while the *j*th column of matrix **X** represents the signal vector that will be transmitted in the *j*th time slot across N_t transmit antennas. As a result, the spatial rate is defined as:

$$R_M = \frac{Q}{T}$$

With this notation, the raw bit rate of a multi-antenna scheme is increased by a factor of R_M with respect to the corresponding Single Input Single Output (SISO) scheme.

7.1 Candidates of Space-Time (ST) Codes for DVB-NGH

7.1.1 List of Candidates of ST Codes in the NGH Project

A good many of ST codes are proposed for the DVB-NGH program. It has been distinguished between MIMO codes of rate 1 and rate 2. The former provide diversity gains and are compatible with single antenna transmitters and receivers. The latter provide diversity and multiplexing gains but require the implementation of multiple antennas at the transmitter and receiver side. The gain achieved by MIMO rate 2 codes is relevant for high SNRs as it is illustrated in Figure 112 which represents outage capacity against *signal to noise ratio* (SNR). For SNR values below 10 dB MIMO codes of rate 1 and rate 2 have very similar performance. For SNR values above 10 dB MIMO codes of rate 2 have a significant gain compared to MIMO codes of rate 1 and therefore the cost due to the implementation of multiple transmit antennas at both the transmitter and receiver is justified.

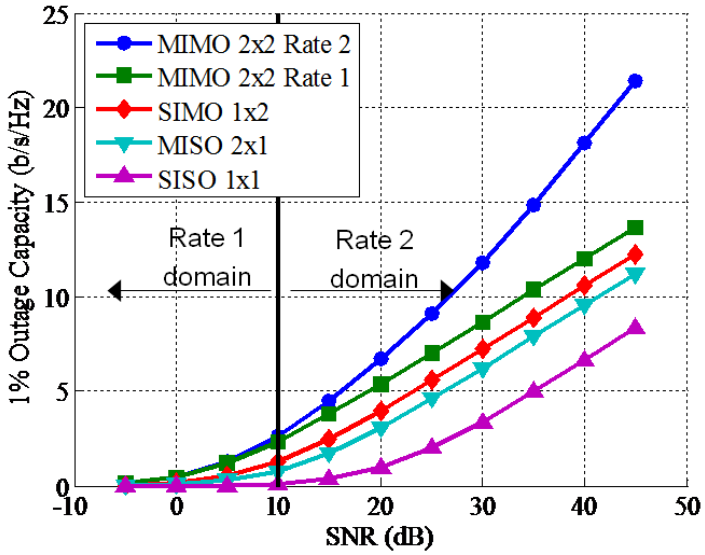

Figure 112: Outage capacity for a target outage probability of 1% in Rayleigh channel

More precisely, the ST codes studied in the framework of ENGINES project are:

Rate-One (diversity coding)

- Alamouti code [79]
- Single-Input-Multiple-Output (SIMO) [82][83]

Rate-Two (spatial multiplexing)

- Rotated-Constellation-based Spatial Multiplexing scheme proposed by Telecom Bretagne [84]

4 Transmit antennas codes

- L_2 code by University of Turku[85]
- MUMIDO code by University of Turku[85]
- Restricted Enhanced Spatial Multiplexing (RESM) code by University of Turku[85]

Hybrid satellite/terrestrial transmission scheme

- 3 transmit antennas (2x terrestrial, 1x satellite) by University of Turku[86]

In addition, some ST codes are also proposed by other DVB members that are not involved in the ENGINES project:

Rate-One (diversity coding)

- eSFN proposed by Technische Universität Braunschweig (TUB) [87][88]
- Transmit Antenna Switching (TxAS) proposed by LG [89]

Rate-Two (spatial multiplexing)

- Enhanced Spatial Multiplexing (eSM) by LG [90]
- Phase Hopping Spatial Multiplexing (PH-eSM) by LG [92]
- Unequal power code by ETRI [93]
- Multi-layer Spatial Multiplexing (ML-SM) by Politecnico di Torino and RAI [94]

7.1.2 Rate-One

The utilization of MIMO rate 1 schemes increase the system capacity and/or the coverage area by means of increased spatial diversity. In a SFN scenario signals transmitted from multiple transmitters have to be added at the receiver position in amplitude and phase. In case of high correlation between them (e.g., line-of-sight components), the received signals can cancel each other due to destructive interference or suffer a significant reduction of the total received power. In order to cope with aforementioned problem, DVB-NGH adopts for its baseline two MIMO rate 1 schemes: the MISO 2x1 scheme of DVB-T2 with Alamouti coding, and a new scheme proposed by TUB known as eSFN (*enhanced Single Frequency Networks*).

7.1.2.1 Alamouti code

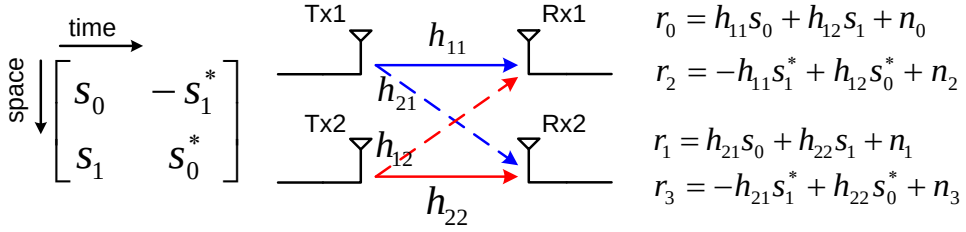

Figure 113: Alamouti ST code scheme.

The Alamouti code [79] is the most known ST coding scheme with full diversity and code rate one. The received signal can be written as:

$$\begin{bmatrix} r_0 \\ r_1 \\ r_2^* \\ r_3^* \end{bmatrix} = \underbrace{\begin{bmatrix} h_{11} & h_{12} \\ h_{21} & h_{22} \\ h_{12}^* & -h_{11}^* \\ h_{22}^* & -h_{21}^* \end{bmatrix}}_{\mathbf{H}} \begin{bmatrix} s_0 \\ s_1 \end{bmatrix} + \begin{bmatrix} n_0 \\ n_1 \\ n_2 \\ n_3 \end{bmatrix}.$$

The advantage of the Alamouti coding scheme is that it creates an orthogonal MIMO channel structure, i.e. $H^{\mathrm{H}}H$ is diagonal matrix, which enables low-complexity *maximum-likelihood* (ML) symbol detection using the simple *zero forcing* (ZF) decoding:

$$\hat{\mathbf{s}} = \left(\mathbf{H}^{\mathrm{H}}\mathbf{H}\right)^{-1}\mathbf{H}^{\mathrm{H}}\mathbf{r}$$

The disadvantage of this scheme is that in order to decode the received signal, all four channel links, i.e. $h_{11}, h_{12}, h_{21}, h_{22}$ should be estimated. Therefore, it requires twice pilots as much as that is needed in the SISO case.

The modified version of the Almouti scheme for DVB-T2 permits the extraction of all available spatial diversity in the MIMO channel. It is applied between different transmitters of the network. It reutilizes the current network structure with one transmit antenna. The receivers have to be aware of the Alamouti transmission to correctly receive the data but can be implemented with a single antenna. Assuming a transmission system with two transmitters and one receive antenna, two consecutive carriers with modulated symbols s_1 y s_2 are mapped to the first transmitter whereas the modulated symbols $-s_2$* y s_1* are mapped to the second transmitter, where * denotes the complex conjugate. At the receiver side appropriate signal processing extracts the available spatial diversity. The Alamouti code can be extended for schemes with multiple receive antennas by means of space-frequency codes in OFDM systems. The benefit compared to SFN networks is the increased spatial diversity. On the other hand, it needs twice as many pilots as in comparison with single antenna transmission.

7.1.2.2 SIMO

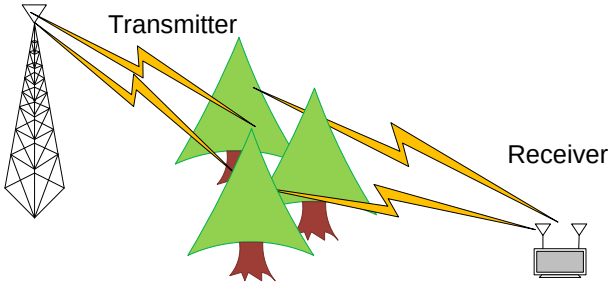

Figure 114: SIMO scheme.

The Single-Input-Multiple-Output (SIMO) is a receive antenna diversity scheme. Multiple antennas are used at the receiver side in order to increase the robustness of the reception. As the geographical separation of the receive antennas are small compared to the signal propagation distance, the received signals on different antennas commonly have correlated shadowing processes and uncorrelated multipath processes.

The advantage of this scheme is that it increases the robustness of the reception while does not require additional pilot overhead.

However, according to the theoretical analysis [82] and simulation results [83], MIMO channel capacity is greater than or equal to the average capacity of the two SIMO channels, even in the worst case ($\det(H) = 0$).

7.1.3 Rate-Two

7.1.3.1 Spatial Multiplexing (SM)

Spatial multiplexing (SM) [88] uses all the degrees of freedom of the MIMO channel to exploit spatial and multiplexing diversity providing both coverage and capacity gain. The incoming stream is divided in multiple independent streams which are modulated and directly fed to the transmitters as it is illustrated at Figure 115.

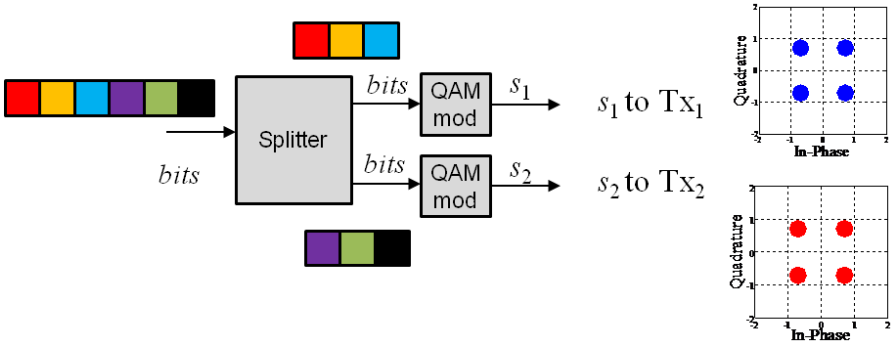

Figure 115: Example diagram of SM for 4 bits per cell (16-QAM)

The received signal by each one of the cross-polarized antennas is described as follows:

$$r_1 = s_1 h_{11} + s_2 h_{12}$$
$$r_2 = s_1 h_{21} + s_2 h_{22}$$

where the additive noise has been neglected to ease the notation. Here, r_1, r_2 are the signals at the receive antennas 1, 2 respectively; s_1, s_2 are the modulated symbols at the transmitter; and h_{11}, h_{12}, h_{21}, h_{22} are the MIMO path channel components of Figure 2. From expression (1), it can be seen that modulated symbol s_1 is transmitted through h_{11} and h_{21} while s_2 is transmitted through h_{12} and h_{22}. This means that each transmitted symbol will be able to obtain spatial diversity from 2 channel paths.

7.1.3.2 Rotated Constellation-based Spatial Multiplexing scheme (rSM)

The so-called "rotated Spatial Multiplexing" or rSM scheme was studied by Telecom Bretagne in the framework of ENGINES and this rate 2 code was afterwards proposed to DVB-NGH to compete with the other proposed Spatial Multiplexing schemes, in particular the so-called "enhanced Spatial Multiplexing" or eSM scheme.

7.1.3.2.1 A brief recall about rotated constellations

Let us denote by $X = I + jQ$ a QAM symbol to be transmitted, prior to the constellation rotation. After the constellation is turned by angle θ, the transmitted symbol S can be expressed as:

$$S = Xe^{j\theta} = \underbrace{(I\cos\theta - Q\sin\theta)}_{S_I} + j\underbrace{(I\sin\theta + Q\cos\theta)}_{S_Q}$$

The rotation aims at correlating the in-phase (I) and quadrature (Q) components. When rotated constellations are used in a SISO context, the two components of each QAM symbol S have to be transmitted separately in different cells, thanks to delay insertion for instance. Thus, the binary information contained in each original constellation point is transmitted twice over the channel. Consequently, the rotated constellation can be seen in a way as a repetition code proceeding at the constellation or signal space level. The DVB-T2 standard specifies the set of values for angle θ for 4-, 16-, 64- and 256-QAM constellations [97].

7.1.3.2.2 Extension of the constellation rotation principle to 2x2 MIMO systems

When the constellation rotation is applied to 2x2 MIMO systems, two rotated QAM symbols can be transmitted simultaneously on the two transmit antennas. Let us denote by $X_1 = I_1 + jQ_1$ and $X_2 = I_2 + jQ_2$ the two QAM symbols to be transmitted jointly.

First, both QAM symbols are rotated by θ, as illustrated in Figure 116, in order to correlate the in-phase (I) and quadrature (Q) components:

$$S_1 = X_1 e^{j\theta} = \underbrace{(I_1\cos\theta - Q_1\sin\theta)}_{S_{1,I}} + j\underbrace{(I_1\sin\theta + Q_1\cos\theta)}_{S_{1,Q}}$$
$$S_2 = X_2 e^{j\theta} = \underbrace{(I_2\cos\theta - Q_2\sin\theta)}_{S_{2,I}} + j\underbrace{(I_2\sin\theta + Q_2\cos\theta)}_{S_{2,Q}}$$

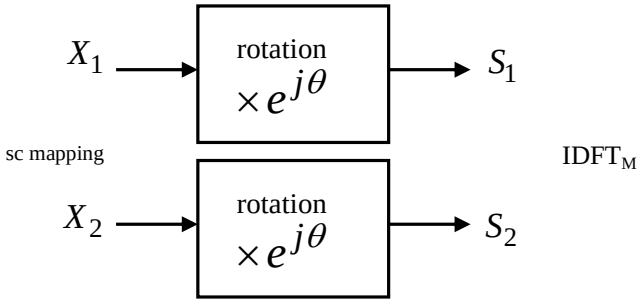

Figure 116: rSM encoding, phase 1: constellation rotation.

Then, the proposed MIMO encoder swaps the Q components on the two antennas: $S_{1,I}$ and $S_{2,Q}$ are mapped onto the first antenna and $S_{2,I}$ and $S_{1,Q}$ are mapped onto on the second antenna as shown in Figure 117.

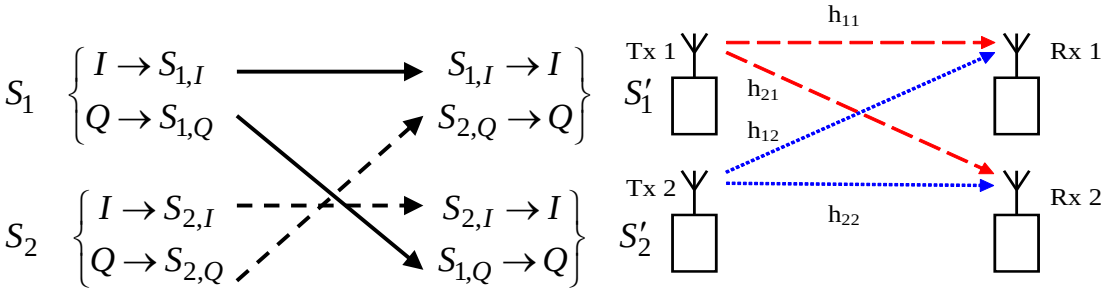

Figure 117: rSM encoding, phase 2: component swapping and transmission

The two transmit antennas finally sent the following signals:

$$S'_1 = S_{1,I} + jS_{2,Q}$$
$$S'_2 = S_{2,I} + jS_{1,Q}$$

The resulting code has a transmit diversity of 2 since it sends one component from each symbol S_i on each antenna. The cyclic delay adopted in DVB-T2 to spread I and Q components in different transmitted cells is no longer required.

If a time interleaver is inserted into the transmission chain between the rotation and the swapping phases, one has to take care that antennas 1 and 2 must carry I and Q components stemming from 2 different rotated SAM symbols only, in order to keep a reasonable detection complexity.

The proposed code is particularly appropriate for transmission scenarios with high antenna mismatch, since this produces erasure events. It is also expected to behave well under high correlation between antennas, since the information to be transmitted is distributed between the antennas.

7.1.3.2.3 Maximum-likelihood detection of rSM

At the receiver side, the symbols R_1 and R_2 received on antennas 1 and 2 can be written as:

$$R_1 = h_{11}\left(S_{1,I} + jS_{2,Q}\right) + h_{12}\left(S_{2,I} + jS_{1,Q}\right) + N_1$$
$$R_2 = h_{21}\left(S_{1,I} + jS_{2,Q}\right) + h_{22}\left(S_{2,I} + jS_{1,Q}\right) + N_2$$

where N_1 and N_2 represent complex additive white Gaussian noise terms.

The maximum likelihood (ML) receiver for this code has to compute the following metrics.

$$D_{euc}^2 = \left\| R_1 - h_{11}\left(S_{1,I} + jS_{2,Q}\right) - h_{12}\left(S_{2,I} + jS_{1,Q}\right)\right\|^2 + \left\| R_2 - h_{21}\left(S_{1,I} + jS_{2,Q}\right) - h_{22}\left(S_{2,I} + jS_{1,Q}\right)\right\|^2$$

for all possible $S_{1,I}$, $S_{1,Q}$, $S_{2,I}$ and $S_{2,Q}$.

If S_1 and S_2 belong to a M-QAM constellation, since $S_{i,I}$ and $S_{i,Q}$ belong to the same rotated QAM symbol S_i (i = 1, 2), the number of metrics to be computed is M^2. Thus, the detection complexity for rSM is the same as the detection complexity of classical or enhanced spatial multiplexing schemes.

7.1.4 Four Transmit Antennas Codes

A number of ST coding schemes are proposed for the four transmit antennas scenario aiming at increasing the robustness (diversity) of the code and decreasing the computational complexity.

7.1.4.1 L_2 Code

The L_2 code is a rate-one ST code with a similar structure as Jafarkhani's quasi-orthogonal code [98]. Compared to the Jafarkhani's code, the L_2 code achieves full diversity and hence has non-vanishing coding gain. The coding matrix is expressed as:

$$(s_0, s_1, s_2, s_3) \mapsto \boldsymbol{X}_{L_2} = \begin{bmatrix} s_0 & js_1 & -s_2^* & -s_3^* \\ s_1 & s_0 & js_3^* & -s_2^* \\ s_2 & js_3 & s_0^* & s_1^* \\ s_3 & s_2 & -js_1^* & s_0^* \end{bmatrix}_{4\times 4} = \begin{bmatrix} \boldsymbol{A} & -\boldsymbol{B}^H \\ \boldsymbol{B} & \boldsymbol{A}^H \end{bmatrix},$$

where $\boldsymbol{A}^H$ is the complex conjugate transpose of matrix $\boldsymbol{A}$. Some characteristics of the L_2 code are:

- Full diversity,
- Rate-One, enabling high-quality reception also in the presence of correlation,
- Quasi-Orthogonal,
- Non-vanishing coding gain,
- Complex sphere decoding with reduced complexity (at most $2M^2$, given M the size of the constellation).

7.1.4.2 MUMIDO Code

MUMIDO code is a rate-two code with lower decoding complexity when the sphere decoding is used. The use of one 4-dimentional sphere decoder can be replaced by two parallel 3-dimentional ones. The coding matrix is expressed as:

$$(s_0, s_1, s_2, s_3) \mapsto \boldsymbol{X}_{MUMIDO} = \begin{bmatrix} s_0 + s_2\zeta & -s_1^* + s_3^* j\zeta \\ s_1 + s_3\zeta & s_0^* - s_2^* j\zeta \\ s_0 - s_2\zeta & -s_1^* - s_3^* j\zeta \\ s_1 - s_3\zeta & s_0^* + s_2^* j\zeta \end{bmatrix}_{4\times 2} = \begin{bmatrix} \boldsymbol{A} \\ f(\boldsymbol{A}) \end{bmatrix},$$

where $\zeta = e^{j\frac{2\pi}{8}}$ and the function f maps ζ to $-\zeta$ and keeps others unchanged. Some characteristics of MUMIDO code are:

- Not full diversity,
- Rate-two code,
- Decoding complexity at most $2M^3$.

7.1.4.3 Restricted Enhanced SM (RESM) Code

Another rate-two ST code with reduced decoding complexity is:

$$(s_0, s_1) \mapsto \boldsymbol{X}_{RESM} = \begin{bmatrix} s_0 + s_1\zeta \\ s_0^* - s_1^* j\zeta \\ s_0 - s_1\zeta \\ s_0^* + s_1^* j\zeta \end{bmatrix}_{4\times 1},$$

Some characteristics of RESM code are:

- Rate-two,
- Decoding complexity at most M^2,
- Real value sphere decoder is needed.

7.1.5 Hybrid Satellite/Terrestrial Transmission

MIMO codes for hybrid satellite/terrestrial use case are proposed for NGH standardization for optimal utilization of the hybrid network. Two options for the network are currently seen, namely SFN where satellite and terrestrial transmitters operate on same frequency and multi frequency network (MFN) where satellite and terrestrial are transmitted on different frequencies. Naturally OFDM transmission for the satellite is required for SFN operation.

7.1.5.1 One Satellite Antenna and Two Terrestrial Antenna

Rate one hybrid Alamouti + QAM:

$$(s_0, s_1) \rightarrow \begin{pmatrix} s_0 & s_1^* \\ s_0 & s_1^* \\ s_1 & -s_0^* \end{pmatrix}_{3x2}$$

- First row corresponds to satellite transmitter, that transmits the same symbols as one terrestrial transmitter
- Sphere decoding complexity M

Rate 3/2 UTU hybrid L3:

$$(s_0, s_1, s_2) \rightarrow \begin{pmatrix} s_0 + s_1 e^{j\pi/4} & s_2^* \\ s_0 - s_1 e^{j\pi/4} & s_2^* \\ s_2 & -s_0^* + s_1^* e^{-j\pi/4} \end{pmatrix}_{3x2}$$

- Intermediate rate
- Sphere decoding complexity M^2

Rate 2 UTU hybrid:

$$(s_0, s_1, s_2, s_3) \rightarrow \begin{pmatrix} s_0 + s_1 e^{j\pi/4} & s_2^* + s_3^* e^{-j\pi/4} \\ s_0 + s_1 e^{j\pi/4} & s_2^* + s_3^* e^{-j\pi/4} \\ s_2 + s_3 e^{j\pi/4} & -s_0^* - s_1^* e^{-j\pi/4} \end{pmatrix}_{3x2}$$

- Sphere decoding complexity M^2

7.1.6 ST Codes Proposed by other DVB members

7.1.6.1 eSFN

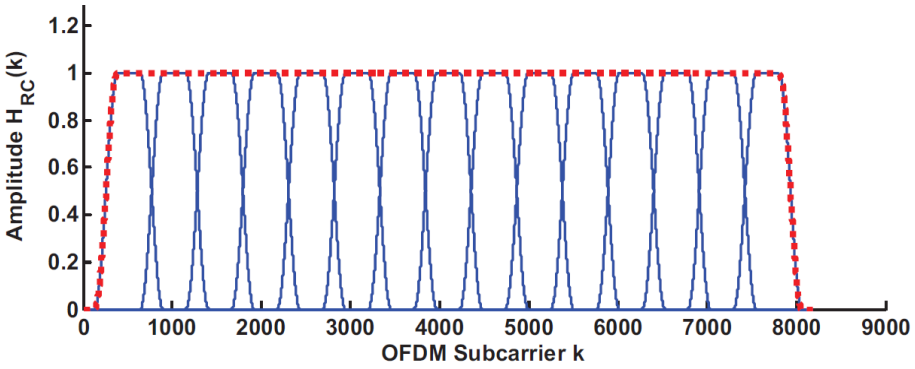

Figure 118: eSFN scheme.

In Single Frequency Network (SFN) configuration, signals from different transmit antennas may incur destructive superposition in certain spots in the landscape. The coherence bandwidth of the deep fades can reach the entire channel bandwidth. The reception in that location becomes very difficult. This problem also happens in the mixed (namely, time multiplexed) SISO/MIMO transmission scenarios. In the SISO transmission time slots, identical data is transmitted on both vertical- and horizontal antennas. This can result in the similar wideband fading problem as in SFN. One antenna may have to be switched off during the SISO transmission, which means a 3 dB transmission power loss.

eSFN (enhanced – Single Frequency Networks) [87][88] is a SFN scheme with improved robustness in face of the deep fading within a wideband. It de-correlates the transmitted signals from different antennas using independent phase distortions. More precisely, the OFDM data for transmission is first divided into a number of groups with equal size. The phases of the subcarriers in each group are distorted with a common shift. The phase shift linearly increases with the with respect to different groups of one antenna, while the phases of different antennas are uncorrelated. In addition, the envelope of each group is shaped by the Raised Cosine Function, as shown in Figure 118, to smooth the phase transition between two adjacent groups.

The advantage of this eSFN scheme is that it avoids the wideband, deep fading that may appear in the SFN configurations. It is almost invisible for receivers and does not require any additional pilots compared to SISO transmissions. In the mixed SISO/MIMO transmission scenario, the same signal can be transmitted on both antennas in the SISO transmission time slot, which not only increases the transmission power but also introduces some diversity. Moreover, the linear distortion permits transmitter identification for monitoring the network. The disadvantage of this scheme is that the channel estimation may suffer from the phase pre-distortion.

MISO Alamouti and eSFN can be combined in the same transmission chain. Figure 119 shows the signal processing applied to each of the transmitters is a SFN network. For the first transmitter (upper branch), the cells output from the frequency interleaver are processed by the eSFN block. For the second transmitter (bottom branch) before eSFN distortion the signal is processed by Alamouti coding. The colored shadowed boxes represent different phases for each group of carriers in eSFN scheme.

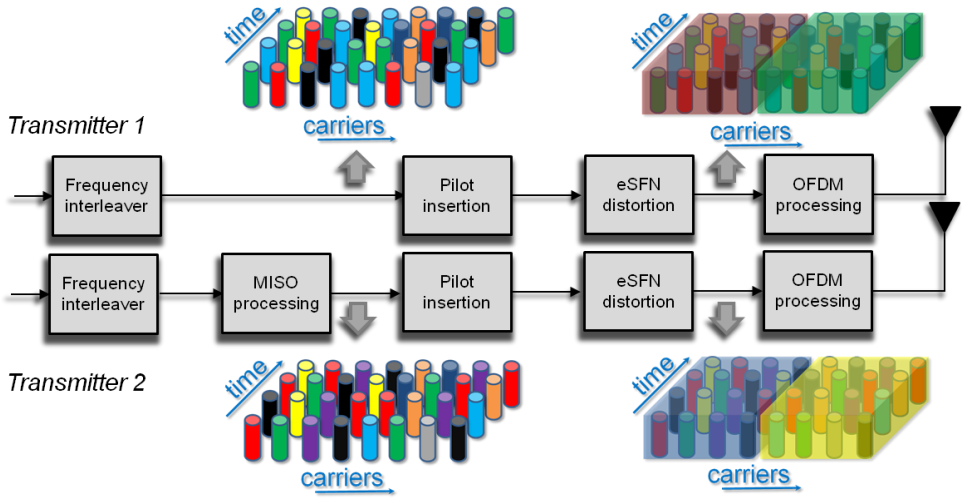

Figure 119: MIMO rate 1 signal processing with a combination of MISO Alamouti and eSFN. The first transmitter applies only linear eSFN distortion (different phase modulation along frequency bins). The second transmitter applies MISO processing (Alamouti coding in frequency direction) and eSFN. The colored boxes after eSFN processing illustrate the different phase modulation applied along transmitters (different for each transmitter in the network).

7.1.6.2 Transmit Antenna Switching (TxAS)

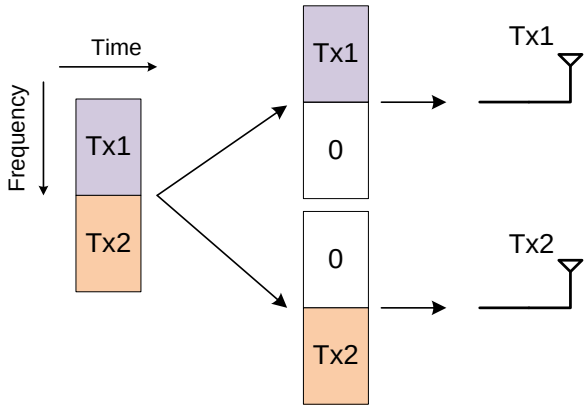

Figure 120: TxAS scheme.

The Transmit Antenna Switching (TxAS) is a simple ST coding scheme aiming at collecting the transmit diversity using the channel coding. It separates the OFDM subcarriers into several disjoint groups. Each subcarrier group is associated with a specific antenna. For each antenna, only the subcarriers in the assigned group are active. The rest subcarriers are not used for data transmission. That is, data on different antennas is transmitted via orthogonal frequency subbands to achieve transmit diversity. At the receiver side, the decoding process involves the data from all transmit antennas. In other words, the transmit diversity is easily collected by the channel coding without the need of the ST coding.

The advantage of this scheme is that it is very easy to implement. As the data on different antennas is transmitted in orthogonal subbands, the channel can be seen as a single-transmitter one at the receiver side. Therefore, there is no need to increase the number of pilots as in the Alamouti scheme even though multiple transmit antennas are used.

The disadvantage of this scheme is that some more pilots are needed for the border area of each group to guarantee reliable channel estimation.

7.1.6.3 eSM/hSM

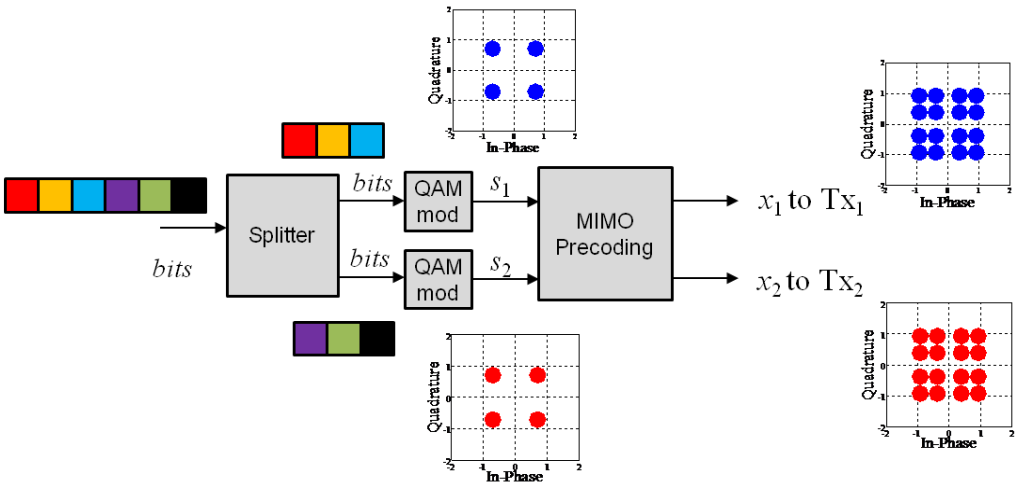

Figure 121: Example diagram of pre-coded SM for 4 bits per cell (16-QAM)

In SFN or mixed SISO/MIMO scenarios, the same signal is transmitted from several transmit antennas over the same channel. The destructive superposition of the signals from different transmitters can result in deep fading over a wide frequency band, i.e. an erasure event, in some geographic locations. Transmitted information is totally lost when the erasure event happens. This kind of the channel situation is referred to as the erasure channel. The conventional Spatial Multiplexing scheme encounters serious decoding error in the erasure channel, because it maximizes the transmission rate but is vulnerable in the bad channel conditions.

The conventional Spatial Multiplexing scheme can be improved applying a linear pre-coding before mapping the independent symbol streams to the transmit antennas. It increases the spatial diversity of the transmitted data. Enhanced Spatial Multiplexing (eSM) [104] is one such proposal which increases the system performance under erasure channels where conventional SM reduces its efficiency. The pre-coding applied by eSM maintains both multiplexing gain under spatially uncorrelated channels and spatial diversity under correlated channels. Figure 121 shows an example diagram of a pre-coded eSM transmission. A linear precoding is performed to the transmitted symbol in order to correlate the signals transmitted signal on different transmit antennas, so that, even if one or more channel links encounter erasure event, the transmitted signal can still be recovered from the signals from other links. The precoded data symbol is expressed as:

$$\mathbf{x} = \boldsymbol{\Theta}\mathbf{s},$$

where $\boldsymbol{s} = [s_1, s_2]^T$ are the normalized QAM symbols before the linear pre-coding and $\boldsymbol{x} = [x_1, x_2]^T$ are the pre-coded QAM symbols to be mapped to transmitters 1 and 2, respectively. The precoding matrix is written as:

$$\boldsymbol{\Theta} = \begin{bmatrix} \cos\theta & -\sin\theta \\ \sin\theta & \cos\theta \end{bmatrix}.$$

The rotation phase θ has two options:
$\theta = 33.3° \Longrightarrow$ eSM,
$\theta = 45° \Longrightarrow$ Hadamard SM (hSM).
While it is proved that the rotation phase θ has very little impact on performance [95].

In this case the received signal by each of the cross-polarized antennas is:

$$r_1 = h_{11}(s_1 \cos\theta - s_2 \sin\theta) + h_{12}(s_1 \sin\theta + s_2 \cos\theta)$$
$$r_2 = h_{21}(s_1 \cos\theta - s_2 \sin\theta) + h_{22}(s_1 \sin\theta + s_2 \cos\theta)$$

where r_1, r_2 are the signals at the receive antennas 1 and 2; s_1, s_2 are the modulated symbols at the transmitter and h_{11}, h_{12}, h_{21}, h_{22} are the MIMO path channel components. From the above expression, it can be seen that modulated symbols s_1 and s_2 are transmitted through all MIMO paths, improving the spatial diversity in comparison with conventional SM. Since the precoding matrix Θ is unitary, the eSM has identical performance as the conventional SM method in non-erasure channels.

Iterative decoding scheme can also be used in the eSM scheme. Some discussions can be found in [96].

7.1.6.4 Phase Hopping-Spatial Multiplexing (PH-SM)

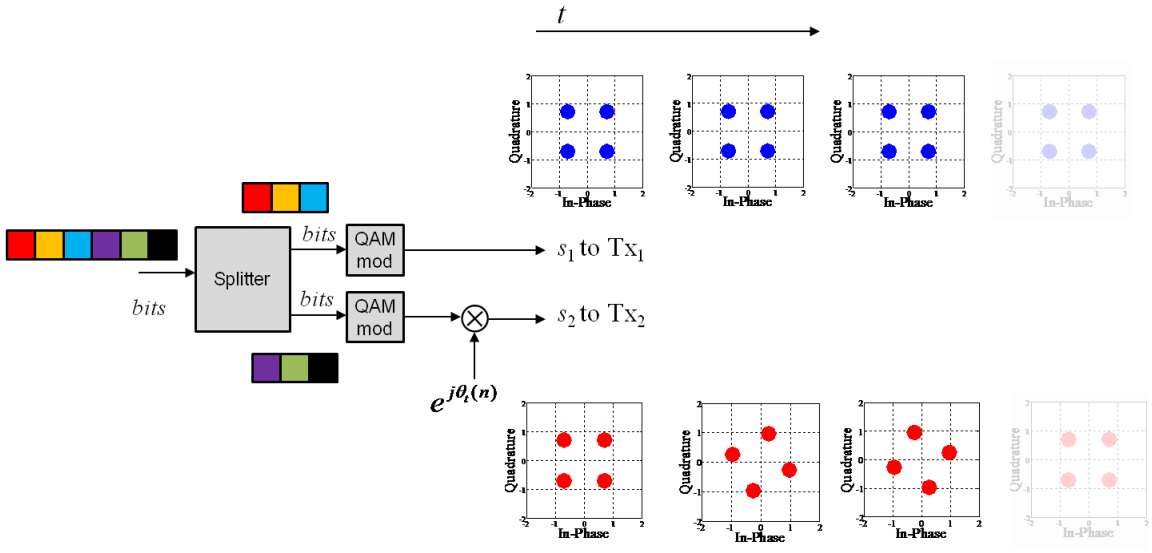

Figure 122: Example diagram of un-coded PH-SM for 4 bits per cell (16-QAM) and N = 3

Another variant of eSM is proposed by adding a circularly hopping phase to the second transmitter before mapping the streams to the transmit antennas in order to enhance the robustness against the transmit antenna orientation and to increase the diversity as well. Such a technique is known in DVB-NGH as phase hopping (PH) [105]. A simplified diagram is shown in Figure 122 for SM with 4 bits per cell (16-QAM).

The PH-SM pre-coding is expressed by following 2x2 matrix for the case of two transmit antennas:

$$\mathbf{x} = \boldsymbol{\Phi}\mathbf{s}$$

where $\boldsymbol{s} = [s_1, s_2]^T$ are the normalized QAM symbols before the linear pre-coding and $\boldsymbol{x} = [x_1, x_2]^T$ are the pre-coded QAM symbols to be mapped to transmitters 1 and 2, respectively. The precoding matrix is written as:

$$\boldsymbol{\Phi} = \begin{bmatrix} \mathbf{1} & \mathbf{0} \\ \mathbf{0} & \mathbf{e^{j\phi_t(n)}} \end{bmatrix}$$

with $\phi_t(n) = \frac{2\pi n}{N}, n = 1, \ldots, N-1$ given a hopping period N. New rotation angle is applied every two independent modulated symbols. An example of the constellations at the output of the second transmitter branch are illustrated in Figure 123 with rotation period $N = 3$.

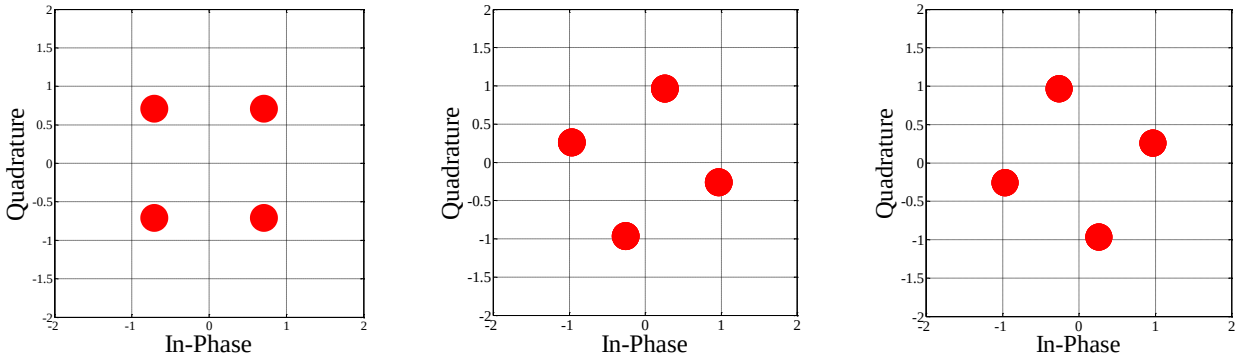

Figure 7:

Figure 123: Phase hopping rotation with un-coded SM with parameter $N = 3$

In this case the received signal by each of the cross-polarized antennas is:

$$r_1 = s_1 h_{11} + e^{j\theta_t(n)} s_2 h_{12}$$
$$r_2 = s_1 h_{21} + e^{j\theta_t(n)} s_2 h_{22}$$

The variables are defined as in previous cases. The spatial diversity of the received symbols is the same as in the case of SM but with increased diversity within a codeword

7.1.6.5 Phase Hopping enhanced Spatial Multiplexing (PH-eSM)

Phase hopping can be implemented with any pre-coded MIMO scheme as eSM, the combination of eSM with PH is called phase hopping-enhanced spatial multiplexing (PH-eSM), the chosen MIMO rate 2 scheme for DVB-NGH base-line. PH-eSM has both, increased spatial diversity due eSM pre-coding and increased diversity within LDPC code word due to PH term. An example diagram of PH-eSM coding chain is showed in Figure 124 for 4 bits per carrier (16-QAM) and rotation period N =3.

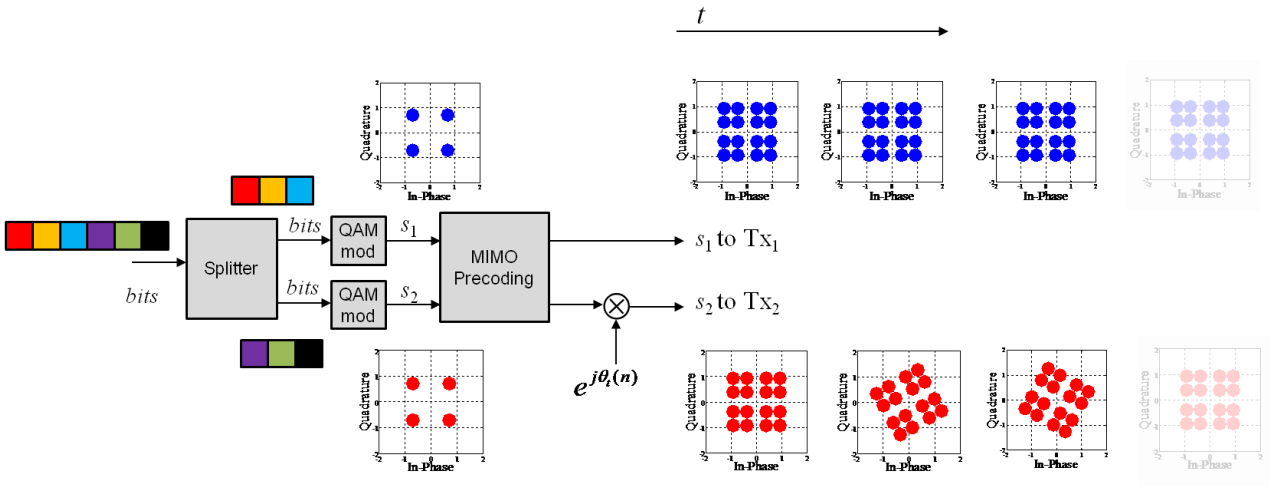

Figure 124: Example diagram of PH-eSM for 4 bits per cell (16-QAM) and N = 3.

More precisely, the precoded data symbol with phase hopping is written as:

$$\mathbf{x} = \mathbf{\Phi\Theta s}$$

where $\boldsymbol{s} = [s_1, s_2]^T$ are the normalized QAM symbols before the linear pre-coding and $\boldsymbol{x} = [x_1, x_2]^T$ are the pre-coded QAM symbols to be mapped to transmitters 1 and 2, respectively. The precoding matries $\mathbf{\Theta}$ and $\mathbf{\Phi}$ are written as:

$$\mathbf{\Theta} = \begin{bmatrix} \cos\theta & -\sin\theta \\ \sin\theta & \cos\theta \end{bmatrix},$$

with the rotation phase θ as defined in section 7.1.6.3 and

$$\mathbf{\Phi} = \begin{bmatrix} \mathbf{1} & \mathbf{0} \\ \mathbf{0} & \mathbf{e^{j\phi_t(n)}} \end{bmatrix}$$

with $\phi_t(n) = \frac{2\pi n}{N}, n = 1, \dots, N-1$ given a hopping period N. And the corresponding received signals are:

$$r_1 = h_{11}(s_1\cos\theta - s_2\sin\theta) + h_{12}e^{j\phi_t(n)}(s_1\sin\theta + s_2\cos\theta)$$
$$r_2 = h_{21}(s_1\cos\theta - s_2\sin\theta) + h_{22}e^{j\phi_t(n)}(s_1\sin\theta + s_2\cos\theta)$$

An example of the constellations at the output of the second transmitter branch are illustrated in Figure 125 with rotation period $N = 3$.

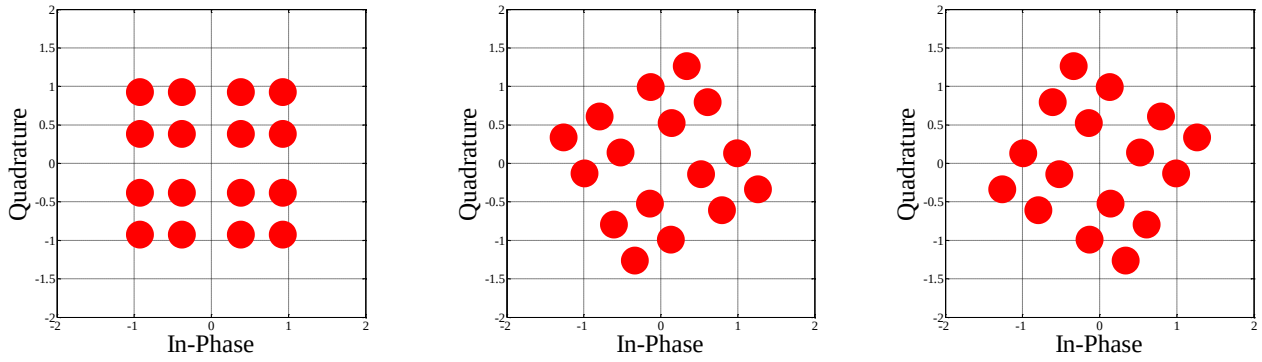

Figure 125: Phase hopping rotation with eSM pre-coding with parameter N = 3

7.1.6.6 Multi-layer Spatial Multiplexing (ML-SM)

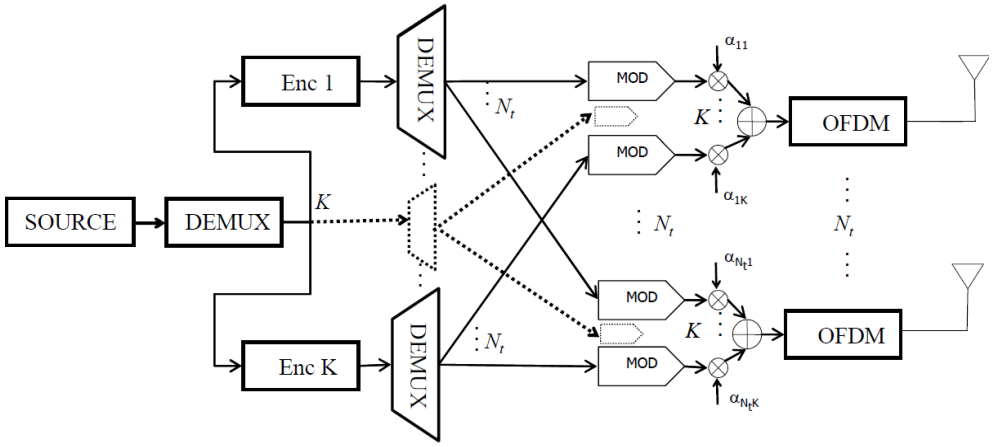

Figure 126: Multi-layer SM scheme.

The optimal (ML) decoding of conventional SM scheme is realized through an exhaustive search among all possible combinations of the transmitted symbols. Therefore, the computational complexity of the decoding grows exponentially with the number of transmit antennas and the modulation efficiency.

A generalization of SM scheme adopts a multilayer architecture in the purpose of reducing the decoding complexity associated to the SM scheme. Each layer is a QPSK symbol stream, weighted by a coefficient, and superimposed on the other layers. The layered structure enables the receiver to decode the superimposed layers one at a time. That means the complexity of the suboptimal decoding grows linearly, instead of exponentially, with respect to the number of layers (i.e. modulation efficiency).

7.1.6.7 Unequal Power Code

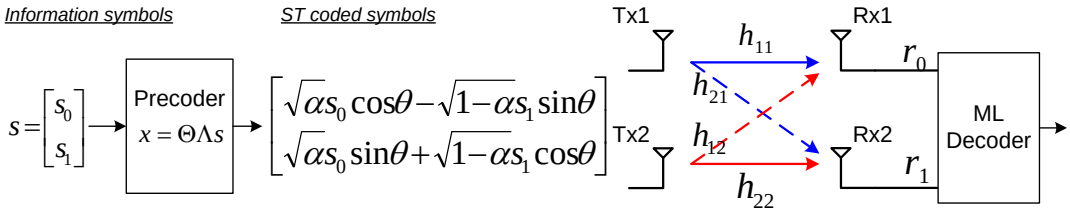

Figure 127: Unequal power code scheme.

A variant of the eSM scheme is proposed in the case that different modulations are applied on the two antennas. The basic idea behind this scheme is to allocate more power to the modulation with higher order which is more vulnerable to the noise. The ST coded data symbols with unequal power can be written as:

$$\mathbf{x} = \mathbf{\Theta\Lambda s},$$

where

$$\mathbf{\Lambda} = \begin{bmatrix} \sqrt{\alpha} & 0 \\ 0 & \sqrt{1-\alpha} \end{bmatrix},$$

is matrix to scales the power between two antennas. For instance, when QPSK and 16QAM are applied to the two antennas, respectively, α is set to $1/3$. That is, twice power are allocated to 16QAM than QPSK symbols. This is to increase the robustness of the higher order constellation under the constrain of the total signal power.

7.2 Performance Comparisons among the Candidates

7.2.1 SM codes

In this section the performance of SM, eSM and PH-eSM are compared by means of simulations. The new channel model developed under the DVB-NGH standardization process is used. The system parameters chosen for the simulations are illustrated in Table 29 and are the same parameters employed in the standardization process of DVB-NGH for the evaluation of the MIMO schemes.

Figure 10 illustrates BER against SNR for the three schemes under evaluation. For this simulation, the channel model detailed in [80] is modified from its original description, removing the frequency shift for the first line of sight (LOS) tap of the cross-polar term. Moreover the simulation includes power imbalance matrices specified in [80], which model asymmetries between the H/V components of the transmit antennas. Results showed in Figure 10 illustrate similar performance of the three simulated schemes. Due to the similar robustness of the schemes under the simulated scenario, a set of corner cases are defined to highlight differences modifying some of the channel parameters like correlation and Rice parameter *K*.

Table 29: Simulation parameters

Signal Definition
FFT size: 4K
Number active carriers: 3409 (no pilots used)
GI fraction: 1/4
Constellation: 8 bits per carrier (16QAM + 16QAM)
LDPC code: 16K, code rates 4/9 and 2/3
Time interleaver (TI) memory size: 525Kcells
Type 1 PLP
Channel
Helsinki 2 portable outdoor
Doppler spread: 33.3 Hz
A new realization is generated for each TI block
A different sequence of random seeds is used for each SNR point.
A same sequence of random seeds is used for all MIMO schemes per SNR point
Receiver
Ideal channel estimation
Simulation stop conditions
Minimum simulated TI blocks: 1e3
Maximum TI blocks: 1e4
Erroneous TI blocks: 1e2
Erroneous TI block = at least one erroneous bit

Starting from the scenario described for simulations in Figure 128, power imbalance matrices due to asymmetries are removed and the TI memory is reduced to 100 Kcells to speed up the simulations. Figure 129 and Figure 130 show BER vs. SNR performance results where the correlation of the standard channel model is increased. For code rate 4/9 PH-eSM outperforms eSM and SM by 0.20 dB and 0.35 dB respectively whereas for code rate 2/3 eSM and PH-eSM have similar performance outperforming SM by 0.26 dB approximately. For Figure 131 and Figure 132 the Rice K factor is increased and the performance order is similar as in the previous case. For code rate 4/9 PH-eSM outperforms eSM and SM by the other two schemes by 0.30 dB and 0.36 dB respectively, finally for code rate 2/3 PH-eSM outperforms eSM and SM by 0.10 and 0.17 dB respectively.

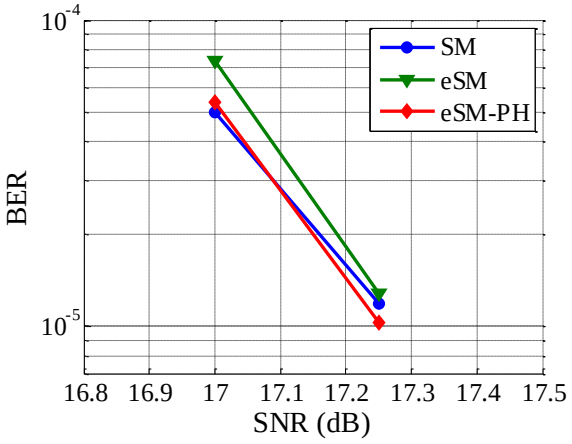

Figure 128: BER vs. SNR curve for standard case with code rate 2/3

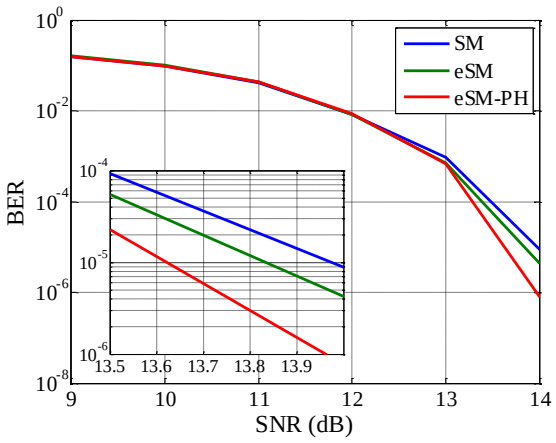

Figure 129: BER vs. SNR curve for high correlation corner case with code rate 4/9

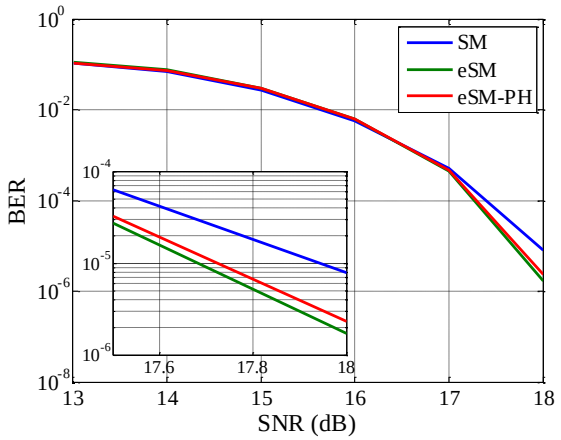

Figure 130: BER vs. SNR curve for high correlation corner case with code rate 2/3

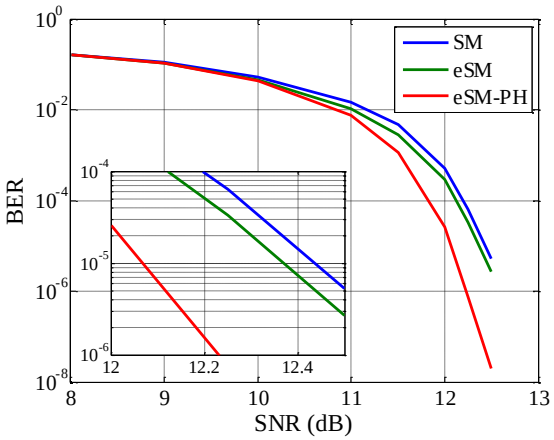

Figure 131: BER vs. SNR curve for high K corner case with code rate 4/9

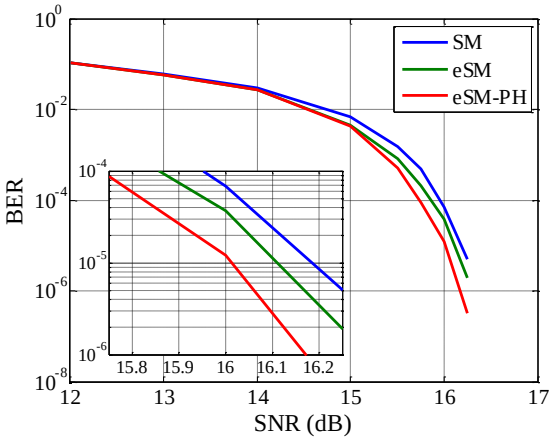

Figure 132: BER vs. SNR curve for high K corner case with code rate 2/3

7.2.2 Rotated constellation-based Spatial Multiplexing scheme (rSM)

The rotated constellation-based space code proposed by Telecom Bretagne has been simulated and compared with its competitors in DVB-NGH, in particular with the eSM scheme. The simulation conditions are list in. Two simulation campaigns have been carried out. For the first campaign, the "Helsinki 2 MIMO outdoor portable model", defined in [80] was adopted. The following figures provide some examples of performance results, targeting 16-QAM constellations, obtained by Telecom Bretagne during the first simulation campaign.

Table 30: Simulation parameters

Parameter	Value
Channel Bandwidth	8 MHz
FFT size	4k
Guard interval	1/4
Carrier frequency	600 MHz
Time interleaver depth	100 ms
LDPC length	16k
Code rates	1/5, 1/3, 4/9, 2/3
Channel estimation	ideal
Time interleaver depth	100 ms
LDPC decoding algorithm	product algorithm, 50 layered iterations
Number of simulated samples	Number of simulated samples: 2000 FEC frames in error for BER > 10^{-3}, 1000 FEC frames in error for BER < 10^{-3}

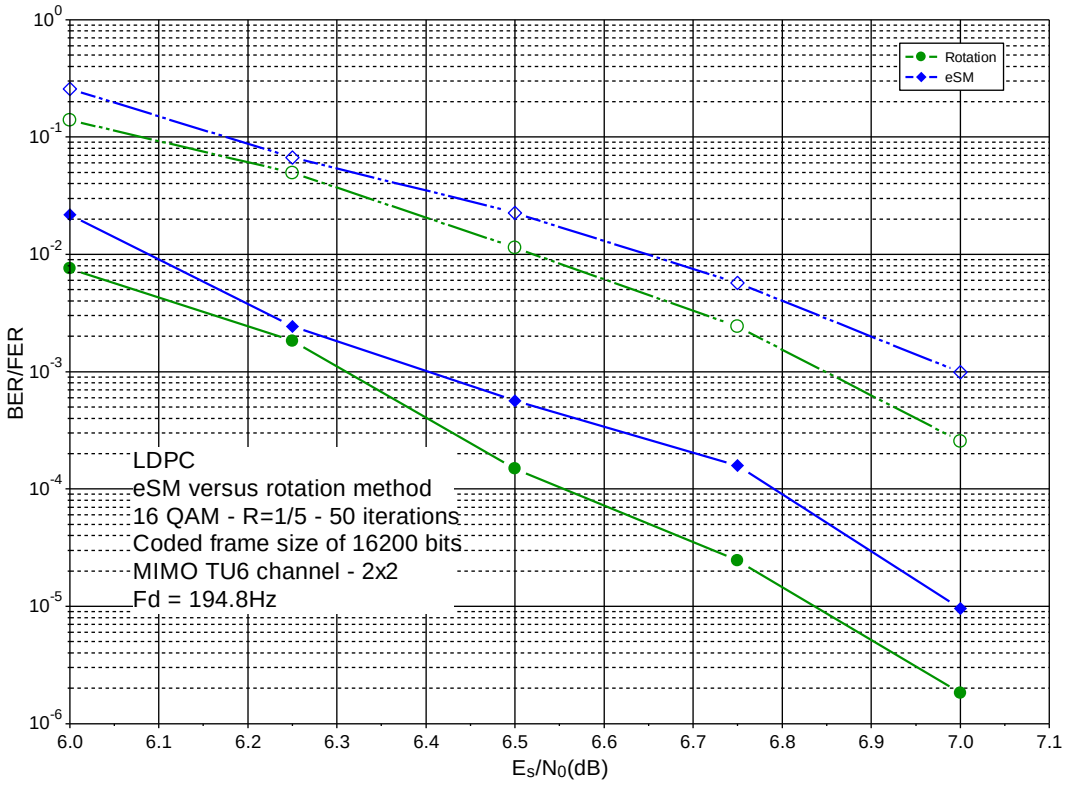

Figure 133: BER/FER comparison of rSM and eSM schemes. 16-QAM constellation, Doppler frequency f_d =194.8 Hz, coding rate R =1/5.

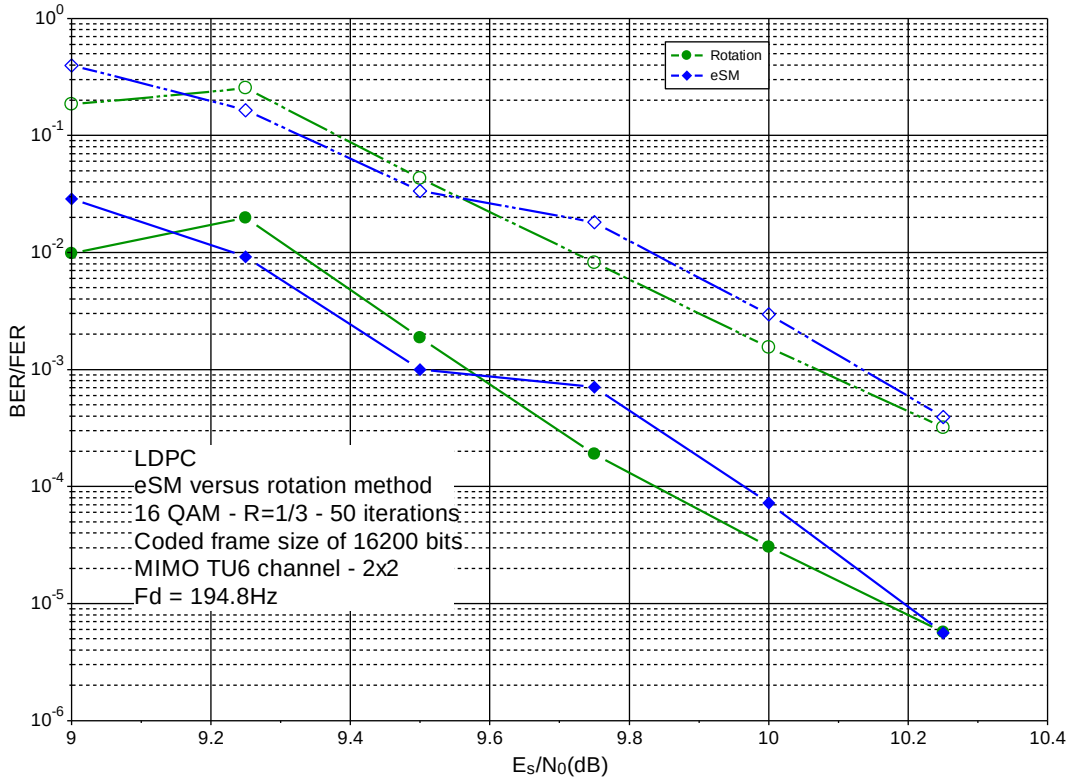

Figure 134: BER/FER comparison of rSM and eSM schemes. 16-QAM constellation, Doppler frequency f_d =194.8 Hz, coding rate R =1/3.

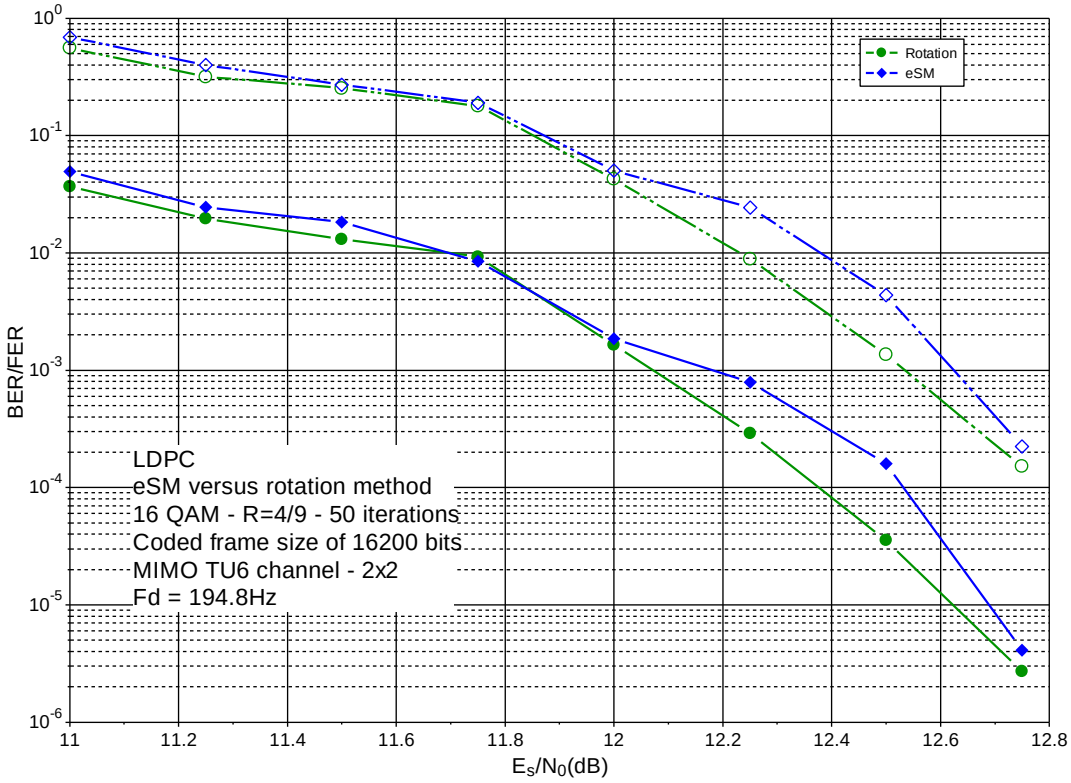

Figure 135: BER/FER comparison of rSM and eSM schemes. 16-QAM constellation, Doppler frequency f_d =194.8 Hz, coding rate R =4/9.

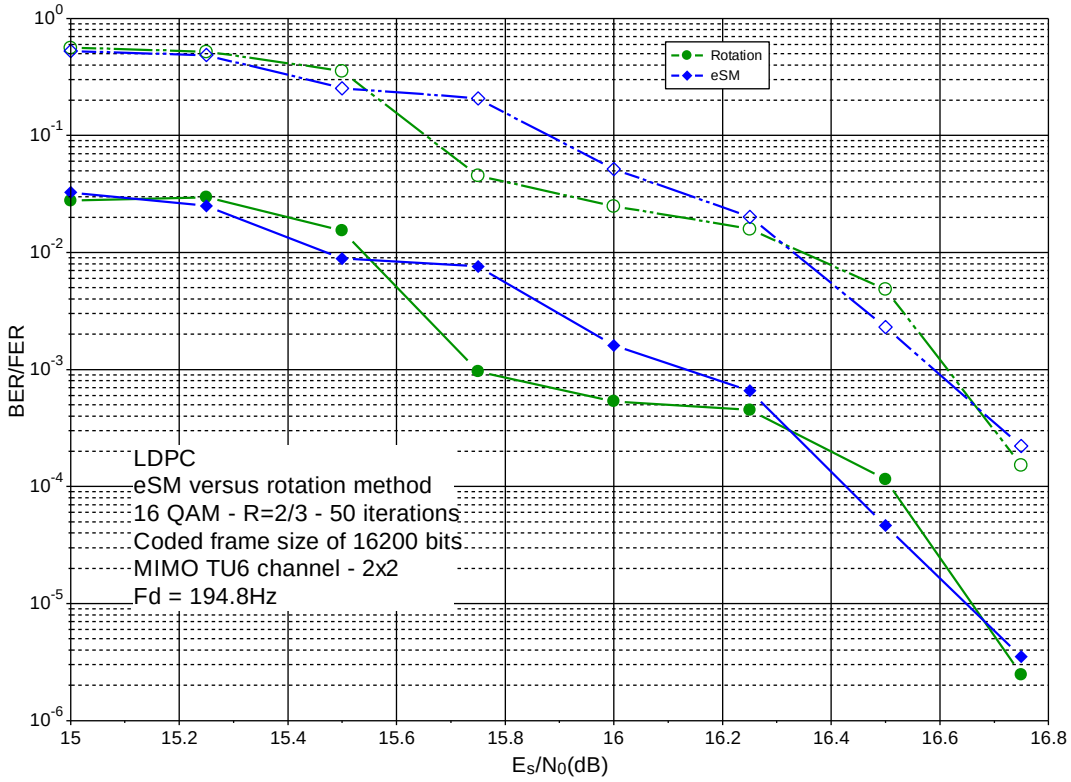

Figure 136: BER/FER comparison of rSM and eSM schemes. 16-QAM constellation, Doppler frequency f_d =194.8 Hz, coding rate R =2/3.

The main conclusion of the first simulation campaign was that eSM and rSM shows very similar performance for all coding rates. Thus, a second simulation campaign was carried out in order to decide between the different proposed solutions. During the second simulation campaign, *corner cases* were agreed to supplement the previously defined NGH "Helsinki 2" outdoor channel model: different values of Doppler frequency, power imbalance (PI), Ricean *K* factor and cross-polar discrimination (XPD) factor were used. A high correlation scenario was also added.

The following figures illustrates, in the case of 16-QAM constellation and coding rate 4/9, the different corner cases that have been simulated during this second simulation campaign in order to get a winning technique.

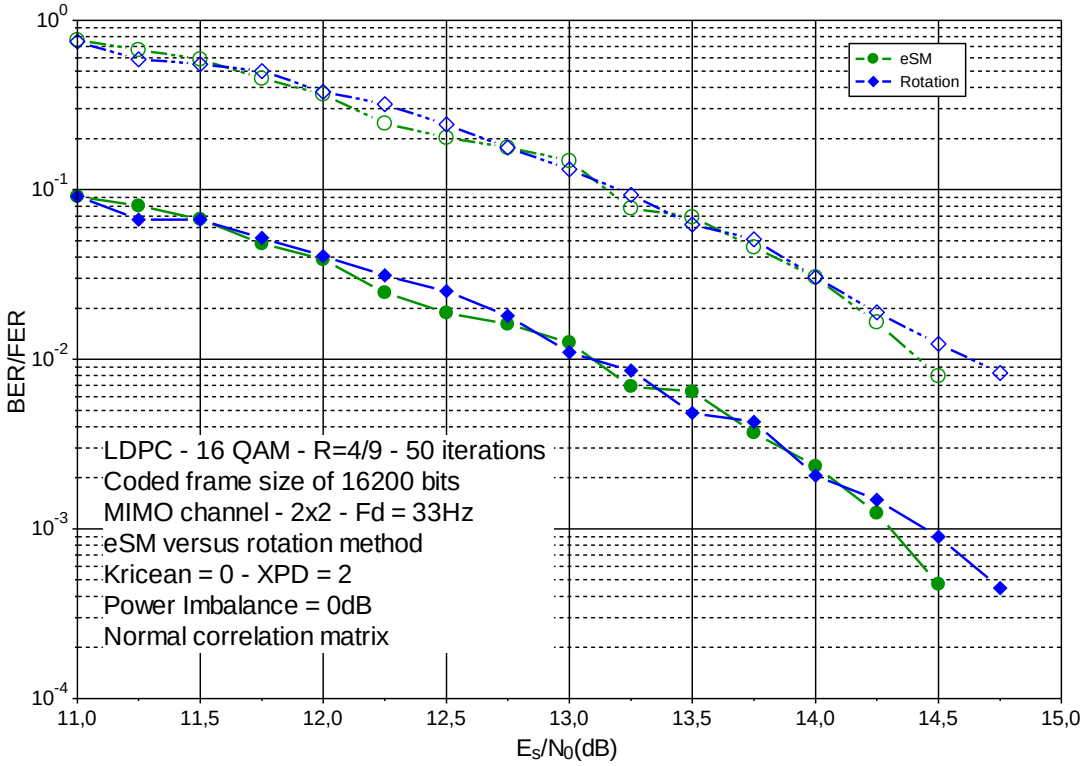

Figure 137: BER/FER comparison of rSM and eSM schemes. 16-QAM constellation, Doppler frequency f_d =33.3 Hz, K = 0, XPD = 2, PI = 0dB, normal correlation matrix, coding rate R =4/9.

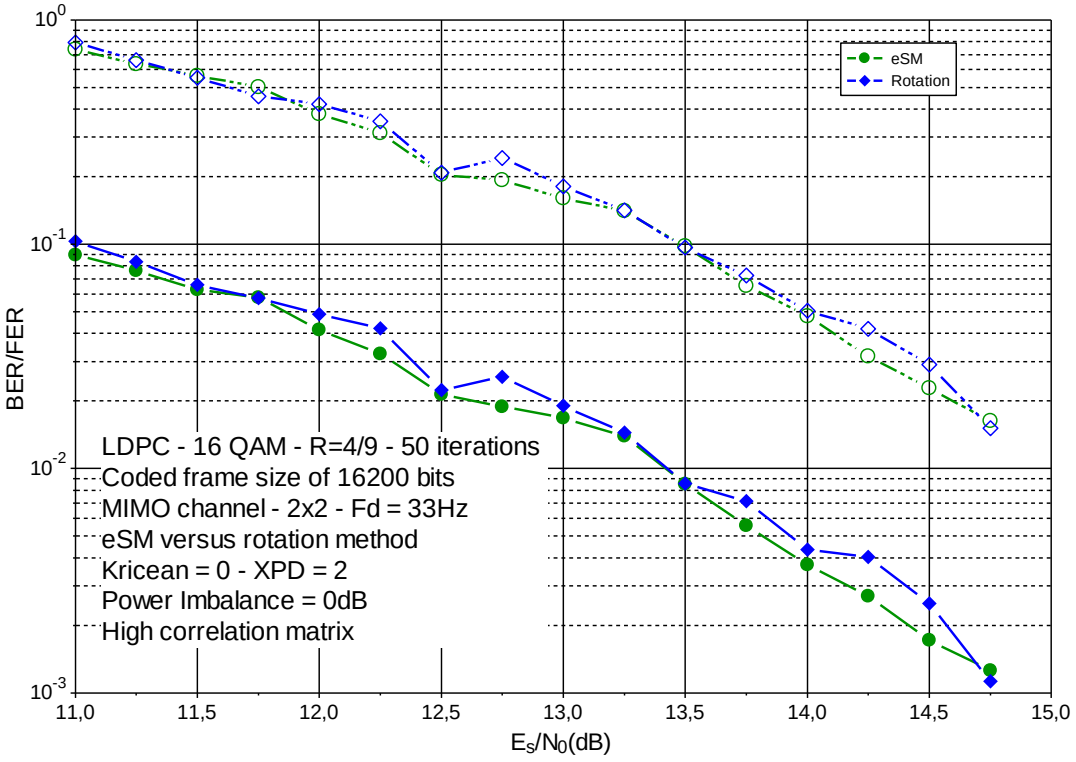

Figure 138: BER/FER comparison of rSM and eSM schemes. 16-QAM constellation, Doppler frequency f_d =33.3 Hz, K = 0, XPD = 2, PI = 0dB, high correlation matrix, coding rate R =4/9.

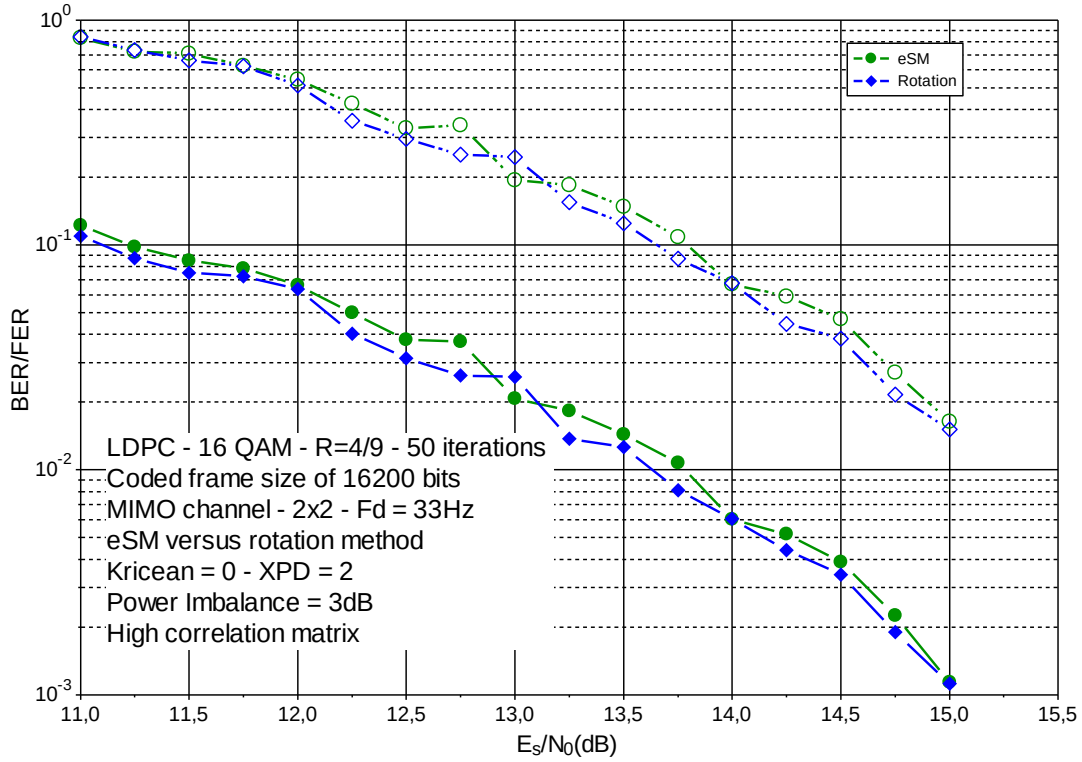

Figure 139: BER/FER comparison of rSM and eSM schemes. 16-QAM constellation, Doppler frequency f_d =33.3 Hz, K = 0, XPD = 2, PI = 3dB, high correlation matrix, coding rate R =4/9.

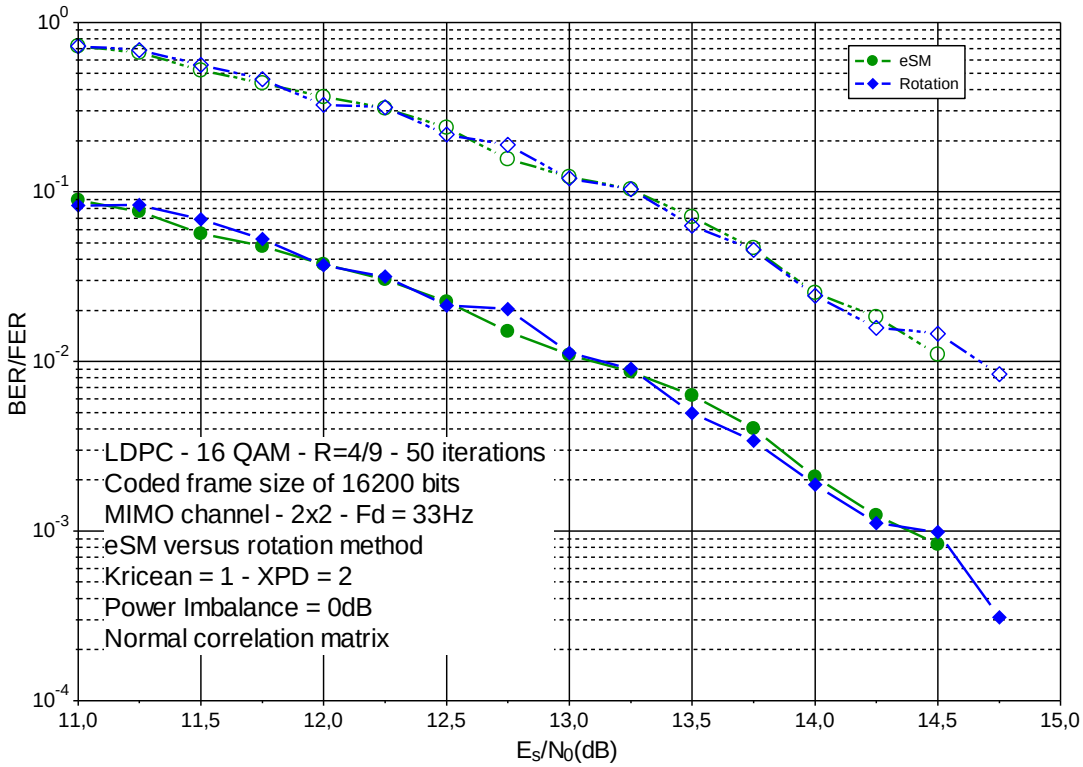

Figure 140: BER/FER comparison of rSM and eSM schemes. 16-QAM constellation, Doppler frequency f_d =33.3 Hz, K = 1, XPD = 2, PI = 0dB, normal correlation matrix, coding rate R =4/9.

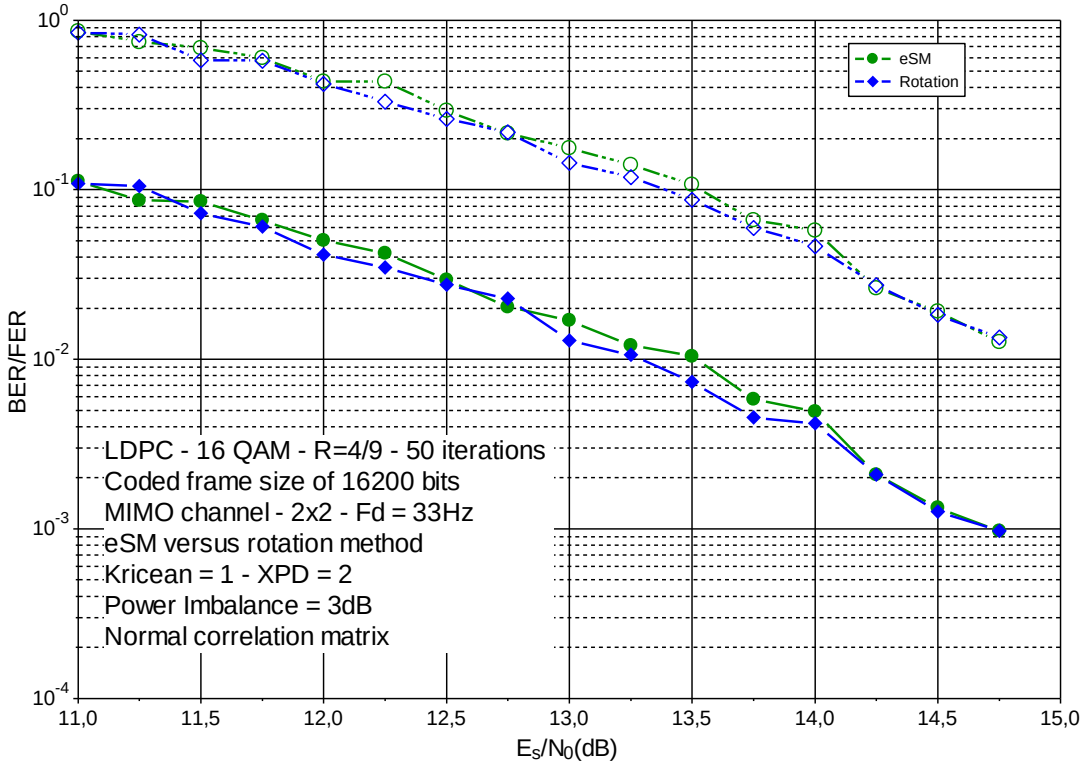

Figure 141: BER/FER comparison of rSM and eSM schemes. 16-QAM constellation, Doppler frequency f_d =33.3 Hz, K = 1, XPD = 2, PI = 3dB, normal correlation matrix, coding rate R =4/9.

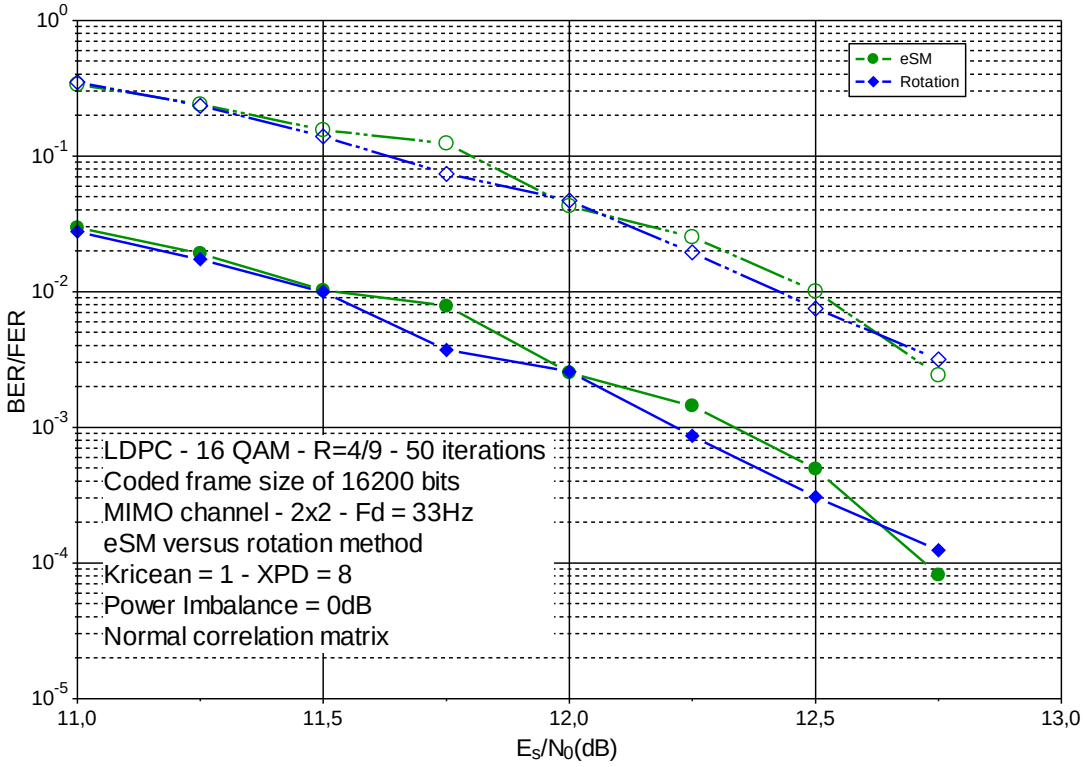

Figure 142: BER/FER comparison of rSM and eSM schemes. 16-QAM constellation, Doppler frequency f_d =33.3 Hz, K = 1, XPD = 8, PI = 0dB, normal correlation matrix, coding rate R =4/9.

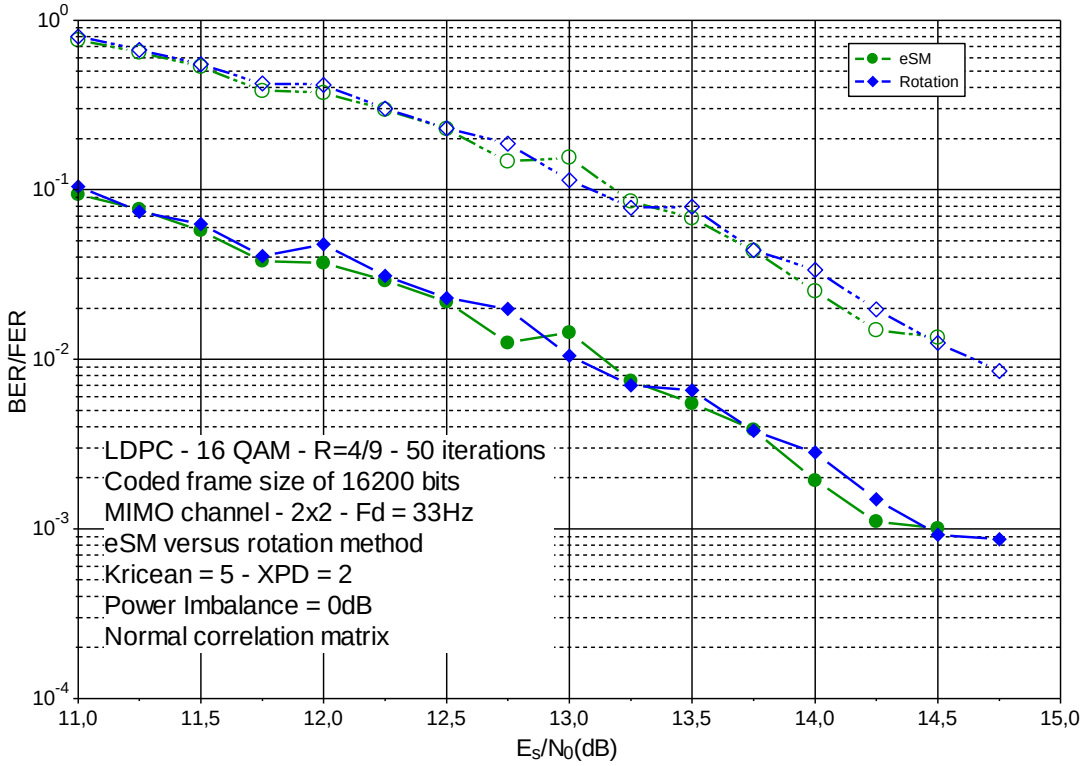

Figure 143: BER/FER comparison of rSM and eSM schemes. 16-QAM constellation, Doppler frequency f_d =33.3 Hz, K = 5, XPD = 2, PI = 0dB, normal correlation matrix, coding rate R =4/9.

Although the corner cases were intended to decide between the competing techniques, rSM and eSM still showed similar performance, with very small gaps between the curves. The eSM technique was finally adopted in DVB-NGH as 2x2 code.

7.2.3 4x2 codes

The performance comparison of the proposed 4x2 schemes to selected 2x2 schemes and SISO and SIMO are shown here. The simulated channel is NGH outdoor channel with Doppler frequency of 33.3 Hz and delay of 0.05 times the guard interval length for the second transmitter pair with respect to the first one. The other system parameters used in the simulations are shown in Table 31.

Table 31: System parameters used in the simulations

Parameter	Value
Bandwidth	8 MHz
FFT size	4k
Guard interval	1/4
Modulation	QPSK
LDPC length	16k
Code rates	1/4, 1/3, 2/5, 1/2, 3/5, 2/3
Channel estimation	ideal
Time interleaver	2^{18} cells

The SNR vs. bpcu curves are presented in Figure 144. To obtain the spectral efficiency (bpcu) pilot density of 1/24 for SISO, 1/12 for 2x2 and 1/6 for 4x2 is assumed. All codes are decoded using soft output sphere decoder with max-log approximation. Ideal channel estimation is applied.

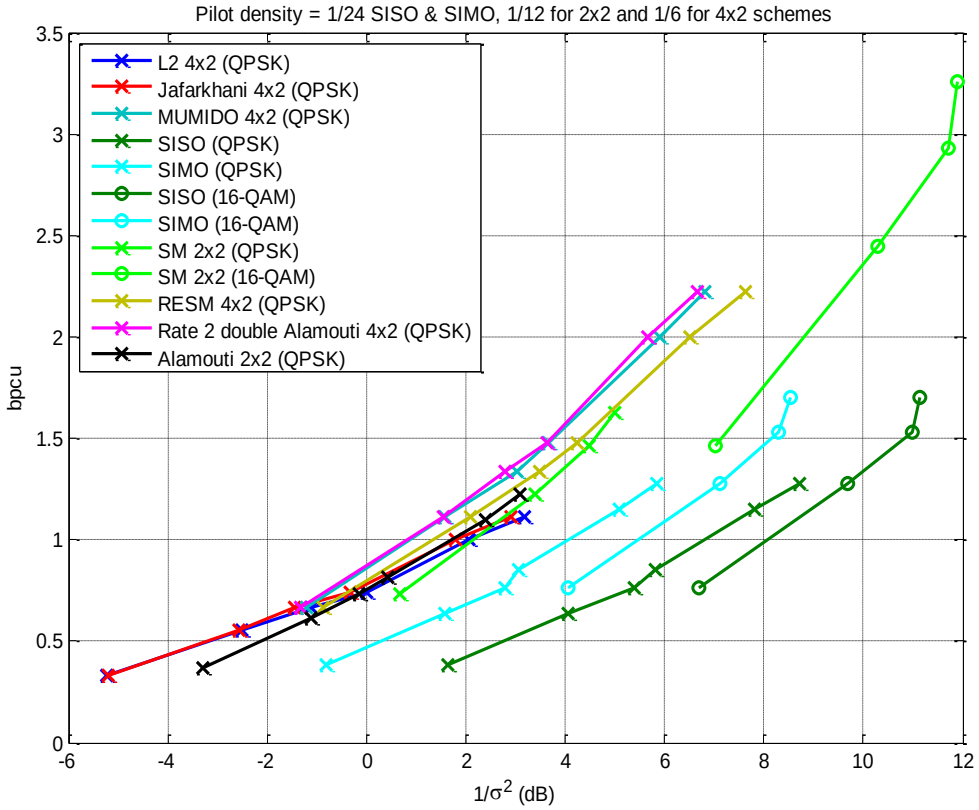

Figure 144: Performance comparison of 4x2 MIMO schemes.

To obtain the capacity curves, LDPC code rates 1/4, 1/3, 2/5, 1/2, 3/5 and 2/3 for all studied SFBCs are simulated and the SNR for reaching BER 10^{-4} is searched. Thus, each point in the curves corresponds to SNR required to reach the BER criterion. This BER criterion was selected as a compromise between the simulation time and accuracy. First of all, it is visible that multi antenna techniques provide gain over SISO and SIMO due to increased diversity. Also, rate 1 4x2 codes show good performance at low signal-to-noise levels. Further, rate 2 4x2 codes outperform 2x2 SM (Spatial Multiplexing). It is important to note that altering the pilot carrier density does not affect the order of 4x2 curves, but changes the bpcu point where the capacity curves cross. Also, if 4x2 schemes are compared to 2x2 schemes, having denser pilot pattern, for example 1/12 for SISO, 1/6 for 2x2 and 1/3 for 4x2, begins to eat out the performance gain of 4x2 schemes.

7.3 Advanced Modulation and MIMO Schemes

7.3.1 Distributed Coded MIMO Application in Terrestrial TV Broadcasting

To increase area coverage, single frequency networks (SFN) are commonly used for terrestrial TV broadcasting. SFNs are based on the simple addition of lower power transmitters at various sites throughout the coverage area. In an SFN, several transmitters transmit at the same moment the same signal on the same frequency. SFN can provide lower transmitted powers, increased bit rates and better performance. A 3-dimensional (3D) space-time-space block code (STSBC) [109] for broadcasting systems with an SFN deployment supporting mobile and portable reception is presented in this section. The use of one additional space dimension is due to the SFN deployment. The STSBC consists of 2 layers: one layer corresponding to an inter-cell ST coding, the second corresponding to an intra-cell ST coding.

More precisely, we consider a distributed MIMO scheme using ($2\times N_t$) transmit antennas (Tx) and N_r receive antennas (Rx), which represents a SFN deployment with 2 geographically separated transmit sites. Each site implements N_t transmission antennas. The transmission could therefore be seen as a double layer scheme in the space domain. The first layer is seen between the 2 sites separated by D km (distributed MIMO scheme). The second layer is seen between the antennas separated by d m within one site. For the first layer, an STBC encoding scheme is applied between the 2 signals transmitted by each site. In the second layer, we use a second STBC encoder for each subset of N_t signals transmitted from the same site. For the first layer, the STBC encoder takes L sets of Q data complex symbols each ($s_1,\ldots,s_Q$) and transforms them into a $2\times U$ output matrix according to the STBC scheme. In the second layer (the second step), the encoder transforms each component of the first layer matrix into $N_t \times T$ output matrix according to the second layer STBC scheme. The number of rows of the encoding matrix in the first layer is equal to two since, the STBC scheme is applied between the signals of two different sites. The output signal of each site is fed to N_t OFDM modulators, each using N sub-carriers. The reader could construct a double layer Alamouti code, for example, by considering 2 sets of 2 symbols each and then, by applying Alamouti encoding between the 2 symbols' sets and another Alamouti encoding between the signals in each site. More generally, the double layer encoding matrix is described by:

$$\mathbf{X}^{(1)} = \begin{pmatrix} \mathbf{X}_{11}^{(2)} & \cdots & \mathbf{X}_{1U}^{(2)} \\ \mathbf{X}_{21}^{(2)} & \cdots & \mathbf{X}_{2U}^{(2)} \end{pmatrix}$$

$$\mathbf{X}_{ij}^{(2)} = \begin{pmatrix} f_{ij,11}(s_1,\ldots s_Q) & \cdots & f_{ij,1T}(s_1,\ldots s_Q) \\ \vdots & \ddots & \vdots \\ f_{ij,M_T1}(s_1,\ldots s_Q) & \cdots & f_{ij,M_TT}(s_1,\ldots s_Q) \end{pmatrix} \quad \textbf{(7.3-1)}$$

In (7.3-1), the superscript indicates the layer, $f_{ij,mt}(s_1,\cdots,s_Q)$ is a function of the input complex symbols sq and depends on the STBC encoder scheme. The time dimension of the resulting 3D code is equal to $U\times T$ and the resulting coding rate is $R = \frac{Q\times L}{U\times T}$. In order to have a fair analysis and comparison between different STBC codes, the signal power at the output of the ST encoder at each site is normalized by $2\times N_t$.

We restrict our study to N_t =2 transmit antennas by site and N_r =2 receive antennas. We construct the first layer with the Alamouti scheme, since it is the most resistant for the case of unequal received powers. In a complementary way, we propose to construct the second layer with the Golden code since it offers the best results in the case of equal received powers. After combination of the 2 layers, (7.3-1) yields:

$$X = 1/\sqrt{5}\begin{pmatrix} \alpha(s_1+\theta s_2) & \alpha(s_3+\theta s_4) & \alpha(s_5+\theta s_6) & \alpha(s_7+\theta s_8) \\ j\bar{\alpha}(s_3+\bar{\theta}s_4) & \bar{\alpha}(s_1+\bar{\theta}s_2) & j\bar{\alpha}(s_7+\bar{\theta}s_8) & \bar{\alpha}(s_5+\bar{\theta}s_6) \\ -\alpha^*(s_5^*+\theta^* s_6^*) & -\alpha^*(s_7^*+\theta^* s_8^*) & \alpha^*(s_1^*+\theta^* s_2^*) & \alpha^*(s_3^*+\theta^* s_4^*) \\ j\bar{\alpha}^*(s_7^*+\bar{\theta}^* s_8^*) & -\bar{\alpha}^*(s_5^*+\bar{\theta}^* s_6^*) & -j\bar{\alpha}^*(s_3^*+\bar{\theta}^* s_4^*) & \bar{\alpha}^*(s_1^*+\bar{\theta}^* s_2^*) \end{pmatrix} \quad \textbf{(7.3-2)}$$

where $\theta = \frac{1+\sqrt{5}}{2}$, $\bar{\theta} = 1-\theta$, $\alpha = 1+j(1-\theta)$, $\bar{\alpha} = 1+j(1-\bar{\theta})$ and (.)* stands for complex conjugate.

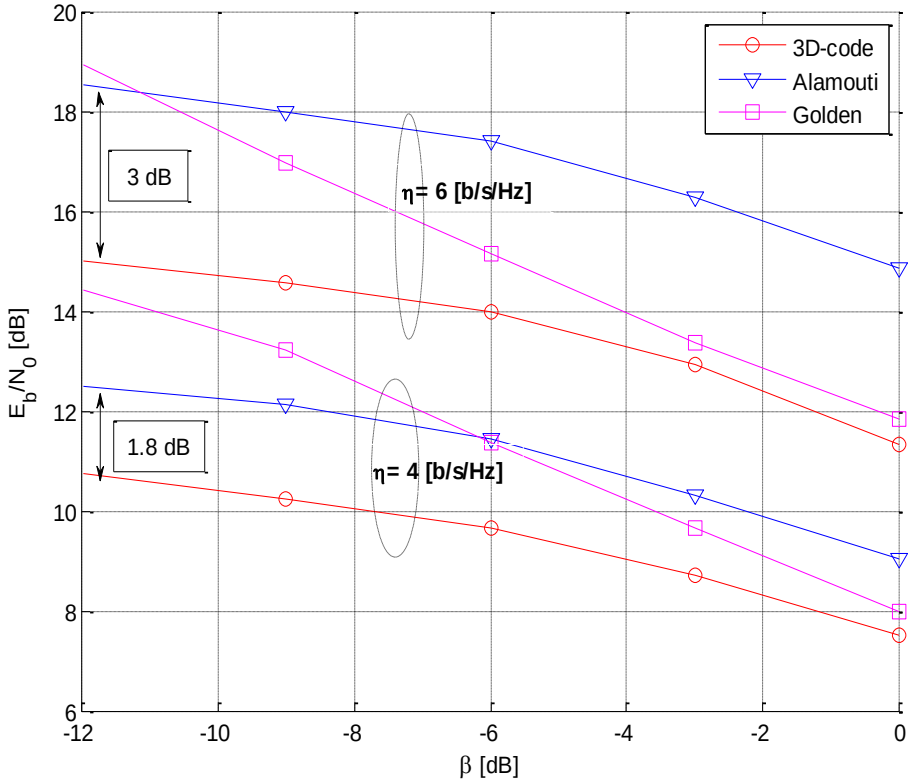

Figure 145: Performance of 3D MIMO codes, Required Eb/N0 to obtain a BER=10^{-4}, double layer case, DVB-T parameters,

η=4 [b/s/Hz]: Alamouti code: 64-QAM, R=1, Rc =2/3.
Other schemes: 16-QAM, R=2, Rc =1/2.
η=6 [b/s/Hz]: Alamouti code: 256-QAM, R=1, Rc =3/4.
Other schemes: 64-QAM, R=2, Rc =1/2.

In the following, we will compare different STBC schemes assuming that a portable or mobile terminal receives signals from the 2 sites with unequal powers. It is a real case in SFN where the terminal receives signals from the 2 sites transmitters. We will assume that the relative power imbalance factor between the received signals from the two sites is equal to β. At the receiving side, we assume that a sub-optimal iterative receiver is used for non-orthogonal STBC schemes. The sub-optimal solution proposed here consists of an iterative receiver where the ST detector and the channel decoder exchange extrinsic information in an iterative way until the algorithm converges.

Figure 145 shows the results in terms of required E_b/N_0 to obtain a BER equal to 10^{-4} for different values of β and 3 STBC schemes i.e. the 3D code scheme, the 1-Layer Alamouti and the Golden code schemes. It can be seen that our proposed scheme presents the best performance whatever the spectral efficiency and the factor β. Indeed, it is optimized for SFN systems owing to the robustness of the Alamouti scheme to unbalanced received powers and the full rank of the Golden code. For β = -12 dB, the proposed 3D code offers a gain equal to 1.8 dB (respectively 3 dB) with respect to the Alamouti scheme for η = 4 [b/s/Hz] (resp. η = 6 [b/s/Hz]). This gain is even greater when it is compared to the Golden code. Moreover, the maximum loss of our code due to unbalanced received powers is only equal to 3 dB in terms of E_b/N_0. These results confirm that the proposed 3D code is very robust whatever the spectral efficiency and the imbalance factor β. Eventually, we should note that the factor β could be related to the channel impulse response delay and to the power path loss. Then, it can be used to adjust synchronisation problems.

7.3.2 Distributed Coded MIMO Application in Hybrid Terrestrial / Satellite TV Broadcasting

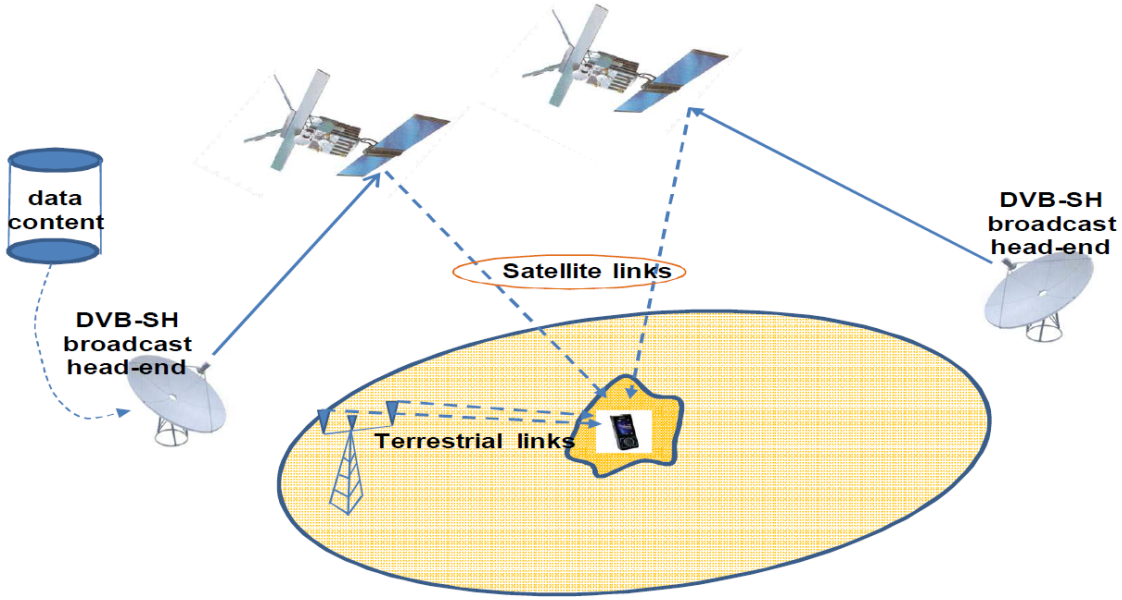

Figure 146: Hybrid terrestrial/satellite transmission scheme for DVB-NGH.

Besides terrestrial broadcasting, the DVB-NGH system can operate in combination with a satellite component to enhance the coverage and the quality of the service in a large area. As shown in Figure 146, the satellites as well as the terrestrial sites are used to transmit the same program to the TV receivers. The transmission can be arranged as either SFN or MFN. In the following presentation, we will focus on the SFN deployment where the philosophy of the 3D MIMO coding presented in the previous section can also be adopted [110].

More precisely, the satellites and terrestrial sites can be viewed as two different "cells". Each cell consists of purely satellite or terrestrial transmitters. Therefore, a space-time-space block code can be formed based on a two level construction of ST coding: inter-cell (i.e. satellite-terrestrial signal) coding and intra-cell (i.e. intra-satellite and intra-terrestrial, respectively) coding. Hence, the double layer encoding matrix can also be described by (7.3-1) given in section 7.3.1. A very important work is to find the suitable ST coding scheme for each layer.

In order to construct the first layer, i.e. the ST encoding between the terrestrial and satellite sites, we consider one antenna by each site. In other words, one terrestrial site with single transmit antenna cooperates with one satellite. The second layer matrix $\mathbf{X}^{(2)}$ in (7.3-1) thus turns to one element. Due to the mobility, the mobile receiver is assumed to move among different locations. According to the typical land mobile satellite (LMS) channel model [106], the signal transmitted from satellite may experience moderate or deep shadowing. Therefore, the first layer ST scheme must be efficient face to shadowing.

In the sequel, we present first the results obtained with different elevation angles and spectral efficiencies using an Alamouti and Golden code scheme at the first layer. The main simulation parameters are list in Table 32. Two spectral efficiencies, i.e. η = 2, and 6 b/s/Hz, are evaluated in the simulation. The corresponding modulation and channel coding to reach these spectral efficiencies are list in Table 33. COST 207 TU-6 channel model [107] is used for terrestrial link while the narrow-band LMS is used for the satellite

link. The received signal is assumed to follow Loo distribution [108]. The value of different parameters in the Loo distribution is given in Table 34.

Figure 147 shows the required E_b/N_0 to obtain a BER equal to $10^{-4}$for a spectral efficiency of $\eta = 2$, and 6 b/s/Hz and two elevation angles. The results depicted in this figure show that for deep shadowing levels ($\Phi = 50°$), the Alamouti scheme presents almost better results. The Golden code presents better results only for low shadowing levels ($\Phi = 30°$) and high spectral efficiency ($\eta = 2$ b/s/Hz).

Table 32: System parameters used in the simulations

Parameter	Value
Sampling frequency	9.14 MHz
FFT size	256
Guard interval	1/4
Modulation	QPSK, 16-QAM, 64QAM and 256QAM
Channel coding	Convolutional codes
Code rates	1/4, 1/3, 2/5, 1/2, 3/5, 2/3
Channel estimation	ideal
Spectral efficiencies	η = 2, and 6 b/s/Hz

Table 33: Modulation and channel coding for different MIMO schemes.

Spectral efficiency	ST scheme	ST coding rate	Constellation	Channel coding rate
η = 2 b/s/Hz	Alamouti	1	16 QAM	1/2
	Golden	2	QPSK	1/2
	3D code	2	QPSK	1/2
η = 6 b/s/Hz	Alamouti	1	256 QAM	3/4
	Golden	2	64 QAM	1/2
	3D code	2	64 QAM	1/2

Table 34: Average Loo model parameters in dB for various angles.

Elevation Φ	Case 1: LOS			Case 2: moderate shadowing			Case 3: deep shadowing		
	M	Σ	MP	M	Σ	MP	M	Σ	MP
10°	-0.1	0.5	-19	-8.7	3	-12	-12.1	6	-25
30°	-0.5	1	-15	-4.7	1.5	-19	-7	3	-20
50°	-0.5	1	-17	-6.5	2.5	-17	-14	2.5	-20

Considering the whole 3D MIMO code construction, we have to find ST coding scheme for the second layer of the hybrid system, that is, the ST coding for inside each "cell". The proposed code should be robust face to the low, moderate and deep shadowing levels. In the first step, we restrict our study to two transmit antennas by cell. According to the results from Figure 147, we propose to construct the first layer with Alamouti scheme, since it is the most resistant for deep shadowing case. In a complementary way, we propose to construct the second layer with the Golden code since it offers the best results in the case of low shadowing levels and high spectral efficiency. After combination of the two layers, it yields the same 3D MIMO code (7.3-2) as in the terrestrial broadcasting case.

Figure 148 shows the results in terms of required E_b/N_0 to obtain a BER equal to 10^{-4} for different values of Φ and 3 STBC schemes including our proposed 3D MIMO scheme. The results obtained in this figure assume that the transmission from the satellite to the receiver is achieved through a LMS channel where a COST 207 TU-6 channel model is assumed for terrestrial transmission. This figure shows the superiority of our 3D MIMO scheme. Its gain compared to the Alamouti scheme is about 1 dB for η= 2b/s/Hz and it could

reach 4 dB for η = 6 b/s/Hz. Moreover, its performance remains quasi unchanged when the terminal changes its elevation angle Φ. This means that it leads to a powerful code for SFN architectures and NGH systems.

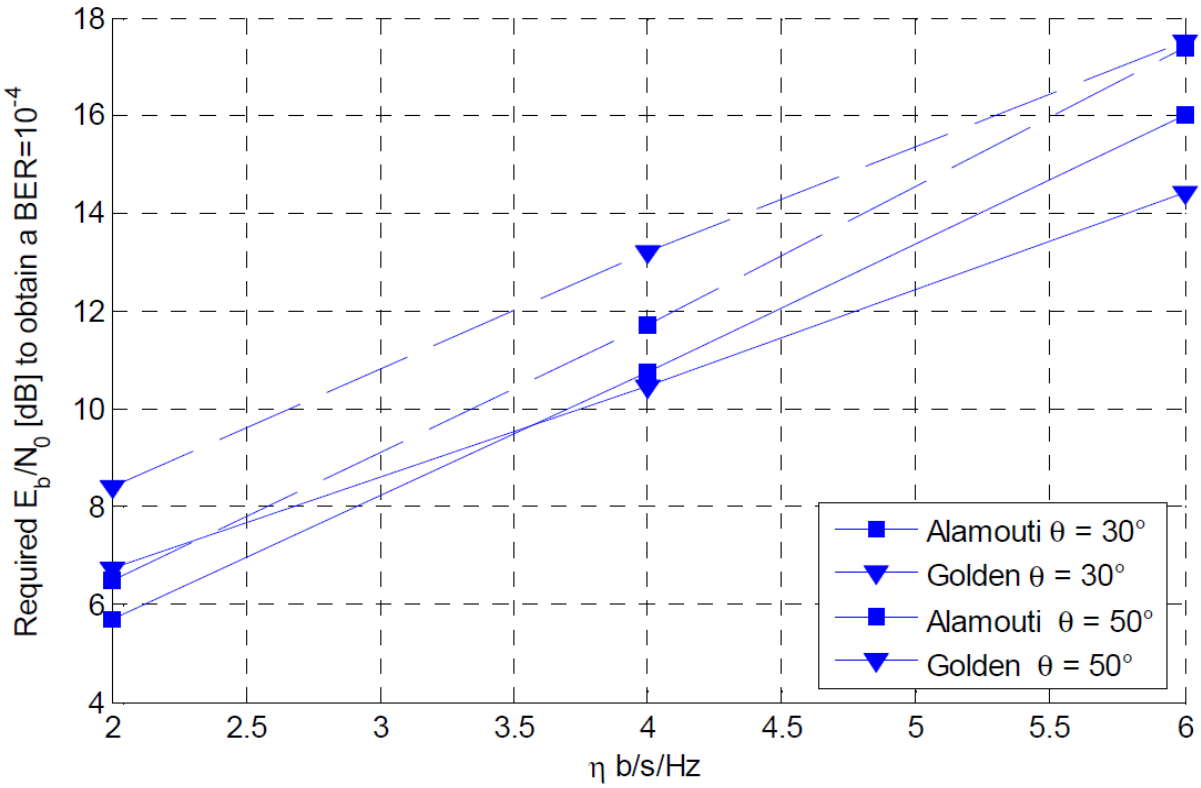

Figure 147: Required E_b/N_0 to obtain a BER=10^{-4}, single layer case.

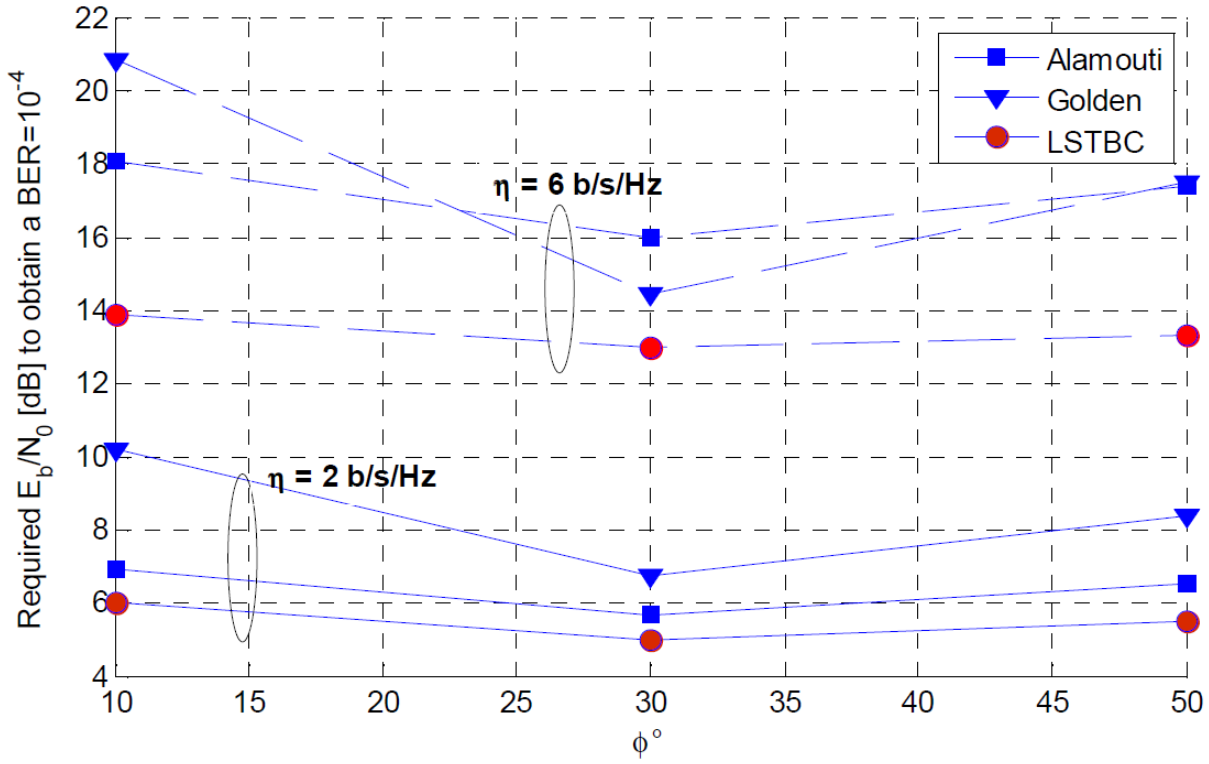

Figure 148: Required E_b/N_0 to obtain a BER=10^{-4}, double layer case.

7.4 High Diversity Multi-Block Space-Time Code

This section presents a Space-Time Code (STC) that was initially proposed by Telecom Bretagne as a response to the DVB-NGH Call for Technology. The proposed code calls for a 2 times 2x2 matrix seen as a two-block matrix. It enjoys a flexible transmission rate and a diversity order of 8 for a 2x2 MIMO system by exploiting additional time diversity. Its decoding complexity is only proportional to the power of four of the constellation size. The STC parameters have been optimized to suit fading channels with and without erasure events. These events are typical of single frequency networks that are becoming a popular topology thanks to their low bandwidth requirements. Unlike state-of-the art quasi-orthogonal structures, the proposed multi-block STC can be jointly optimized for shaping and coding gain.

Since the channel measurements carried out showed that the Multiple Input Multiple Output (MIMO) channels to be considered for NGH were highly correlated, MIMO techniques have only been adopted as an option. Consequently, only proposals with very little additional complexity were actually considered. Thus, this STC code was early withdrawn from the NGH proposals. However further studies have been carried out in order to show its suitability to a broadcast systems, especially in the case of single frequency networks.

7.4.1 Introduction

Next generation telecommunication and broadcasting systems should be designed to satisfy the need for high data rate transmissions while improving robustness to severe channel conditions. On one hand, reliable transmissions over deeply faded channels require an increase in the diversity order. On the other hand, multiple antenna systems can achieve high throughputs without requiring additional bandwidth. Therefore the introduction of STC for MIMO systems is considered to be a promising mean of fulfilling these constraints. Indeed, STCs have been introduced in several communications standards like the Long Term Evolution (LTE) of the 3rd Generation Partnership Project (3GPP) [111] and the second generation of the Worldwide Interoperability for Microwave Access (WiMAX 2) [112].

Broadcast standards have not introduced full rate MIMO yet. Indeed, one major difference with respect to telecommunication systems resides in the absence of return channel carrying crucial information about transmission quality. It enables adaptive throughput via varying coding and modulation schemes. In addition, broadcast network topology can play a significant role in the definition of the constraints of the system. Indeed, Single Frequency Networks (SFN), where several transmitters simultaneously send the same signal over the same frequency channel, are increasingly used in broadcasting applications due to their efficient usage of the radio spectrum. However, SFNs entail undesirable effects on the transmission channel since their deployment leads to the introduction of deep fades. In addition to multipath in the case of a single transmitter, several echoes of the same signal are also received due to presence of several transmitters in the SFN case. The constructive or destructive addition of these echoes, also known as self-interference, results in additional deep fades. Frequently, they have a dynamic range beyond the reach of a standard receiver due to quantization error. In this case, deep fades can be modelled by erasure events causing a significant performance penalty.

A possible solution to mitigate the impact of SFN on performance can be found by using diversity techniques. Indeed, the introduction of Signal Space Diversity (SSD) for Single Input Single Output (SISO) broadcast systems has proven to improve performance for deeply faded or erased channels [113]. Therefore, MIMO for broadcasting should consider introducing STC with high diversity. The Golden code [114] is one of the best known Space-Time Block Codes (STBC) due to its remarkable properties in terms of full rate, full diversity and having a non-vanishing determinant. However, the Maximum Likelihood (ML) decoding complexity of such a code remains relatively high especially for high order constellation schemes. Therefore, alternative STBC structures have been proposed lately [115][118][119][120][121][122] that enjoy what is

known as fast decoding. They are generally based on a quasi-orthogonal structure that allows for a lower complexity decoding under a channel invariability constraint. Based on the STBC structure of [115], we propose the introduction of SSD between modulation symbols of two STBC blocks. The resulting Multi-Block STBC (MB-STBC) is shown to enjoy full rate and a linear increase in diversity with increasing number of blocks. By using the quasi-orthogonal structure, the proposed STBC remains fast decodable with a complexity of the same order as the Golden code. In addition, it has been designed to withstand different scenarios of severe SFN channel conditions where one or more transmit antennas suffer from deep fading or erasure events during one or more symbol periods.

7.4.2 Channel models

Two channel models have been considered in this study: the classical Rayleigh fading channel and a variation of this channel to which we have added additional deep fade events. Both are based on the fading channel model of [123].

7.4.2.1 The fading channel model

We adopt the classical frequency non-selective memoryless Rayleigh fading channel model. The received discrete time baseband complex signal r_j on antenna j can be written as:

$$\begin{bmatrix} r_1 \\ r_2 \end{bmatrix} = \begin{bmatrix} h_{11} & h_{12} \\ h_{21} & h_{22} \end{bmatrix} \begin{bmatrix} s_1 \\ s_2 \end{bmatrix} + \begin{bmatrix} n_1 \\ n_2 \end{bmatrix} \quad (1)$$

where s_l represents the complex transmitted signal on antenna l, h_{jl} is a Rayleigh distributed fading coefficient with $E(h_{jl}^2) = 1$, and n_j is a complex white Gaussian noise with spectral density $N_0/2$ in each component axis. We assume coherent detection and perfect Channel State Information (CSI) knowledge so that h_{jl} and the phase of the signal are perfectly estimated and available at the receiver.

7.4.2.2 The fading channel model with erasures

In addition to the classical Rayleigh fading described above, additional erasure events can affect the transmitted signal. In addition, if a properly designed channel interleaver is introduced, these events can be modeled by a discrete random processes e taking value 0 with a probability of P_e and value 1 with a probability of $1-P_e$. The received discrete time baseband complex signal r_j becomes:

$$\begin{bmatrix} r_1 \\ r_2 \end{bmatrix} = \begin{bmatrix} e_1 h_{11} & e_2 h_{12} \\ e_1 h_{21} & e_2 h_{22} \end{bmatrix} \begin{bmatrix} s_1 \\ s_2 \end{bmatrix} + \begin{bmatrix} n_1 \\ n_2 \end{bmatrix} \quad (2)$$

The occurrence of erasure events sets a bound on the coding rate R. In fact, with an erasure probability of P_e a reliable coded transmission cannot be ensured with a redundancy ratio lower than P_e, or in other words with a coding rate greater than $1-P_e$. This prevents the conventional system from operating at high coding rates and sets a bound on the achievable spectral efficiency.

7.4.3 Description of the proposed MB-STBC

7.4.3.1 Encoding procedure

The proposed STBC calls for a 2x4 matrix of the following form:

$$\mathbf{X} = \begin{bmatrix} s_1'' & s_3'' & s_5'' & s_7'' \\ s_2'' & s_4'' & s_6'' & s_8'' \end{bmatrix} \qquad (3)$$

This structure allows the transmission of 8 signals $s_1'' \cdots s_8''$ through 2 antennas over 4 time slots. The first (second) row of the matrix contains the 4 signals successively sent through the first (second) transmit antenna.

We assume that the channel coefficients are constant during the two first and the two last time slots. In other words, a quasi-orthogonal STBC structure spread over 4 slots. In a multi-carrier transmission system, this property can be obtained by transmitting the signals of columns 1 and 2 (respectively of columns 3 and 4) of **X** over adjacent subcarriers while the signals of columns 1 (respectively 2) and 3 (respectively 4) are transmitted over distant subcarriers.

Two different channel matrices have then to be considered: **H** for the transmission of signals in columns 1 and 2 and H' for the transmission of signals in columns 3 and 4:

$$\mathbf{H} = \begin{bmatrix} h_{11} & h_{12} \\ h_{21} & h_{22} \end{bmatrix} \text{ and } \mathbf{H}' = \begin{bmatrix} h_{11}' & h_{12}' \\ h_{21}' & h_{22}' \end{bmatrix} \qquad (4)$$

Let us consider 8 modulation symbols $s_1 \ldots s_8$ taken from an M-order 2-dimensional constellation **C**, where in-phase I and quadrature Q components are correlated. This correlation can be obtained by applying a rotation to the original constellation. The rotation angle should be chosen such that every constellation point is uniquely identifiable on each component axis separately. This is equivalent to the first step performed for SSD [113]. The representation of s_i in the complex plane is given by, $s_i = I_i + jQ_i$, $i = 1 \cdots 8$. The proposed construction of **X** involves the application of two steps:

Step 1: the first step consists of defining two subsets S_1' and S_2' of modified symbols s_i' obtained from *I* and *Q* components belonging to different symbols s_i. Each subset must only contain one component of each symbol s_i of **C**. For instance:

$$S_1' = \{s_1', s_2', s_3', s_4'\} \text{ and } S_2' = \{s_5', s_6', s_7', s_8'\}$$

$$\text{where } \begin{matrix} s_1' = I_1 + jQ_7 \\ s_2' = I_2 + jQ_8 \\ s_3' = I_3 + jQ_5 \\ s_4' = I_4 + jQ_6 \end{matrix} \text{ and } \begin{matrix} s_5' = I_5 + jQ_3 \\ s_6' = I_6 + jQ_4 \\ s_7' = I_7 + jQ_1 \\ s_8' = I_8 + jQ_2 \end{matrix}.$$

Symbols s_i' belong to an extended constellation **C'** of size M^2.

Step 2: the symbols $s_1'' \cdots s_8''$ transmitted by **X** are defined as

$$\begin{matrix} s_1'' = as_1' + bs_2' \\ s_2'' = as_3' + bs_4' \\ s_3'' = -cs_3'^{*} - ds_4'^{*} \\ s_4'' = cs_1'^{*} + ds_2'^{*} \end{matrix} \text{ and } \begin{matrix} s_5'' = as_5' + bs_6' \\ s_6'' = as_7' + bs_8' \\ s_7'' = -cs_7'^{*} - ds_8'^{*} \\ s_8'' = cs_5'^{*} + ds_6'^{*} \end{matrix}.$$

where *s** represents the complex conjugate of *s*.

a, *b*, *c* and *d* are complex-valued parameters of the STBC. Signals *s*'' belong to the STBC constellation signal set **C''** different from **C'**.

7.4.3.2 Decoding the MB-STBC code

The proposed MB-STBC code enjoys a structure that enables a simplified detection. Indeed, inspired by the decoding process in [115], the decoding complexity can be greatly simplified without the need for a sphere decoder [124]. If we denote by r_k^j the signal received by the j^{th} reception antenna, j = 1, 2, during time slot k, where $k = 1 \ldots 4$.

The four signals successively received by antenna 1 can be written as:

$$\begin{aligned} r_1^1 &= h_{11}\left[a(I_1 + jQ_7) + b(I_2 + jQ_8)\right] \\ &\quad + h_{12}\left[a(I_3 + jQ_5) + b(I_4 + jQ_6)\right] + n_1^1 \end{aligned} \tag{5}$$

$$\begin{aligned} r_2^1 &= h_{11}\left[-c(I_3 - jQ_5) - d(I_4 - jQ_6)\right] \\ &\quad + h_{12}\left[c(I_1 - jQ_7) + d(I_2 - jQ_8)\right] + n_2^1 \end{aligned} \tag{6}$$

$$\begin{aligned} r_3^1 &= h'_{11}\left[a(I_5 + jQ_3) + b(I_6 + jQ_4)\right] \\ &\quad + h'_{12}\left[a(I_7 + jQ_1) + b(I_8 + jQ_2)\right] + n_3^1 \end{aligned} \tag{7}$$

$$\begin{aligned} r_4^1 &= h'_{11}\left[-c(I_7 - jQ_1) - d(I_8 - jQ_2)\right] \\ &\quad + h'_{12}\left[c(I_5 - jQ_3) + d(I_6 - jQ_4)\right] + n_4^1 \end{aligned} \tag{8}$$

Simplified decoding is possible under the condition that the *I* and *Q* components of any s_i constellation symbol are mapped to two different *s*' symbols who are multiplied by the same STBC parameter *a*, *b*, *c* or *d*. This constraint is respected in the structure of the STBC matrix **X.** Therefore, by re-arranging equations (5) to (8) we obtain y_k^j terms:

$$\begin{aligned} y_1^1 &= r_1^1 - b\left[h_{11}(I_2 + jQ_8) + h_{12}(I_4 + jQ_6)\right] \\ &= a\left[h_{11}(I_1 + jQ_7) + h_{12}(I_3 + jQ_5)\right] + n_1^1 \end{aligned} \tag{9}$$

$$\begin{aligned} y_2^1 &= r_2^1 - d\left[h_{12}(I_2 - jQ_8) - h_{11}(I_4 - jQ_6)\right] \\ &= c\left[h_{12}(I_1 - jQ_7) - h_{11}(I_3 - jQ_5)\right] + n_2^1 \end{aligned} \tag{10}$$

$$\begin{aligned} y_3^1 &= r_3^1 - b\left[h'_{11}(I_6 + jQ_4) + h'_{12}(I_8 + jQ_2)\right] \\ &= a\left[h'_{11}(I_5 + jQ_3) + h'_{12}(I_7 + jQ_1)\right] + n_3^1 \end{aligned} \tag{11}$$

$$\begin{aligned} y_4^1 &= r_4^1 - d\left[h'_{12}(I_6 - jQ_4) - h'_{11}(I_8 - jQ_2)\right] \\ &= c\left[h'_{12}(I_5 - jQ_3) - h'_{11}(I_7 - jQ_1)\right] + n_4^1 \end{aligned} \tag{12}$$

In equations (9) to (12), the first line terms are only dependent on *I* and *Q* components of even symbols *s*. Vice-versa, second line terms depend solely on odd symbols. Therefore, applying a detection conditioned by the knowledge of even terms is possible. In other words, for a loop on all possible values for $S_2 = I_2 + jQ_2$, $S_4 = I_4 + jQ_4$, $S_6 = I_6 + jQ_6$ and $S_8 = I_8 + jQ_8$ (for a total of M^4 terms where *M* represents the order of the constellation *s*) intermediate Z_k terms can be computed as follows:

$$Z_1 = \frac{h_{11}^* y_1^1 + h_{21}^* y_1^2}{a} + \frac{h_{12} y_2^{1*} + h_{22} y_2^{2*}}{c^*} \quad (13)$$

$$Z_2 = \frac{h_{12}^* y_1^1 + h_{22}^* y_1^2}{a} - \frac{h_{11} y_2^{1*} + h_{21} y_2^{2*}}{c^*} \quad (14)$$

$$Z_3 = \frac{h_{11}'^* y_3^1 + h_{21}'^* y_3^2}{a} + \frac{h_{12}' y_4^{1*} + h_{22}' y_4^{2*}}{c^*} \quad (15)$$

$$Z_4 = \frac{h_{12}'^* y_3^1 + h_{22}'^* y_3^2}{a} - \frac{h_{11}' y_4^{1*} + h_{21}' y_4^{2*}}{c^*} \quad (16)$$

By properly combining Z_k terms, we obtain:

$$\begin{aligned} &\mathrm{Re}\{Z_1\} + j\,\mathrm{Im}\{Z_4\} = \left(|h_{11}|^2 + |h_{12}|^2 + |h_{21}|^2 + |h_{22}|^2\right) I_1 \\ &+ j\left(|h_{11}'|^2 + |h_{12}'|^2 + |h_{21}'|^2 + |h_{22}'|^2\right) Q_1 + \mathrm{Re}\{N_1\} + j\,\mathrm{Im}\{N_4\} \end{aligned} \quad (17)$$

$$\begin{aligned} &\mathrm{Re}\{Z_2\} + j\,\mathrm{Im}\{Z_3\} = \left(|h_{11}|^2 + |h_{12}|^2 + |h_{21}|^2 + |h_{22}|^2\right) I_3 \\ &+ j\left(|h_{11}'|^2 + |h_{12}'|^2 + |h_{21}'|^2 + |h_{22}'|^2\right) Q_3 + \mathrm{Re}\{N_2\} + j\,\mathrm{Im}\{N_3\} \end{aligned} \quad (18)$$

$$\begin{aligned} &\mathrm{Re}\{Z_3\} + j\,\mathrm{Im}\{Z_2\} = \left(|h_{11}'|^2 + |h_{12}'|^2 + |h_{21}'|^2 + |h_{22}'|^2\right) I_5 \\ &+ j\left(|h_{11}|^2 + |h_{12}|^2 + |h_{21}|^2 + |h_{22}|^2\right) Q_5 + \mathrm{Re}\{N_3\} + j\,\mathrm{Im}\{N_2\} \end{aligned} \quad (19)$$

$$\begin{aligned} &\mathrm{Re}\{Z_4\} + j\,\mathrm{Im}\{Z_1\} = \left(|h_{11}'|^2 + |h_{12}'|^2 + |h_{21}'|^2 + |h_{22}'|^2\right) I_7 \\ &+ j\left(|h_{11}|^2 + |h_{12}|^2 + |h_{21}|^2 + |h_{22}|^2\right) Q_7 + \mathrm{Re}\{N_4\} + j\,\mathrm{Im}\{N_1\} \end{aligned} \quad (20)$$

With the noise terms N_k being:

$$N_1 = \frac{h_{11}^* n_1^1 + h_{21}^* n_1^2}{a} + \frac{h_{12} n_2^{1*} + h_{22} n_2^{2*}}{c^*} \quad N_2 = \frac{h_{12}^* n_1^1 + h_{22}^* n_1^2}{a} - \frac{h_{11} n_2^{1*} + h_{21} n_2^{2*}}{c^*} \quad N_3 = \frac{h_{11}'^* n_3^1 + h_{21}'^* n_3^2}{a} + \frac{h_{12}' n_4^{1*} + h_{22}' n_4^{2*}}{c^*}$$

$$N_4 = \frac{h_{12}'^* n_3^1 + h_{22}'^* n_3^2}{a} - \frac{h_{11}' n_4^{1*} + h_{21}' n_4^{2*}}{c^*}$$

Equations (17) to (20) show that the combinations of Z_k dependent terms are each a function of only one $s_i = I_i + jQ_i$ symbol. Therefore a simple linear detection can be performed separately on all symbols in the same loop since every I_i and Q_i couple is unique. In addition, the diversity of 8 is clearly observed since the I and Q components of every symbol depend on 4 different channel coefficients. Therefore, since SSD is applied, every complex s_i signal enjoys an overall diversity of 8.

The detection of odd symbols on the second antenna is similar to the first antenna. For the joint detection of even symbols, the following distance should be minimized:

$$
\begin{aligned}
D(s_2,s_4,s_6,s_8) = & \left|y_1^1 - a\left[h_{11}(I_1+jQ_7)+h_{12}(I_3+jQ_5)\right]\right|^2 \\
& + \left|y_2^1 - c\left[h_{12}(I_1-jQ_7)-h_{11}(I_3-jQ_5)\right]\right|^2 \\
& + \left|y_3^1 - a\left[h'_{11}(I_5+jQ_3)+h'_{12}(I_7+jQ_1)\right]\right|^2 \\
& + \left|y_4^1 - c\left[h'_{12}(I_5-jQ_3)-h'_{11}(I_7-jQ_1)\right]\right|^2 \\
& + \left|y_1^2 - a\left[h_{21}(I_1+jQ_7)+h_{22}(I_3+jQ_5)\right]\right|^2 \\
& + \left|y_2^2 - c\left[h_{22}(I_1-jQ_7)-h_{21}(I_3-jQ_5)\right]\right|^2 \\
& + \left|y_3^2 - a\left[h'_{21}(I_5+jQ_3)+h'_{22}(I_7+jQ_1)\right]\right|^2 \\
& + \left|y_4^2 - c\left[h'_{22}(I_5-jQ_3)-h'_{21}(I_7-jQ_1)\right]\right|^2
\end{aligned} \quad (21)
$$

The distance $D(s_2,s_4,s_6,s_8)$ of equation (21) can be directly computed from y_k^j terms (which depend on s_2,s_4,s_6 and s_8) of equations (9) to (12) and by replacing the *I* and *Q* components of odd constellation symbol terms by their detected values from equations (17) to (20). Since $D(s_2,s_4,s_6,s_8)$ should be computed for all possible combinations of even constellation symbols, the total number of computed terms is in the order of M^4.

Note that the simplified detection does not depend on the choice of the STBC parameters *a*, *b*, *c* and *d*. These should be chosen depending on the rank, determinant, and shaping considerations.

7.4.4 Selection of the MB-STBC parameters

7.4.4.1 Conventional STBC design criteria

The minimization of the union bound for the Pairwise Error Probability (PEP) leads to the well-known rank-determinant [125]:

1) *Rank Criterion:* To achieve the maximum diversity, the rank R_a of the codeword difference matrix $\Delta = \mathbf{X} - \hat{\mathbf{X}}$ must be maximized for all possible transmitted codeword pairs $(\mathbf{X}, \hat{\mathbf{X}})$. When $R_a = N_t$ (N_t being the number of transmit antennas), the STBC is said to reach full diversity.

2) *Determinant Criterion:* The STBC minimum determinant δ is defined as:

$$\delta = \min_{\mathbf{X}\neq\hat{\mathbf{X}}} \det\left[\left(\mathbf{X}-\hat{\mathbf{X}}\right)\left(\mathbf{X}-\hat{\mathbf{X}}\right)^H\right] \quad (22)$$

Where *H* denotes the Hermitian transpose. For high SNRs, in order to obtain the best performance, δ should be maximized. Indeed, the dominant parameter is the diversity gain which defines the slope of error rate curves. Therefore, it is important to ensure the full diversity of the STBC and then maximize its coding gain δ^{1/N_t}.

The search for the minimum determinant is performed over an ensemble that spans all possible values of **X** and **X**'. For the proposed MB-STBC, this ensemble includes M^{16} different values. Taking into account that the STBC is linear and that the difference between two STBC codewords is a codeword, a simplified determinant criterion can be computed as follows:

$$\delta' = \min_{\mathbf{X}'} \det\left[\mathbf{X}\mathbf{X}^H\right] \qquad (23)$$

The search over δ' reduces the search ensemble to M^8 values.

7.4.4.2 STBC design criteria for channels with erasures

Designing STBC codes that can withstand erasure events follows the same procedure as the conventional criteria followed by additional steps based on the computation of the simplified determinant criteria where the erased position(s) are replaced by null value(s). The resulting **X** matrix parameters should be chosen such that the simplified determinant remains as high as possible. Four cases have been considered in our study:

Case 1: A classical Rayleigh fading channel as defined in section II-A. The conventional STBC design criteria apply.

Case 2: A classical Rayleigh fading channel with one erased transmit antenna during two symbol periods. The channel follows section II-B for the erased antenna. The erasure event spans two symbol periods due to the quasi-orthogonal structure of the STBC.

Case 3: A classical Rayleigh fading channel with one erased transmit antenna during the four symbol periods (all of the time).

Case 4: A classical Rayleigh fading channel with both transmit antennas erased during two symbol periods.

7.4.4.3 Choice of MB-STBC parameters

The choice of STBC parameters follows several constraints:

Transmit power of each antenna is normalized.

Rotation angle for SSD.

$|a| = |b| = |c| = |d| = 1/\sqrt{2}$ in order to guarantee identical transmit average energy per antenna .

Having to divide by a and c^* during the simplified detection process (equ (13) to equ (16)), we have chosen these two parameters to be real valued and therefore $a = c = 1/\sqrt{2}$.

$d = e^{-j\frac{\pi}{2}} b$, or $angle(d) = angle(b) - \pi/2$. Therefore, the search space is limited to finding the angle of b : $angle(b) = \Phi$ satisfying the design criteria.

On one side, parameters a et c being real numbers should not be a limiting factor for the search space. Indeed, the chosen $angle(b) = \Phi$ values satisfying the constraints are still valid when a and c are complex numbers. Indeed, the only requirement is that a, b, c, d parameters respect the following constraint:

angle(a) = Φ_a, $angle(c) = -\Phi_a$, $angle(b) = \Phi + \Phi_a$ and $angle(d) = \Phi - \Phi_a - \pi/2$, whatever the value taken by Φ_a.

On the other side, search for the $angle(b) = \Phi$ can be limited to the interval [0, π] due to the symmetry of the $\mathcal{C}''$ constellation with respect to axes origin. Consequently, angles α and $\alpha + \pi$ result into equivalent STBC codes with respect to the design criteria.

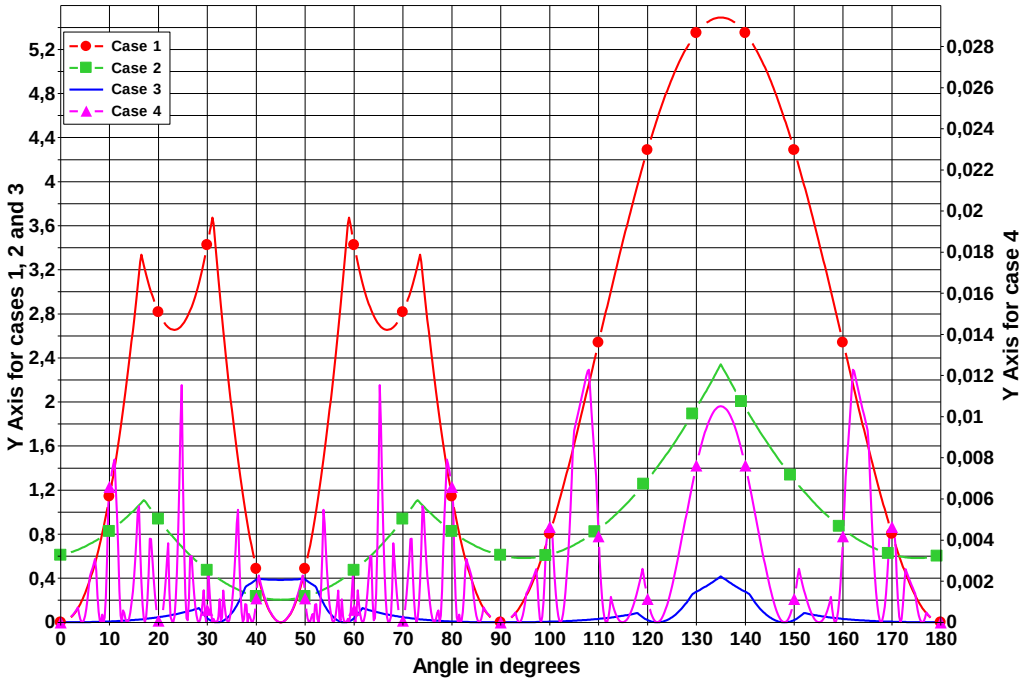

Figure 149: Simplified minimum determinant criteria as a function of angle(b) = Φ for the 4 considered cases of section 7.4.4.2.

The minimum determinant as a function of the angle of parameter *b* for the 4 different cases of section 7.4.4.2 is shown in Figure 149. For cases 1, 2 and 3, $\Phi = 135°$ represents the value that maximizes the simplified determinant. For this same angle, MB-STBC achieves one of the highest determinant values for case 4. Therefore, $angle(b) = \Phi = 135°$ can be considered as a compromise that enables good performance for the proposed MB-STBC structure under considered scenarios.

In addition, MB-STBC with $\Phi = 135°$ enjoys a high shaping gain. Indeed, the introduction of SSD increases the number of possible constellation points to be transmitted on every antenna. Parameters should be chosen such that this shaping gain is as high as possible since it plays a role on performance for low E_b/N_0 values. Unlike classical 2x2 quasi-orthogonal structures where the shaping gain and the coding gain are in general competing and not complementing, the MB-STBC with $\Phi = 135°$ shows the best coding and shaping gain since the resulting code exhibits the best error rate performance for low and high E_b/N_0 regions among all Φ values leading to non-zero rank.

7.4.5 Simulation results

Simulations have been carried out over a Rayleigh fading channel with and without erasures. When erasures were simulated, studied cases in section 7.4.4.2 were considered. The erasure events are then applied on an antenna all of the time. This is equivalent to having $P_e = 1$ in section 7.4.2.2. These two simulated cases represent extreme cases since a realistic scenario should lie between $P_e = 0$ (Rayleigh channel) and $P_e = 1$ (Rayleigh channel with erased antennas all of the time).

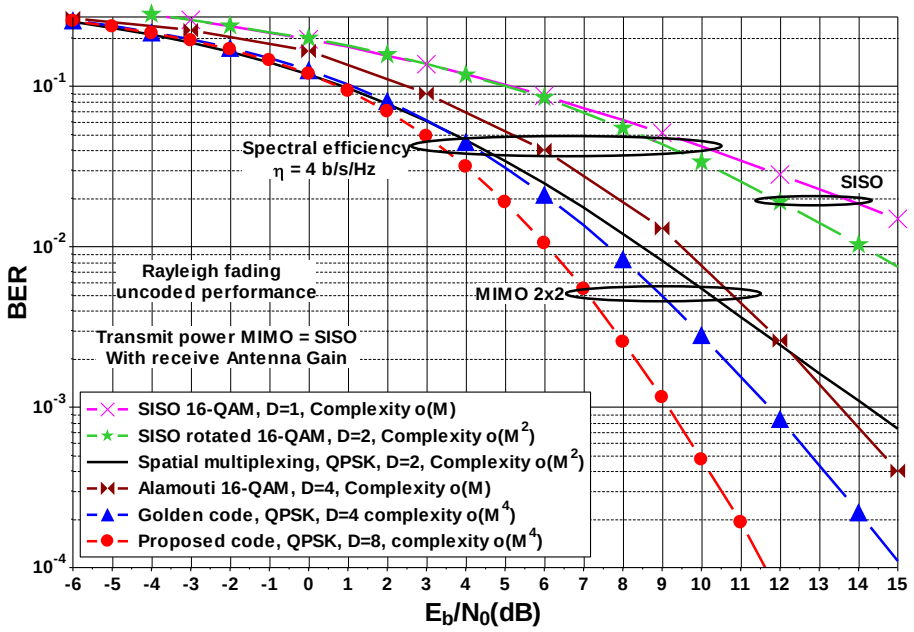

Figure 150: BER comparison between proposed MB-STBC, Alamouti 2x2, Golden code, spatial multiplexing, SISO and SISO with SSD over a Rayleigh fading channel for 4 bits/channel use.

A comparison in terms of Bit Error rate (BER) between the proposed MB-STBC, the Alamouti 2X2 code, the Golden code, spatial multiplexing, SISO and SISO with SSD are presented in Figure 150 over a Rayleigh fading channel for a spectral efficiency of 4 bits/channel use. It can be observed that the proposed MB-STBC outperforms all codes for high E_b/N_0 values since it achieves a diversity order of 8.

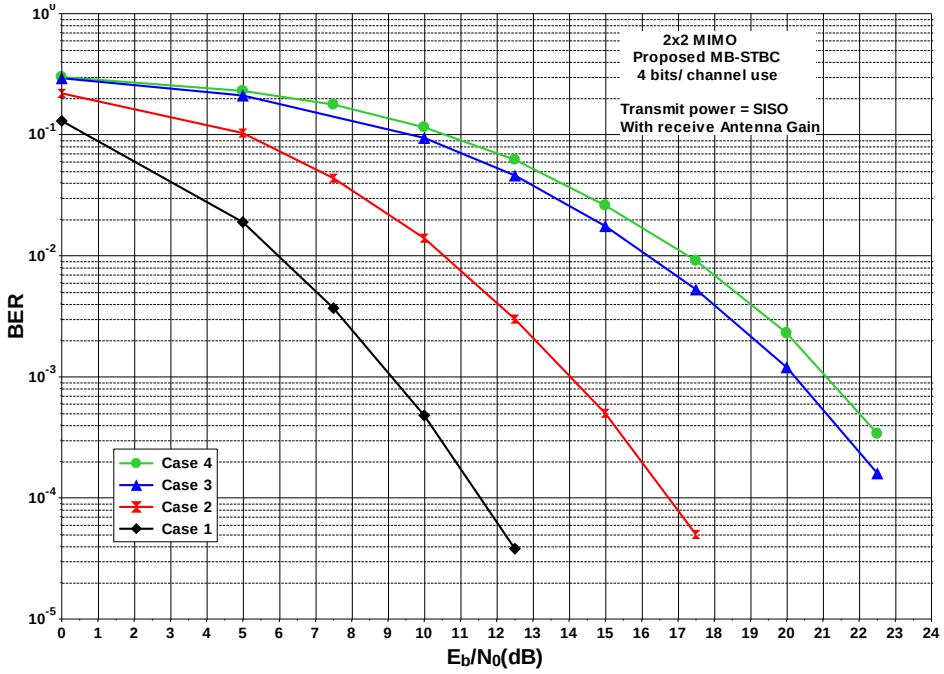

Figure 151: BER performance of the proposed MB-STBC, for cases 1, 2, 3 and 4 of section 7.4.4.2 and 4 bits/channel use.

Figure 151 shows BER performance of the MB-STBC for the 4 different channel cases. Despite the extreme nature of considered scenarios, the proposed code is still able to detect all transmitted constellation symbols.

It achieves a diversity order of 4 for cases 3 and 4 where half of the transmitted signal power is not received.

When concatenated with a powerful outer Forward Error Correcting (FEC) code that also exploits time and spatial diversity, the gain of the proposed STBC will depend on the actual coding rate and the amount of erasure events. Indeed, as mentioned in section 7.4.2.2, the amount of erasure events or P_e sets a bound on the FEC coding rate. If the chosen rate is larger than this bound, the FEC decoder will not achieve iterative convergence unless concatenated with the proposed STBC.

7.4.6 Conclusion

We have proposed a new multi-block space-time block code that follows a quasi-orthogonal structure and achieves a diversity order of 8 for a 2x2 MIMO system by exploiting additional time/frequency diversity. Its decoding complexity remains reasonable thanks to its structure that allows for a simplified detection. Its parameters have been optimized under several scenarios where the transmit antennas can suffer from erasure events. These scenarios are particularly interesting for a transmission over single frequency networks. The resulting code compares favorably to existing STBC codes and exhibits high robustness to erasure events.

7.5 Distributed MIMO techniques for the future broadcasting systems

In order to meet the ever-increasing demand of mobile digital television (DTV) broadcasting, the Digital Video Broadcasting (DVB) consortium started the standardization process of the Next Generation Handheld specification (DVB-NGH) [126] at the beginning of 2010. DVB-NGH will be finalized in the first half of 2012 to acquire the leading position in the future mobile DTV market.

Owing to the future extension frame (FEF) defined in DVBsecond generation Terrestrial (DVB-T2) [127], DVB-NGH can inherit many state-of-the-art transmission technologies such as low density parity check (LDPC) code, orthogonal frequencydivision multiplexing (OFDM) and, more importantly, can share the hardware as well as the frequency channel in a time division manner with the fixed DTV services. Being different from DVB-T2, the new DVB-NGH is expected to be able to deliver DTV services to the battery-powered mobile receivers efficiently, flexibly and reliably. To fulfill these requirements, DVB-NGH incorporates the multiple-input, multiple-output (MIMO) technique aiming at achieving higher throughput and improving the robustness of the mobile reception in severe broadcasting scenarios.

We investigate the application of MIMO techniques in the DTV broadcasting. We first show that the distributed MIMO scheme is the best choice among typical broadcasting scenarios from the channel capacity perspective. With this knowledge, we consequently evaluate several distributed space-time (ST) coding proposals for DVB-NGH. The performance of these STBCs is compared by simulations with DVB-NGH specifications in realistic channel conditions.

7.5.1 Broadcasting Scenarios

7.5.1.1 Channel capacity analysis

7.5.1.1.1 Single frequency network

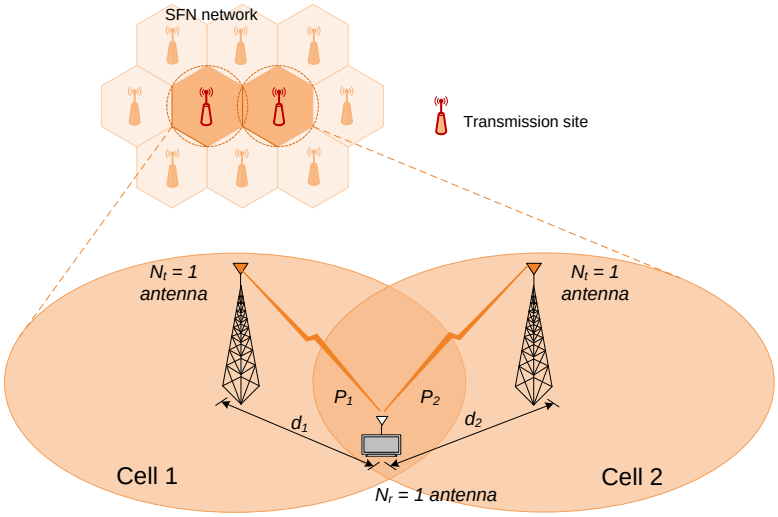

Figure 152: An example of single frequency network.

Single frequency network (SFN) is a popular and spectrally efficient network implementation in the modern digital TV broadcasting systems [132]. Several geographically separated transmitters in an SFN simultaneously transmit the same signal (TV program) in the same TV frequency band. Hence, SFN can easily achieve a large coverage without requiring extra frequency bands. a shows a simple example of an SFN with two transmission sites.

In the orthogonal frequency-division multiplexing (OFDM) based DVB system with N subcarriers, the ergodic capacity of SFN channel with two transmission sites can be computed as:

$$C_{\mathrm{SFN}} = \mathbb{E}\left\{\frac{1}{N}\sum_{k=0}^{N-1}\log_2\left(1+\frac{P}{2N\sigma_n^2}\left(\lambda_1^2|H_1(k)|^2+\lambda_2^2|H_2(k)|^2\right)\right)\right\},$$

where $H_j(k), j = 1, 2$ are the frequency response of the kth subcarrier of the channel connecting jth transmission site and the receiver; λ_1^2 and λ_2^2 are the power scale factor representing the path losses associated with the two channels, respectively; P is the overall transmission power of the two sites; σ_n^2 is the variance of the noise; $\mathbb{E}\{\cdot\}$ is the expectation value.

7.5.1.1.2 Distributed MIMO broadcasting network

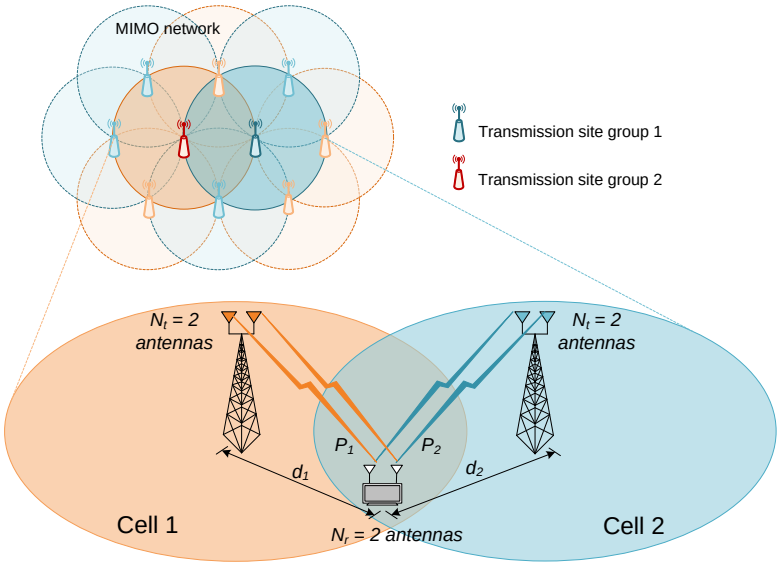

Figure 153: Distributed MIMO broadcasting network

Traditionally, MIMO is realized using several co-located transmit antennas on the same transmission site. In fact, MIMO transmission can also be implemented among multiple cooperated, geographically separated transmission sites. This yields the so-called distributed MIMO which not only extends the coverage of the services but improves the efficiency and reliability of the transmission. As shown in Figure 152, we investigate the distributed MIMO scenario where two adjacent transmission sites cooperate with each other. Each transmission site has two transmit antennas and receiver has two receive antennas as well. It is worth noting that we consider the distributed MIMO with two sites in order to limit the decoding complexity and the user cost.

Yet, the two-cell distributed MIMO structure can be easily applied in a network with larger number of transmission sites. In fact, the transmission sites of the network can be divided into two groups. The distributed MIMO designed for the two-cell case are applied to the two site groups. With proper planning of the locations of transmission sites, the broadcasting network can be easily extended to a large area. For example, one implementation of distributed MIMO network is presented in Figure 152. The geographical locations of the transmission sites are the same as in the traditional SFN, which suggests a good compatibility with the existing broadcasting networks. More precisely, this network can be implemented by simply adding a second transmit antenna on each transmission site and performing proper MIMO coding over different sites.
Since the channel information is unknown for the transmitter in the broadcasting scenarios, the channel capacity is achieved when the symbols transmitted by different antennas have same power. The ergodic capacity of the DVB system through distributed MIMO channel is expressed as:

$$C_{\mathrm{MIMO}} = \mathbb{E}\left\{\frac{1}{N}\log_2\left(\det\left(\mathbf{I} + \frac{P}{2NN_t\sigma_n^2}\sum_{j=1}^{2}\lambda_j^2\mathbf{H}_j\mathbf{H}_j^{\mathcal{H}}\right)\right)\right\},$$

where $\mathbf{H}_j = \mathrm{diag}([\mathbf{H}_j(1), \ldots \mathbf{H}_j(N)])$ is a block diagonal matrix representing the channel matrix associated with the jth transmission site; its kth element $\mathbf{H}_j(k)$ is an $N_r \times N_t$ matrix in which the (p,q)th element $H_{pq}(k)$ is the frequency response of the channel link from the qth transmit antenna to the p th receive antenna; $\det(\cdot)$ is the determinant of the matrix.

7.5.1.2 Comparison

The capacity improvements brought by the distributed MIMO over the traditional SISO SFN is evaluated with the two-cell broadcasting network implementation as shown in Figure 152. Figure 154 presents the ratios of the two channel capacities (C_{MIMO}/C_{SFN}) in different geographical locations. The two transmission sites locate in "A" and "B" positions in Figure 154. The distance between two sites is 15 km. The total transmission power *P* is 10 kW. Suppose that the signal experiences independent and identically distributed (i.i.d.) Rayleigh small-scale fading and signal power exponentially decays with respect to the distance between receiver and transmitter. The power decaying factor is chosen as 3.5 which represents the typical propagation scenario in the urban area. The channel capacities of the two broadcasting scenarios are computed according to the results given in previous sections. It can be seen that the distributed MIMO broadcasting can achieve around twice channel capacity than the traditional SFN broadcasting within the coverage of the two-cell network with the same overall transmission power. More interestingly, the improvements are more significant in the border area of the two cells, which leads to a better coverage in the edges of the cells. This example shows that the distributed MIMO broadcasting has better potential in terms of transmission efficiency.

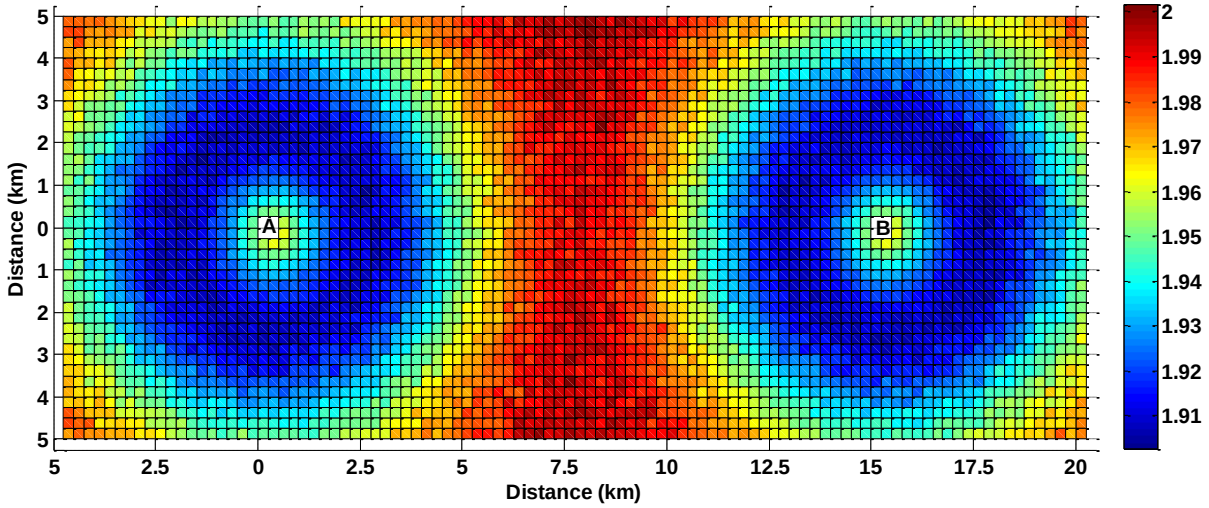

Figure 154: Capacity comparison between classical SISO-SFN scheme and a distributed MIMO-SFN strategy. The color scale gives the capacity improvement from SISO to MIMO.

7.5.2 Space-Time Coding Schemes with Four Transmit and Two Receive Antennas

It has been well known that the spatial multiplexing (SM) technique provides higher communication capacity than the traditional SISO transmission [133]. The orthogonal space-time block coding (STBC) such as Alamouti scheme can easily extract the spatial diversity by linear processing [129]. Since last decades, various STBCs [132][134][135][136][137]have been proposed for different application scenarios achieving different trade-offs among efficiency (coding rate), reliability (diversity) and orthogonality (decoding complexity).

As far as the distributed MIMO broadcasting scenario is concerned, one significant characteristic of the propagation scenario is the unequal power levels of the received signals. More specifically, signals coming from different transmission sites experience different path losses. This yields power imbalances between signals sent from different cells at the receiver side. In contrast, signals sent from the same transmission site may have the same average power level. This characteristic should be taken into account when designing a suitable STBC for distributed MIMO broadcasting.

Intuitively, the STBC can be designed in a hierarchical manner. That is, information symbols of the same cell can be encoded using a STBC scheme. This is called intra-cell ST coding. According to the propagation characteristic, the intra-cell ST coding should be efficient with balanced received signal power. Consequently, the resulting encoded symbols of different transmission sites are encoded by a second ST coding scheme, namely inter-cell ST coding. In contrast to the intra-cell counterpart, inter-cell ST scheme should be robust against signal power imbalances.

With the knowledge of the characteristics of distributed MIMO broadcasting and using the hierarchical ST encoding methodology, a so-called 3D MIMO code has been proposed for the distributed MIMO scenarios. The Golden code is selected as the intra-cell ST coding, because it is the most efficient 2×2 ST coding scheme with equal received signal power [137]. The Alamouti scheme is adopted as the inter-cell ST coding because it offers full diversity and is robust against power imbalances. The combination of Alamouti and Golden codes achieves strong adaptability to different signal power situation while preserving the transmission efficiency offered by the Golden code. The resulting 3D MIMO codeword provides a ST coding rate of 2 with high diversity.

In addition, several STBCs in the literatures can be applied in the distributed MIMO broadcasting as well. For instance, the simple SM scheme [133]can adapt to the 4×2 distributed MIMO scenarios. More specifically, two transmission sites transmit the same signals at the same time forming an SFN. For each site, two independent information symbols are transmitted via the two antennas forming a SM transmission. It yields a 4×2 distributed SM scheme with ST coding rate of 2.

The classical quasi-orthogonal Jafarkhani code [136]is also a potential candidate for the distributed MIMO broadcasting. The Alamouti scheme is applied in both intra-cell and inter-cell ST codings providing a ST coding rate of 1. The Jafarkhani code has a quasi-orthogonal structure [136]which enables group-wise decoding at a low complexity cost.

Recently, some STBCs were proposed based on the group-wise orthogonal structures aiming at providing efficient performance with low decoding complexity. For instance, the Biglieri-Hong-Viterbo (BHV) code [135]is constructed based on two Jafarkhani codewords. The underlying Jafarkhani code structure provides implicit group-wise orthogonality that enables low complexity decoding. Similarly, the Srinath-Rajan code [134]is formed by two coordinated interleaved orthogonal design (CIOD) which also yields simple decoding algorithm. Both BHV and Srinath-Rajan codes offer a ST coding rate of 2.

The most important features of the STBCs involved in the study are listed in Table 35. The decoding complexities are presented in terms of the number of possible STBC codewords visited during the sphere decoding. If the exhaustive search is used for the decoding, the maximum likelihood (ML) can be found after evaluating M^Q codewords where M is the size of the constellation and Q is the number of information symbols stacked within one STBC codeword. That is, for a given modulation order, the more information symbols in one codeword, the more difficult the decoding process. Yet, due to the embedded group-wise orthogonality, lower complexity can be expected when the sphere decoder is used. As shown in Table 35, Jafarkhani, Srinath-Rajan and BHV codes require decoding complexities of $O(M^2)$, $O(M^{4.5})$ and $O(M^7)$, instead of $O(M^4)$, $O(M^8)$ and $O(M^8)$, respectively. Moreover, these STBCs are designed with different trade-offs between efficiency and complexity. In order to know which of them are appropriate for the distributed MIMO broadcasting, it is important to compare them with the real system settings.

Table 35: STBCs for distributed MIMO broadcasting scenarios.

STBC	Rate	Structure of STBC				ST decoding complexity
		Nb. info. symb.	Nb. channel uses	Intra-cell ST coding	Inter-cell ST coding	
Jafarkhani	1	4	4	Alamouti	Alamouti	$O(M^2)$
3D MIMO	2	8	4	Golden	Alamouti	$O(M^8)$
SM 4x2	2	2	1	SM 2x2	SFN	$O(M^2)$
BHV	2	8	4	Based on 2 Jafarkhani codes		$O(M^7)$
Srinath-Rajan	2	8	4	Based on 2 CIOD codes		$O(M^{4.5})$

7.5.3 Evaluation and Performance Comparison

7.5.3.1 Simulation setups

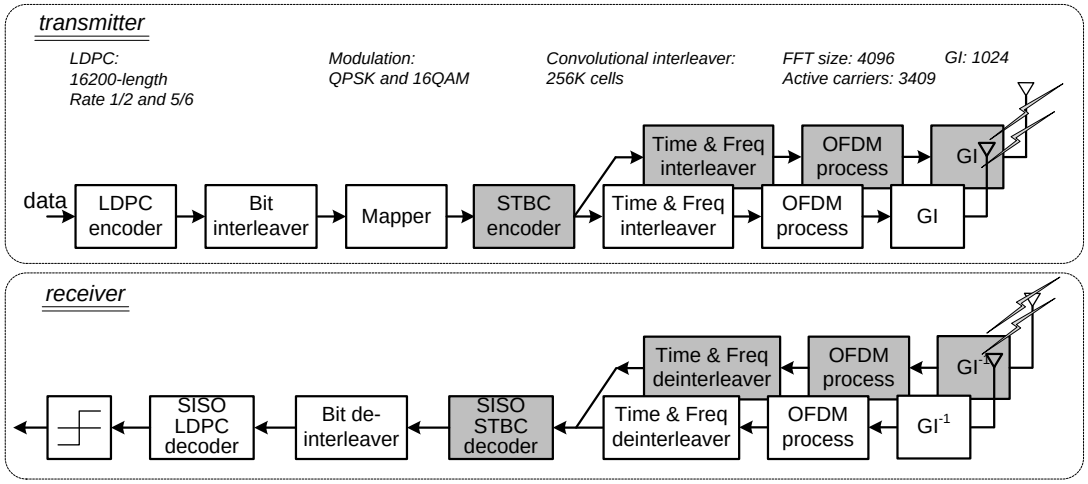

Figure 155: Generic block diagram of the DVB-NGH system. The shaded blocks are the new functionalities of DVB-NGH while others are inherited from DVB-T2.

Different STBCs are evaluated using the latest DVB-NGH specifications which is, up to now, the only TV broadcasting standard that supports MIMO transmission. The generic block diagram of the DVB-NGH system and some important simulation parameters are illustrated in Figure 154. QPSK and 16QAM are used for the rate-2 and rate-1 STBCs, respectively, in order to achieve the same spectral efficiency in the comparison. Two channel coding rates namely 1/2 and 5/6 are used in the simulation. The soft-output sphere decoder [131] is used to decode the received MIMO signal. The performance of STBCs is evaluated using the realistic DVB-NGH MIMO outdoor channel which simulates a cross-polarized 2×2 MIMO transmission in the UHF band [130]. The two-cell distributed MIMO propagation scenarios are simulated using two uncorrelated DVB-NGH 2×2 MIMO channels. Moreover, the channel coefficients related to the farther transmission site contain a time delay and power attenuations reflecting the difference of propagation distances. We assume the perfect synchronization and perfect channel information at the receiver side.

7.5.3.2 Simulation results

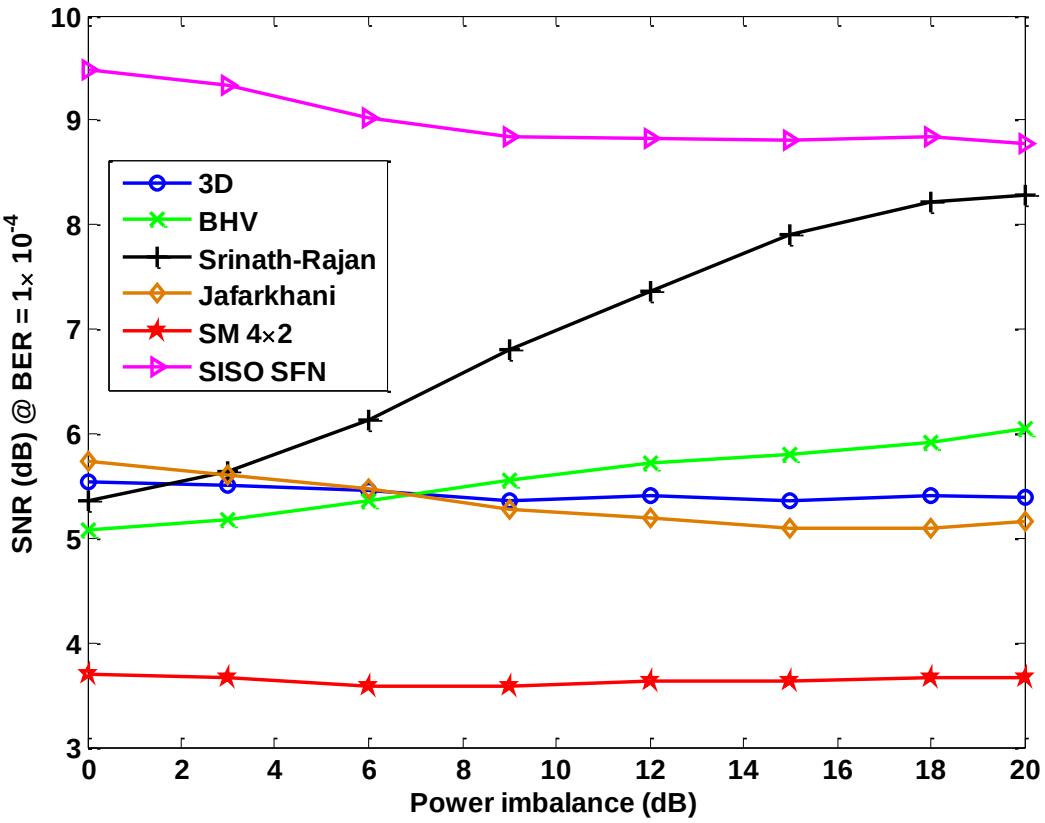

Figure 156: Required SNR to achieve the BER level of 1×10^{-4} with respect to different values of received power imbalance, LDPC rate 1/2, DVB-NGH outdoor MIMO channel, Doppler frequency 33.3 Hz.

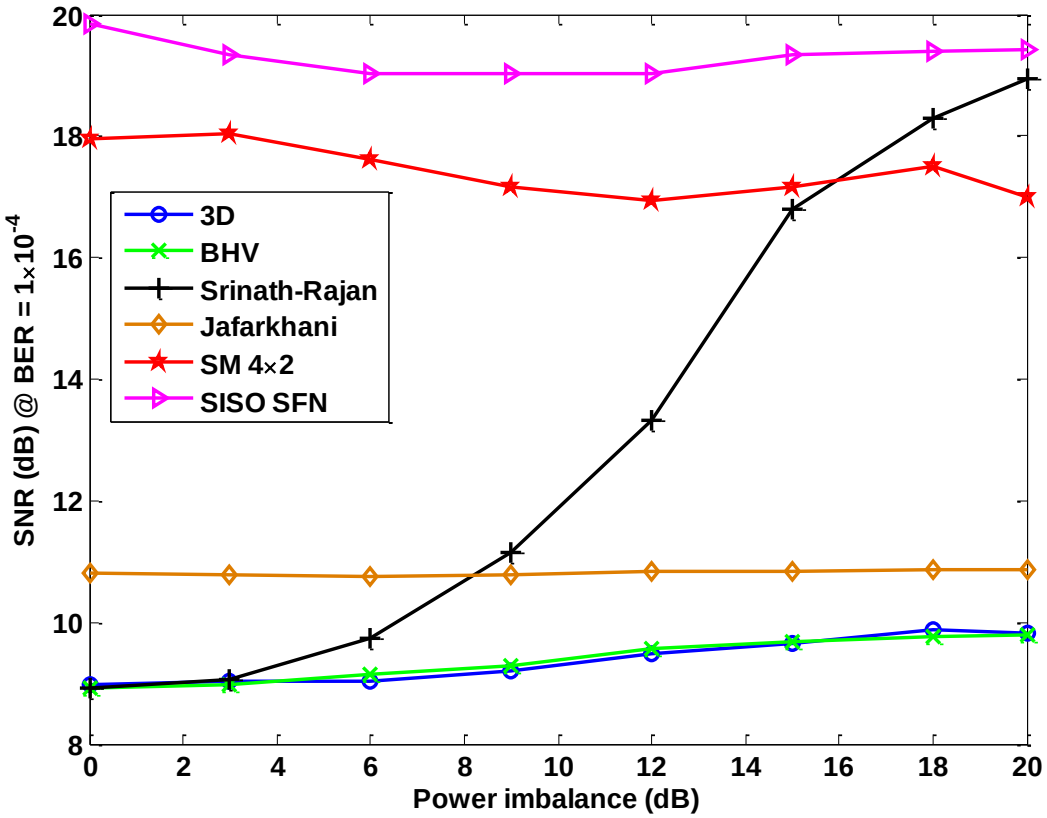

Figure 157: Required SNR to achieve the BER level of 1×10^{-4} with respect to different values of received power imbalance, LDPC rate 5/6, DVB-NGH outdoor MIMO channel, Doppler frequency 33.3 Hz

Figure 156 shows the required SNR to achieve a BER level of 1×10^{-4} with respect to different values of power imbalances. Since the power imbalance is determined by the signal path losses, this experiment suggests the performance in different geographical locations. In fact, the robustness of STBCs against power imbalances is crucial for distributed MIMO broadcasting because the broadcasters should guarantee equally good quality of service for all users within the coverage of the services no matter where they locate. The performance of the classical SISO SFN broadcasting is also given for comparison. From Figure 156, it can be seen that STBCs significantly outperform SFN with both balanced and imbalanced power. For instance, SM 4×2, 3D MIMO and Jafarkhani codes achieve 5.7 dB, 4 dB and 3.8 dB gains over SISO SFN with balanced signal power. These gains become 5 dB, 3.3dB and 3.5 dB when the power imbalance is 20 dB. Moreover, 3D MIMO, Jafarkhani and SM 4×2 codes are robust against received signal power imbalances. In contrast, Srinath-Rajan and BHV codes suffer 3 dB and 1 dB degradations compared with the balanced power case when the power imbalance level is 20 dB. Interestingly, the simple SM 4×2 code achieves the best performance among all STBCs when the strong LDPC code with rate 1/2 is used. Thanks to the strong error-correction capability of the low-rate LDPC code and long time interleaver, the LDPC decoding process can extract high time diversity and can efficiently correct the error in the received signal. Therefore, the effect of the diversity extracted by the STBCs is less significant in such case. On the other hand, accurate STBC decoding becomes more difficult when there are many information symbols stacked in one STBC codeword. Therefore, the simplest SM 4×2 code achieves best performance among all STBCs when strong forward error correction (FEC) scheme is used.

Figure 157 presents the BER performance against power imbalances with a weaker FEC configuration. LDPC with rate 5/6 is used in this experiment while other settings remain the same as the previous part.

STBCs show similar power imbalance resistance behaviors as in Figure 156. Jafarkhani, 3D MIMO, BHV and SM 4×2 codes are still robust within a wide range of power imbalances with weaker FEC. Srinath-Rajan code suffers 10 dB degradation when the power imbalance value is 20 dB compared with the balanced power case. Moreover, the SM 4×2 code is not efficient with weak FEC configuration. It is 7~9 dB worse than the sophisticated STBCs such as 3D MIMO and BHV codes. Because the diversity embedded in the STBCs is crucial for the error-correction process when a weaker FEC is adopted. It is worth noting that the better performance of the sophisticated STBCs comes along with the higher decoding complexity. More specifically, as indicated in Table 35, BHV and 3D MIMO codes require higher complexities ($O(M^7)$ and $O(M^8)$, respectively) than simple STBC such as SM 4×2 scheme.

It can be concluded from the comprehensive experiments that STBCs outperform the traditional SISO SFN in the typical broadcasting scenarios. Moreover, different STBCs have different preferred application scenarios. For example, simple STBC, i.e. SM 4×2 scheme offers satisfactory performance in combination with strong FEC configurations, namely low-rate channel coding and low-order modulations. In addition, it requires much less decoding complexity compared with other more sophisticated STBCs. Therefore, SM 4×2 scheme is suitable to deliver low data rate services for portable or mobile receptions.

On the other hand, the sophisticated STBCs such as 3D MIMO and BHV codes are suitable solutions for high date rate services, because they can be used in combination with weaker FEC configurations are used. In the contrary, simple solution such as SM 4×2 scheme is not efficient with such configurations any more. Furthermore, high rate services are commonly delivered to the fixed receivers belonging to family, business and public users. The fixed receivers can afford higher decoding complexity and power consumption than the battery-powered handheld devices. Therefore, the sophisticated STBCs are suitable solutions for high date rate services.

7.5.4 Complexity Analysis

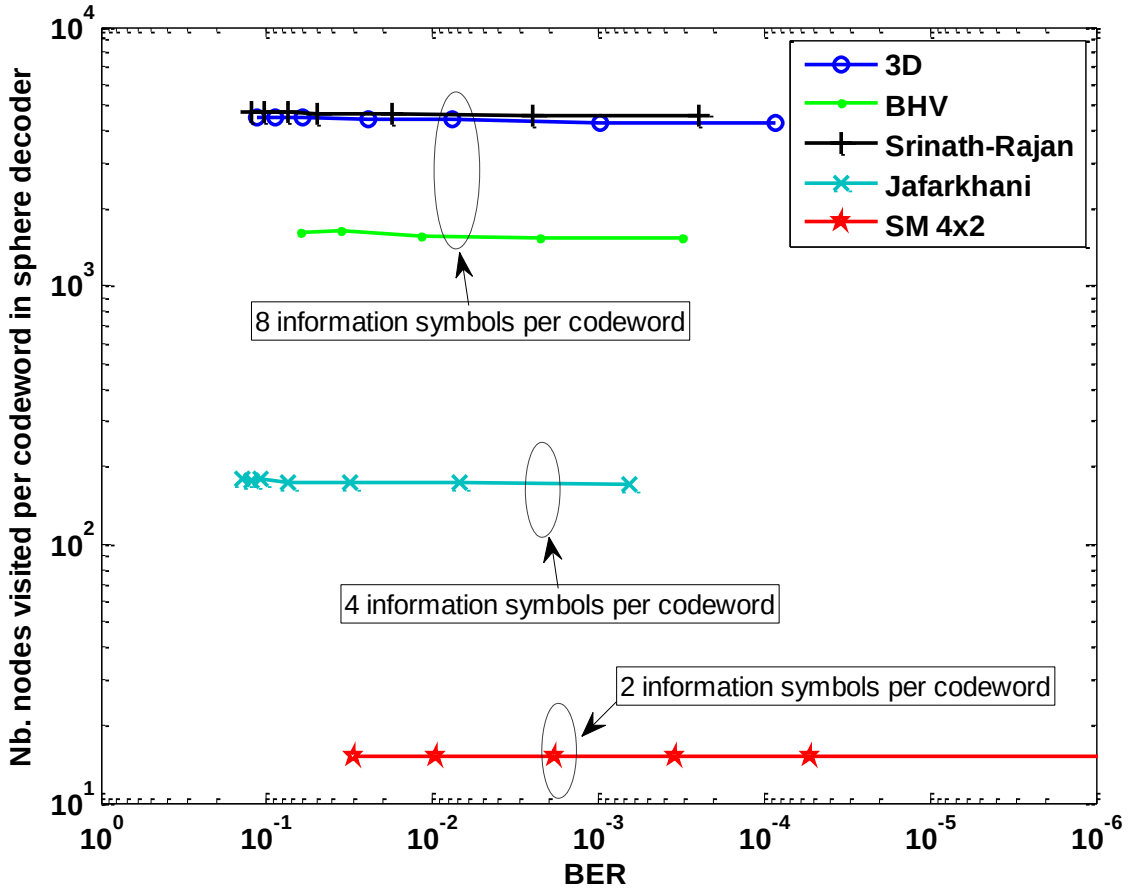

Figure 158: Complexities of the soft-output sphere decoding, LDPC rate 4/9, DVB-NGH MIMO channel with f_D=33.3Hz.

The maximum likelihood (ML) decoding finds the best solution of the received STBC codewords through an exhaustive search over all possibilities. The sphere decoding simplifies this cumbersome traversal by restricting the search space within a hypersphere centered at the received signal point. Hence, the number of codewords to be examined can be greatly reduced. Figure 158 shows the computational complexity of the sphere decoding in terms of the number of nodes (possible STBC codewords) "visited" during the search. It can be seen that the decoding complexity mainly depends on the number of information symbols that are stacked within one STBC codewords. For instance, the sphere decoder has to check about 13 possible codewords to decode each SM 4×2 codeword which contains two information symbols. This number increases to about 170 for Jafarkhani code which stacks four information symbols in a codeword. For those containing eight information symbols, the sphere decoder has to examine 1500~4500 possibilities for each codeword. The more information symbols stacked in one codeword, the more complex the decoding process. In addition, the decoding complexities are notably reduced compared with the brutal force ML search. Meanwhile, the SNR value (represented by different BER levels) does not significantly affect the decoding complexity.

7.5.5 Conclusion

In this work, distributed MIMO, a promising technique for the future TV broadcasting system, is presented. We first show that the distributed MIMO outperforms the traditional SISO SFN broadcasting network in terms of the channel capacity, which indicates that distributed MIMO has the potential to provide higher system capacity. Consequently, we investigate several STBCs that can be applied for the distributed MIMO

broadcasting scenarios. Performance of the STBCs is evaluated using the real system configurations and realistic MIMO broadcasting channel models. It can be seen that the simple STBCs are more suitable for low data-rate services while the sophisticated ones are more preferred by the high data-rate services. In general, simple and sophisticated STBCs can be applied in mutually complementary application scenarios.

8 RELAYING STUDIES FOR BROADCAST NETWORKS

Cooperative communications in wireless networks have recently been introduced as a new method to increase the throughput, the reliability and the robustness of wireless systems. Relay techniques in cooperative networks where relay nodes assist the transmission between a source and a destination have been widely explored in the literature, namely, the *decode-and-forward* [138], the *amplify-and-forward* [139] and the *compress-and-forward* [140] techniques.

Most commonly, relaying with time sharing between the source and the relay has been widely explored in the literature. However, time sharing is not an efficient solution for broadcast scenarios, i.e., it is not convenient that the base station transmits half the time and remains silent the other half. We propose two new approaches suitable for broadcast scenarios. The first approach is based on frequency sharing, where the available bandwidth is shared between the base station and the relay to achieve orthogonality at the receiver side. The second approach is a distributed coding/modulation scheme which allows at efficiently exploit the available resources (time, frequency).

The remainder of this part will be as follows. In Section 8.1, we provide coverage analysis based on achievable rates. We consider relays operating in both half-duplex and full-duplex modes. In Section 8.2, we present a distributed coding scheme suitable for broadcast scenarios with OFDM based transmission under the half-duplex constraint (frequency sharing). In Section 8.3, we present a new relaying strategy for full-duplex mode called decode-rotate-and-forward based on constellation rotation at the relay. The latter coding scheme has been filed as a patent and the application is under process.

8.1 Coverage Extension through Cooperative Relaying

Radio signals traveling from the transmitter antenna to the receiver antenna exhibit attenuation due to the natural diffusion of the signal, absorption and diffraction phenomena. This attenuation called path-loss is generally assumed proportional to at least the square of the distance between the transmitter and the receiver. In wireless infrastructures, receivers can exhibit severe attenuation which results in low throughput, poor coverage and reliability. Enhanced capacity and extended coverage are among the desired requirements for wireless communication systems. Relaying offers a promising solution to improve reliability, achieve higher throughput or provide coverage extension. In this work, we investigate the effect of fixed relay deployment on coverage in a wireless infrastructure.

8.1.1 Coverage Analysis for the Decode-and-Forward Strategy

For coverage study, as for outage analysis, we fix a target rate and seek to maximize the geographic region outside which an outage occurs. We compute the coverage area for the cooperative relay network.

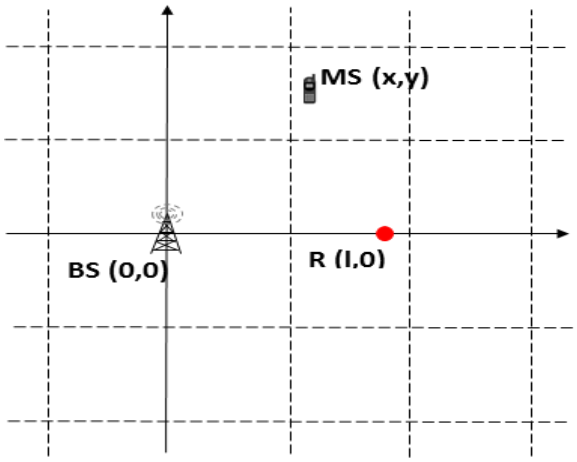

Figure 159: Representation of the wireless relay network in two-dimension model

We consider the wireless relay network in two dimensions as depicted in Figure 159. Without loss of generality, downlink transmission is considered in this work. A base station *BS* communicates data to a mobile station *MS* cooperating through a relay *R*. The relay is fixed and its location is given by coordinates $(l, 0)$, the coordinates of the base station are set to $(0,0)$ and the mobile station location is given by coordinates (x, y). This two-dimension model allows to assess the performance of relay transmission under realistic deployment scenarios. The base station transmits with power P_{BS} and the relay with power P_R. We further assume that the relay is at best as powerful as the base station, i.e. $P_R \leq P_{BS}$.
We denote by $l_{BS,MS}$ the link between the base station and the mobile station, $l_{BS,R}$ the link between the base station and the relay, and $l_{R,MS}$ the link between the relay and the mobile station and we denote by $\gamma_{BS,MS}$, $\gamma_{BS,R}$ and $\gamma_{R,MS}$ the signal-to-noise ratio in dB of the base station-to-mobile station channel, the base station-to-relay channel, and the relay-to-mobile station channel, respectively. Likewise, we denote by $d_{BS,MS}=\sqrt{x^2+y^2}$, $d_{BS,R}=l$ and $d_{R,MS}=\sqrt{(x-l)^2+y^2}$ the distance from *BS* to *MS*, from *BS* to *R*, and from *R* to *MS*, respectively. The channels are modeled as additive white Gaussian noise (AWGN) channels with path loss attenuation. The mean power of the signals decreases with distance d as $d^{-\alpha}$, where α denotes the path-loss exponent and it is often assumed to be $2 \leq \alpha \leq 6$. For propagation in free space, the path-loss exponent α is assumed to be 2. For lossy environments, α can be in the range of 4. The path-loss exponent is assumed to be constant over the two dimensional plane. Therefore, $\gamma_{BS,R}$ is given by

$$\gamma_{BS,MS} = \frac{P_{BS}}{d_{BS,MS}^{\alpha} N} \qquad (1)$$

where *N* denotes the noise power. Similar expressions are obtained for $\gamma_{BS,R}$ and $\gamma_{R,MS}$.

Let $R > 0$ denote a desired transmission rate. We denote by G the coverage region. For direct transmission where a base station transmits without the help of the relay, the coverage region is given by

$$G(d_{BS,MS}) = \{d_{BS,MS} : C(d_{BS,MS}) \geq R)\} \qquad (2)$$

where *C* denotes the capacity of the direct link.
In the two dimensional plane, this is equivalent to find coordinates (x, y) which verify (2). By solving (2), we have that the mobile station is out of coverage if

$$d_{BS,MS} > \left(\frac{P_{BS}}{N(2^R - 1)}\right)^{\frac{1}{\alpha}} \quad (3)$$

8.1.2 Coverage Extension with Half-Duplex Mode

For the cooperative scheme, we recall that the achievable rate R' for the decode-and-forward strategy with relay operating in half-duplex mode [141] is given by

$$R' = \min\left\{\frac{1}{2}\log(1 + \frac{P_{BS}}{Nd_{BS,R}^{\alpha}}), \frac{1}{2}\log(1 + \frac{P_{BS}}{Nd_{BS,MS}^{\alpha}}) + \frac{1}{2}\log(1 + \frac{P_R}{Nd_{R,MS}^{\alpha}})\right\} \quad (4)$$

As described in Section 8.1.1, the relay position is fixed at distance l from the base station. l is chosen such that it verifies

$$l \leq \left(\frac{P_{BS}}{N(2^{2R} - 1)}\right)^{\frac{1}{\alpha}} \quad (5)$$

If l verifies (5), the relay is still able to decode the information transmitted by the base station.

For a fixed distance l between the source and the relay, we define the coverage region as

$$\mathrm{G}(l) = \{d_{BS,MS}: R'(d_{BS,MS}, l) \geq R)\} \quad (6)$$

This is equivalent to find the pair (x, y) which verifies

$$\frac{1}{2}\log(1 + \frac{P_{BS}}{N(x^2 + y^2)^{\frac{\alpha}{2}}}) + \frac{1}{2}\log(1 + \frac{P_R}{N((x - l)^2 + y^2)^{\frac{\alpha}{2}}}) \leq \mathrm{R} \quad (7)$$

In Figure 160, we plot the coverage area for both direct transmission and cooperative transmission. Here, we consider $R=1/2$, $P_{BS}/N=P_R/N=2$ dB and a path-loss exponent $\alpha = 3.52$.
As shown in Figure 160, the coverage is extended especially at the side where the relay is located. However, a loss in the coverage is observed with respect to direct transmission in some regions. This is due to the half-duplex constraint, i.e. the available resource is shared between the base station and the relay.

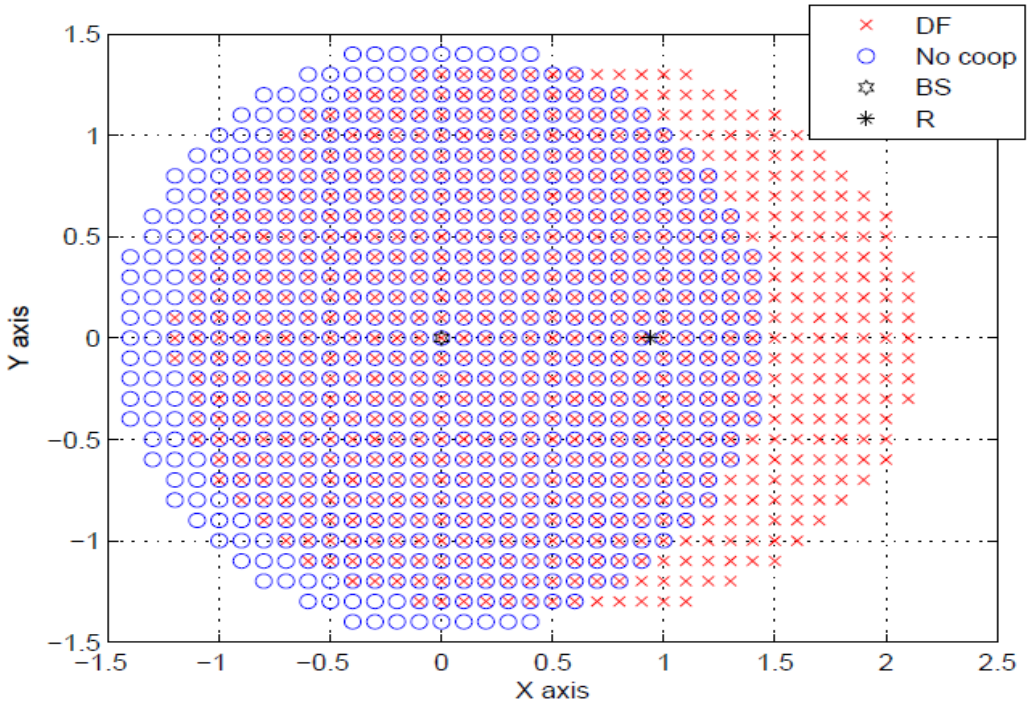

Figure 160: Coverage area of the base station for both direct and cooperative half-duplex relay transmission. R=1/2, PBS/N=PR/N=2 dB and α=3.52.

8.1.3 Coverage Extension with Full-Duplex Relay

The coverage study for the full-duplex relay scenario remains valid. The achievable rate of decode-and-forward relaying scheme is given by

$$R' = \min\left\{\log(1+\frac{P_{BS}}{Nd_{BS,R}^{\alpha}}), \log(1+\frac{P_{BS}}{Nd_{BS,MS}^{\alpha}}+\frac{P_R}{Nd_{R,MS}^{\alpha}})\right\} \quad (8)$$

The relay position l is chosen such that it verifies

$$l \leq \left(\frac{P_{BS}}{N(2^{2R}-1)}\right)^{\frac{1}{\alpha}} \quad (9)$$

and the coverage area for a given distance l is obtained by finding the coordinates (x, y) which verify

$$\log(1+\frac{P_{BS}}{Nd_{BS,MS}^{\alpha}}+\frac{P_R}{Nd_{R,MS}^{\alpha}}) \leq \mathrm{R} \quad (10)$$

In Figure 161, we plot the coverage area of the base station with and without the full-duplex relay cooperation. We assume a rate $R=1/2$, $P_{BS}/N=P_R/N=2$ dB and a path-loss exponent $\alpha=3.52$.

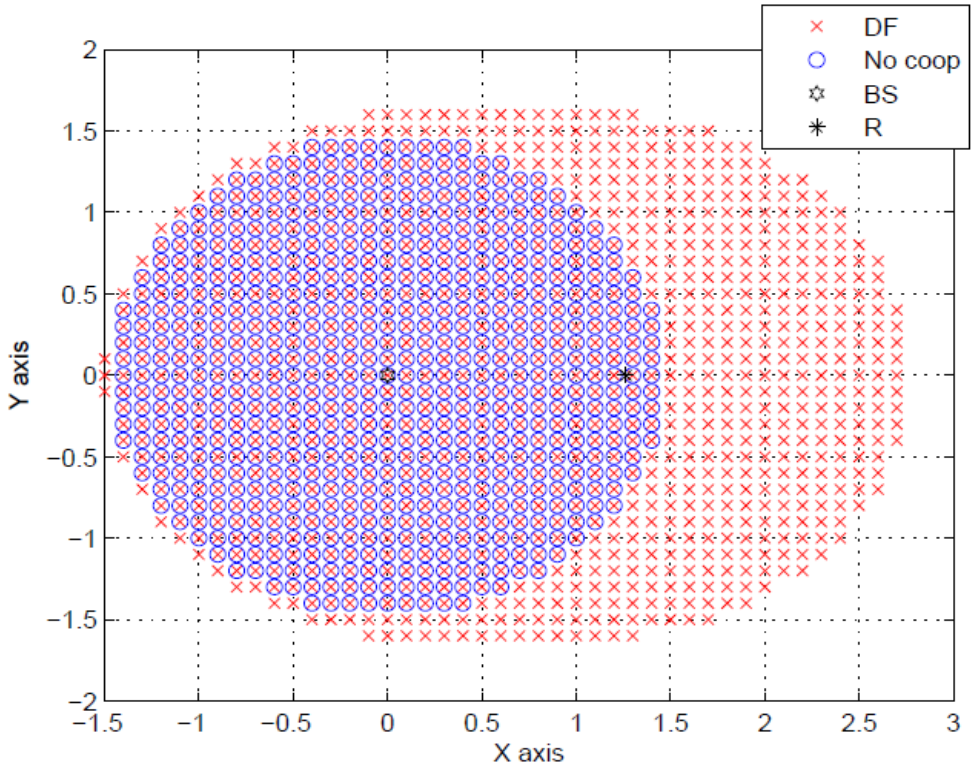

Figure 161: Coverage area of the base station for both direct and cooperative full-duplex relay transmission. R=1/2, PBS/N=PR/N=2 dB and α=3.52.

Unlike the half-duplex case, the coverage is always extended compared to direct transmission. While full-duplex relaying outperforms half-duplex relaying in terms of coverage, full-duplex scenario requires additional complexity at the receiver since signals from both base station and relay are received simultaneously and also at the relay to tackle potential interference between the relay transmitting and receiving antennas [142]. The choice between half-duplex and full-duplex relaying should be made in a compromise between coverage extension and complexity. In the next sections, we propose distributed coding schemes with relay operating in both half-duplex and full-duplex modes.

8.2 Distributed Coding for OFDM-Based Transmission in Cooperative Broadcast Networks

8.2.1 System Description

We consider the wireless relay network depicted in Figure 159. We consider an OFDM transmission waveform where the available bandwidth is divided into N_{FFT} subcarriers. N_{BS} subcarriers are allocated to the base station transmission and N_R subcarriers to the relay with $N_{FFT}=N_{BS}+N_R$.

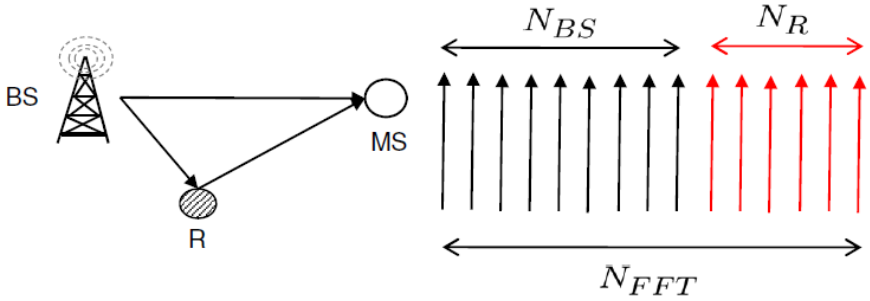

Figure 162: A wireless relay network: a base station broadcasts to a mobile station with the help of a relay.

At the base station *BS*, the information sequence $\boldsymbol{u}_{BS}$, of length k_{BS} bits, is encoded by encoder $\mathcal{C}_{BS}$ of rate R_{BS} into codeword $\boldsymbol{c}_{BS}$ of length $n_{BS}=k_{BS}/R_{BS}$ bits. Codeword $\boldsymbol{c}_{BS}$ is modulated and then mapped onto OFDM symbol $\boldsymbol{x}_{BS}$ with N_{BS} subcarriers and then transmitted over a wireless channel. Here, we use the binary phase shift keying (BPSK) modulation; however, our scheme can be extended to higher order modulations. The transmitter at the base station is depicted in Figure 163. Due to the broadcast nature of the wireless channel, the relay receives a noisy version of symbol $\boldsymbol{x}_{BS}$, denoted by $\boldsymbol{y}_{BS,R}$, from the base station *BS*. It then cooperates with the base station *BS* by transmitting its own parity sequence $\boldsymbol{x}_R$ to the mobile station *MS*. The mobile station decodes the information of the base station by jointly exploiting the received sequence $\boldsymbol{y}_{BS,MS}$ from the base station and the sequence $\boldsymbol{y}_{R,MS}$ from the relay.

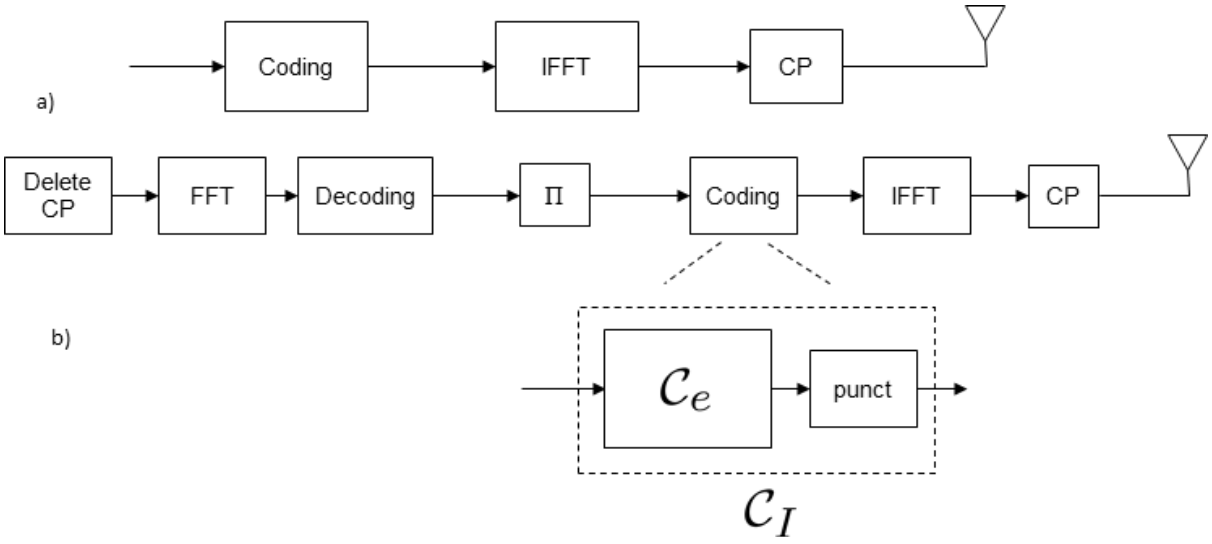

Figure 163: a) The transmitter at the base station. b) The receiver and the transmitter at the relay node.

Based on the two observations $\boldsymbol{y}_{BS,MS}$ and $\boldsymbol{y}_{R,MS}$ from the base station and the relay, respectively, an iterative decoding is performed at the mobile station.

The proposed relaying scheme can be regarded to as a *decode-and-forward* scheme. The relay receives a noisy version of symbol $\boldsymbol{x}_{BS}$ from the base station, it decodes it, and generates an estimate of codeword $\boldsymbol{c}_{BS}$. The estimated bits are then interleaved by an interleaver Π. The bits at the output of the interleaver are encoded by a recursive inner encoder $\mathcal{C}_e$ of rate R_e punctured to rate $R_I=R_e/\rho$ through a puncturer. ρ denotes the permeability ratio of the puncturer, giving the ratio of bits that survive puncturing. Parameter ρ determines the amount of redundancy transmitted by the relay and can be adjusted according to requirements

in terms of performance, throughput and/or power. The resulting codeword is then modulated by BPSK modulation and mapped onto OFDM symbol $\boldsymbol{x}_R$ with N_R subcarriers and transmitted to the mobile station.

The subcarriers can be optimally allocated between the base station and the relay in order to achieve higher rates [143]. Furthermore, the coding/decoding scheme can be extended to scenarios where multiple relays aid the communication from the base station to the mobile station. If successful decoding is achieved at the relays, the relays process the received signal according to the encoding strategy described above and SFN-like transmission at the relays, i.e., the relays are allocated the same subcarriers N_R in order to efficiently exploit the radio spectrum [143].

8.2.2 Numerical Results

The performance of the proposed scheme is evaluated through simulations. The 4-state, rate-1/2, recursive convolutional encoder with generator polynomials *(1,5/7)* in octal form is used at the base station. The *4*-state, rate-*1*, recursive convolutional encoder with generator polynomial *(5/7)* is used at the relay.
In Figure 164 we give bit error rate (BER) results of the proposed scheme for block length $k_{BS}=1024$ bits over a Rayleigh fast fading channel as a function of $\gamma_{BS,MS}$. An S-random interleaver and a maximum of ten decoding iterations were considered. We also assumed that $d_{BS,R}=(1/4)d_{BS,MS}$ and $d_{R,MS}=(3/4)d_{BS,MS}$.
A total number of $N_{FFT}=4096$ subcarriers is considered. $N_{BS}=2048$ subcarriers and parameter ρ is set so that $N_R=2048$ subcarriers. Therefore, the effective global rate of the overall system $R_{eff}=1/4$. For comparison purposes, we also consider the non-cooperation scenario where the base station transmits to the mobile station without the help of the relay.
For fair comparison, we plot the non-cooperative curve assuming that the base station transmits with a rate *1/4* which corresponds to the effective rate of the cooperative system. We consider the use of convolutional codes (CCs) and turbo codes (TCs) at the base station. The proposed distributed turbo-like code shows a significant gain with respect to the non-cooperation scenario. It also outperforms the non-cooperation scheme where a turbo code is used at the base station.
We also consider a scenario where the transmission from the base station to the mobile station is assisted by a *gap filler* which simply amplifies the received signal from the base station and forwards it to the mobile station. The proposed cooperative scheme presents better performance in terms of error rate compared to the *gap filler* scenario. The observed gain is due to the iterative decoding process in the proposed scheme.

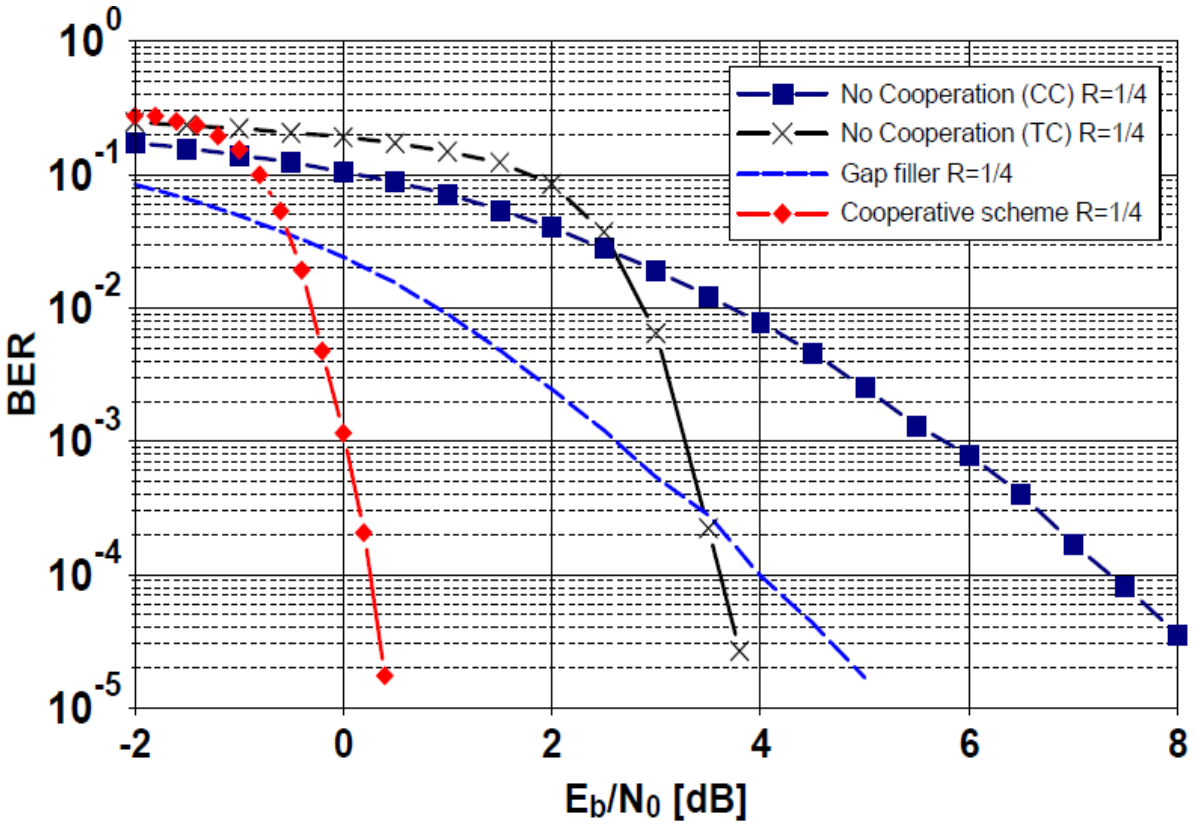

Figure 164: BER curves of the non-cooperative system and the turbo-like coding scheme over Rayleigh fast fading channel. kBS=1024 bits, NFFT=4096 subcarriers, Reff=1/4, 10 iterations. The dashed curve corresponds to a broadcast scenario employing gap

8.3 A New Decode-Rotate-and-Forward Strategy for Cooperative Relay Networks

8.3.1 System Description

We propose a new relaying strategy, called *decode-rotate-and-forward* for wireless relay networks. We consider a scenario where a source communicates with a destination with the help of a relay. The source and the relay are allowed to transmit simultaneously.

We consider a full-duplex relay, i.e., the relay is allowed to transmit and receive simultaneously.

We consider the wireless relay network depicted in Figure 165. The network consists of a source *S* which communicates statistically independent data to a single destination *D* cooperating through a relay *R*.

Except for the first transmission, the source and the relay transmit simultaneously. At source *S*, the information sequence $\boldsymbol{u}_s$, of length *k* bits, is encoded by encoder C_s of rate R_s into codeword $\boldsymbol{c}_s$. Codeword $\boldsymbol{c}_s$ is then modulated into $\boldsymbol{x}_s$ and transmitted over a wireless channel. For simplicity, we first consider BPSK modulation.

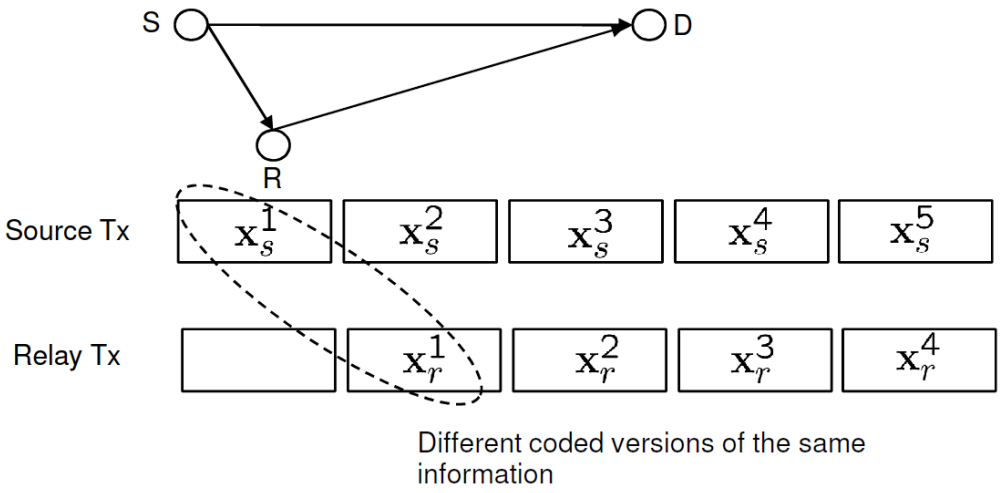

Figure 165: Simultaneous transmission: the source and the relay transmit simultaneously; the relay forwards a coded version of the data source of the previous slot.

Due to the broadcast nature of the wireless channel the relay receives a noisy version of codewords $\boldsymbol{c}_s$, denoted by $\boldsymbol{y}_{s,r}$, from the source. During the same time slot, the relay transmits a new version $\boldsymbol{x}_r$ of the source data received in the previous slot. The destination receives the signals from the source and the relay simultaneously and decodes the information of the source by jointly exploiting the received sequence $\boldsymbol{y}_d$ from the source and the relay simultaneously. The transmission scheduling is illustrated Figure 165.

The relay receives a noisy version of codewords $\boldsymbol{c}_s$ from the source, it decodes it, and generates an estimate of the information bits $\boldsymbol{u}_s$. The estimated sequence $\hat{\boldsymbol{u}}_s$ is then interleaved into $\tilde{\boldsymbol{u}}_s$ by an interleaver Π, and re-encoded by another encoder C_r into codeword $\boldsymbol{c}_r$. Codeword $\boldsymbol{c}_r$ is then modulated into $\boldsymbol{x}_r$ using BPSK modulation rotated by an angle φ. Here, we consider a rotation angle $\varphi=90°$. The proposed distributed coding scheme is depicted in Figure 166.

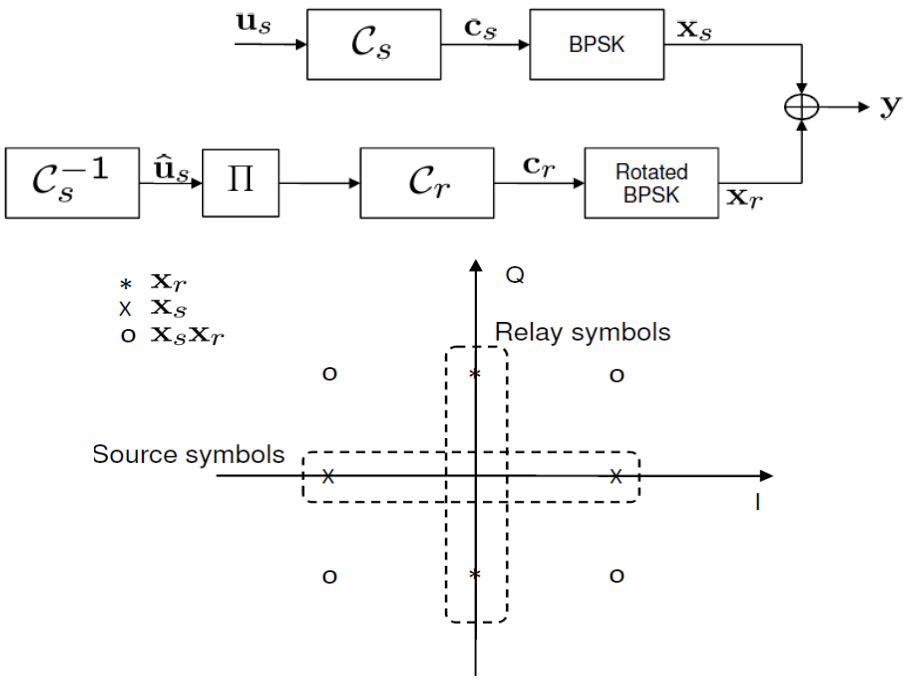

Figure 166: Block diagram of the proposed decode-rotate-and-forward strategy: Encodings at the source and the relay. Equivalent distributed constellation between the source and the relay.

The modulation used in the proposed scheme can be seen as a distributed higher order modulation between the source and the relay (here, the resulting higher order modulation is a QPSK modulation) where the BPSK modulation at the source accounts for modulation on the I axis (Inphase axis) of the QPSK modulation and the BPSK modulation at the relay accounts for modulation on the Q axis (Quadrature axis). The equivalent distributed constellation is depicted in Figure 166.

At the destination *D*, a higher order demodulator is used to jointly demodulate the received sequence $\boldsymbol{y}_d$ and generate the channels log-likelihood ratios (LLRs) LLR($\boldsymbol{x}_s$) and LLR($\boldsymbol{x}_r$). Here, since BPSK modulation is used at the source and the relay, a QPSK demodulator is considered. LLR($\boldsymbol{x}_s$) and LLR($\boldsymbol{x}_r$) are then passed to decoders $\mathcal{C}^{-1}{}_s$ and $\mathcal{C}^{-1}{}_r$ of the source code and the relay code, respectively. Decoding of the source information is performed in the classic way of a distributed turbo code [139], i.e., in an iterative fashion by exploiting the additional redundancy provided by the relay.

This work has recently been filed as a patent and is currently under review at the National Institute of Intellectual Properties (INPI France).

8.3.2 Numerical Results

The performance of the proposed scheme is evaluated through simulations. For simplicity, the *4*-state, rate-*1/2*, recursive convolutional encoder with generator polynomial $(1,5/7)_8$ is used at the source and the relay. However, different constituent encoders at the sources and the relay can be considered. An S-random interleaver Π and a maximum of ten decoding iterations are assumed.

For comparison purposes, we also consider the non-cooperation scenario where a source transmits to the destination without the help of the relay. For fair comparison, we consider that the source uses an encoder rate *R=1/4* and QPSK modulation in order to be at the same spectral efficiency of our proposed scheme.

In Figure 167, we give BER results for the proposed decode-rotate-and-forward scheme over AWGN channels as a function of γ_{sd} and a block length *k=128* bits. We also assume that $d_{rd}=d_{sd}$ and we assume that

the source-to-relay link is reliable enough to guarantee a low error probability at the relay which is a necessary condition for the *decode-and-forward* strategy [141], and therefore for the new *decode-rotate-and-forward* strategy. In Figure 167, BPSK modulation is used at the source and a rotated BPSK of angle $\varphi=90°$ is used at the relay. The resulting constellation is a QPSK constellation as described in Section 8.3.1.

The proposed distributed coding/modulation scheme shows a significant gain with respect to the non-cooperation scenario. For instance, a gain of almost 3 dB is observed at BER=10^{-3} compared to direct transmission. Moreover, it allows at efficiently exploiting the radio channel and achieves higher spectral efficiency compared to schemes time or frequency sharing transmission.

8.4 Conclusions

In this work, we provide coverage analysis for cooperative relays networks based on achievable rates. We also proposed a distributed turbo-like coding scheme for a wireless relay network based OFDM in a broadcast scenario where a base station transmits to a mobile station with the help of one or more relays. The proposed scheme achieves a significant gain with respect to the non-cooperation case and it also outperforms gap filler scenarios traditionally used in broadcast systems.

We, further, proposed a new relaying strategy, *decode-rotate-and-forward*, for a wireless relay network where a source transmits to a destination with the help of a relay where the source and the relay are allocated the same transmission time and transmit in the same bandwidth. The proposed scheme achieves a significant gain with respect to the non-cooperation case in terms of error rate. Moreover, it allows to efficiently exploit the channel resources and to achieve higher spectral efficiency compared to schemes where the transmission time is shared between the source and the relay. Furthermore, it is flexible in terms of the modulation order choice used at the source and the relay and the extension to multiple relays is straightforward.

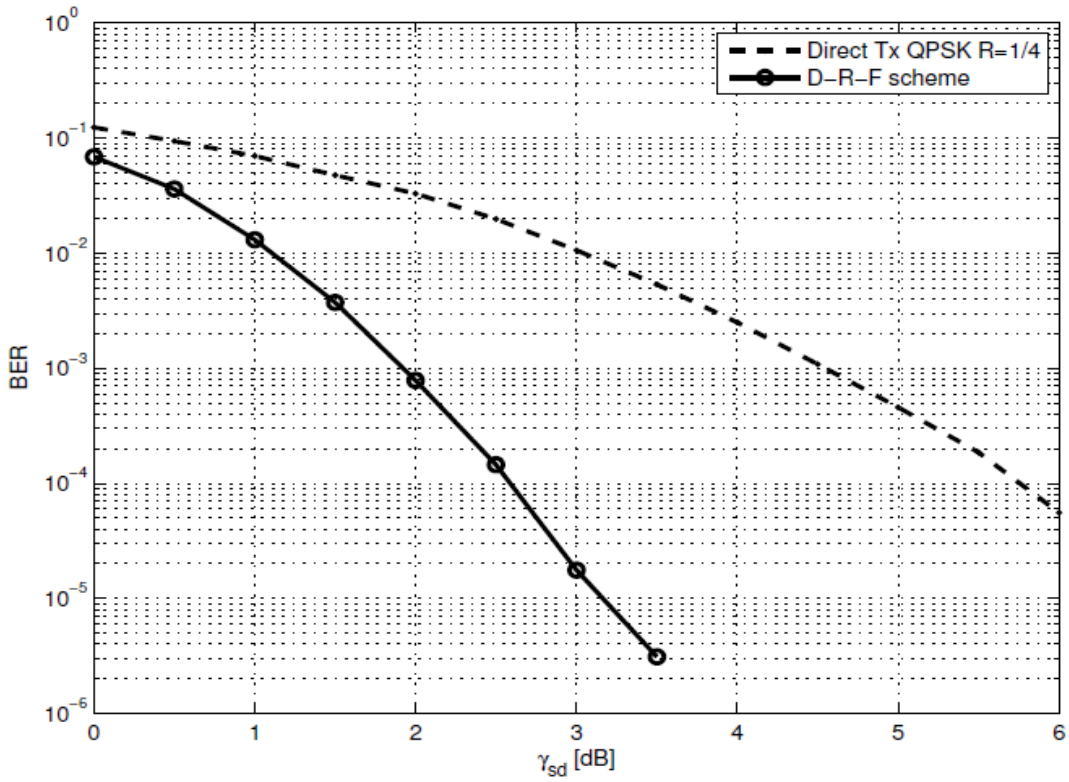

Figure 167: BER curves for the decode-rotate-and-forward (φ=90°) scheme over AWGN channels. ks=128 bits, BPSK modulation, 10 iterations.

9 SUMMARY

This deliverable is dedicated to the presenting studies related to advanced component techniques that have been devised or refined in order to solve fundamental issues for reaching required capacity and performance for DVB-NGH. Vast amount of work performed within ENGINES project has been directed to DVB-NGH standardization. Therefore some of the mechanisms presented here have been adopted to the nearly finished DVB-NGH physical layer specification.

Studies on Forward Error Correction (FEC) coding techniques and constellations for data and signalling were presented. Both LDPC and turbo codes were investigated together with Base Band interframe FEC (BB-iFEC) mechanism. The application of rotated constellations was investigated. Further, contributions of the project on optimisation of channel interleaving mechanism and scheduling were considered.

OFDM-OQAM modulation which is particularly efficient against frequency distortions such as Doppler Effect was studied. Performance comparison of PAPR reduction techniques for DVB-NGH was presented. Further, a study on the optimization of the channel estimation pilots, used jointly for PAPR reduction process was performed.

Analysis of Time-Frequency Slicing (TFS) adopted for DVB-NGH was presented. TFS mechanism and its feasibility and requirements were considered.

Multiple antenna technique studies and their outcomes were presented. Space Time (Frequency) codes presented for the DVB-NGH were presented together with performance studies. Further, distributed MIMO schemes are considered.

Finally a study on relaying on broadcasting networks was presented. Cooperative communications in wireless networks have recently been introduced as a new method to increase the throughput, the reliability and the robustness of wireless systems.

10 REFERENCES

[1] Digital Video Broadcasting (DVB) TM-H NGH, Call for Technologies (CfT), v 1.0 19, November 2009, available at http://www.dvb.org/technology/dvb-ngh/DVB-NGH-Call-for-Technologies.doc.

[2] Digital Video Broadcasting (DVB), Framing Structure, channel coding and modulation for satellite services to handheld devices (SH) below 3 GHz, ETSI EN 302 583, v 1.2.1, Dec. 2011.

[3] Digital Video Broadcasting (DVB), Frame structure channel coding and modulation for a second generation digital terrestrial television broadcasting system (DVB-T2), ETSI EN 302 755, v1.3.1, Oct. 2011.

[4] Digital Video Broadcasting (DVB) CM-NGH, Commercial Requirements for DVB-NGH, v 1.01, June 2009, available at http://www.dvb.org/technology/dvb-ngh/DVB-NGH-Commercial-Requirements.pdf.

[5] A. Guillén i Fàbregas, A. Martinez and G. Caire , Bit-Interleaved Coded Modulation, Foundations and Trends in Communications and Information Theory, Vol. 5, No 1-2, pp 1-153, Now publishers, 2008.

[6] M. Eroz, F.-W. Sun, and L.-N. Lee, "An innovative low-density parity-check code design with near-shannon-limit performance and simple implementation," IEEE Trans. Commun., vol. 54, no 1, pp. 13–17, Jan. 2006.

[7] H. Jin, A. Khandekar, and R.J. McEliece, "Irregular Repeat–Accumulate Codes," in Proc. 2nd Int'l Symp. on Turbo Codes and Related Topics, pp. 1-8, Brest, France, Sept. 2000.

[8] G. D. Forney Jr. and L.-F. Wei, "Multidimensional constellations – Part I: Introduction, figures of merit and generalized cross constellations," IEEE Journal on Select. Areas in Commun., vol. 1, no 6, Aug. 1989.

[9] M. Makni, J. Robert and E. Stare, "Performance analysis of time frequency slicing," 14th ITG Conf. on Electronic Media Technology (CEMT), pp. 1-6, Dortmund, Germany, March 2011.
[10] C. E. Shannon, "Communication in the presence of noise," Proc. Institute of Radio Engineers, vol. 37 (1): pp. 10–21, Jan. 1949.
[11] Digital Video Broadcasting (DVB), Frame structure channel coding and modulation for a second generation digital terrestrial television broadcasting system (DVB-T2), ETSI EN 302 755, v1.3.1, 2011.
[12] C. Berrou, Y. Saouter, C. Douillard, S. Kerouédan and M. Jézéquel, "Designing good permutations for turbo codes: towards a single model," *Proc. of ICC'04*, Paris, France, June 2004.
[13] Y. Saouter, "Selection procedure of turbocode parameters by combinatorial optimization," Proc. *Int'l Symp. on Turbo Codes and Iterative Information Processing*, Brest, France, Sept. 2010.
[14] F. Kienle, N. When and H. Meyr, "On complexity, energy- and implementation-efficiency of channel decoders," submitted to *IEEE Trans. Commun.* in March 2010. Download at http://ems.eit.uni-kl.de/uploads/tx_uniklwehn/ARXIV_Efficiency_Channel_Decoders.pdf.
[15] TM-NGH 795, "Continuous_N_periodic_L1_sul", Jan Zöllner.
[16] TM-NGH 866, "L1-Pre performance with NGH signaling PLP", Jan Zöllner.
[17] TM-NGH 843, "Reduced overhead for L1-config and L1-dynamic" Erik Stare.
[18] TM-NGH 875, "L1 Signalling Optimization", Ismael Gutiérrez.
[19] J. Zöllner, "Further Considerations on n-periodic Transmission of L1-pre and L1-config", 17.05.2011
[20] D. Gómez-Barquero, P. F. Gómez, D. Gozálvez, B. Sayadi, and L. Roullet, "BB-iFEC for Next Generation Handheld DVB-NGH," *Proc. Of IEEE BMSB*, Erlangen, Germany, 2011.
[21] F. Pérez-Fontán, *et al*., "Statistical modelling of the LMS channel," *IEEE Trans. on Vehicular Technology*, vol.50, no. 6, pp. 1549-1567, 2001.
[22] D. Gómez-Barquero, D. Gozálvez and N. Cardona, "Application layer FEC for mobile TV delivery in IP datacast over DVB-H Systems," *IEEE Trans. on Broadcasting*, vol. 55, no. 2, pp. 396-406, 2009.
[23] D. Gómez-Barquero, P. Unger, T. Kurner, and N. Cardona, "Coverage estimation for multi-burst FEC mobile TV services in DVB-H systems," *IEEE Trans. on Vehicular Technology*, vol. 59, no. 7, pp. 3491-3500, 2010.
[24] M. A. Ismail, W. Dabbous, and A. Clerget, "A multi-burst sliding encoding for mobile satellite TV broadcasting," *Proc. IEEE INFOCOM*, Rio de Janeiro, Brasil, 2009
[25] B. Sayadi, Y. Leprovost, S. Kerboeuf, M. L. Alberi-Morel, and L. Roullet, "MPE-iFEC: an enhanced burst error protection for DVB-SH systems," *Bell Labs Technical Journal*, vol. 14, no. 1, pp. 25-40, 2009.
[26] ETSI TS 102 772 v1.1.1, "Multi-Protocol Encapsulation – inter-burst Forward Error Correction (MPE-iFEC)," 2010.
[27] ETSI TS 102 584 v1.2.1, "Guidelines for the Implementation for Satellite Services to Handheld devices (SH) below 3GHz," 2011.
[28] C. Abdel Nour and C. Douillard, "Rotated QAM Constellations to Improve BICM Performance for DVB-T2*," Proc. IEEE ISSSTA*, Bologna.
[29] ETSI EN 302 755 v1.2.1, "Frame Structure Channel Coding and Modulation for a Second Generation Digital Terrestrial Television Broadcasting System (DVB-T2)," 2011.
[30] ETSI draft TR 102 831 v0.10.4, "Implementation Guidelines for a Second Generation Digital Terrestrial Television Broadcasting System (DVB-T2)," 2010.
[31] DVB Document, "Commercial Requirements for DVB-NGH," 2009.
[32] M.-L. Alberi, S. Kerboeuf, B. Sayadi, Y. Leprovost, and F. Faucheux, "Performance Evaluation of Channel Change for DVB-SH Streaming Services," *Proc. IEEE ICC*, Cape Town, South Africa, 2010.
[33] ETSI TS 102 591-2 v1.1.1, "Digital Video Broadcasting (DVB); IP Datacast: Content Delivery Protocols (CDP) Implementation Guidelines; Part 2: IP Datacast over DVB-SH," 2010.

[34] J. Boutros and E. Viterbo, "Signal space diversity: A power- and bandwidth-efficient diversity technique for the Rayleigh fading channel," *IEEE Trans. Inform. Theory*, vol. 44, no. 4, pp. 1453–1467, July 1998.
[35] C. Abdel Nour and C. Douillard, "Improving BICM performance of QAM constellations for broadcasting applications," *5th International Symposium on Turbo Codes & Related Topics*, Lausanne, Switzerland, Sept. 2008, pp. 55-60.
[36] ENGINES Technical Report TR4.1 "Interim report on Hybrid Access Technologies", September 2011.
[37] B. Le Floch, M. Alard, and C. Berrou, "Coded Orthogonal Frequency Division Multiplex," *Proceedings of the IEEE*, vol. 83, pp. 982–996, June 1995.
[38] D. Pinchon, P. Siohan, and C. Siclet, "Design techniques for orthogonal modulated filter banks based on a compact representation," *IEEE Trans. Signal Processing*, vol. 52, no. 6, pp. 1682 – 1692, June 2004.
[39] N. Laurenti and L. Vangelista, "Filter design for the conjugate OFDM-OQAM system" *First International Workshop on Image and Signal Processing and Analysis*, July 14-15, 2000, pp: 267-272.
[40] H. S. Malvar "Modulated QMF Filter Banks with Perfect Reconstruction", *Electronics Letters*, June 1990, vol.26,nb.13,pp: 906-907
[41] A. Skrzypczak, P. Siohan and J.-P. Javaudin "Analysis of the Peak-to-Average Power Ratio for OFDM/OQAM", *7th IEEE Workshop on Signal Processing Advances in Wireless* Communications, *SPAWC'06*, July 2006, Cannes, France.
[42] B. R. Saltzberg, "Performance of an efficient parallel transmission system'', *IEEE Transactions on Communication Technology*, pp. 805-811, Vol. 15, N° 6, Dec. 1967.
[43] B. Farhang-Boroujeny and R. Kempter, "Multicarrier communication techniques for spectrum sensing and communication in cognitive radios'', *IEEE Communication magazine*, pp. 80-85, Vol. 46, 2008.
[44] "European union 7th Framework programme: Project PHYDYAS,'' http://www.ict-phydyas.org
[45] P. Siohan, C. Siclet and N. Lacaille, "Analysis and design of OFDM/OQAM systems based on filterbank theory'', *IEEE Transactions on Signal Processing*, pp. 1170-1183, Vol. 50, N° 5, May 2002.
[46] C. Cariolaro and F. Vagliani, "An OFDM scheme with a half complexity'', *IEEE Journal on Selected Areas in Communications*, pp. 1586-1599, Vol. 13, N° 9, Dec. 1995.
[47] A. Jalali, D. Lacroix and P. Combelles, "Multicarrier modulation using weighted prototype functions'', *Patent FR-97 08547, 01/07/1997, International Extension PCT/FR98/01398, WO99/01967,* Jan. 1999.
[48] L. Vangelista and N. Laurenti, "Efficient implementations and alternative architectures for OFDM-OQAM systems'', *IEEE Transactions on Communications*, pp. 1170-1183, Vol. 50, N° 5, May 2002.
[49] T. Nguyen and R. Koilipillai, "The theory and design of arbitrary-length cosine-modulated filter banks and wavelets, satisfying perfect reconstruction'', *IEEE Transactions on Signal Processing*, pp. 473-483, Vol. 44, N° 3, March 1996.
[50] Y. Dandach and P. Siohan, "FBMC/OQAM modulators with half complexity'', *Globecom*, Houston (USA), December 5-9, 2011.
[51] J. W. Cooley and J. W. Tukey, "An algorithm for the machine calculation of complex Fourier series'', *Math computations*, 1965.
[52] P. Duhamel and H. Hollmann, "Implementation of "split-radix" FFT algorithms for complex, real and real symmetric data'', in *ICASSP*, Tampa (USA), Vol. 10, pp. 784-787, April 1985.
[53] A. Saidi, "Decimation-in-time-frequency FTT algorithm '', in *ICASSP*, Adelaide (Australia), Vol. 3, pp. 453-456, April 1994.
[54] C. Burrus and T. W. Parks, "*DFT/FFT and convolution algorithms''*, Wiley, New-York, 1985.
[55] H. Sorensen, D. Jones and C. Burrus, "Real-valued algorithms for the FFT'', in *ICASSP*, Vol. 12, pp. 1831-1834, April 1987.

[56] T. Ihalainen, A. Iklef, J. Louveaux and M. Renfors, "Channel equalization for multi antenna FBMC/OQAM receivers'', *IEEE Transactions on Vehicular Technology*, pp. 2070-2085, Vol. 60, N° 5, 2011.
[57] G. Ndo, H. Lin and P. Siohan, "FBMC/OQAM equalization: Exploiting the imaginary interference'', in *PIMRC 2012, Sydney (Australia), Sepember 2012.*
[58] H. Lin and P. Siohan, "Capacity analysis for PLC with different multi-carrier modulations", *IEEE Transcations on Power Delivery*, pp. 113-124,Vol. 25, N° 1, 2010.
[59] M. Renfors, T. Ihalainen, T. H. Stitz, A block-Alamouti scheme for filter bank based multicarrier transmission, *European wireless Conference*, Lucca, Italy, April 2010.
[60] R. Van Nee and R. Prasad, "OFDM for Wireless Multimedia Communications", *Artech House Publisher*, March 2000.
[61] M. J. F.-G. Garcia, O. Edfors and J. M. Paez-Borrallo, "Peak Power Reduction for OFDM Systems with Orthogonal Pilot Sequences", *IEEE Transactions on. Wireless Commun*ications, vol. 5, no. 1, pp 47-51, Jan. 2006.
[62] S. H. Han and J. H. Lee, "An overview of Peak-to-Average Power Ratio reduction techniques of multicarrier transmission", *IEEE Wireless Commun*ications, vol. 12, no. 2, pp. 56-65, April 2005.
[63] X. Li and and J. L. Cimini, "Effect of Clipping and Filtering on the performance of OFDM", *47th IEEE Vehicular Technology Conference*, vol. 3, pp. 1634-1638, Phoenix, USA, May 1997.
[64] S. H. Muller and J. B. Huber, "OFDM with reduced Peak-to-Average Power Ratio by Optimum Combination of Partial Transmit Sequences", *Electronics Letters*, vol. 32, no. 5, pp. 368-369, Feb. 1997.
[65] R. W. Bauml, R. F. H. Fisher and J. B. Huber, "Reducing the Peak-to-Average Power Ratio of multicarrier Modulation by Selected Mapping", *Electronics Letters*, vol. 32, no. 22, pp. 2056-2057, Oct. 1996.
[66] D. S. Jayalath and C. Tellambura, "Reducing the Peak-to-Average Power Ratio of Orthogonal Frequency Division Multiplexing signal through bit of symbol interleaving", *Electronics Letters*, vol. 36, no. 13, pp. 1161-1162, June 2000.
[67] J. Tellado-Mourelo, "Peak-to-Average Power Ratio reduction for multicarrier Modulation", *PhD thesis, Stanford University*, Sept. 1999.
[68] M. Mahafeno, Y. Louet and J.-F. Helard, "PAPR reduction using SOCP-based Tone Reservation for Terestrial DVB Systems", *IET Communications Journal*, vol. 3, no. 7, pp. 1250-1261, July 2009.
[69] Aggarwal and T. H. Meng, "Minimising the Peak-to-Average Power Ratio of OFDM Signals Using Convex Optimization," *IEEE Transactions on Signal Processing*, vol. 54, no. 8, pp. 3099-3110, Aug. 2006.
[70] S. Zabre, J. Palicot, Y. Louet and C. Lereau, "SOCP Approach for OFDM Peak-to-Average Power Ratio Reduction in the Signal Adding Context", *IEEE Symposium on Signal Processing and Information Technology*, pp. 834-839, Vancouver, Canada, Aug. 2006.
[71] M. Sharif, M. Gharavi-Alkhansari and B. H. Khalaj, "On the peak-to-average power of OFDM signals based on oversampling", *IEEE Transactions on Communications*, vol. 51, no. 1, pp. 72-78, Jan. 2003.
[72] R. Van Nee and A. de Wild, "Reducing the peak-to-average power ratio of OFDM", *48th IEEE Vehicular Technology Conference*, vol. 3, pp. 2072-2076, Ottawa, Canada, May 1998.
[73] DVB "Implementation guidelines for a second generation digital terrestrial television broadcasting system (DVB-T2)", *ETSI TR 102 831 V0.9.17*, Nov. 2009.
[74] DVB BlueBook A122, "Digital Video Broadcasting (DVB); Frame structure channel coding and modulation for a second generation digital terrestrial television broadcasting system (DVB-T2)", July 2011.
[75] E. Stare, "Time-Frequency Slicing (TF-Slicing). A new concept for DVB-T2", TM-T20112.
[76] D. Gozálvez, D. Gómez-Barquero, D. Vargas and N. Cardona, "Time Diversity in DVB-T2 Systems"
[77] E. Stare and S. Bergsmark, "Time-Frequency Slicing gains", TM-T20280, 2007-09-24.

[78] M. Makni, J. Robert and E. Stare, "Performance Analysis of Time Frequency Slicing", 14th ITG Conference on Electronic Media Technology in Germany, March 2011.
[79] S. M. Alamouti, "*A simple transmit diversity technique for wireless communications*", IEEE Journal on Selected Areas in Communications, 1998.
[80] "*MIMO Channel Models*", Taskforce report TR 3.1, ENGINES project, June 2011.
[81] "*Digital Video Broadcasting (DVB); Frame structure channel coding and modulation for a second generation digital terrestrial television broadcasting system (DVB-T2)*", European Standard, ETSI EN 302 755, v1.2.1, February 2011.
[82] Peter Moss, "*MIMO vs SIMO*", DVB document TM-NGH499r1, October 2010.
[83] Joerg Robert, "*Revised Capacity Figures*", DVB document TM-NGH478r1, October 2010.
[84] C. A. Nour, "Rotated Constellations as MIMO Space Code for DVB-NGH", DVB document TM-NGH564, October 2010.
[85] Camilla Hollanti and Tero Jokela, "Rate-1 and Rate-2 UTU Codes for the 4x2 MIMO channel--Detailed Descriptions for Cross-Check Simulations", DVB document TM-NGH523r1, November 2010.
[86] Camilla Hollanti and Tero Jokela, "Hybrid MIMO configurations and code complexities", DVB document TM-NGH1042, June 2011.
[87] Joerg Robert, "*Simulation Results on MIMO Performance*", DVB document TM-NGH587, December 2010.
[88] Joerg Robert, "Improved Robustness and Transmitter Identification for Multi-Antenna Systems", DVB document TM-NGH616, February 2011.
[89] Volker Pauli, "Low-Complexity Tx Diversity Scheme for DVB-NGH: Tx Antenna Switching", DVB document TM-276, June 2010.
[90] JaeHwui Bae, "New Spatial Multiplexing Scheme for Erasure Fading Channels", DVB document TM-NGH338, July 2010.
[91] Sangchul Moon, "Consideration about eSM and Multilayer SM", DVB document TM-NGH503, October 2010.
[92] M. Petrov, Y. Murakami, T. Kimura, M. Ouchi, "*The Effect of LoS Components on MIMO Performance*", DVB document TM-NGH591, December 2010.
[93] JaeHwui Bae, "*ETRI's Unequal Tx Power MIMO SM and Simulation results*", DVB document TM-NGH406, September, 2010.
[94] Alberto Morello and Vittoria Mignone, "MIMO for Broadcast in DVB-NGH", DVB document TM-NGH074, March, 2010.
[95] Mihail Petrov, "*Final MIMO Simulations for Phase 2–eSM vs. hSM*", DVB document TM-NGH815, March 2011.
[96] Sangchul Moon, "*Consideration about eSM and Multilayer SM*", DVB document TM-NGH518, November 2010.
[97] C. A. Nour and C. Douillard, "*Rotated QAM constellations to improve BICM performance for DVB-T2*", in the Proceedings of the ISSSTA, 2008.
[98] H. Jafarkhani, "*A quasi-orthogonal space-time block code*", IEEE Transactions on Communications, 2001.
[99] David Tse and Pramod Viswanath, "*Fundamentals of Wireless Communication*", Cambridge University Press, 2005.
[100] A. Paulraj and R, Nabar, "*MIMO Communications Systems*", Chapter in Wiley Encyclopedia on Telecommunications. Ed. J. Proakis, 2003.
[101] Emre Telatar, "*Capacity of Multi-antenna Gaussian Channels*", Technical Report BL0112170950615-07TM, AT&T Bell Laboratories, 1995.
[102] F. Oggier, and E. Viterbo, "*Algebraic number theory and code design for Rayleigh fading channels*", Foundations and Trends in Communications and Information Theory, 1 (3). pp. 333-415, 2004.
[103] H. Bölcskei and A. J. Paulraj, "*Space-Frequency Coded Broadband OFDM Systems*," Proc. IEEE Wireless Commun and Networking Conf., Chicago, IL, Sept. 2000, pp. 1–6.
[104] W. Ko, H. Hong, S. Moon, P. Fertl, "*LG Response to NGH Call for Technology*," TM-NGH076, 2010
[105] M. Petrov, Y. Murakami, T. Kimura, M. Ouchi, "The Effect of LoS Components on MIMO Performance," TM-NGH652, 2011.

[106] F. Fontan, M. Vazquez-Castro, C. Cabado, J. Garcia, E. Kubista, "Statistical modeling of the LMS channel," *IEEE Trans. Vehicular Technology*, vol. 50, No.6, pp. 1549-1567, Nov. 2001.
[107] "*COST 207 Report, Digital land mobile radio communications*," Commission of European Communities, Directorate General, Telecommunications Information Industries and Innovation, Luxemburg, 1989.
[108] C.Loo, "*A Statistical Model for a Land Mobile Satellite Link*", IEEE Trans. Vehicular Technology, Vol. VT-34, No.3, August 1985.
[109] Y. Nasser, J.-F. Helard and M. Crussiere, "3D MIMO scheme for broadcasting future digital TV in single-frequency networks," *Electronics Letters* , vol.44, no.13, pp.829-830, June 2008.
[110] Y. Nasser and J.-F. Helard, "Double Layer Space-Time Block Code for Hybrid Satellite-Terrestrial Broadcasting Systems," *Proc. IEEE Vehicular Technology Conference Fall (VTC 2009-Fall),* pp.1-5, Sept. 2009.
[111] LTE; Evolved Universal Terrestrial Radio Access (E-UTRA); Physical layer procedures, 3GPP TS 36.213, Version 10.3.0, Release 10, Oct. 201.
[112] IEEE 302.16m, IEEE Standard for local and metropolitan area networks - Part 16: Air Interface for Broadband Wireless Access Systems, Amendment 3: Advanced Air Interface, May 2011.
[113] C. Abdel Nour and C. Douillard, "Improving BICM Performance of QAM constellations for broadcasting applications," Int. Symp. on Turbo Codes and Iterative Techniquee, Lausanne, Switzerland, Sept. 2008.
[114] J. C. Belfiore, G. Rekaya, and E. Viterbo, "The Golden code: a 2x2 full-rate space-time code with non vanishing determinants", IEEE Trans. Inform. Theory, vol. 51, n° 4, pp. 1432-1436, April 2005.
[115] S. Sezginer and H. Sari, "Full-rate full-diversity 2×2 space-time codes
[116] of reduced decoder complexity," IEEE Commun. Lett., vol. 11, no. 12,
[117] pp. 973–975, Dec. 2007.
[118] J. Paredes, A.B. Gershman, and M. G. Alkhanari, ``A 2x2 space--time code with non-vanishing determinants and fast maximum likelihood decoding," in Proc IEEE Int. Conf. on Acoustics, Speech, and Signal Processing (ICASSP2007), Honolulu, Hawaii, USA, pp. 877-880, April 2007.
[119] M. Samuel and M. P. Fitz, ``Reducing the detection complexity by using 2x2 multi-strata space--time codes," in Proc IEEE Int. Symp. Inform. Theory (ISIT 2007), pp. 1946-1950, Nice, France, June 2007.
[120] E. Biglieri, Y. Hong and E. Viterbo, "On fast-decodable space-time block codes,"IEEE Trans. On Information Theory, pp. 524-530, vol. 55, n. 2, Feb. 2009.
[121] C. Hollanti, J. Lahtonen, K. Ranto, R. Vehkalahti, and E. Viterbo, ``On the Algebraic Structure of the Silver Code," in IEEE Information Theory Workshop, Porto, Portugal, May 2008.
[122] O. Tirkkonen and A. Hottinen, ``Square-matrix embeddable space-time block codes for complex signal constellations," in IEEE Trans. Inform. Theory, vol. 48, no. 2, , pp. 384-395, February 2002.
[123] W. C. Jakes, Microwave Mobile Communications, Wiley-Interscience, May 1994.
[124] B. M. Hochwald and S. ten Brink, "Achieving near-capacity on a multiple-antenna channel," IEEE Trans. Communications, vol. 51, pp. 389-399, Mar. 2003.
[125] V. Tarokh, N. Seshadri, and A. R. Calderbank, "Space-time codes for high data rate wireless communications: Performance criterion and code construction," IEEE Trans. Inf. Theory, vol. 44, no. 2, pp. 744–765, Mar. 1998.
[126] "DVB-NGH, Next Generation Handheld," http://www.dvb.org/technology/dvb-ngh/.
[127] *Frame structure channel coding and modulation for a second generation digital terrestrial television broadcasting system* (DVB-T2), ETSI Std. EN 302 755, Rev. 1.2.1, 2011.
[128] V. Tarokh, N. Seshadri and A. Calderbank, "Space-time codes for high data rate wireless communication: Performance criterion and code construction," IEEE Trans. Inf. Theory, vol. 44, no. 2, 1998, pp. 744–765.
[129] S. Alamouti, "A simple transmit diversity technique for wireless communications," IEEE J. Sel. Areas Commun., vol. 16, no. 8, Oct. 1998, pp. 1451–1458.
[130] P. Moss, T. Y. Poon and J. Boyer, "A simple model of the UHF cross-polar terrestrial channel for DVB-NGH," Research & Development White Paper WHP205, Sept. 2011.

[131] C. Studer and H. Bolcskei, "Soft-input soft-output single tree-search sphere decoding," IEEE Trans. Info. Theory, vol. 56, no. 10, 2010, pp. 4827–4842.
[132] Y. Nasser, J.-F. Hélard and M. Crussière, "3D MIMO scheme for broadcasting future digital TV in single-frequency networks," Electronics Letters, vol. 44, no. 13, June 2008, pp. 829–830.
[133] P. W. Wolniansky, G. J. Foschini, G. D. Golden and R. A. Valenzuela, "V-BLAST: an architecture for realizing very high data rates over the rich-scattering wireless channel," in Proc. URSI International Symposium on Signals, Systems, and Electronics (ISSSE 98), 1998, pp. 295–300.
[134] K. Srinath and B. Rajan, "Low ML-decoding complexity, large coding gain, full-rate, full-diversity STBCs for 2×2 and 4×2 MIMO systems," IEEE J. Sel. Topics Signal Process., vol. 3, no. 6, 2009, pp. 916–927.
[135] E. Biglieri, Y. Hong and E. Viterbo, "On fast-decodable space-time block codes," IEEE Trans. Inf. Theory, vol. 55, no. 2, 2009, pp. 524–530.
[136] H. Jafarkhani, "A quasi-orthogonal space-time block code," IEEE Trans. Commun., vol. 49, no. 1, 2001, pp. 1–4.
[137] J. Belfiore, G. Rekaya and E. Viterbo, "The Golden code: a 2×2 full-rate space-time code with nonvanishing determinants," IEEE Trans. Inf. Theory, vol. 51, no. 4, 2005, pp. 1432–1436.
[138] M. Valenti and B. Zhao, "Distributed turbo codes: towards the capacity of the relay channel," in *Proc. IEEE Vehicular Technology Conference (VTC)*, pp. 322–326, Oct. 2003.
[139] J. Laneman, D. N. C. Tse, and G. W. Wornell, "Cooperative diversity in wireless networks: Efficient protocols and outage behavior," *IEEE Trans. Inf. Theory*, vol. 50, pp. 3062–3080, Dec. 2004.
[140] G. Kramer, M. Gastpar, and P. Gupta, "Cooperative strategies and capacity theorems for relay networks," *IEEE Trans. Inf. Theory*, vol. 51, pp. 3037–3063, Sept. 2005.
[141] Y. Liang and V. V. Veeravalli, "Gaussian orthogonal relay channels: Optimal resource allocation and capacity," *IEEE Trans. On Inform. Theory*, vol. 51, pp. 3284–3289, Sept. 2005.
[142] T. Riihonen, S. Werner, and R. Wichman, "Rate-interference trade-off between duplex modes in decode-and-forward relaying," in *Proc. IEEE Int. Symp. Pers. Indoor Mob. Radio Commun., Toronto, Canada*, pp. 690–695, Sept. 2010.
[143] R. Youssef,M. Helard,M. Crussiere, and J. Helard, "Distributed coding for OFDM-based transmission in cooperative broadcast networks," in *Proc. International Workshop on Cross Layer Design (IWCLD)*, Nov. 2011.